Influence of spectrum compatible earthquake records on the inelastic behavior of reinforced concrete structures

by

RAMÓN LUIS GASCOT LOZADA

A thesis submitted in partial fulfillment of the requirements for the degree of

MASTER OF SCIENCE
IN
CIVIL ENGINEERING

UNIVERSITY OF PUERTO RICO
MAYAGÜEZ CAMPUS
MAYAGÜEZ, PUERTO RICO
2013

Approved by:

_____	_____
Luis E. Suárez-Colche, PhD. Member, Graduate Committee	Date
_____	_____
Ricardo R. López-Rodríguez, PhD. Member, Graduate Committee	Date
_____	_____
Luis A. Montejo-Valencia, PhD. President, Graduate Committee	Date
_____	_____
Miguel F. Canals-Silander, PhD. Representative of Graduate Studies	Date
_____	_____
Ismael Pagán-Trinidad, MSCE Chairperson of the Department	Date

ABSTRACT

Seismic designed structures are expected to resist minor level earthquakes without significant damage as well as major level earthquakes without collapse. Over the last years the number of seismic instrumentation networks has increased over highly active seismic regions raising considerably the number of strong motion records available. Despite the increase in the number of available strong motion records, artificial spectrum compatible records are still widely used for seismic design/assessment in zones where the number of available records is scarce and/or to reduce the number of analysis required while complying with design codes requirements.

There are different methodologies used to generate spectrum compatible records and three of them are evaluated in this report: wavelet based modification of seed records, seed record adjustment based on the Continuous Wavelet Transform and synthetic record generation in the frequency domain. Different sets of compatible records are generated using each of these methodologies. The compatible records are evaluated based on the level of match with the target spectrum and its strong motion characteristics. The effect on the nonlinear seismic response is evaluated using these records as input motions for nonlinear time history analyses of a typical RC bridge bent column model developed and calibrated using a distributed plasticity fiber based finite element approach. It was found that the three methodologies are capable of generating compatible records with an acceptable level of matching the characteristics. However, the records generated using the frequency domain approach exhibit unrealistic strong motion characteristics and a tendency to induce less inelastic demand in the structures. In the case of methodologies based on modification of actual earthquake records it was found that when the

seed records are selected based on their initial compatibility with the target spectrum, the resultant compatible record not only retains better the original characteristic of the records but the variability in the structural response is reduced.

RESUMEN

Una estructura diseñada sísmicamente se espera que resista sin mayor daño un terremoto de baja intensidad, así como que no colapse con uno de gran magnitud. Durante los pasados años la instrumentación sísmica ha aumentado considerablemente en regiones de alta actividad sísmica, como resultado el número de registros de movimientos fuertes disponible se ha elevado de manera copiosa. A pesar de este aumento, los terremotos compatibles a un espectro de diseño siguen siendo ampliamente utilizados en el diseño o evaluación sísmica de estructuras en zonas donde la cantidad de registros disponibles es escasa o simplemente para reducir el número de análisis requeridos y todavía cumplir con las especificaciones requeridas por los códigos de diseño.

Existen distintos tipos de métodos para generar terremotos compatibles con un espectro, tres de éstos son evaluados en este reporte: modificaciones basadas en la adición de "wavelets" a registros semilla, ajustes a los registros semilla a base de la trasformada continua "Wavelet" y generación de terremotos completamente sintéticos en el dominio de la frecuencia. Diferentes grupos de registros compatibles con un espectro fueron generados con cada una de estas metodologías. Los registros compatibles fueron evaluados basándose en el nivel de coincidencia con el espectro objetivo y sus características de movimiento fuerte. Los registros fueron utilizados para evaluar la respuesta sísmica no lineal de un modelo numérico de una columna típica de hormigón reforzado de un puente. El modelo de la columna fue desarrollado usando elementos finitos de plasticidad distribuida basados en fibras. Se encontró que las tres metodologías son capaces de generar registros compatibles con un nivel aceptable de

coincidencia con el espectro objetivo. Sin embargo, los registros generados en el dominio de la frecuencia presentaron características de movimiento fuerte poco realistas y una tendencia a inducir menor demanda inelástica en las estructuras. En el caso de las metodologías basadas en la modificación de los registros reales, se encontró que cuando los registros de semillas se seleccionan en base a su compatibilidad inicial con el espectro objetivo, los terremotos resultantes no sólo retuvieron mejor las características originales de la registros, sino que se redujo la variabilidad en la respuesta no lineal de la estructura.

To God and the two most important people in my world,

my parents Ramón L.and Violeta,

they are my inspiration to succeed and be a better person every day,

to my sister, niece and friends for always being there.

ACKNOWLEDGMENTS

First of all, I want to thank God for giving me the opportunity to complete one of my goals, obtain my master degree completely healthy and for being a continuous guide for me throughout my life. I am very grateful for the guidance and the advice of my mentor Dr. Luis A. Montejo Valencia, who inspired me and was very important on the completion of this research. To my graduate committee Dr. Luis E. Suárez, Dr. Ricardo R. López and Dr. Miguel F. Canals for believe in me and guide me to accomplish this project. My special thanks are extended to Prof. Ismael Pagán and the administrative staff of the Civil Engineering Department.

I would like to thank the University of Puerto Rico fellowship program in Nuclear Structural Engineering for providing the funding during the major part of this research. This work was performed at the University of Puerto Rico at Mayagüez under award NRC-HQ-12-G-38-0018 from the US Nuclear Regulatory Commission. The statements, findings, conclusions, and recommendations are those of the authors and do not necessarily reflect the view of the US Nuclear Regulatory Commission.

TABLE OF CONTENTS

LIST OF TABLES

LIST OF FIGURES

CHAPTER 1

1.1 Introduction

Earthquakes, one of the most dangerous nature events that exist, can be defined as the sudden slip on a fault and the resulting ground shaking due to seismic waves and radiated seismic energy. Earthquakes do not directly cause the structures to collapse, ground motions are the real cause of seismic damage. Since the beginning of its study, engineers and scientists have no real means to predict or make an accurately forecast of this event, the only genuine possibility is to try to mitigate its consequences. (Gioncu & Mazzolani, 2011).

The most important fact that induces the damage in buildings and structures is their dynamic response to the ground motions. At present, with all the techniques and computer programs developed in the structural engineering area, the structural response of most structural systems can be safely predicted. The same cannot be said for the seismic engineering area. Due to the complexity of the seismic phenomena it is very hard to predict a ground motion, and that is the mystic and the challenge of earthquake engineering. Further challenge is to design without knowing the ground motion.

Modern seismic design started on the 1950s, when Housner proposed the idea that seismic energy is dissipated through plastic deformation. In the 1960s Velestos and Newmark developed the first study on the inelastic response spectrum. They obtained the maximum response deformation for elastic-perfectly plastic structures. Another new concept was proposed in 1969 by Newmark and Hall, by constructing spectra based on acceleration, velocities and

displacements in the short, medium and long period ranges, respectively. (Gioncu & Mazzolani, 2002)

In the 1990s two seismic events completely changed the view and approach of earthquake resistant design: the Northridge earthquake in Los Angeles, California and the Kobe earthquake in Japan. After these earthquakes the new goal of the design methodology is to produce structures that have a predictable seismic performance under multiple levels of earthquake intensity. This design philosophy is commonly referred as performance based design (PBD), (Bertero and Bertero, 2000). To accomplish the objectives of PBD, a displacement based design approach is better suited than the traditional force based design. (Priestley et al. , 2007).

1.2 Justification and previous research

Independent of the approach selected, displacement or force based, current seismic design of civil structures is performed using equivalent lateral load approaches or other variations of the response spectrum method, where the ground motion is represented as a design response spectrum that is representative of the seismic hazard on the site. The pseudo-acceleration or displacement design response spectrum is used to estimate the force or deformation demand imposed in the structure. This technique is promoted in the majority of the design codes and standards, for example the Minimum Design Loads for Buildings and Other Structures developed by the American Society of Civil Engineers (ASCE 7-10, 2010). The main goal of this technique is to translate the ground motion into forces acting on the building.

It should be noticed that codes do not always allow the use of the equivalent lateral load approach. In ASCE 7-10 for example, the structure must be first classified as regular or irregular.

The irregularities are divided in two groups, vertical irregularities and horizontal irregularities, and they are explained in the ASCE 7-10 guidelines, specifically in Chapter 12. If the structure is regular one can follow straightforward the requirements that the code dictates and construct the design response spectrum for the specific site to obtain the spectral response acceleration. With this acceleration and other parameters like the response modification factor and the importance factor, one can calculate the total base shear and then distribute it along the height of the structure. However, if the structure is irregular or meets the characteristic necessary to be considered as irregular, dynamic analyses are required to verify the design of the structure. Other instances where dynamic time history analyses are required are in the seismic design and/or assessment of critical infrastructure like nuclear power plants (NRC, 2007).

While current design codes accept elastic time history analyses for design verification, it should be noticed that this type of analysis will not provide any information on the behavior of the structure beyond its yield limit. On the other hand, inelastic time history analysis provides the most accurate method for verifying that inelastic deformations satisfy the design limits (Priestley et al. , 2007). Charney (2011) concluded that nonlinear dynamic analysis is generally regarded as the best method of analysis available, but there exists a number a barriers to a broad acceptance in the design community. These barriers include the lack of a comprehensive design basis that makes direct use of the analysis, concern (real or perceived) about the complexity of the analysis, a general lack of training in dynamic response history analysis and in nonlinear analysis, and the necessity to select ground motions for the analysis. Notice that, independent of what type of analysis is performed, elastic or inelastic, dynamic time history analyses require the seismic input to be defined as acceleration records and to comply with code requirements, the acceleration series used should be compatible with the design spectrum. By compatible it is

meant that the response spectrum of the acceleration time history matches in average the design spectrum.

To select these input records one can look at real historic records with amplitude scaled by a factor to optimize the fitting over the design spectrum (e.g. Bommer & Acevedo, 2004) or one can use different methodologies available to generate "artificial" spectrum compatible records. When using the first option, amplitude scaling, a larger number of records is required to obtain a reliable average of the structural response due to the natural scatter of the records. However, the use of spectrum compatible records substantially reduces the number of analyses required to obtain a reliable estimate of the structural response (e.g. Watson-Lamprey & Abrahamson, 2006; Heo et al, 2011; Hancock et al, 2008; Jun, 2010). Additionally, since the spectral amplitude characteristics are quite similar for a set of spectrum compatible records, this type of records can be used to explore the effect of other strong motion parameters in the structural response (Hancock & Bommer, 2007; Montejo & Kowalsky, 2008). Nevertheless, spectrum compatible records have been criticized for being too severe due to its unrealistic energy content (e.g. Naeim al, 1995; Bommer & Ruggeri, 2002; Bommer & Acevedo, 2004). *The purpose of this work is to analyze the effect of spectrum compatible earthquake records generated using different approaches on the inelastic response of reinforced concrete structures.*

1.3 Objectives

The specific objectives of this research work can be summarized as follows:

- Evaluate different methodologies available for the generation of spectrum compatible earthquake records. Examine the level of matching obtained and how well are the characteristics of the seed record retained on the compatible record.
- Evaluate the influence of the seed record on the efficiency of the different methodologies. Investigate how close to the target spectrum the response spectrum of the seed record needs to be.
- Evaluate the effect of the compatible earthquakes on the inelastic response of the structure. Examine whether there is any significant difference on the results obtained using records generated with different methodologies. Study if any of the methodologies produces more "severe" records.
- Examine which strong motion parameters, other than the spectral amplitude, have influence on the inelastic response. Since all of the records that will be used have basically the same response spectrum, the effect of other parameters like strong motion duration can be examined.

1.4 Methodology

The activities to be performed as part of this research work involve:

(1) Selection of historic earthquake records: The records are selected from the PEER Ground Motion Database (PEER 2012) based on how the spectral shapes resemble the target design spectrum. In order to analyze the effect of the seed record on the performance of the different modification methodologies, two sets of 10 records will be assembled. One set will consist of the available records that best match the design spectrum and the other set will be formed by records whose response spectrum shape differs largely from the target spectrum. Figures 1.4.1 and 1.4.2

show examples for both cases. Since the comparison is based on shape, the amplitude of the records is scaled to provide a best fit.

(2) Modification of these records to obtain spectrum compatible records using three different methodologies: time domain adjustment by adding wavelets to the original time history (Hancock et al., 2006), adjustment of the wavelet coefficients of the original time history (Suárez & Montejo, 2005) and frequency domain modification of an initial random process using an historic record to define the amplitude modulation (similar to Gasparini & Vanmarcke, 1976).

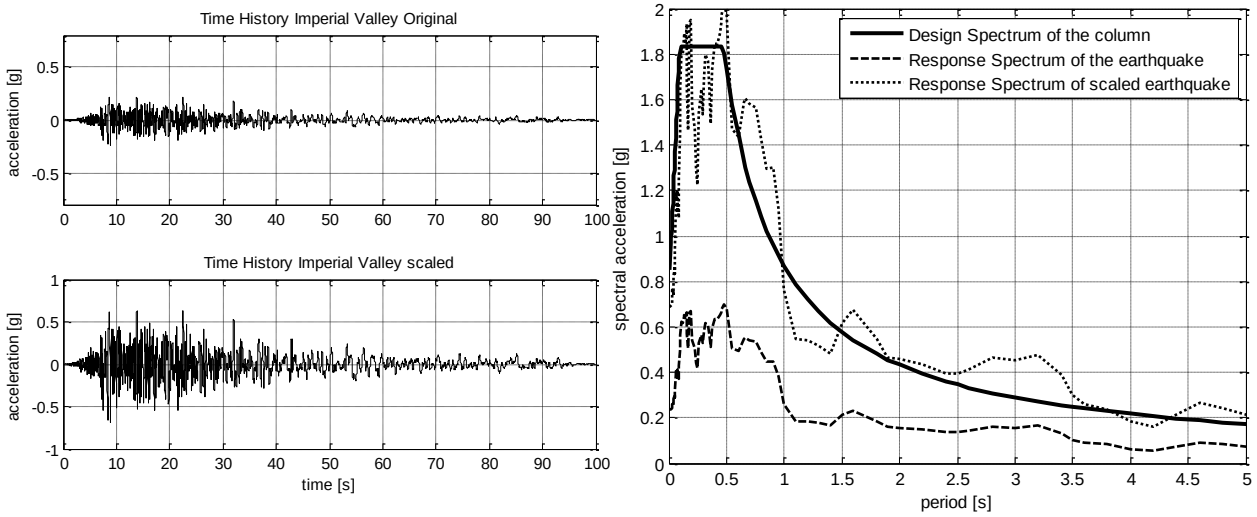

Figure 1.4.1. Imperial Valley Earthquake, Imperial Valley scaled Earthquake, Design Spectrum and Response Spectra

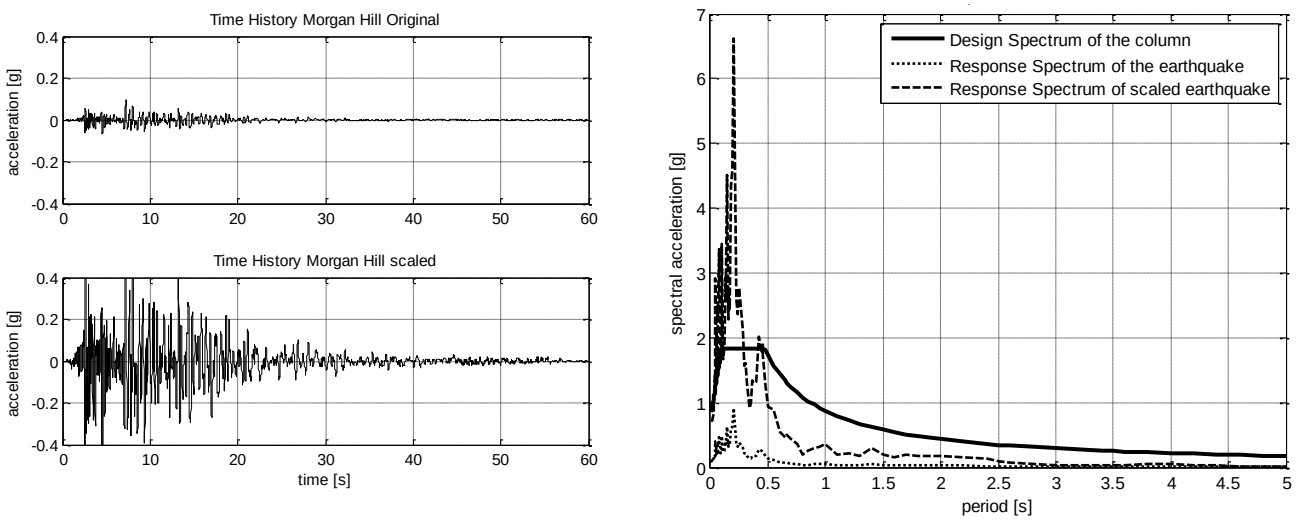

Figure 1.4.2. Morgan Hill Earthquake, Morgan Hill scaled Earthquake, Design Spectrum and Response Spectra

(3) Development of a numerical model capable of replicating, as close as possible, the actual nonlinear seismic response of a reinforced concrete structure: A fiber-based distributed plasticity approach will be used to develop a finite element model for the large scale reinforced concrete bridge column tested on the outdoor shake table at the University of California at San Diego (Figure 1.4.3.). This structure was selected because the experimental data is available from the NEEShub repository, so that validation and calibration of the model is possible. Figure1.4.4. shows an example of the results obtained.

Figure 1.4. 3. UCSD column pre-test setup (UCSD report)

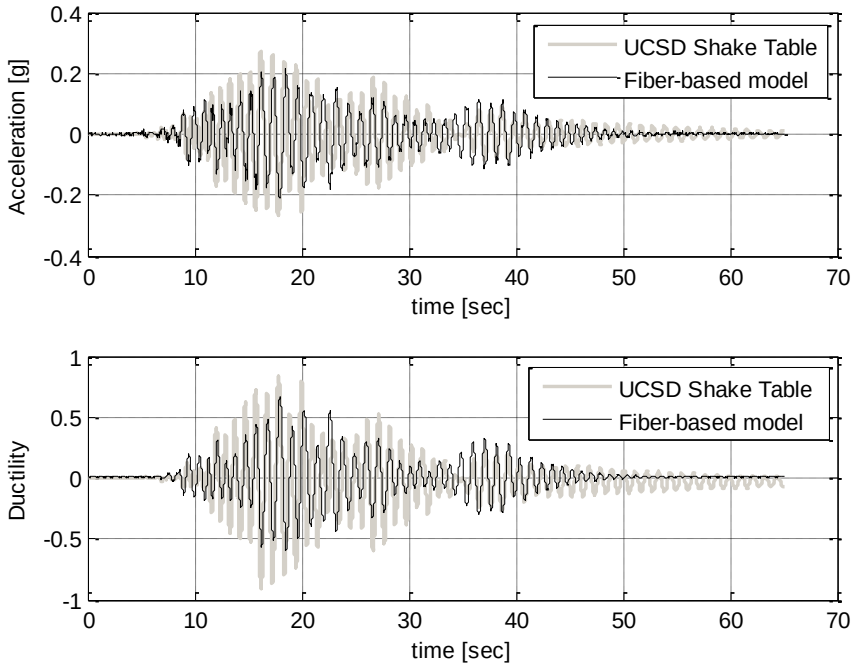

Figure 1.4.4. (a) Acceleration time-histories for EQ1, (b) Ductility time-histories for EQ1

(4) Perform incremental dynamic analyses (Vamvatsikos & Cornell, 2002). The spectrum compatible records will be used to perform incremental dynamic analyses of the structural model. This will allow the examination of the effect of compatible records over a large range of inelastic demand levels.

1.5 Thesis Organization

1.5.1. Seed records selection, generation and examination of the resulting compatible records

Chapter 2 presents the development of the spectrum compatible records generated for this study. There are different methodologies used to generate these types of records; three of them are evaluated in this report: (1) time domain adjustment by adding wavelets to the original time

history (as implemented by the program *SeismoMatch*), (2) adjustment of the wavelet coefficients via Continuous Wavelet Transform CWT, (as implemented by the program *ArtifQuakeLet II*) and (3) frequency domain modification of an initial random process (as implemented by the program *SeismoArtif*). These records are examined in detail on how well the characteristics of the original seed record are retained in the compatible record. The characteristics/parameters examined are peak ground acceleration (PGA), peak ground velocity (PGV), peak ground displacement (PGD), Arias intensity (AI), significant duration (SD), cumulative absolute velocity (CAV), mean period (Tm), and frequency content via Fourier spectra and Wavelet Maps.

1.5.2. Effect of spectrum compatible records on the seismic demand of a typical RC bridge bent column

Chapter 3 examines the effect of using the records generated in Chapter 2 as input motions for nonlinear time history analyses of a full scale reinforced concrete (RC) bridge column. To accomplish this, a fiber based distributed plasticity model of of the structure is developed and calibrated using actual large scale experimental data. Once the model is calibrated, incremental dynamic analyses (IDA) are performed in order to analyze the inelastic demand imposed in the structure by the different records over a wide range of seismic intensities.

1.5.3. Effect of spectrum compatible records on the seismic demand of RC bridge columns with different periods of vibration

Chapter 4 extends the analysis performed in Chapter 3 by analyzing the behavior of 4 RC bridge columns with different natural periods. To achieve this, the cantilever length of the specimen was changed in order to obtain columns with aspect ratios (L/D) of 3.4, 4.2,6 and 8. The main reason

for this change is obtain different natural periods so that each structure fits under different regions of the design spectrum. The objective is to identify if there are any significant differences in the inelastic demand imposed in the structure by the spectrum compatible records, this time taking into account also the period vibration of the structure.

1.6 References

ASCE (2010). *Minimum Design Loads for Buildings and Other Structures* (ASCE 7-10), American Society of Civil Engineers, Reston, Virginia.

Bertero.R.D., and Bertero, V. V. (2000). Application of a Comprehensive Approach For The Performance-Based Earthquake Resistant Design Buildings. *12th World Conference on Earthquake Engineering, New Zealand , v 2*, 847-855.

Bommer, J. J., and Acevedo, A. B. (2004). The Use of Real Earthquake Accelerograms as Input to Dynamic Analysis . *Journal of Earthquake Engineering (Special Issue 1), v 8*, 43-91.

Bommer, J. J., and Ruggeri, C. (2002). The Specification of Acceleration Time-Histories in Seismic Codes. *Euro Earthquake Engineering , v 16*, 3-16.

Charney, F. (2011). Use of Nonlinear Analysis in the Context of the ASCE 7 Seismic Load Provisions. *Structural Congress 2011* , 782-790.

Gasparini, D. A., and Vanmarcke, E. H. (1976). Simulated Earthquake Motions Compatible with Prescribed Response Spectra [SIMQKE]. *Issue 2 of Evaluation of seismic safety of buidings, Research report, Massachusetts Institute of Technology Dept. of Civil Engineering* .

Gioncu, V., and Mazzolani, F. M. (2002). *Ductility of Seismic Resistant Steel Structure* . London: Spon Press.

Gioncu, V., and Mazzolani, F. M. (2011). *Earthquake Engineering for Structural Design* . London: Spon Press.

Hancock, J., and Bommer, J. J. (2007). Using Spectral Matched Records to Explore the Influence of Strong-Motion Duration on Inelastic Structural Response. *Soil Dynamics and Earthquake Engineering v 27* , 291-299.

Hancock, J., Bommer, J. J., and Stafford, P. J. (2008). Numbers of Scaled and Matched Accelerograms Required for Inelastic Dynamic Analyses. *Earthquake Engineering and Structural Dynamics , v 37,* 1585-1607.

Hancock, J., Watson-Lamprey , J., Abrahamson, N., Bommer , J., Markatis, A., and McCoy, E. (2006). An Improved Method of Matching Response Spectra of Recorder Earthquake Ground Motion Using Wavelets. 5th International Rose-School Seminar, Imperial College Press, 67-89

Heo, Y., Kunnath, S.,and Abrahamson,N.(2011). Amplitude-Scaled versus Spectrum-Matched Ground Motions for Seismic Performance Assessment. *Journal of Structural Engineering, v 137,* 278-288.

Jun, D. H. (2010). Seismic Response of R/C Structures Subjected to Simulated Ground Motions Compatible with Design Spectrum. *The Structural Design of Tall and Special Buildings.* doi: 10.1002/tal.658

Montejo, L. A., and Kowalsky, M. J. (2008). Estimation of Frequency-Depend Strong Motion Duration via Wavelet and its Influence on Nonlinear Seismic Response. *Computer-Aided Civil and Infrastructure Engineering, v 23,* 253-264.

Naeim,F., and Lew, M. (1995). On the Use of Design-Spectrum Compatible Time Histories. *Earthquake Spectra, v 11,* 111-127.

USNRC Regulatory Guide 1.208,"A Performance-Based Approach to Define the Site-Specific Earthquake Ground Motion" Rev. 0, March 2007.

PEER- Pacific Earthquake Engineering Research Center (2012) PEER NGA database. http://peer.berkeley.edu/peer_ground_motion_database. Accessed October 2012

Priestley, M., Calvi, G. M., and Kowalsky, M. J. (2007). *Displacement based seismic design structure.* IUSS Press, Pavia, Italy

Suárez , L. E., and Montejo, L. A. (2005). Generation of Artificial Earthquakes via the Wavelet Transform. *International Journal of Solids and Structures , v 42,* 5905-5919.

Vamvatsikos, D. and Cornell, C;. (2002). Incremental Dynamic Analysis. *Earthquake Engineering and Structural Dynamics, v 32, 491-514* .

Watson-Lamprey , J. A., and Abrahamson, N. A. (2006). Bias Caused by Use of Spectrum Compatible Motions. *8th US National Conference on Earthquake Engineering, San Francisco California,* 8821-8829.

CHAPTER 2

2. Seed records selection, generation and examination of the resulting compatible records

2.1 Introduction

Seismic designed civil structures are expected to resist minor level earthquakes without significant damage as well as major level earthquakes without collapse. While recent advances in finite element modeling allow us to closely track the nonlinear response of a civil structure subjected to seismic accelerations, we still need to specify appropriate input motions to obtain meaningful results. Over the last years seismic instrumentation networks have increased over highly active seismic regions (e.g. Japan, China, and California) rising considerably the number of strong motion records available. Strong motion databases can be searched online in different sites around the world. The sources are rich in information and the search can be performed based on different parameters. For example, mechanism of source, distance to rupture, magnitude and local soil conditions among others parameters. Despite the increase in the number of available strong motion records, artificial spectrum compatible records are still widely used for seismic design/assessment in zones where the number of available records is scarce and/or to reduce the number of analysis required while complying with design codes requirements. Most recent methodologies generate the compatible records from modification of historic (seed) records. This section describes the selection of such seed records, the generation of spectrum

compatible records using three different methodologies and the characteristics of the resulting records.

2.2 Seed records selection

The database used in this study was the Pacific Earthquake Engineering Research Center (PEER) Ground Motion Data Base (PEER 2012). The PEER ground motion database was released in the year 2000 and contains 3,551 three-component records from 173 earthquakes and 1,456 recording stations (PEER Ground Motion Database Technical Report, 2010). The website offers the choice of selecting between scaled earthquakes or non-scaled earthquakes; for effects of this investigation the scaled records option was selected. This option allows you to search for records based on their compatibility with a target response spectrum. The target spectrum used in this particular case was constructed following the provisions in ASCE 7. Since the structure to be analyzed is a typical California bridge bent column, the values of spectral response acceleration at short period (Sds), spectral response acceleration at 1 sec period (Sd1) and long period were set as the maxima occurring in all the state of California according to ASCE 7-10 maps and then modified for type of soil C. These values are presented in Figure 2.2.1 as a recreation of the input window of the website.

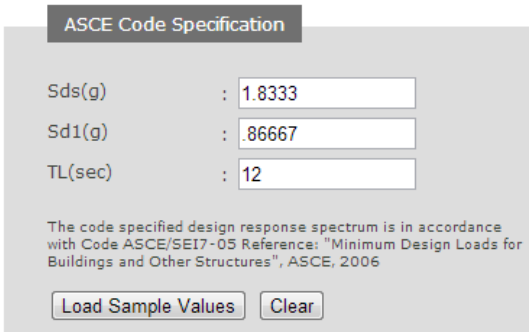

Figure 2.2. 1 Input values for the generation of the target spectrum (PEER Ground Motion Database)

In order to investigate the effect of the initial level of matching of the seed record on the efficiency of the algorithms, two sets of 10 records each were selected. One set contains records whose response spectrum shapes are close to the target spectrum; this set is denoted as the close match records (CM). The other set contains records whose response spectrum shape is distant from the target spectrum; this set is named the distant match records (DM). Records with pulse like characteristics (near source records) were disregarded.

The initial level of matching of the seed records is estimated using the root mean square deviation (D_{rms}) between the spectral amplitudes (Equation 2.1). Note that since the selection is made based on the overall spectral shape resemblance, the seed records are multiplied by a scale factor *a* (Equation 2.2) to reduce the spectral amplitude misfit (Beyer and Boomer, 2007). A limit value of 8 for the scale factor was set in the selection of the CM records; no scale factor limit was set for the DM records. The period range used to examine the level of matching in the response spectra was [0.2 – 4] seconds. The period range used to generate the compatible records was [0.02- 4] seconds.

$$D_{rms} = \sqrt{\frac{1}{N}\sum_{i=1}^{N}\left(aS_{\alpha R}(T_i) - S_{\alpha T}(T_i)\right)^2} \qquad (2.1)$$

where:

N= number of periods at which the spectral shape is specified,

a = scale factor,

$S_{\alpha R}$= spectral acceleration of the record at period T_i , and

$S_{\alpha T}$ = target spectral acceleration at period T_i.

$$a = \sum_{i=1}^{N} \frac{S_{\alpha T}(T_i)}{S_{\alpha R}(T_i)} \qquad (2.2)$$

A summary of the two set of records is presented in Tables 2.1 and 2.2. Besides the earthquakes general information, the table contains the Joyner-Boore distance (Rjb), which is defined as the shortest distance from a site to the surface projection of the rupture depth, and the average shear- wave velocity in the firts 30 meters depth (Vs30). It is seen that the average root mean square deviation for the DM records is more than twice the deviation calculated for the CM records. The response spectra for the scaled seed records are presented in Figures 2.2.2 and 2.2.3 along with the target spectrum. As expected, the CM records response spectra seem to be in closer agreement with the target spectrum than the DM records.

Table 2. 1. Close match records

Record ID	*Magnitude/Year and Historical Earthquake*	*dt (s)*	*Drms*	*a*	*Mechanism*	*Rjb (km)*	*Vs 30 (m/s)*
CM1	M. 6.54 1987 Superstation Hills	0.01	0.164	6.8	Strike-Slip	17	208.7
CM2	M. 6.53 1979 Imperial Valley	0.01	0.271	3.2	Strike-Slip	22	274.5
CM3	M. 6.93 1989 Loma Prieta 1	0.005	0.285	5.8	Reverse-Oblique	39.7	284.8
CM4	M. 6.8 1976 Gazli	0.005	0.334	1.3	Unknown	3.9	659.6
CM5	M. 7.28 1992 Landers	0.005	0.358	7.3	Strike-Slip	27	345.4
CM6	M. 6.2 1999 Chichi-Taiwan 04	0.005	0.37	4.6	Strike-Slip	21.6	258.9
CM7	M. 7.62 1999 Chichi-Taiwan 01	0.005	0.392	2.5	Reverse-Oblique	Unknown	680
CM8	M. 6.93 1989 Loma Prieta 2	0.005	0.393	7.3	Reverse-Oblique	39.3	367.6
CM9	M. 6.2 1999 Chichi-Taiwan 03	0.005	0.394	4.5	Reverse	18.1	475.5
CM10	M. 6.69 1994 Northridge	0.01	0.421	7.6	Reverse	25.6	405.2
Minimum			***0.164***	***1.3***			
Maximum			***0.421***	***7.6***			
Average			***0.338***	***5.1***			

Table 2. 2 Distant match records

Record ID	*Magnitude/ Year/ Historical Earthquake*	*dt (sec)*	*Drms*	*a*	*Mechanism*	*Rjb (km)*	*Vs 30 (m/s)*
DM1	M. 6.69 1994 Northridge 02	0.01	0.451	4.3	Reverse	15.1	1222.5
DM2	M. 6.69 1994 Northridge 01	0.005	0.536	1.5	Reverse	21.2	1015.9
DM3	M. 5.74 1979 Coyote Lake	0.005	0.776	5.0	Strike-Slip	10.2	1428
DM4	M. 6.93 1989 Loma Prieta 2	0.005	0.794	10.7	Reverse-Oblique	76	1249.9
DM5	M. 6.19 1984 Morgan Hill	0.005	0.821	6.5	Strike-Slip	14.9	1428
DM6	M. 6.3 1999 Chichi-Taiwan 06	0.004	0.821	19.3	Reverse	52.3	1528.8
DM7	M. 6.93 1989 Loma Prieta 1	0.005	0.848	8.1	Reverse-Oblique	83.4	1315.9
DM8	M. 7.62 1999 Chichi-Taiwan 03	0.004	0.853	5.0	Reverse-Oblique	52.5	1525.8
DM9	M. 7.62 1999 Chichi-Taiwan 02	0.004	0.994	15.1	Reverse-Oblique	117.3	1022.8
DM10	M. 7.62 1999 Chichi-Taiwan 01	0.005	1.053	21.8	Reverse-Oblique	120.8	1023.5
Minimum			***0.451***	***1.5***			
Maximum			***1.053***	***21.8***			
Average			***0.795***	***9.7***			

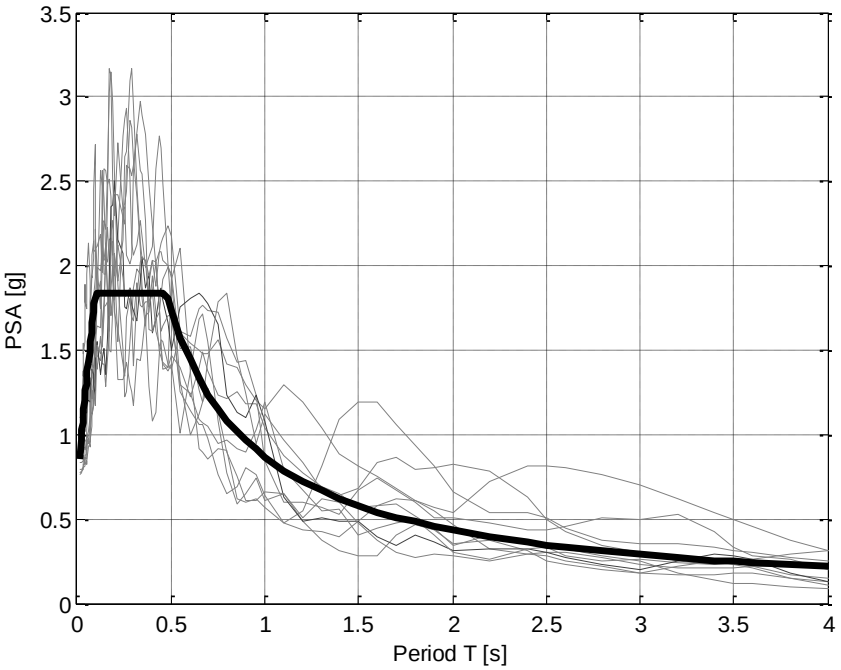

Figure 2.2.2. Design spectrum and scaled CM records response spectra

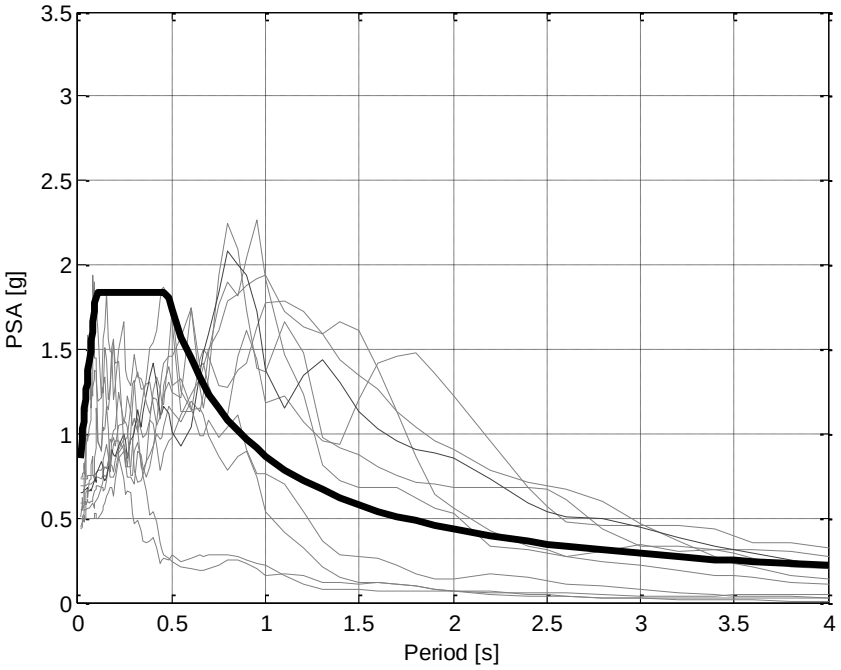

Figure 2.2.3. Design spectrum and scaled DM records response spectra

2.3 Generation of artificial earthquakes

There are different methodologies used to generate spectrum compatible records; three of them are evaluated in this report: (1) time domain adjustment by adding wavelets to the original time history (as implemented by the program *SeismoMatch*), (2) adjustment of the wavelet coefficients via Continuous Wavelet Transform CWT (as implemented by the program *ArtifQuakeLet II*), and (3) frequency domain modification of an initial random process (as implemented by the program *SeismoArtif*).

2.3.1 SeismoMatch:

The first approach used to generated artificial earthquakes was SeismoMatch. This application, developed by the Italian company Seismosoft, is capable of adjusting any earthquake accelerograms to match a specific target response spectrum. The program implements the algorithms proposed by Abrahamson (1992) and later improved by Hancock et al. (2006). The essence of the methodology is described in Hancock et al. (2006) as follows:

> (1) Calculate the response of an elastic SDOF system under the action of the acceleration time-series for each period and damping level to be matched.
>
> (2) Compare the peak of each SDOF response with the target amplitude and determine the mismatch.
>
> (3) Add wavelets to the acceleration time-series with the appropriate amplitudes and phasing so that the peak of each response matches the target amplitude. One wavelet is used to match one SDOF response. Each wavelet is applied to the time series so that the

time of maximum SDOF response under the action of the wavelet is the same as the time of peak response to be adjusted from the unadjusted acceleration time-series.

Note that a fundamental assumption of the method is that the time of the peak response does not change as a result of adding the wavelet adjustment. The records generated by this approach and their response spectra are presented in Figure 2.3.1 and Figure 2.3.2 for the CM and DM records, respectively. Figure 2.3.3 and Figure 2.3.4 shows the comparison of the times histories of acceleration, velocity and displacement between the seed record and the compatible record for the CM1 and the DM4 cases, respectively. The complete time histories comparison can be seen in Appendix A.1 for the close match (CM) and Appendix A.2 for the distant match (DM) records.

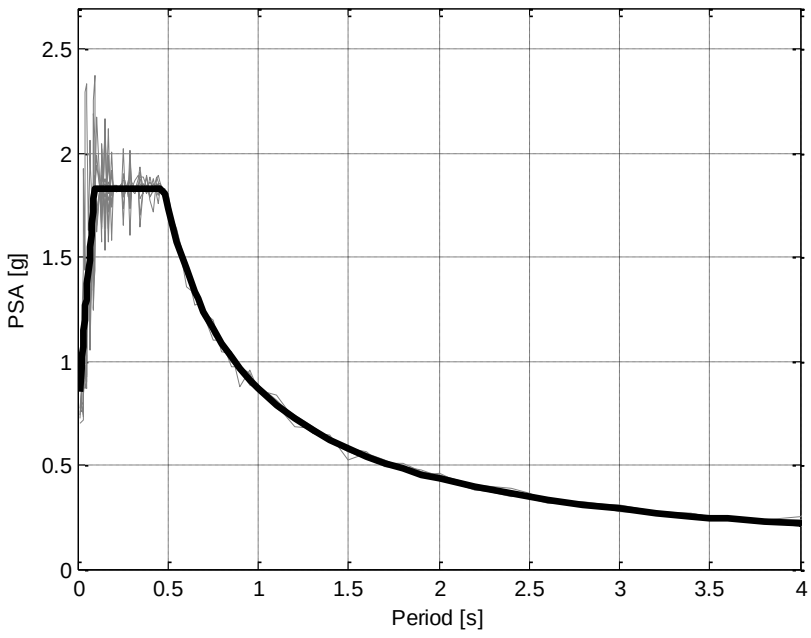

Figure 2.3.1 Design spectrum and SeismoMatch CM compatible records spectra

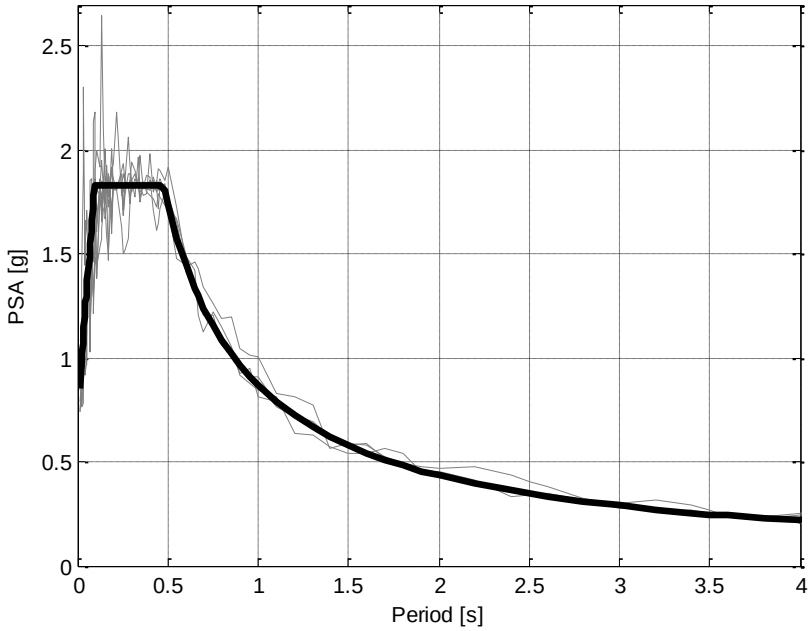

Figure 2.3.2. Design spectrum and SeismoMatch DM compatible records spectra

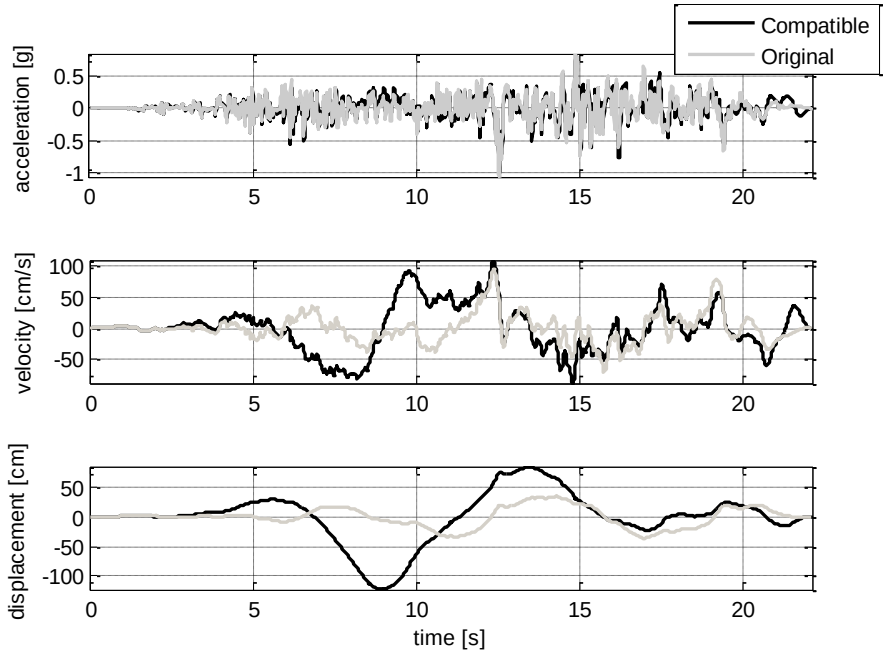

Figure 2.3.3. Time histories of acceleration, velocity and displacement for the scaled record CM1 and the compatible record generated by SeismoMatch

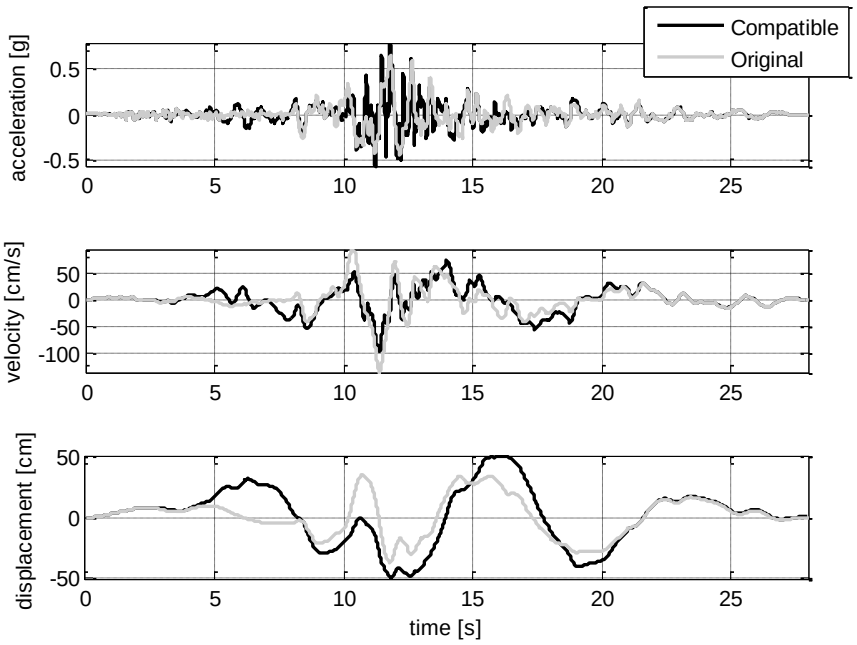

Figure 2.3.4. Time histories of acceleration, velocity and displacement for the scaled seed record DM4 and the compatible earthquake record generated by SeismoMatch

2.3.2 ArtifQuakeLet II:

This code implements a Continuous Wavelet Transform (CWT) based approach to generate spectrum compatible records from the manipulation in the time-frequency domain of a seed record. The algorithm first decomposes the original record in detail functions (i.e. functions with a very dominant frequency and modulated amplitude), the signal is reconstructed using an iterative procedure that independently scale the detail functions to obtain an average match with the target spectrum (Suárez and Montejo, 2005). This approach has been used with success in the past but it has the drawback of the large amount of time that takes the algorithm to run. To improve the process, the ArtifQuakeLet II program computes the wavelet decomposition and constructs the detail functions using a fast convolution implementation by means of the Fast Fourier Transform (FFT) (Montejo and Suárez, 2013). The results obtained are presented in

Figure 2.3.5 and Figure 2.3.6. Just like the Wavelets based method (SeismoMatch), the CWT based method (ArtifQuakeLet II) needs a seed record in order to generate the compatible earthquake record. A graphic comparison between the time histories of acceleration, velocity and displacement of the scaled seed record and the artificial record can be seen in Figure 2.3.7 and Figure 2.3.8 for the CM1 and DM4 cases, respectively. Appendix A.3 and A.4 shows the time histories comparison for the remaining cases.

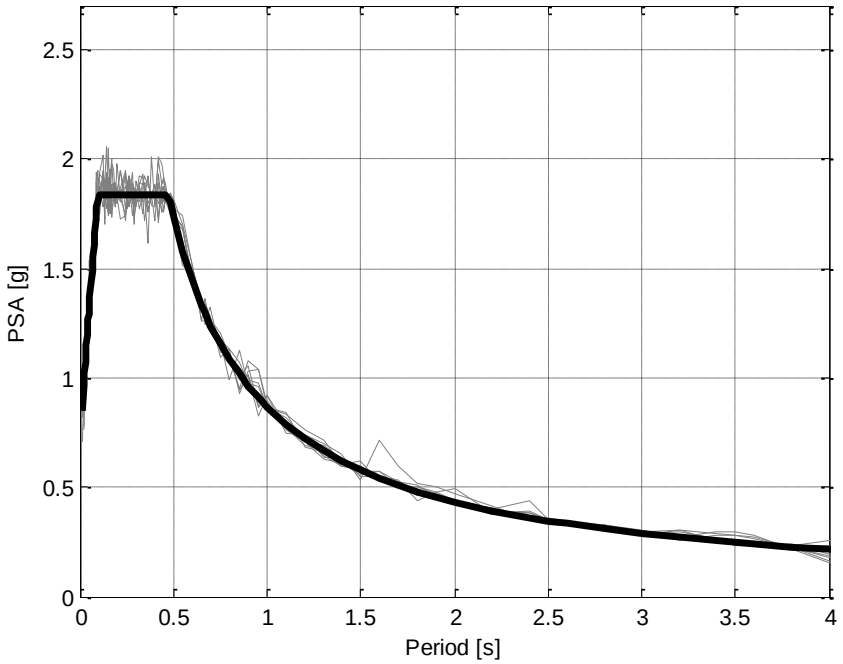

Figure 2.3.5 Design spectrum and ArtifQuakeLet II CM compatible records spectra

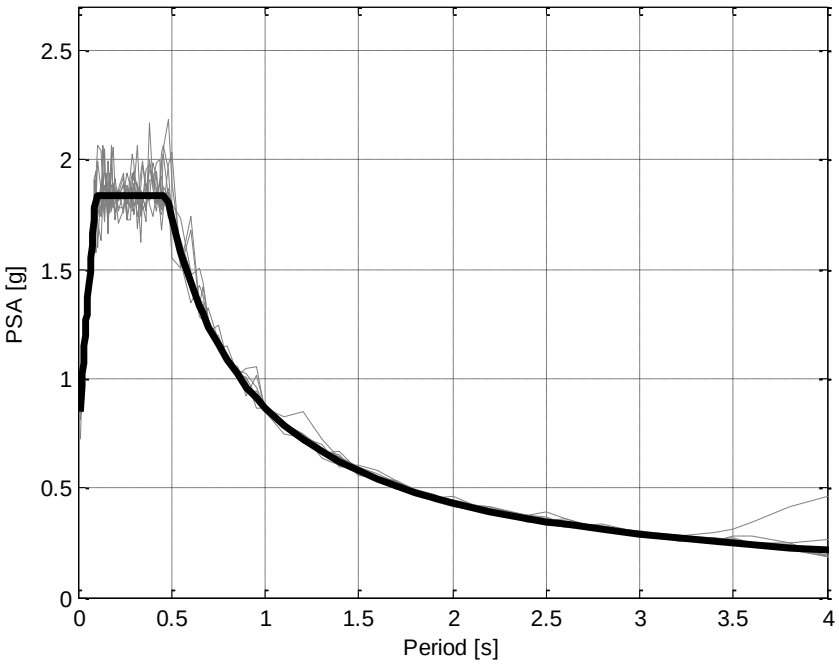

Figure 2.3.6. Design spectrum and ArtifQuakeLet II DM compatible records spectra

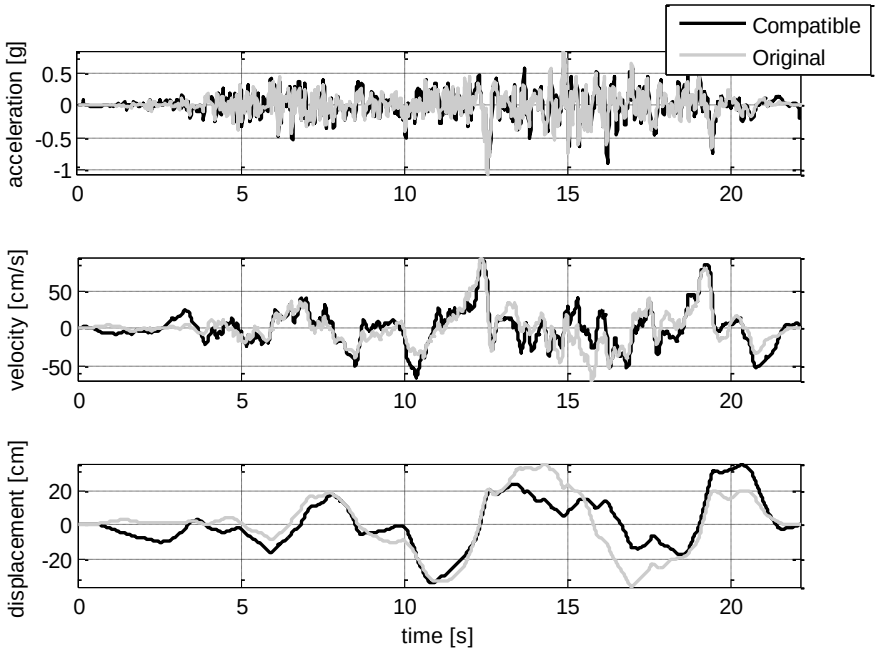

Figure 2.3.7. Time histories of acceleration, velocity and displacement for the scaled seed record CM1 and the compatible earthquake record generated by ArtifQuakeLet II

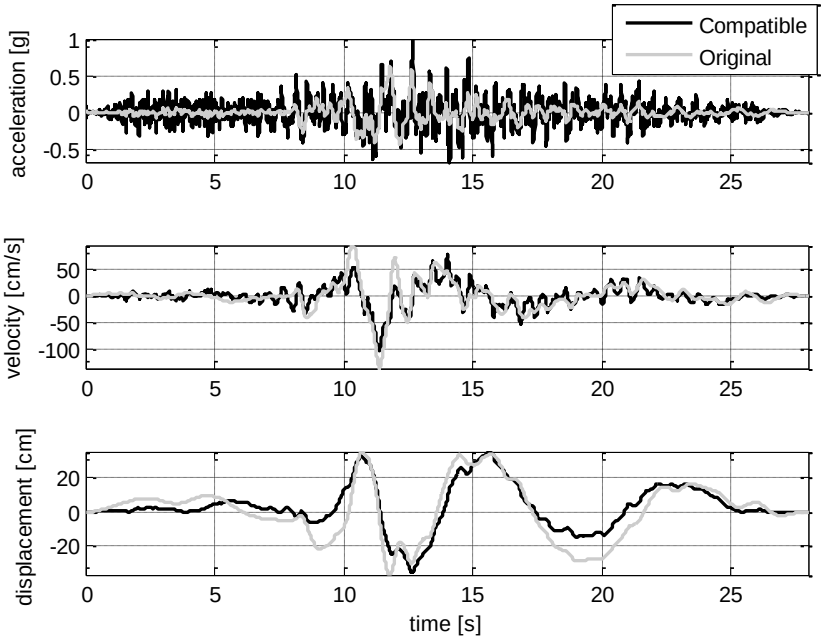

Figure 2.3.8. Time histories of acceleration, velocity and displacement for the scaled seed record DM4 and the compatible earthquake record generated by ArtifQuakeLet II

2.3.3 SeismoArtif:

This program is an application capable of generating artificial earthquake accelerograms matched to a specific target response spectrum using different calculation methods and varied assumptions. The method of calculation selected was the "artificial accelerogram generation and adjustment"; this option can be considered as an evolved version of the popular SIMQKE program by Gasparini and Vanmarcke (1976). The algorithm starts by defining a random process with an amplitude envelope applied in the time domain (a trapezoidal window was selected for all the records generated) and the frequency content is modified using the Fourier Transform. Note that in this approach there is no need for a seed record. A total of 10 compatible records were generated with total durations between 10 and 100 seconds. Figure 2.3.9 presents the spectra of the generated records as well as the target spectrum. The time histories of acceleration,

velocity and displacement for the 50 seconds artificial record is illustrated in Figure 2.3.10 and the complete overview of the times histories can be seen in Appendix A5.

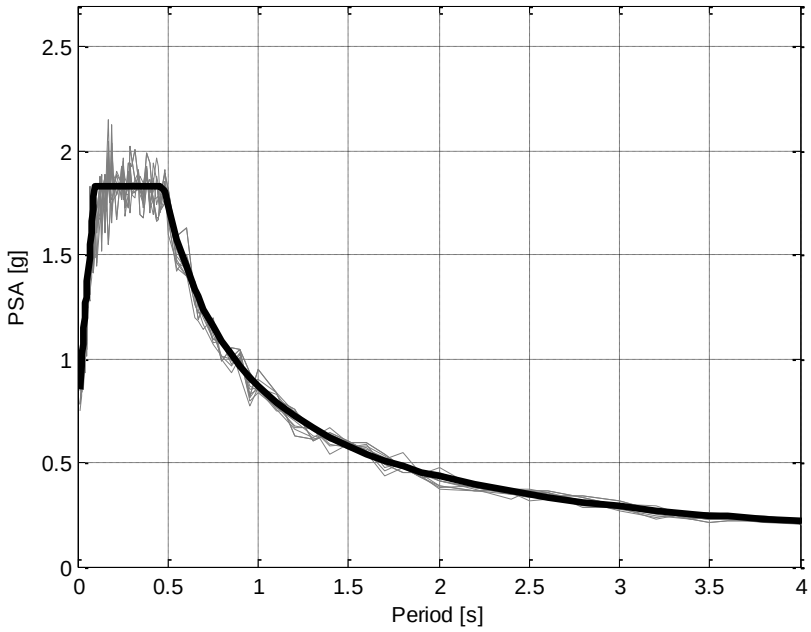

Figure 2.3.9. Design spectrum and SeismoArtif match compatible spectra records

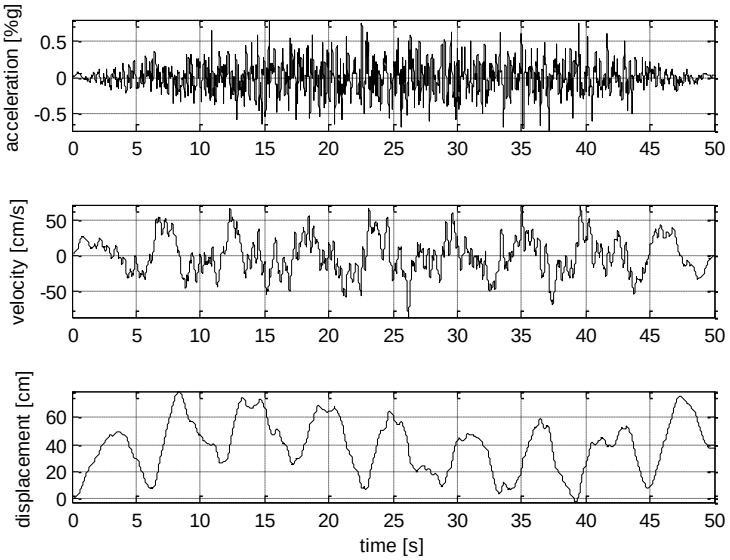

Figure 2.3.10. Time histories of acceleration, velocity and displacement of the 50 seconds artificial earthquake record generated by SeismoArtif

2.3.4 Preliminary observations:

All three methodologies evaluated were able to generate earthquakes records whose response spectra matches closely the target spectrum. Figure 2.3.11 summarizes the mean square root deviations for all the 50 compatible records generated (5 groups of 10). It is seen that the SeismoArtif records exhibit the smallest average spectral amplitude deviation from the target spectrum, followed by the ArtifQuakeLet and SeismoMatch records, respectively. Nevertheless, the SeismoArtif records also exhibited the most unrealistic velocity and displacement time histories (see for example Figure 2.3.10 and Appendix A5).

Looking only at the goodness of the match obtained, the initial level of match of the seed record doesn't seem to play an important role on the generation of compatible records using the

Wavelet (SeismoMatch) or CWT (ArtifQuakeLet II) approaches. The next section presents a more detailed analysis of the characteristic of the resulting compatible records.

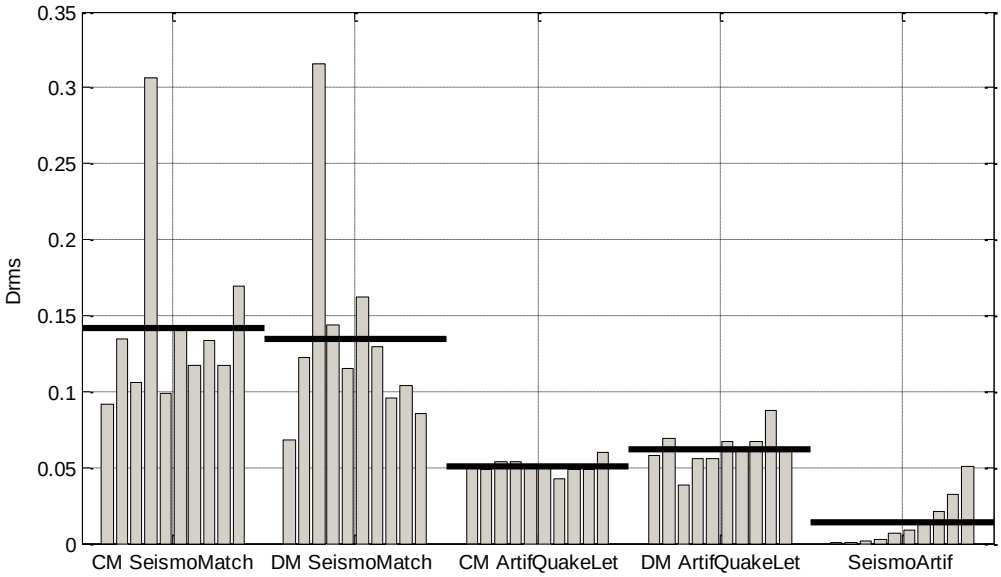

Figure 2.3.11. Goodness of match

2.4 Examination of the resulting compatible records

The results presented in the previous section demonstrated that any of the three methodologies being evaluated is capable of generating records with a response spectrum that closely matches a target spectrum. This section presents a detailed examination of the resulting compatible records. Chapter 3 examines the effect of such records on the nonlinear seismic response of a civil structure. In the case of the methodologies that use seed records, focus is placed on how well the characteristics of the original seed record are retained in the compatible record. The characteristics/parameters being examined are peak ground acceleration (PGA), peak ground velocity (PGV), peak ground displacement (PGD), Arias intensity (AI), significant duration

(SD), cumulative absolute velocity (CAV), mean period (Tm), and frequency content via Fourier spectra and Wavelet Maps.

2.4.1 Peak ground acceleration (PGA):

PGA is defined as the maximum absolute acceleration registered, or in terms of the response spectrum, the spectral amplitude at a period of zero. PGA is usually the principal parameter associated with the severity of the earthquake. Figure 2.4.1 shows a bar graph with the PGA values of the scaled seed records and the artificial records generated by the SeismoMatch and the ArtifQuakeLet II methodologies for the CM records. It is seen that the values are very close between each other. The largest difference between a seed record and an artificial record was 0.25 g (CM3). For the DM case, Figure 2.4.2, the values are not as similar to the scaled seed records. The artificial records generated by the SeismoMatch approach exhibit the larger PGA values as well as the largest gaps when compared with the scaled seed records. The PGA values for the SeismoArtif method are presented in Figure 2.4.3 and all ten ground movements shows a PGA value between 0.8 g and 1.0 g. Finally, Figure 2.4.4 summarizes the PGAs for all the 50 compatibles records. The dashed horizontal lines represent the PGA value of the target spectrum. Recall that the matching was specified in the period range of [0.02 -4] seconds, therefore the PGA values of the compatible records are not necessarily expected to match the target spectrum PGA. It can be seen from Figure 2.4.4 that the majority of the generated records exceed that value, however; the DM cases and SeismoArtif shows the largest disparity.

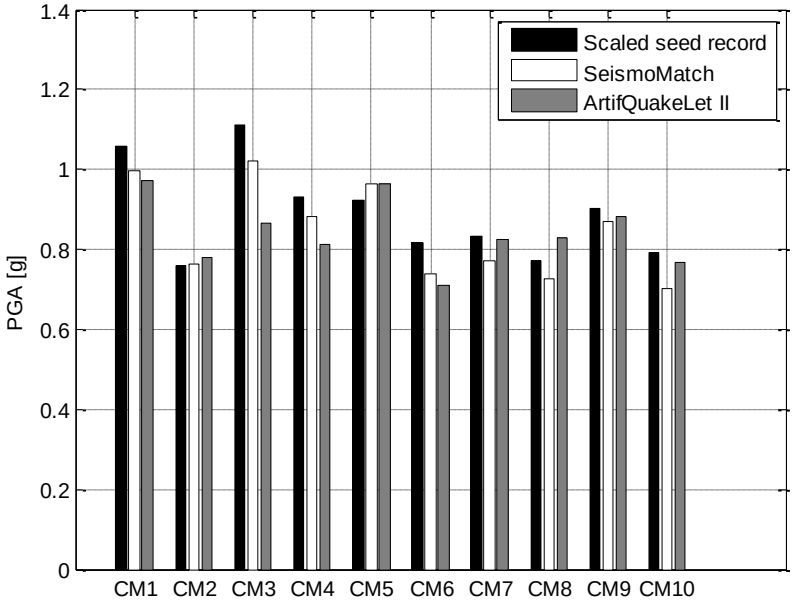

Figure 2.4.1 PGA values for the scaled CM seed records and the artificial records

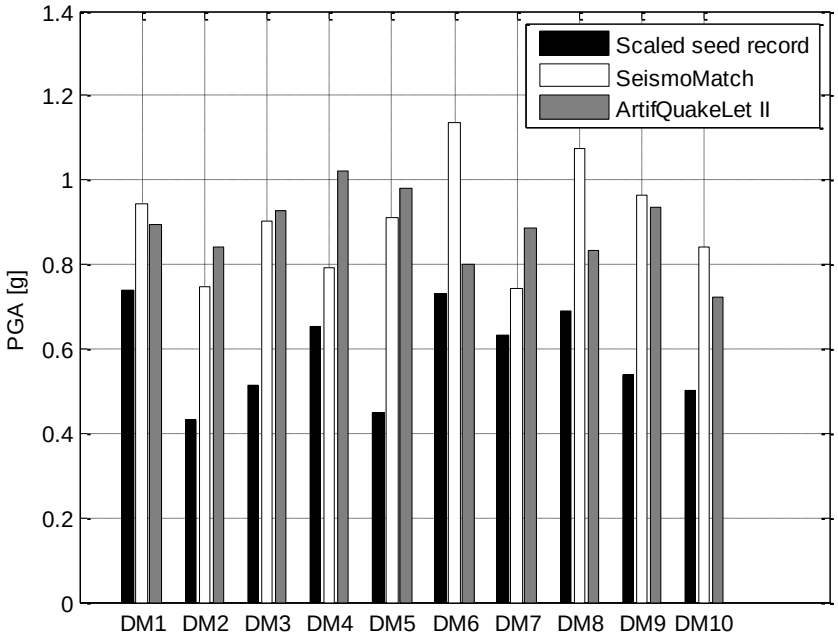

Figure 2.4.2. PGA values for the scaled DM seed records and the artificial records

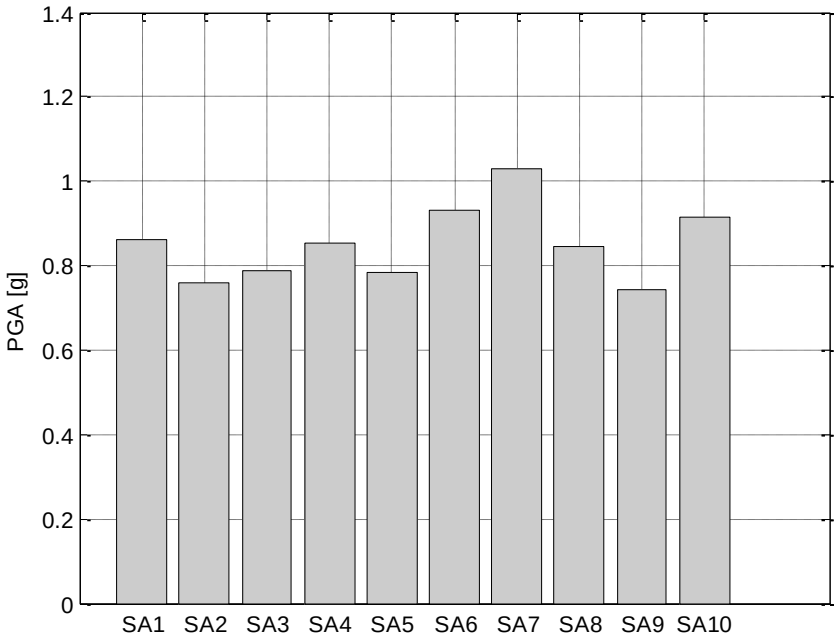

Figure 2.4.3. PGA values for SeismoArtif records

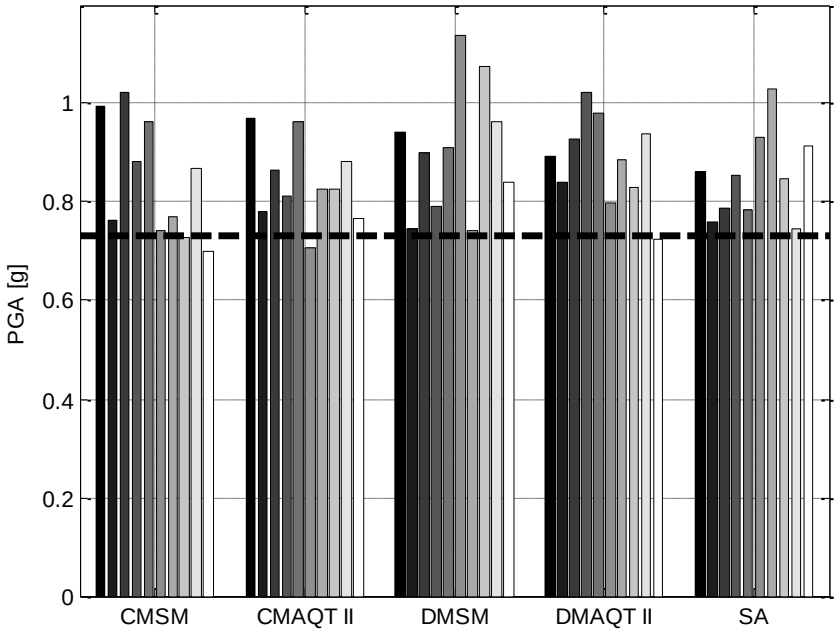

Figure 2.4.4. Compatible records and target spectrum PGAs

2.4.2 Peak ground velocity (PGV):

Another parameter that can provide useful information is the peak ground velocity (PGV). Some authors argue that the PGV provides significant better correlations with seismic demand than other simple instrumental ground motion intensity measures such as the PGA (Bradley, 2012). Figure 2.4.5 and Figure 2.4.6 present the values of PGV for the close match and the distant match records respectively. As for the PGA, it is seen that PGV values are better preserved for the CM cases. PGV values for all the records, including the SeismoArtif earthquakes are illustrated in Figure 2.4.7. It seen from this figure that the records with the largest PGV are those generated with the SeismoMatch approach and for the DM case.

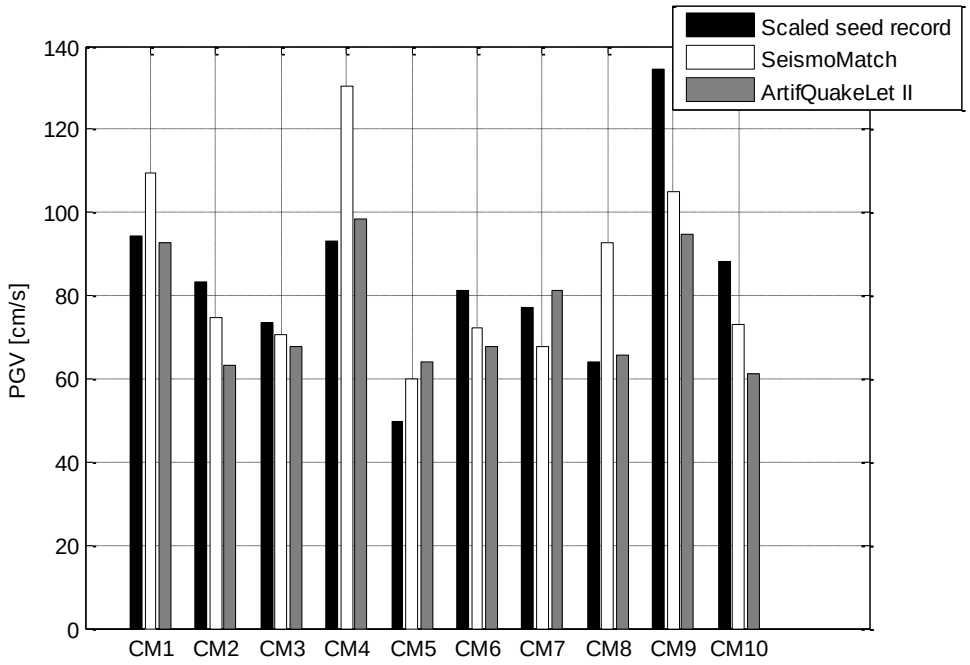

Figure 2.4. 5. PGV values for the scaled CM seed records and the artificial records

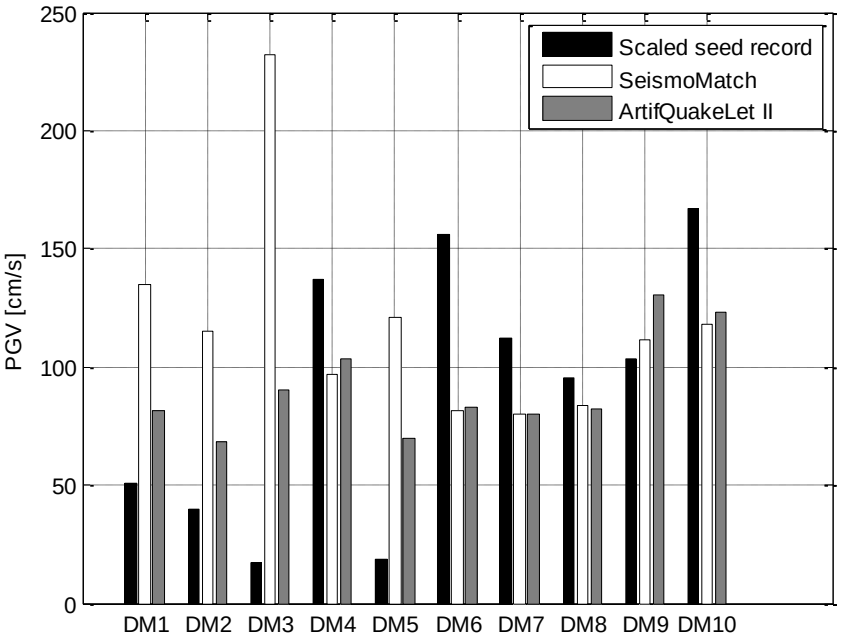

Figure 2.4.6. PGV values for the scaled DM seed records and the artificial records

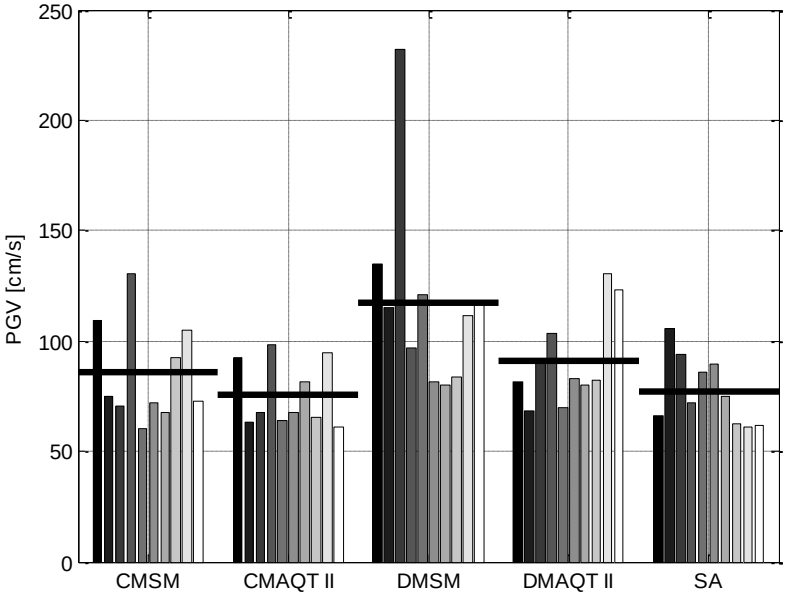

Figure 2.4.7. PGV values for all the generated records

2.4.3 Peak ground displacement (PGD):

From all three peak parameters, the highest variability between the seed records and the artificial earthquakes was observed in the peak ground displacement parameter. As it can be seen in Figure 2.4.8 (CM case) and Figure 2.4.9 (DM case) the difference is very notable, especially in the distant match case. Figure 2.4.10 summarizes the PGD values for all 50 records: it is seen that in some cases the values obtained are quite unrealistic. Because of the difficulty in obtaining a reliable PGD value from the strong motions records due to its sensitivity to low-cut filtering, the value has limited use in most of the fields of the earthquakes engineering. In artificial records, any alteration to the acceleration time series has the potential to severely corrupt the displacement history due to the double integration scheme involved. Nevertheless, the PGD value helps to constrain the long period response spectral displacement (Douglas, 2012).

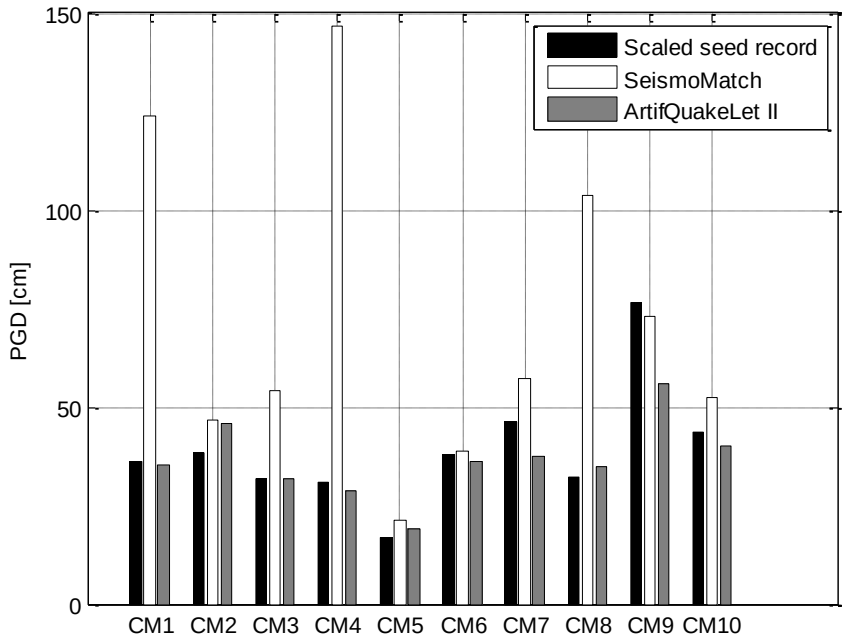

Figure 2.4.8. PGD values for the scaled CM seed records and the artificial records

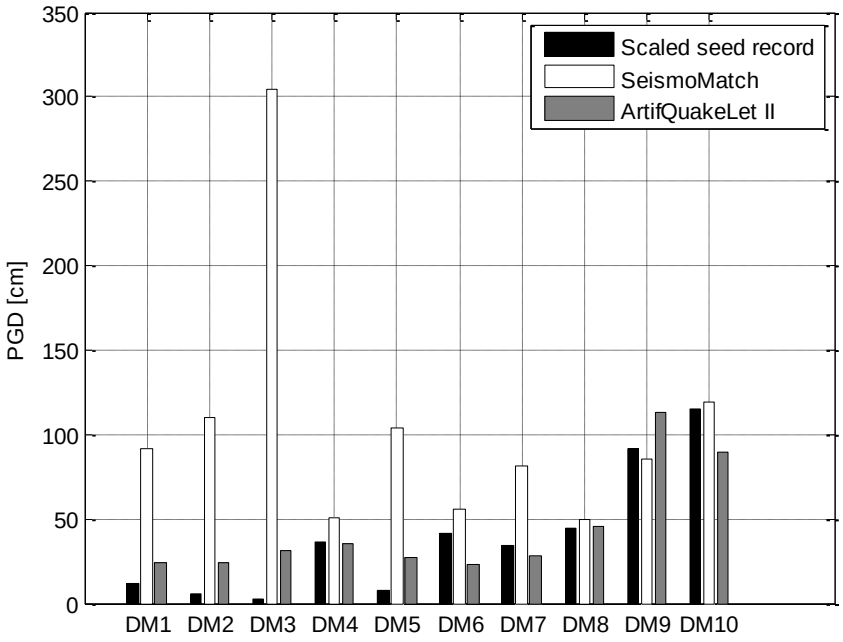

Figure 2.4. 9. PGD values for the scaled DM seed records and the artificial records

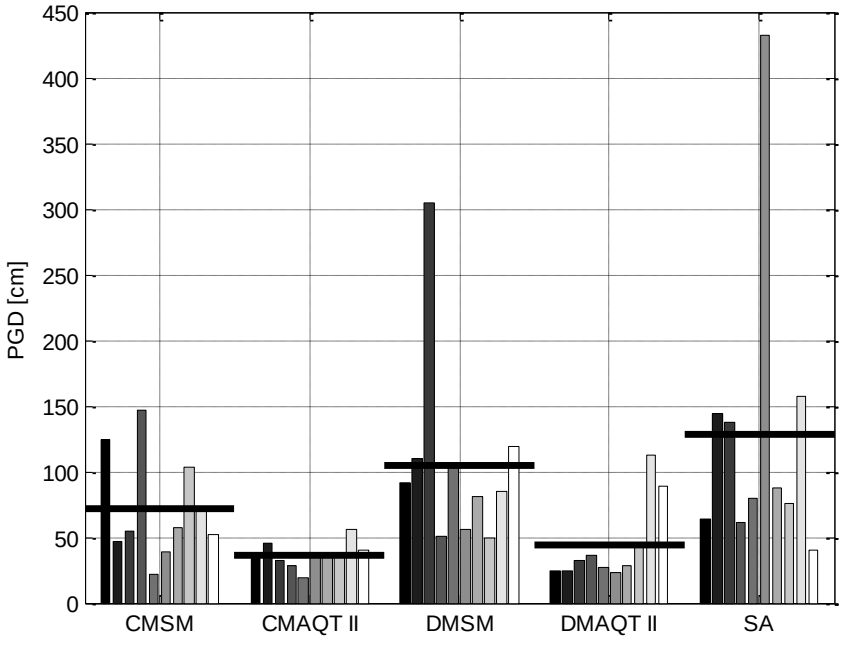

Figure 2.4.10. PGD values for all the generated records

2.4.4 Arias intensity (AI) and significant duration (SD):

The Arias intensity is a quantitative measure of earthquake shaking intensity and was presented by Arturo Arias in 1970 (Arias, 1970). It is defined as the square of the acceleration integrated over the duration of the motion (Equation 2.3) and has been used by several researchers to evaluate the earthquake records damage potential.

$$AI = \frac{\pi}{2g}\int_0^{\infty} a(t)^2 dt \qquad (2.3)$$

where;

g = is the acceleration of gravity

a(t) = acceleration time history

This value can be graphically represented in a Husid Plot, i.e. a plot that shows how the integral in Equation 2.3 is accumulating with time. The AI can be used, as a measure of the energy content of the motion, and it is a reliable parameter in assessing liquefaction potential (Kayen and Mitchell, 1997). The fact that it is independent of the fundamental period of the structural systems increase its applicability over a wide range of problems encountered in engineering practice, including the dynamic response of structures (Travasarou et al; 2003). Moreover, the Arias Intensity is fundamental in the calculation of the significant duration of the earthquake record. The significant duration is defined as the time interval across which a specified amount of energy is dissipated. A common measure of significant duration is the time interval between 5 and 95% of the total Arias intensity accumulated. An example of the Husid

plot and a graphical representation of the significant duration are presented in Figure 2.4.11 for the scaled record and compatible record corresponding to the CM4 case. The horizontal hatched lines denote the value of the 5% and 95% of the Arias intensity; the time difference between the 5% and 95% defines the significant duration of the record. Arias intensities and significant duration (SD) values are summarized in Tables 2.3, 2.4 and 2.5 as well in Figures 2.4.12 through 2.4.15. Husid plots for all the compatibles records are presented in Appendix B. It seen that AIs and SDs of the seed records are better preserved by SeismoMatch, this is particularly evident for the DM records where the ArtifQuakeLet II records exhibit AI and SD values much larger than the observed in the seed records. When the AI's for all the 50 compatible records are compared Figure 2.4.16 it is noticed that the SeismoArtif records reveal values that are unreasonable high.

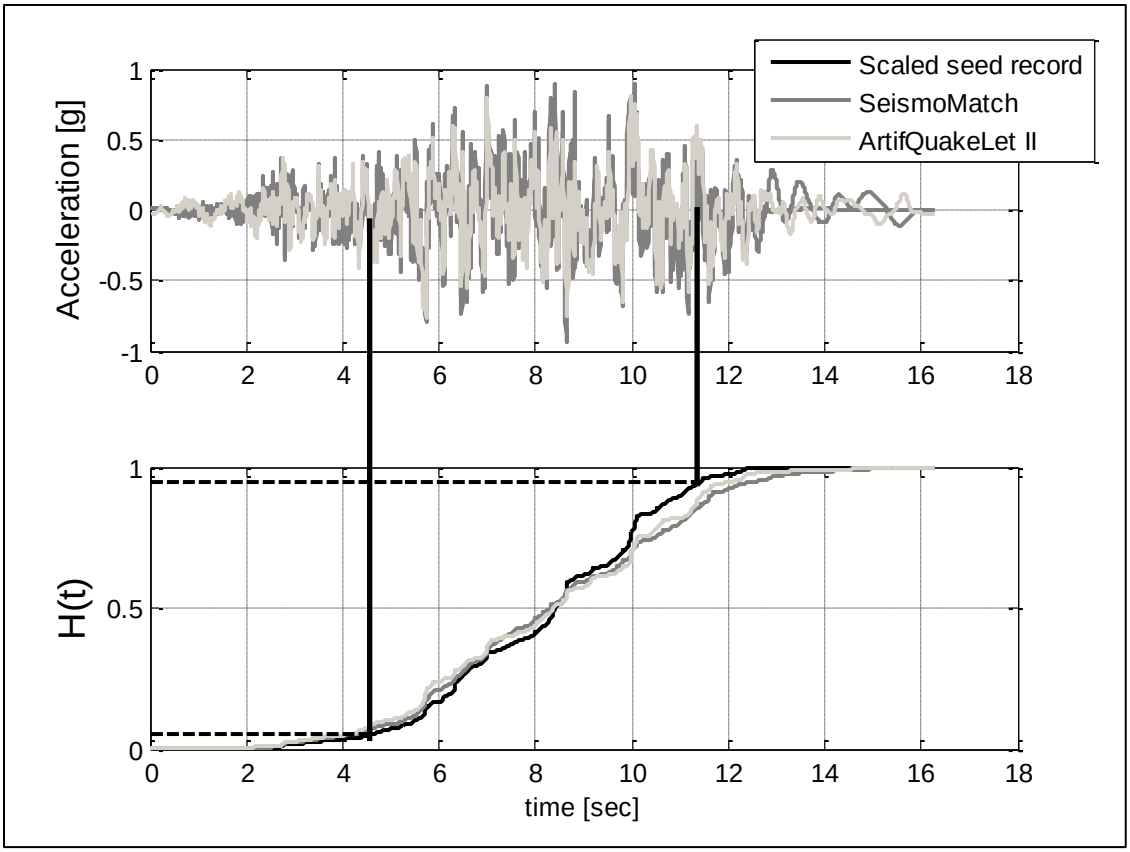

Figure 2.4.11. Husid plot and graphical representation of the significant duration (SD)

Table 2.3. Arias intensity and significant duration for the close match records

Earthquake Label	*Arias intensity [cm/s]*			*Significant duration [sec]*		
	Original	*SeismoMatch*	*ArtifQuakeLet II*	*Original*	*SeismoMatch*	*ArtifQuakeLet II*
CM1	1031.49	1066.94	1198.21	13.53	13.51	14.14
CM2	2454.80	2924.03	2498.79	51.05	59.23	65.18
CM3	1044.73	990.05	1428.75	17.24	18.45	21.40
CM4	844.45	1209.29	992.58	6.84	8.51	8.05
CM5	1927.50	2078.97	2555.38	34.62	36.06	37.87
CM6	831.95	760.16	1124.32	15.51	17.23	22.90
CM7	1875.58	1612.71	2059.66	24.12	24.69	25.11
CM8	1344.79	1268.73	1421.10	16.71	18.21	25.58
CM9	704.76	592.49	847.78	9.26	11.09	17.46
CM10	1302.31	1149.37	1579.27	20.78	21.28	24.22

Table 2.4. Arias intensity and significant duration for the distant match records

Earthquake Label	*Arias intensity [cm/s]*			*Significant duration [sec]*		
	Original	*SeismoMatch*	*ArtifQuakeLet II*	*Original*	*SeismoMatch*	*ArtifQuakeLet II*
DM1	371.59	573.68	878.16	6.67	7.42	11.17
DM2	341.54	617.23	1167.22	8.91	9.16	19.43
DM3	160.08	945.52	618.15	7.31	8.39	8.52
DM4	592.63	567.76	1316.68	9.71	10.87	17.24
DM5	223.32	775.98	1018.42	9.56	9.13	13.58
DM6	649.04	441.34	1784.82	11.64	16.30	22.42
DM7	671.34	562.05	1244.20	8.36	9.87	24.34
DM8	623.13	477.22	2104.12	13.80	22.29	35.24
DM9	791.29	776.32	2122.86	19.29	21.28	31.34
DM10	989.09	797.67	2070.49	23.40	25.34	29.73

Table 2.5. Arias intensity and significant duration for the SeismoArtif records

Earthquake Label	*Arias Intensity [cm/s]*	*Significant Duration [sec]*
SA1	965.80	9.55
SA2	1310.60	14.15
SA3	1859.82	20.43
SA4	2007.29	26.54
SA5	2672.17	33.71
SA6	2845.17	37.65
SA7	3128.22	44.55
SA8	3489.52	49.25
SA9	4183.93	56.89
SA10	4777.60	63.80

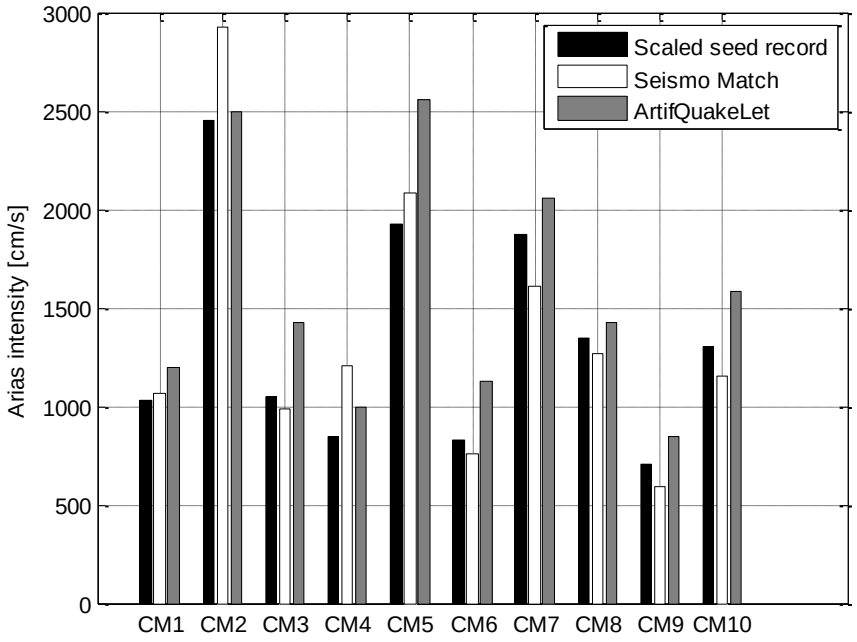

Figure 2.4.12. Arias intensity values for the scaled CM seed records and the artificial records

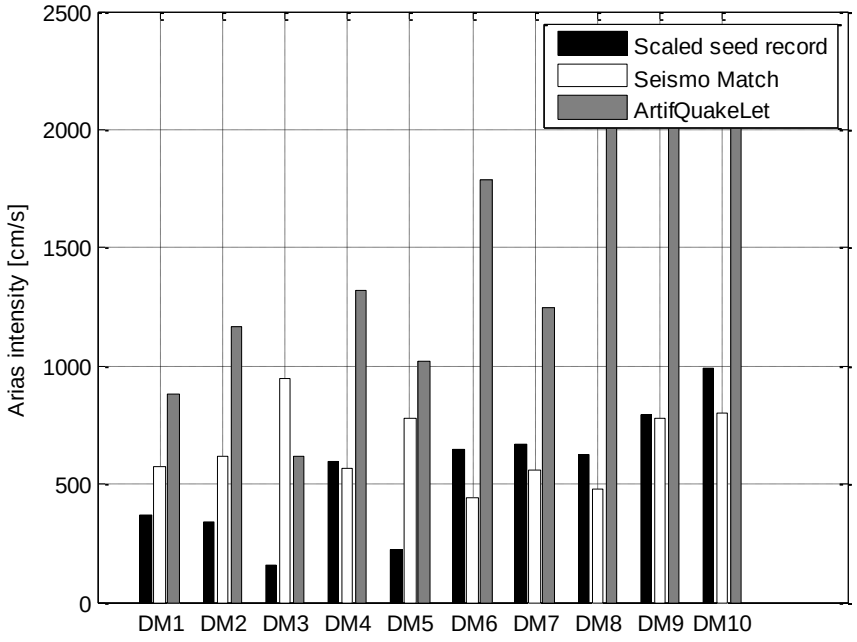

Figure 2.4.13 Arias intensity values for the scaled DM seed records and the artificial records

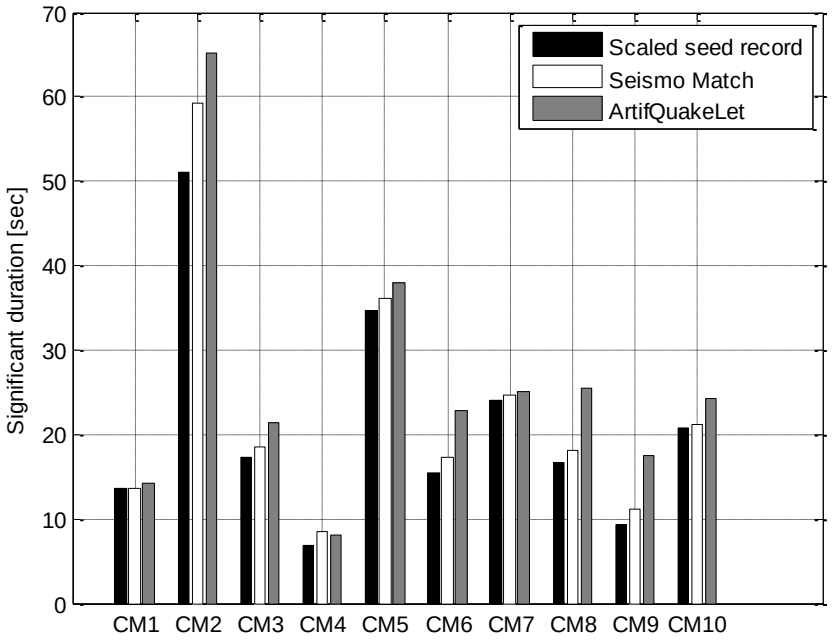

Figure 2.4.14. Significant duration values for the scaled CM seed records and the artificial records

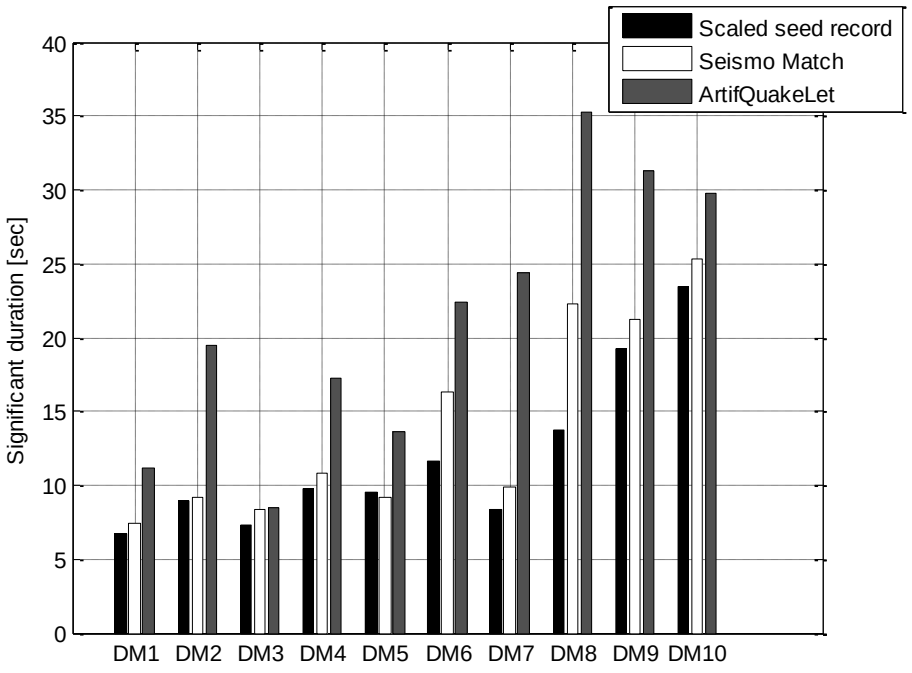

Figure 2.4.15. Significant duration values for the scaled DM seed records and the artificial records

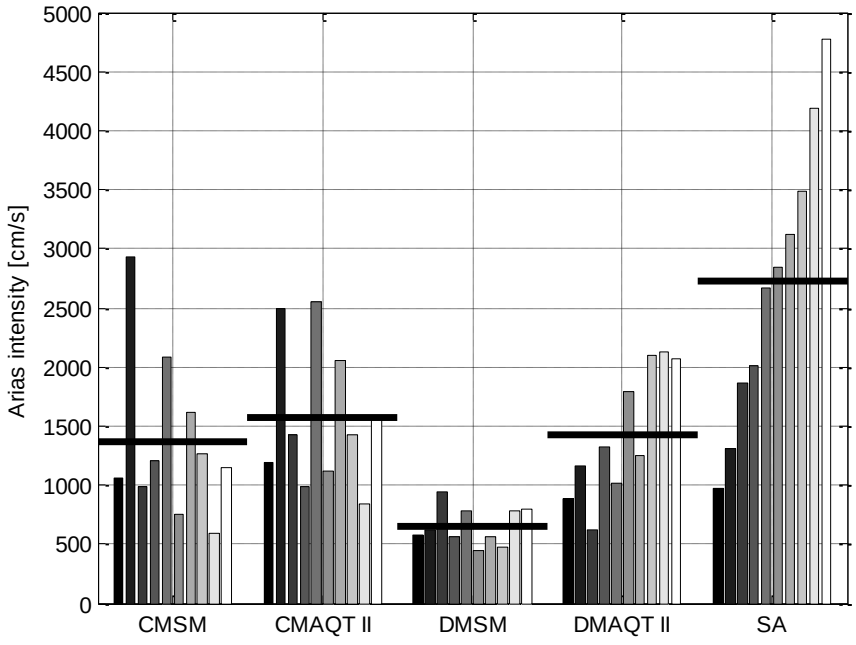

Figure 2.4.16. Arias Intensity values for all the compatible records

2.4.5 Cumulative absolute velocity (CAV):

Defined as the integral of the absolute value of the acceleration time series, CAV offers some advantages over peaks ground motions and response spectral parameters, because it includes the cumulative effects of the ground motions duration (Campbell and Bozorgnia, 2010). The CAV was initially proposed by the Electrical Power Research Institute (EPRI) in 1998 as an index to indicate the beginning of structural damage to engineered structures. Since then, several variants of the CAV have been proposed. According to the United States Nuclear Regulatory Commission (U.S. NRC), CAV was determined to be the best parameter correlating damage with the Modified Mercalli Intensity Scale, (NRC, 2007). There are several approaches proposed to calculate CAV for the purpose of this work the values of CAV are calculated based on the original definition. The CAV values for all the matches can be seen in Tables 2.6, 2.7 and 2.8 as

well in Figures 2.4.17 and 2.4.18. The results obtained are similar to the behavior observed for the AI; the CAVs of the seed records are better preserved by SeismoMatch and this is more notorious for the DM records where the ArtifQuakeLet II records exhibit CAV values much larger than those observed in the seed records. When the CAVs for all the 50 compatible records are compared (Figure 2.4.19), it is noticed that the ArtifQuakeLet records reveal values that are unreasonable high.

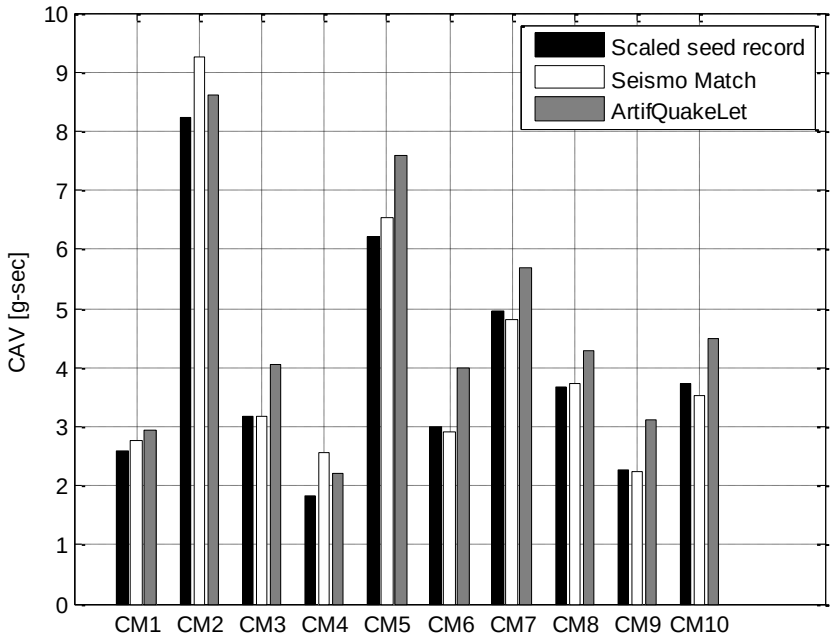

Figure 2.4.17. CAV values for the scaled CM seed records and the artificial records

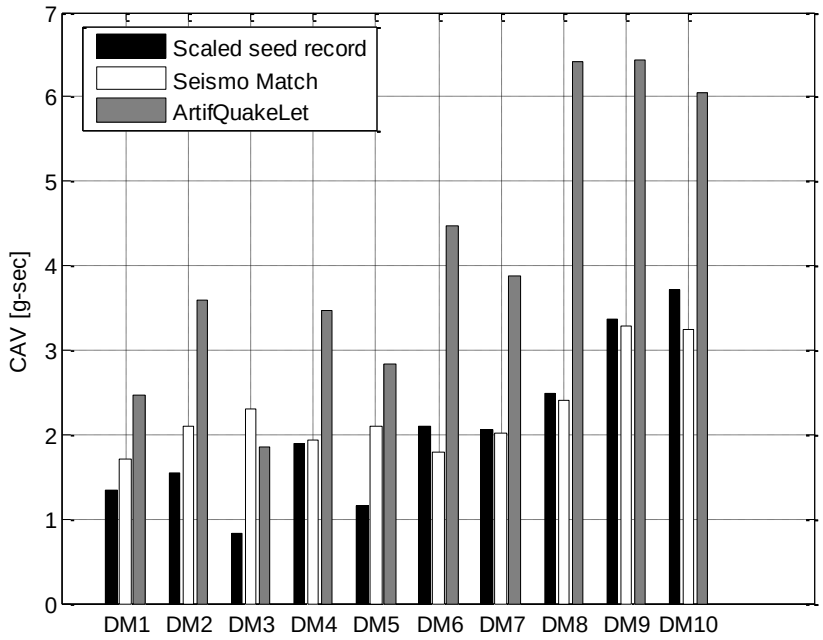

Figure 2.4.18. CAV values for the scaled DM seed records and the artificial records

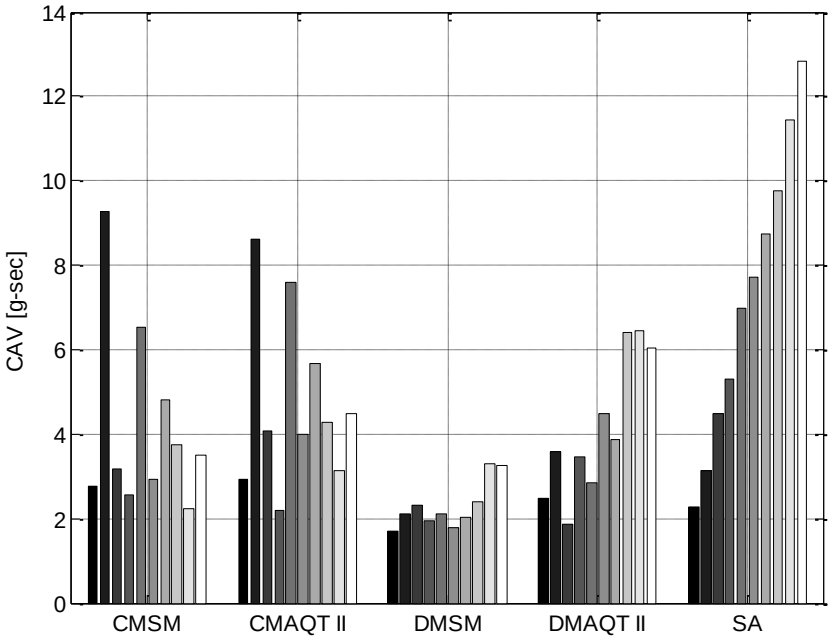

Figure 2.4.19. CAV values for the compatible records

Table 2.6. Cumulative absolute velocity (CAV) values for the close match records

Earthquake Label	*CAV [g-sec]*		
	Original	*SeismoMatch*	*ArtifQuakeLet II*
CM1	2.600	2.762	2.924
CM2	8.231	9.255	8.617
CM3	3.182	3.181	4.064
CM4	1.835	2.553	2.199
CM5	6.216	6.534	7.576
CM6	2.987	2.915	3.980
CM7	4.963	4.823	5.688
CM8	3.675	3.729	4.281
CM9	2.267	2.227	3.119
CM10	3.737	3.515	4.475

Table 2.7. Cumulative absolute velocity (CAV) values for the distant match records

Earthquake Label	*CAV [g-sec]*		
	Original	*SeismoMatch*	*ArtifQuakeLet II*
DM1	1.344	1.708	2.457
DM2	1.539	2.089	3.598
DM3	0.839	2.303	1.846
DM4	1.889	1.927	3.470
DM5	1.157	2.102	2.840
DM6	2.099	1.793	4.467
DM7	2.061	2.023	3.876
DM8	2.478	2.397	6.407
DM9	3.372	3.294	6.433
DM10	3.709	3.248	6.050

Table 2.8. SeismoArtif cumulative absolute velocity (CAV) values

Earthquake Label	*CAV [g-sec]*
SA1	2.278
SA2	3.135
SA3	4.490
SA4	5.300
SA5	6.967
SA6	7.708
SA7	8.745
SA8	9.752
SA9	11.446
SA10	12.823

2.4.6 Measures of frequency content:

The frequency content of an earthquake is a very useful and common parameter for structural earthquake engineering as it can largely influence the response of a civil structure. Historically the amplitude Fourier spectrum (or the Power spectrum), has been the principal tool to gather frequency content information from an earthquake record. A single parameter that can be used to represent the frequency content of a ground motions is the mean period (T_m). It represents the inverse of the mean frequency of a Fourier amplitude spectrum:

$$T_m = \frac{\sum C_i^2 / f_i}{\sum C_i^2} \tag{2.4}$$

where:

C_i = are the Fourier amplitudes at f_i frequencies between 0.25 and 20 Hz.

Mean period values are summarized in Tables 2.9 thought 2.11 and in Figure 2.4.20 and Figure 2.4.21. In terms of preserving the seed records original mean periods, the best results are obtained for the SeismoMatch CM records (Figure 2.4.20). For the DM records the mean periods from the compatible records differ largely when compared to the scaled records value (Figure 2.4.21). In the SeismoArtif records it is noticed that the mean period values are quite similar along all the 10 records (~0.46 seconds). This tendency may be undesirable when selecting records for structural analysis as all the records may tend to excite the same frequency (modes) of the structures.

The frequency content of the records is also analyzed using the traditional Fourier amplitude spectra and Wavelet maps via CWT, so that not only the frequency content is evaluated but also its evolution in time. The CWT was calculated using the complex Morlet wavelet, with bandwidth parameter (*fb)* and central frequency parameter (*fc*) of 2. An example of the results is presented in Figure 2.4.22 through Figure 2.4.28. The first three figures (Figures 2.4.22, 2.4.23 and 2.4.24) show the results for CM1 and present the Fourier spectra and wavelet maps for the scaled seed record, the SeismoMatch artificial record and the ArtifQuakeLet II artificial record, respectively. It is seen that most of the non-stationary characteristics of the records are retained, i.e. the dominant frequencies remain approximately the same (Fourier spectra) and are occurring at about the same times (Wavelet map) for the original and compatible records. Similar results were obtained for the other CM records (see Appendix C).

Figures 2.4.25 through 2.4.27 present the results obtained for the DM4 records. It is seen that the non-stationary characteristics are not retained. Moreover, both methodologies are adding

high frequencies to the original seed record. In the case of SeismoMatch such frequencies are concentrated over the strong motion part of the record, in the ArtifQuakeLet II record the added high frequencies content seems to be distributed over the total duration of the record. Similar results were obtained for all the DM records (see Appendix C). Hence, as it was shown with the mean period and reaffirmed with the Fourier spectrum and wavelet map, the distant match records are not close to the seeds records in terms of frequency content.

Finally, Figure 2.4.28 shows the same analysis for the SeismoArtif record of duration 50 seconds. It is seen that the non-stationary characteristics of this record are not realistic, with most of the dominant frequencies occurring over the total duration of the record. Similar results were obtained for the other 9 SeismoArtif records (see Appendix C).

Table 2.9. Mean period values for the close match records

Earthquake Label	***Mean Period Tm [sec]***		
	Original	***SeismoMatch***	***ArtifQuakeLet II***
CM1	0.438	0.482	0.505
CM2	0.625	0.553	0.544
CM3	0.560	0.597	0.520
CM4	0.398	0.412	0.463
CM5	0.385	0.462	0.485
CM6	0.655	0.548	0.483
CM7	0.464	0.505	0.461
CM8	0.434	0.521	0.575
CM9	1.025	0.624	0.493
CM10	0.731	0.616	0.551

Table 2.10. Mean period values for the distant match records

Earthquake Label	*Mean Period Tm [sec]*		
	Original	*SeismoMatch*	*ArtifQuakeLet II*
DM1	0.456	0.540	0.563
DM2	0.431	0.604	0.527
DM3	0.194	0.572	0.569
DM4	1.059	0.655	0.422
DM5	0.213	0.545	0.552
DM6	1.248	0.802	0.389
DM7	1.093	0.728	0.466
DM8	1.100	0.897	0.372
DM9	0.970	0.745	0.410
DM10	1.375	0.763	0.395

Table 2.11. SeismoArtif mean period values

Earthquake Label	*Mean Period Tm [sec]*
SA1	0.481
SA2	0.486
SA3	0.434
SA4	0.450
SA5	0.453
SA6	0.460
SA7	0.470
SA8	0.457
SA9	0.433
SA10	0.422

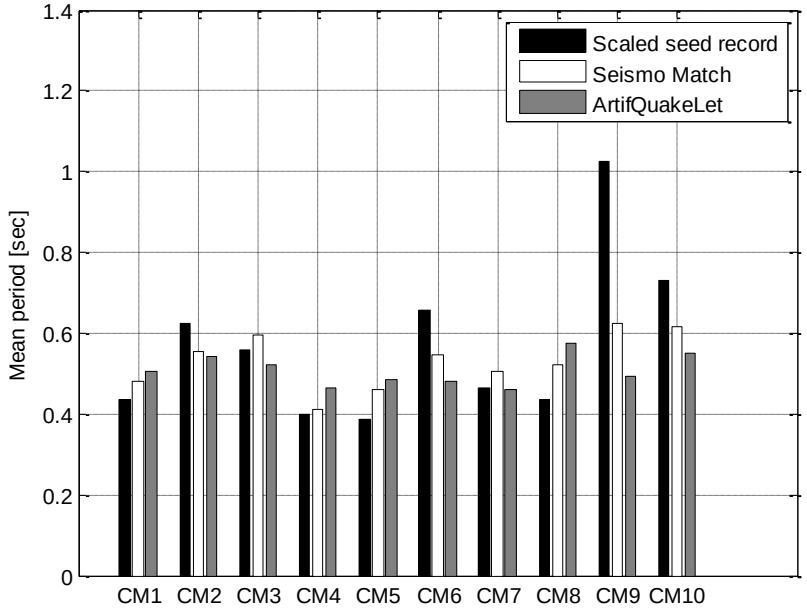

Figure 2.4.20. Mean period (Tm) values for the scaled CM seed records and the artificial records

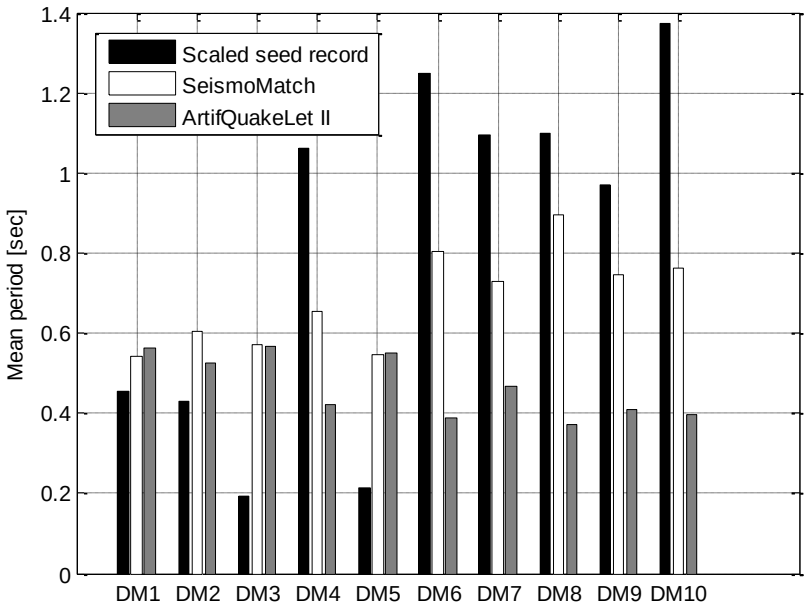

Figure 2.4.21. Mean period (Tm) values for the scaled DM seed records and the artificial records

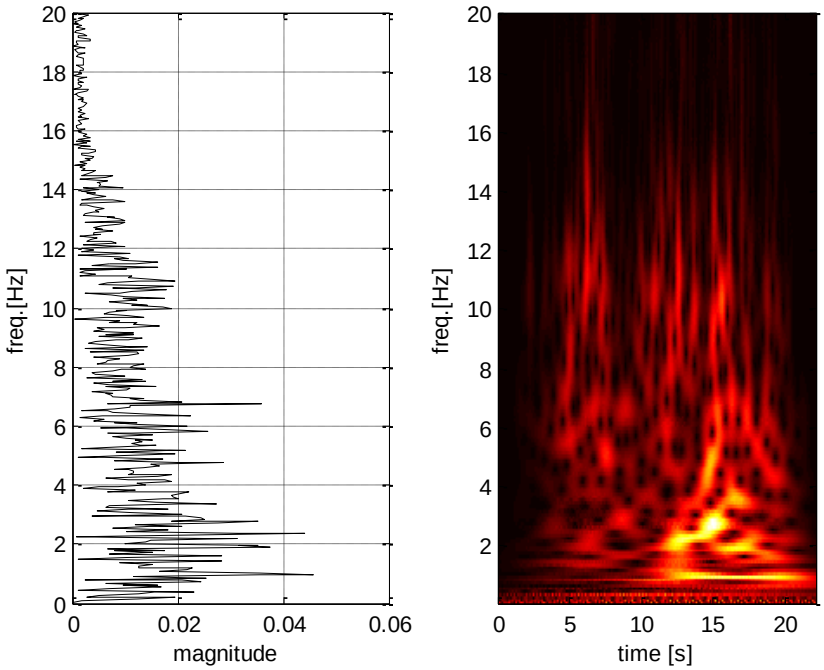

Figure 2.4.22. Fourier spectrum and wavelet map for the scaled seed record (CM1)

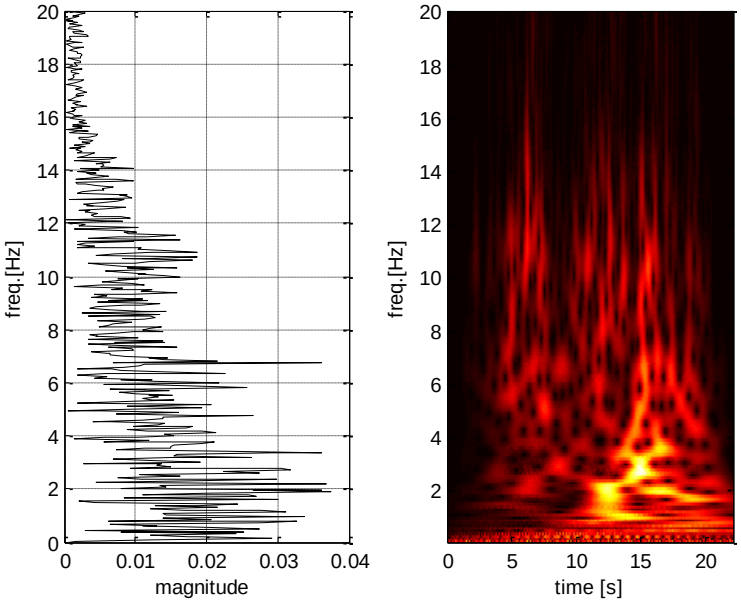

Figure 2.4. 23. Fourier spectrum and wavelet map for the SeismoMatch artificial record (CM1)

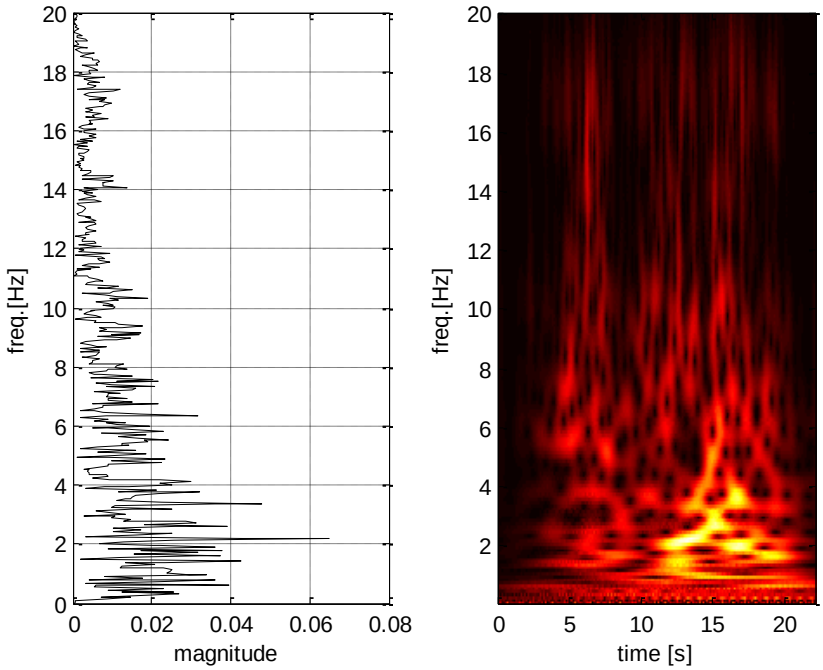

Figure 2.4.24. Fourier spectrum and wavelet map for the ArtifQuakeLet II artificial record (CM1)

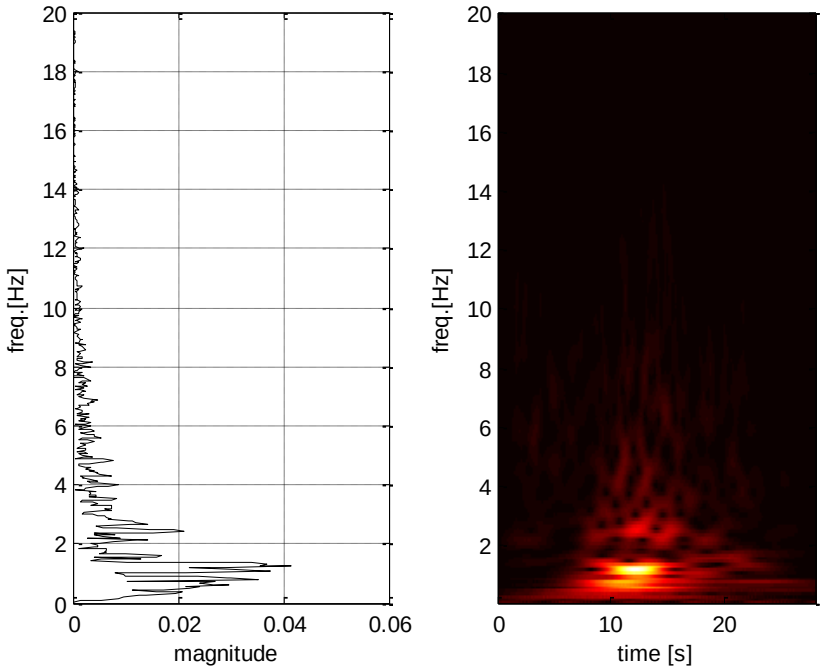

Figure 2.4. 25. Fourier spectrum and wavelet map for the scaled seed record (DM4)

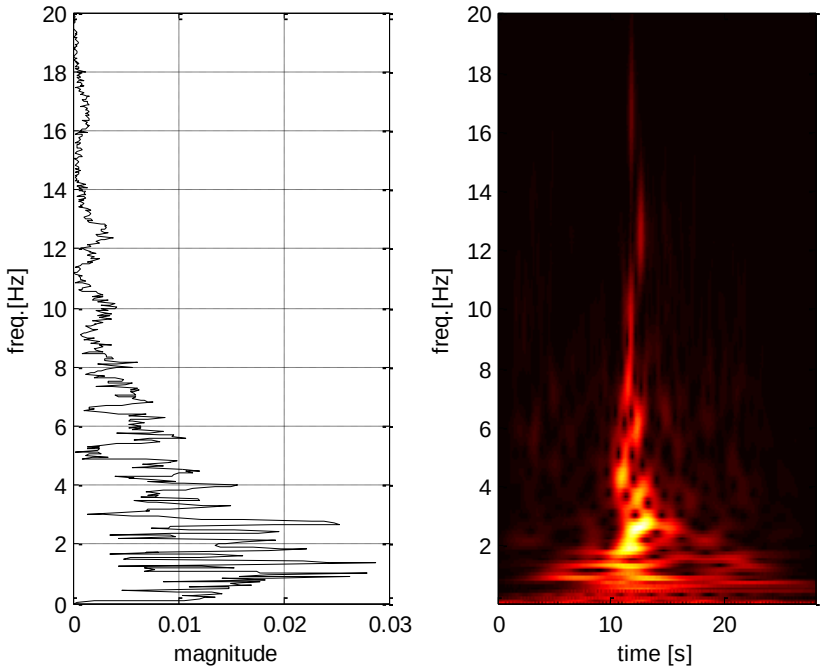

Figure 2.4.26. Fourier spectrum and wavelet map for the SeismoMatch artificial record (DM4)

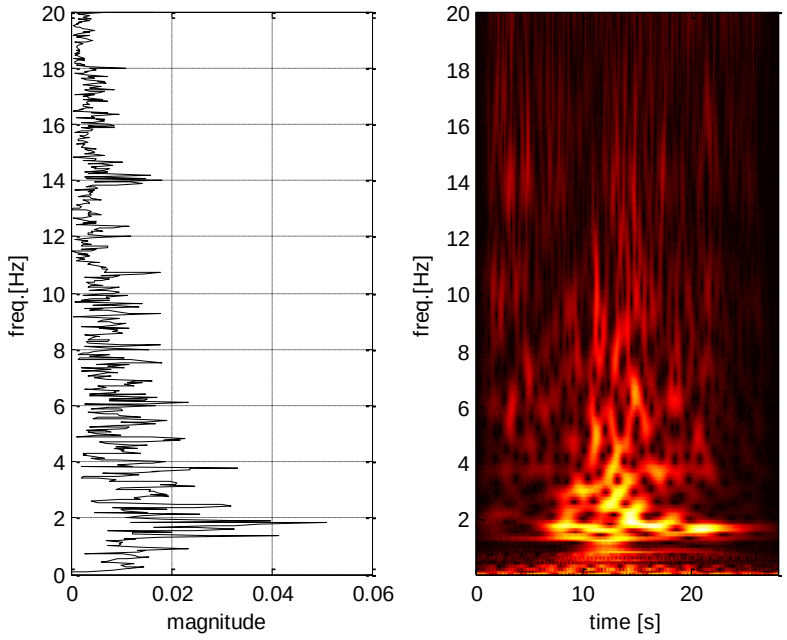

Figure 2.4. 27. Fourier spectrum and wavelet map for the ArtifQuakeLet II artificial record (DM4)

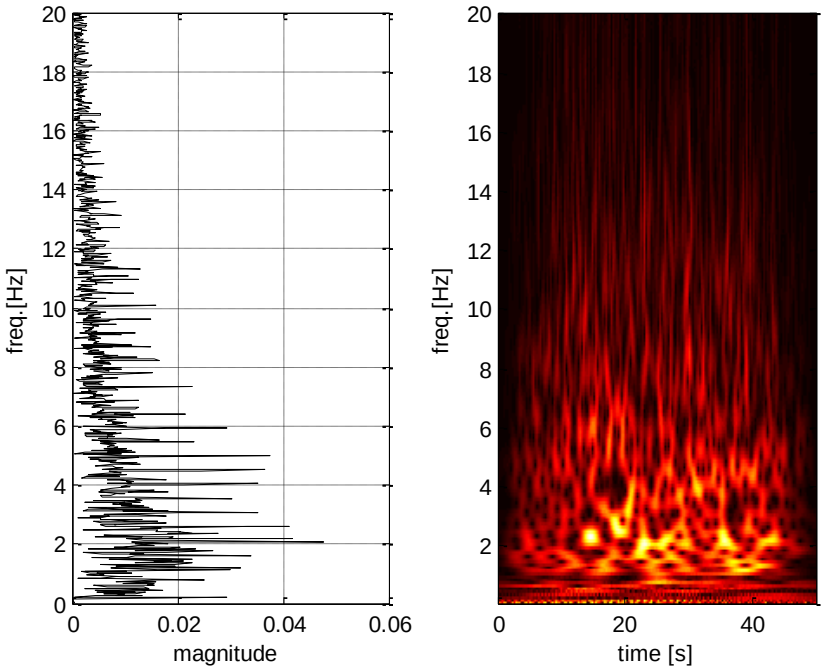

Figure 2.4.28. Fourier spectrum and wavelet map for the SeismoArtif artificial record (SA5)

2.5 Conclusions

Three different methodologies to generate artificial earthquake records compatibles with a design spectrum were evaluated. The main findings are summarized as follows:

- In general, all three methodologies were successful generating acceleration time series with a response spectrum that matches a prescribed design spectrum. The compatible records with the best matching were those generated using a frequency domain approach (SeismoArtif), followed by the CWT based approach (ArtifQuakeLet II) and the Wavelets approach (SeismoMatch), respectively. These results were somehow expected as the frequency domain approach starts from a white noise signal (i.e. frequency content in the whole frequency

range) while the other two methodologies start from an actual earthquake record (i.e. limited frequency content to work with).

- For the methodologies working with seed records it was found that the initial level of match of the record does not significantly affect the level of matching that can be attained for the final compatible record. However, the characteristics of the seed records are better preserved in the compatible records when the initial spectral match is close.
- When working with CM records there is no significant difference between the results obtained for the CWT and the Wavelets based approaches. However, when initial match is distant (DM records), the Wavelet approach tend to preserve better the transient characteristic of the seed record than the CWT approach. Nevertheless, the CWT records exhibited better behaved velocities and displacements time histories.
- Finally, while the frequency domain approach (SeismoArtif) generated the records with better match, the characteristics of such records were quite unrealistic. That is, extremely high energy content and strong motion duration, weird behaved velocities and displacement series, inappropriate frequency content and stationary characteristics.

2.6 References

Abrahamson, N.A. (1992). "Non-Stationary Spectral Matching". *Seismological Research Letters*, v63, 30.

Arias, A. (1970). "A Measure of Earthquake Intensity". *Seismic Design for Nuclear Power Plant*s, MIT Press, Cambridge, Massachusetts, 438-483.

Beyer, K., and Boomer J. J. (2007). “Selection and Scaling of Real Accelerograms for Bi-Directional Loading: A Review of Current Practice and Code Provisions”, *Journal of Earthquake Engineering,* v 11, 13-45.

Bradley, B.A. (2012). “Empirical Correlations between Peak Ground Velocity and Spectrum-based Intensity Measure*”, Earthquake Spectra Feb 2012,* v 28, 17-35.

Campbell, K.W., and Bozorgnia, Y. (2010). “Analysis of Cumulative Absolute Velocity (CAV) and JMA Instrumental Seismic Intensity (I_{JMA}) Using the PEER-NGA Strong Motion Database”. PEER Report, College of Engineering University of California, Berkeley.

Douglas, J. (2012). “Consistency of Ground-Motion Predictions from the Past Four Decades: Peak Ground Velocity and Displacement, Arias Intensity and Relative Significant Duration”. *Bulletin of Earthquake Engineering,* v 10, 1339-1356.

Gasparini,D., and Vanmarcke, E. H. (1976). “SIMQKE: A Program for Artificial Motion Generation”, Department of Civil Engineering, Massachusetts Institute of Technology, Cambridge, MA.

Hancock, J., Watson-Lamprey, J., Abrahamson, N.A., Bommer, J.J., Markatis, A., McCoy,E.,and Mendis, R. (2006). “An Improved Method of Matching Response Spectra of Recorded Earthquake Ground Motion Using Wavelets”. *Journal of Earthquake Engineering,* v 10, 67-89.

Kayen, R. E., and Mitchell, J. K. (1997). “Assessment of Liquefaction Potential during Earthquakes by Arias Intensity”. *Journal of Geotechnical and Geoenvironmental Engineering,* v 123, 1162- 1174.

Montejo, L. A., and Suárez, L. E. (2013). “An Improved CWT Based Algorithm for the Generation of Spectrum Compatible Records”. Submitted for publication.

Pacific Earthquake Engineering Research Center PEER. (2013), Next Generation Attenuation of Ground Motions NGA database,<http://peer.berkeley.edu/nga/index.html>.

Suárez, L. E., and Montejo, L. A. (2005). “Generation of Artificial Earthquakes via the Wavelet Transform”. *International Journal of Solids and Structures*, v 42, 5905-5919.

Travasarou, T., Bray, J. D. nd Abrahamson, N.A. (2003). “ Empirical Attenuation Relationship for Arias Intensity”. *Earthquake Engineering and Structural Dynamics*, v 32, 1133-1155.

USNRC Regulatory Guide 1.208, “A Performance- Based Approach to Define the Site-Specific Earthquake Ground Motion” Rev. 0, March 2007.

CHAPTER 3

3. Effect of spectrum compatible records on the seismic demand of a typical RC bridge bent column

3.1 Introduction

Chapter 2 presented the development of spectrum compatible records using 3 different methodologies and a preliminary assessment of the characteristics of the resulting records. This chapter examines the effect of using these records as input motions for nonlinear time history analyses of civil structures. To accomplish this, a fiber based distributed plasticity model of a typical RC bridge bent column is developed and calibrated using actual large scale experimental data. Once the model is calibrated, incremental dynamic analyses (IDA) are performed using the spectrum compatible records previously generated. This allows us to analyze the inelastic demand imposed in the structure by the different records over a wide range of seismic intensities. The main objective is to identify if there are any significant differences in the inelastic demand imposed in the structure by spectrum compatible records generated using different methodologies. That is, to establish if any of the methodologies being evaluated generate records that are consistently more or less severe than the others. Additional objectives of this study are to confirm the adequacy of different intensity measures and to evaluate the effect of different parameters not related to spectral amplitude (e.g. duration) on the inelastic demand of the structure.

3.2 Structural model

3.2.1 Test and model description:

The structure to be analyzed is a full scale reinforced concrete (RC) bridge column subjected to a seismic motion through a shake table test performed at the Network for Earthquake Engineering Simulation (NEES) Large High Performance Outdoor Shake Table (LHPOST) at the University of California- San Diego. The complete experiment data is available from the NEEShub repository and it was used to calibrate a numerical model capable of replicating the column nonlinear seismic behavior. The test specimen consists of a cantilevered reinforced concrete column, footing and superstructure mass, as seen in Figure 3.2.1. The column replicated a full scaled bridge column designed under the Caltrans design guidelines. In terms of dimensions the diameter of the column was 1.22 m (4 ft) and the height was 7.31 m (24 ft).

Figure 3.2. 1 Test specimen (UCSD report)

The foundation consisted of a 5.49 m (18ft) long, 1.83 m (6 ft) wide and 1.22 m (4 ft) deep reinforced concrete block. The superstructure mass consists of five concrete blocks arranged together and has a combined estimated weight of 2321.5 KN (521.9 kip). The concrete strength of the column was 27.6 MPa (4.0 ksi). The reinforced steel was Grade 60 (414 MPa) steel conforming to ASTM A706 (2009). The longitudinal reinforcement was 18 No. 11 type bars and transverse reinforcement was provided in the form of butt-welded double No. 5 hoops spaced 152 mm (6 in) center to center (Schoettler et al, 2012).

Ten ground motions, starting with low- intensity motions, were applied to the column leaving it on near-collapse conditions. In addition to earthquake loads, low-intensity White Noise (WN) excitations were applied to the column between earthquakes to identify its dynamic properties. No attempts were made to straighten or repair the column between tests.

3.2.2 Finite element model

A distributed plasticity fiber based finite element model was developed in OpenSees (Figure 3.2.2). This method is highly recommended for the nonlinear analysis of structures when softening and degradation of the members is expected (Scott and Fenves, 2006). This approach also provides a more general framework for nonlinear analysis which allows plastic hinges to form at any location and to account for axial force-moment interaction by integrating the force deformation response at sections along the element length. Confined and unconfined concrete fibers are modeled with the OpenSees *Concrete01* material. Each one was modeled separately but using the same constitutive model, proposed by Mander, et al. (1988). The reinforced steel bars fibers are modeled using the *ReinforcingSteel* material suggested by Mohle and Kunntah (2006). This particular steel model has the capability to account for the fatigue and the rupture of

the rebar. To circumvent the localization problem typical of force-based approaches (e.g. Coleman and Spacone, 2001), the number of integration points and element lengths were chosen such that the integration weight of the fixed node matched the expected plastic hinge length.

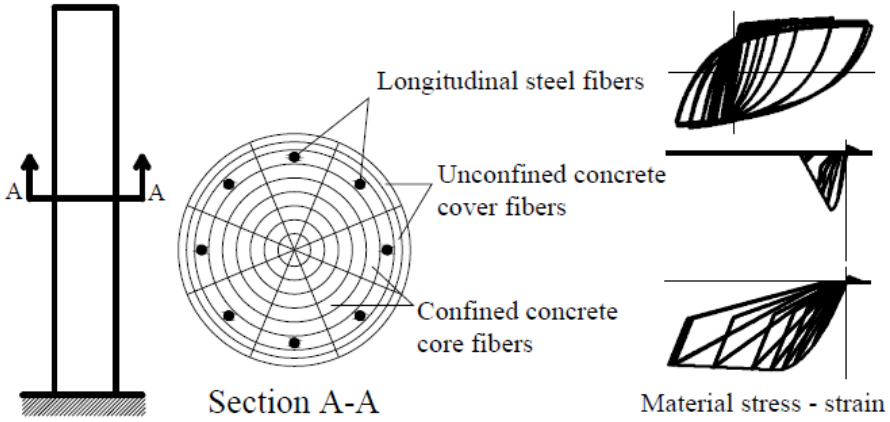

Figure 3.2.2. Distributed plasticity model (Montejo, 2008)

.

The validation of the numerical model is presented in Figures 3.2.3 through Figure 3.2.5. The experimental results were obtained from the UCSD shaking table test and were compared with the result of the total acceleration and the displacement ductility obtained from the numerical model. For the sake of brevity, the figures present the results of acceleration and displacement during earthquakes 1, 4 and 7, which are representative of different levels of inelastic demand in the structure. Note that the accelerations of the experimental results are smooth, unlike those obtained from the numerical model. The reason is that accelerations measured during the test were filtered to remove the high frequencies of the response before they were provided to the general public.

In general, it is seen that the accelerations obtained at the top of the column are in close agreement with the experimental results. In the case of the displacement time histories the agreement in the maximum peaks is also close; however, capturing the column residual displacement is more challenging. As a result, it is seen that in some cases the displacements from the simulations are similar to the experimental results but shifted by some value (Aguirre and Montejo, 2013).

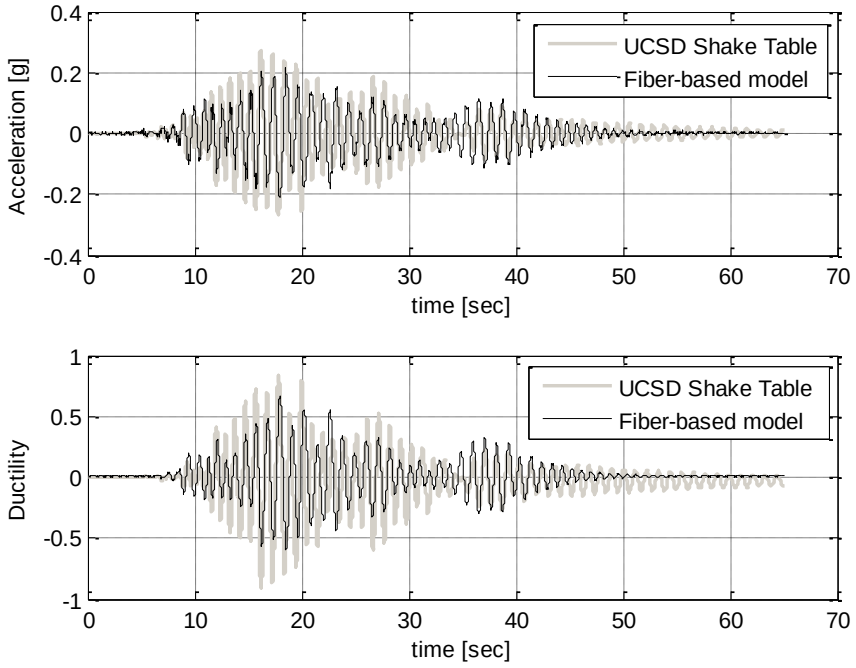

Figure 3.2. 3. (a) Acceleration time-histories for EQ1, (b) Ductility time-histories for EQ1

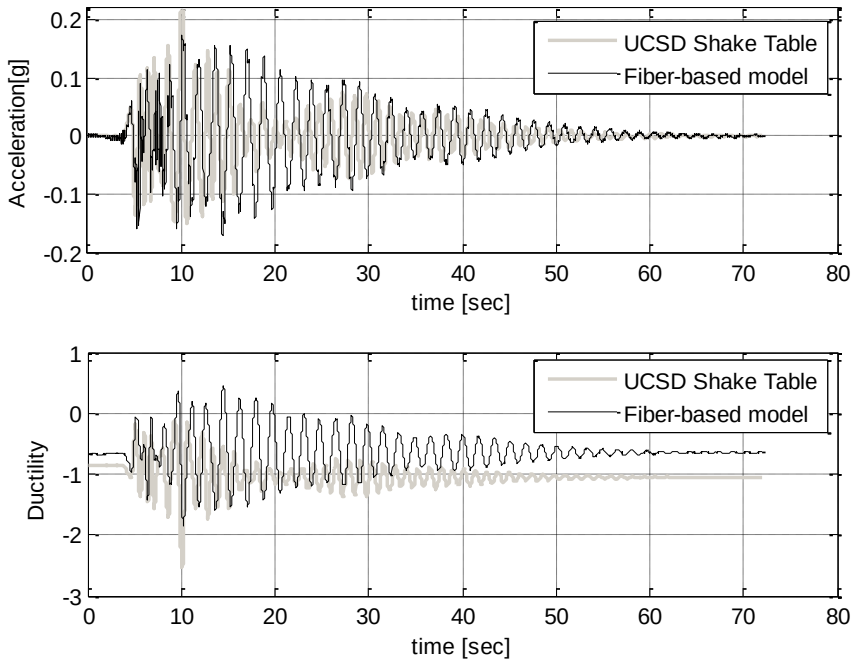

Figure 3.2.4. (a) Acceleration time-histories for EQ4, (b) Ductility time-histories for EQ4

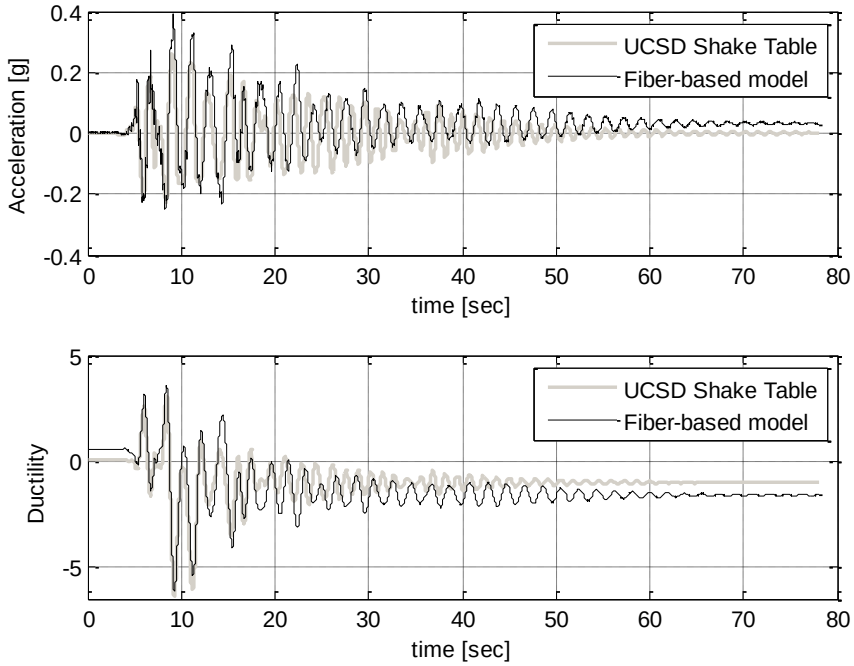

Figure 3.2.5. (a) Acceleration time-histories for EQ7, (b) Ductility time-histories for EQ7

Peak acceleration and displacement are not the only parameters that can give us an indication of the behavior of a civil structure. In general a RC structure can be weakened or damaged when it is subjected to a combination of stress reversals and high stress excursions. For this reason Park and Ang (1985) proposed a damage model which includes not only the maximum response, but also the effect of the repeated cyclic loadings. The proposed damage estimator, named Damage Index (DI), can be expressed as a linear combination of the damage caused by excessive deformation and the contributed by repeated cyclic loading (Equation 3.1).

$$DI = \frac{\delta_M}{\delta_U} + \frac{\beta}{Q_Y \cdot \delta_U} \int dE \qquad (3.1)$$

where;

δ_M = maximum deformation during the earthquake

δ_U = ultimate deformation under monotonic loading

Q_Y = calculated yield strength (if the maximum strength, Q_u, is smaller than Q_Y, Q_y is replaced by Q_u)

β = non-negative parameter that represents the effect of cycling loading on structural damage

dE= incremental absorbed hysteretic energy

The result of the integral in Equation 3.1 is the total absorbed hysteric energy (E) which can be determined by using the load-deformation time history. There are parameters that are independent of the load- deformation time history: δ_U, Q_Y and Q_u, and they were obtained from a

pushover analysis (Table 3.1). The value for β (0.06) was obtained through a trial and error process by identifying different known levels of performance.

Table 3.1. Independent parameters for the DI calculation

Parameter	δ_U	Q_Y	Q_U	Notice that $Q_U < Q_Y$ hence, $Q_Y = 481.65$ kN
Value	106.07 cm	610.20 kN	481.65 kN	

The remaining parameters need to be computed during each earthquake load. Values of the damage index (DI) are such that values of DI ≥ 1.0 imply complete collapse or total damage and a DI ≈ 0.5 corresponds to moderate/reparable damage. Figure 3.2.6 shows the results of the DI for each earthquake applied to the specimen in the original test (UCSD Shake table test). It is seen that the values obtained for DI correlate well with the observed damage, therefor the value used for β is appropriate.

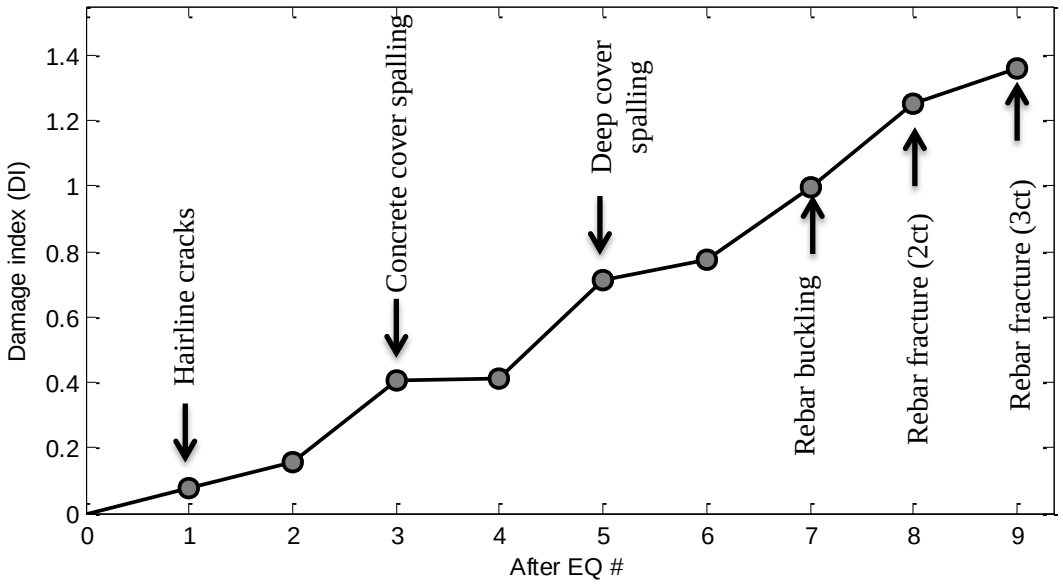

Figure 3.2.6 Calculated damage index (DI) after each earthquake

3.3 Incremental dynamic analysis (IDA)

The incremental dynamic analysis (IDA) is an emerging structural analysis method that offers thorough seismic demand and limit-state capacity by using a series of nonlinear dynamic analyses under a suite of scaled ground motions records (Vamvatsikos and Cornell 2002). This method was first introduced by Bertero (1977) and allows one to study and understand structural response under a variety of ground motions with different intensities and providing a good estimation of the dynamic capacity. In IDA, the quantifications of the response of the structure are provided by a variety of Damage Measures (DMs) which corresponds to systematically increasing ground motion Intensity Measures (IM) and can be interpreted in IDA plots. Damage Measures can be defined as an observable quantity that is part of, or it can be deduced from the output of the corresponding nonlinear dynamic analysis. An example of DMs can be ductility, node rotations and maximum base shear, among others. For this work the DMs selected were ductility, two way ductility, bars tensile strain and damage index (DI). Intensity Measures is a non-negative scalar that constitutes a monotonically increasing function of a selected factor. Examples of IM can be Peak Ground Acceleration (PGA), Peak Ground Velocity (PGV), and the 5% damped spectral acceleration at the structure's first mode period, among others.

There are several steps necessary to perform an IDA analysis. First, a nonlinear structural model needs to be formed as well as a suite of records must be selected. The UCSD column previously presented will be used as the structural model. For the suite of records, all the artificial earthquakes, described and analyzed in Chapter 2 will be engaged. Before using the records for IDA they are normalized so that all of them have the same spectral amplitude at the period of vibration that the structure exhibited at ductility 1. A plot of period of vibration vs.

maximum ductility reached at each test was generated (Figure 3.3.1) and the period at ductility 1 (T*) was estimated from it. The value estimated for T* was 0.75 s. Figure 3.3.2 shows the response spectra of the 50 normalized records.

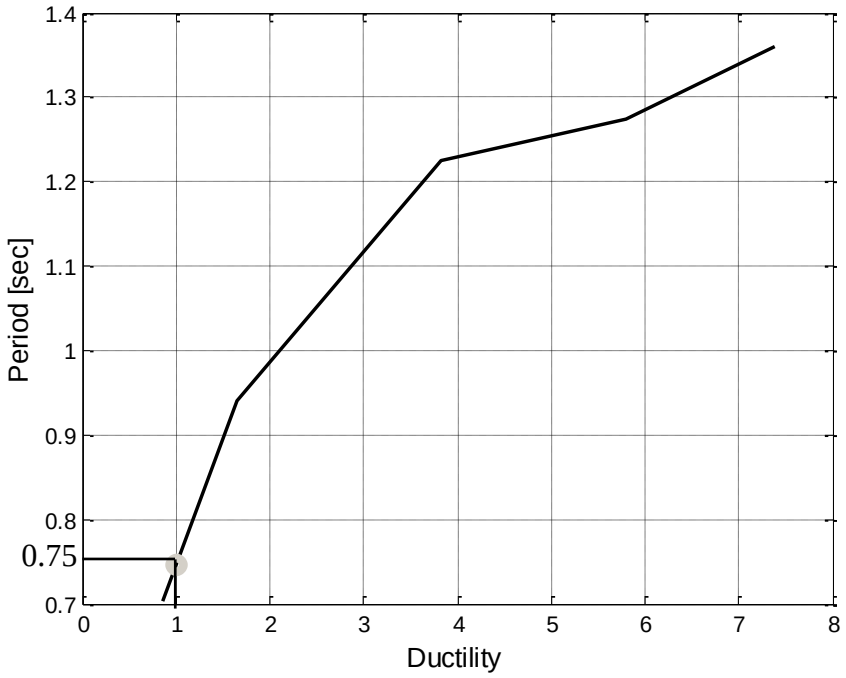

Figure 3.3. 1 Period vs. Ductility plot

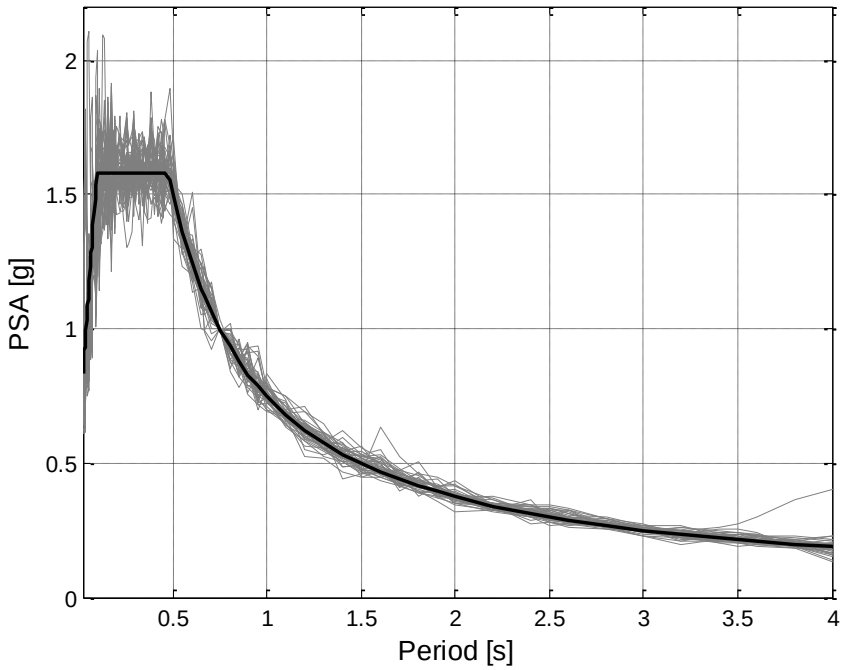

Figure 3.3.2. Target spectrum and response spectra of all 50 artificial earthquakes

The next step is to select the IM vector and the DMs parameters. Several IM and DMs were selected for this work. The feasibility of using spectral acceleration at T* (Sa (T*)), peak ground acceleration (PGA), peak ground velocity (PGV), peak ground displacement (PGD) and cumulative absolute velocity (CAV) as IM was investigated . Peak ductility displacement, two direction average peak ductility (2 way ductility), bars tensile strain and damage index (DI) were selected as DMs. The 2 way ductility parameter is calculated as the average between the positive and negative displacement ductilities. In the next section several combinations of DM and IM are presented in order to identify the most suitable parameter.

3.4 IDA results

3.4.1 Sa(T*) as IM

Figures 3.4.1 to 3.4.6 presents IDA curves for different DMs, all using the spectral acceleration at T*, Sa(T*) as IM. A typical IDA curve is presented in Figure 3.4.1, in this case for the CM SeismoMatch records using Sa(T*) as IM and peak displacement ductility as damage measure. The thick solid line denotes the mean and the dashed lines the mean plus and minus one standard deviation. An important initial observation is that in the expected range of performance, i.e. below ductility 6, the scatter in the results is relatively low with most of the IDA curves being contained on the range mean ± standard deviation. Similar results were obtained for the other sets of records and DMs. For the sake of brevity the IDA plots for the other earthquakes sets and DMs are presented in Appendix D. Figures 3.4.2 to 3.4.5 summarize the results obtained: each figure presents the mean IDA curve obtained for each earthquake set (left figures) and the corresponding coefficient of variation (COV, right figures). It is seen that the record-to-record dispersion for the DMs evaluated is relatively low, e.g. mostly below 0.3, (Cornell et al., 2002). The records generated using the frequency domain approach (SeismoArtif) exhibited a clear tendency to induce lower damage in the structure as measured by all the DMs except by the DI. On the other hand, the records generated through the Wavelet approach (SeismoMatch) using distant match records (DMSM records) exhibited a tendency to induce the large amount of damage in the structure as measured by all the DMs except by the DI. In terms of the DMs the Damage Index (DI) exhibited the lowest dispersion. Table 3.2 summarizes the highest and the lowest values at the last scaling factors (Sa(T*) = 2) for each one of the damage measures, as well as the earthquake that produces the value. It is seen that the same record dominate the extreme values, in the case of the maximum values; all cases were dominated by EQ#2 of the

DMSM approach. The minimum values were obtained from the records, EQ# 6 DMAQT II , EQ#1 SA and EQ#4 DMAQT II.

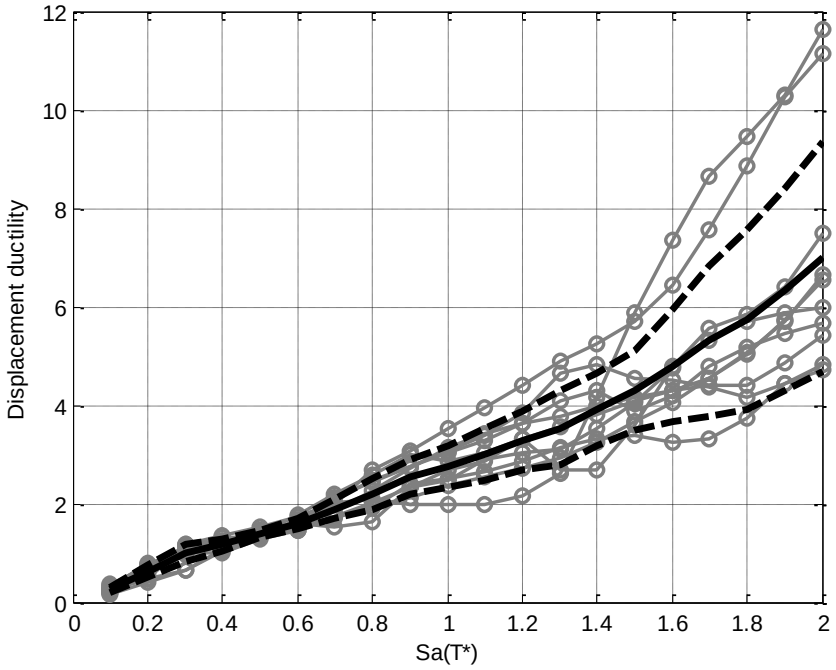

Figure 3.4. 1. CM SeismoMatch IDA curves peak displacement ductility

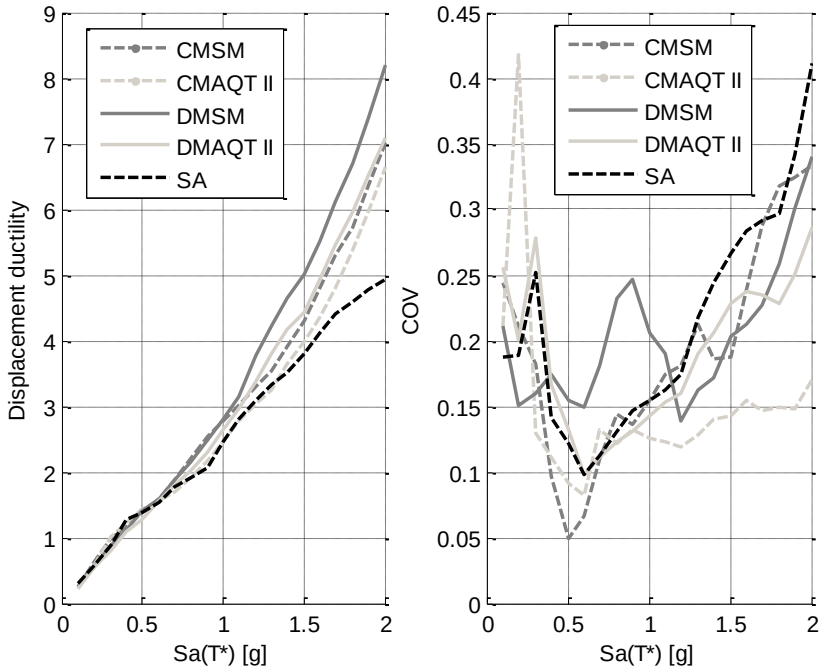

Figure 3.4.2. Average IDA curves (left) and COVs (right) using Sa(T*) as IM and peak displacement ductility as damage measure

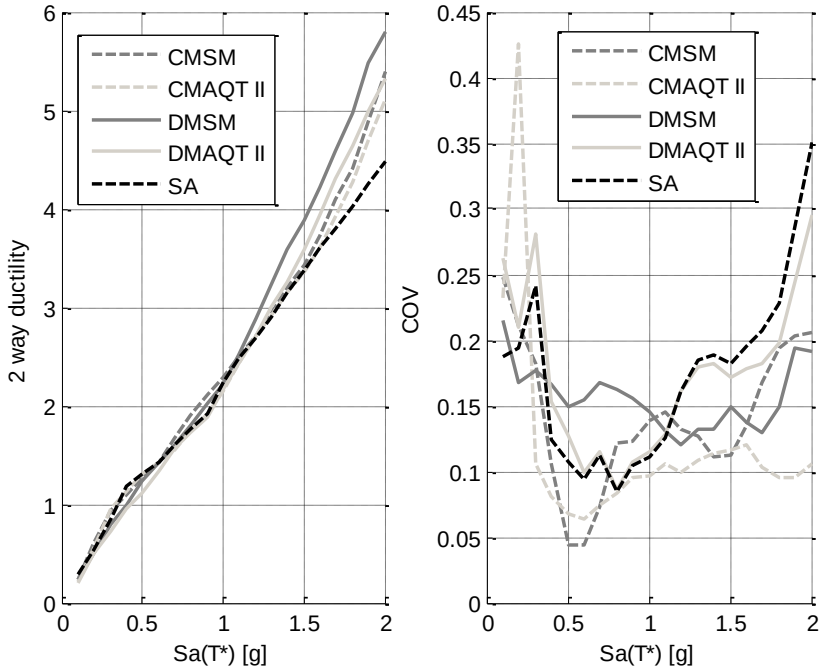

Figure 3.4.3. Average IDA curves (left) and COVs (right) using Sa(T*) as IM and 2 way ductility as damage measure

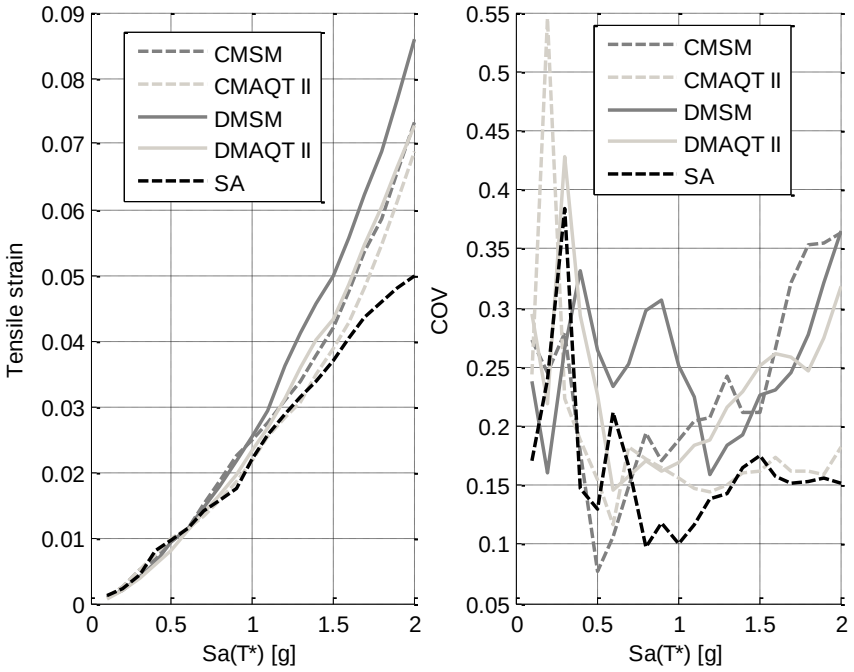

Figure 3.4.4. Average IDA curves (left) and COVs (right) using Sa(T*) as IM and tensile strain as damage measure

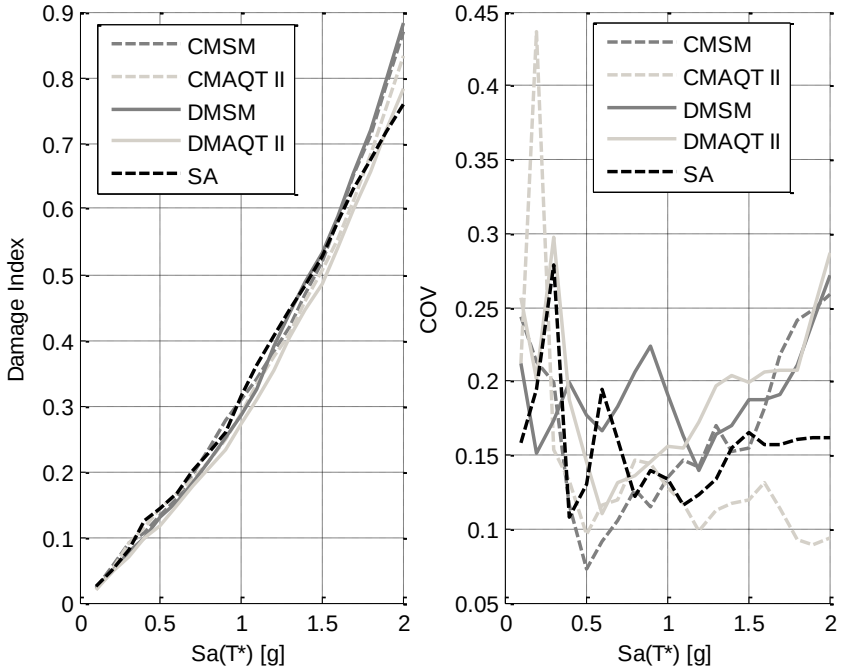

Figure 3.4.5. Average IDA curves (left) and COVs (right) using Sa(T*) as IM and damage index (DI) as damage measure

Table3.2 Maximum and minimum values at Sa(T*) = 2

Damage Measure	*Maximum*	*Approach/ EQ #*	*Minimum*	*Approach/ EQ #*
Displacement ductility	13.69	DMSM/ EQ# 2	3.9964	SA/ EQ# 1
Two way ductility	8.15	DMSM/ EQ#2	3.7842	DMAL/ EQ# 6
Tensile strain	0.1484	DMSM/ EQ#2	0.0386	SA/ EQ# 1
Damage Index	1.31	DMSM / EQ# 2	0.4557	DMAL/ EQ# 4

3.4.2 PGA, PGV, PGD and CAV as IM

The spectral acceleration at T* is not the only parameter that can be used as IM. Others ground motion characteristics can be used as well. In this section we investigate the use of peak ground acceleration (PGA), peak ground velocity (PGV), peak ground displacement (PGD) and cumulative absolute velocity (CAV) as IM. The DMs selected for this group of IDA curves were reduced to peak displacement ductility and damage index, since the other DMs exhibited similar behavior to the peak displacement ductility. For comparison purposes the results for Sa(T*) as IM are shown again in a different fashion. Figures 3.4.6 to 3.4.15 present the IDA curves for these parameters, the plots in the left show the IDA curves for each of the 50 earthquakes records and the right plots show the average IDA curves for each of the earthquake sets.

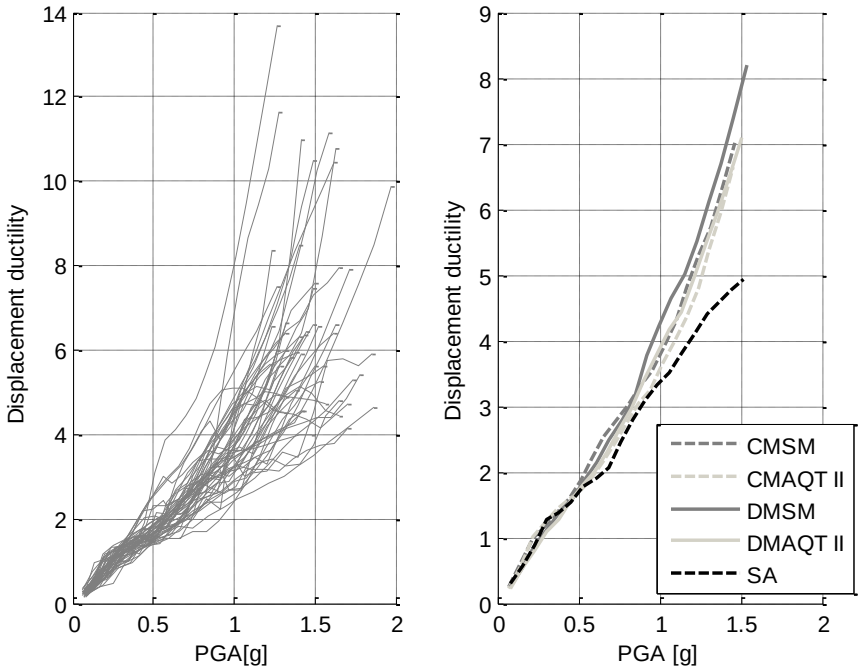

Figure 3.4. 6 (a) IDA curves (Ductility vs. PGA) for all artificial earthquakes (b) Average IDA curves (Ductility vs. PGA) by approach

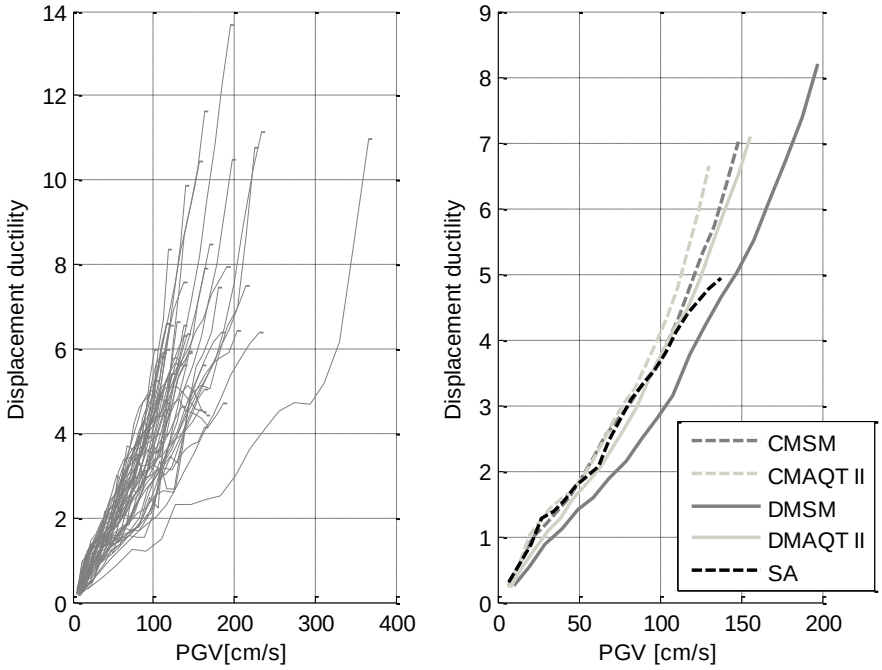

Figure 3.4.7 (a) IDA curves (Ductility vs. PGV) for all artificial earthquakes (b) Average IDA curves (Ductility vs. PGV) by approach

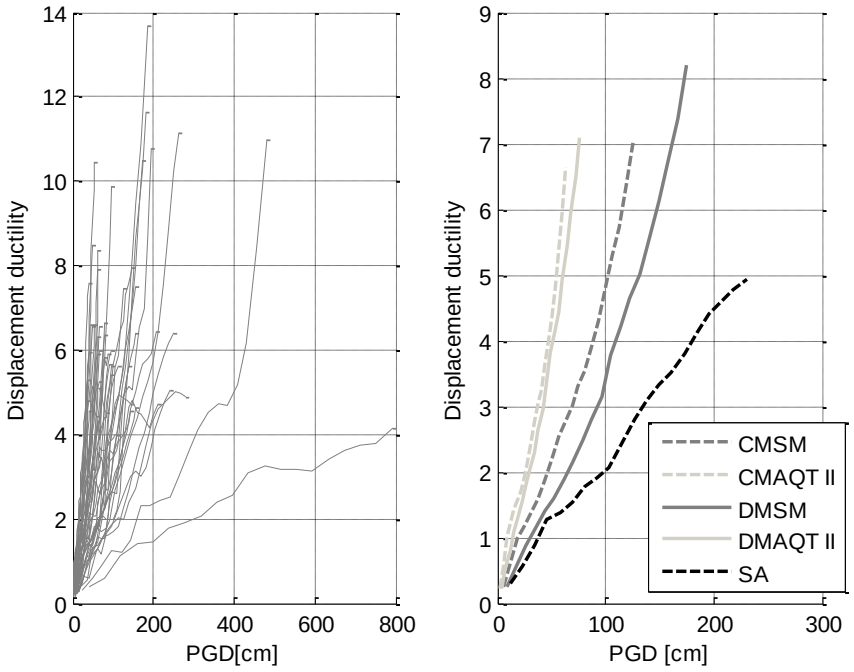

Figure 3.4. 8. (a) IDA curves (Ductility vs. PGD) for all artificial earthquakes (b) Average IDA curves (Ductility vs. PGD) by approach

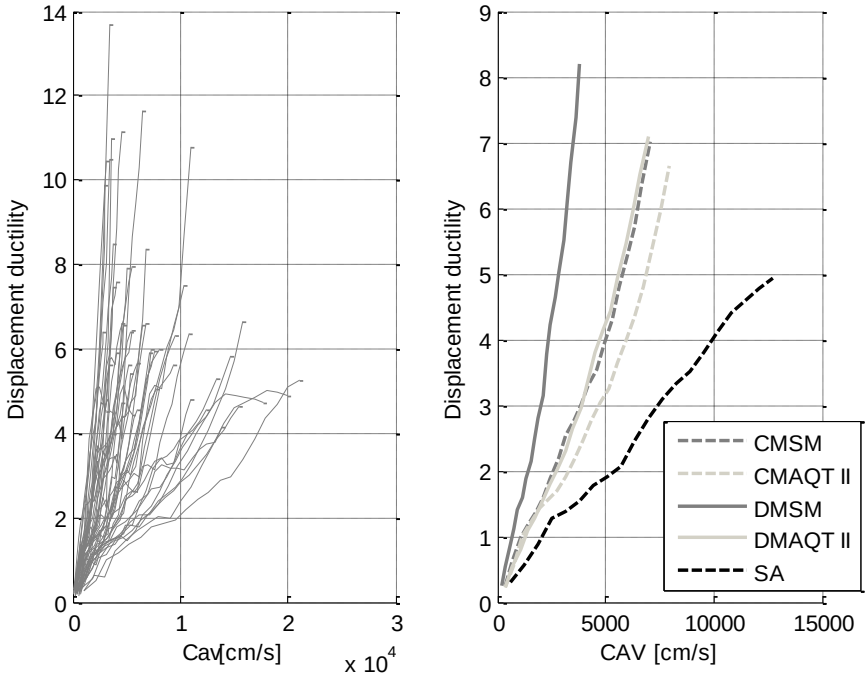

Figure 3.4. 9. (a) IDA curves (Ductility vs. CAV) for all artificial earthquakes (b) Average IDA curves (Ductility vs. CAV) by approach

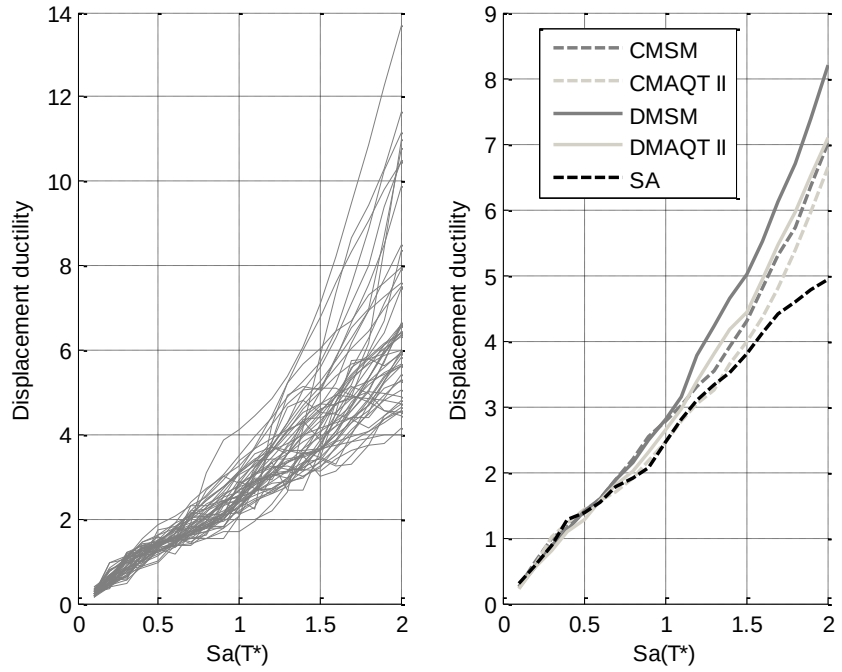

Figure 3.4. 10. (a) IDA curves (Ductility vs. Sa(T*)) for all artificial earthquakes (b) Average IDA curves (Ductility vs. Sa(T*)) by approach

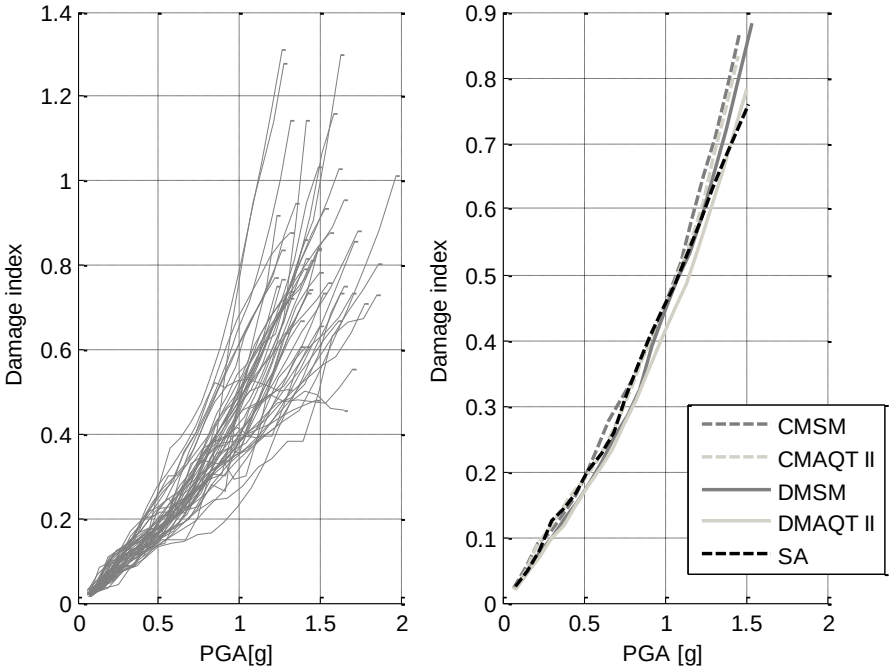

Figure 3.4.11. (a) IDA curves (DI vs. PGA) for all artificial earthquakes (b) Average IDA curves (DI vs. PGA) by approach

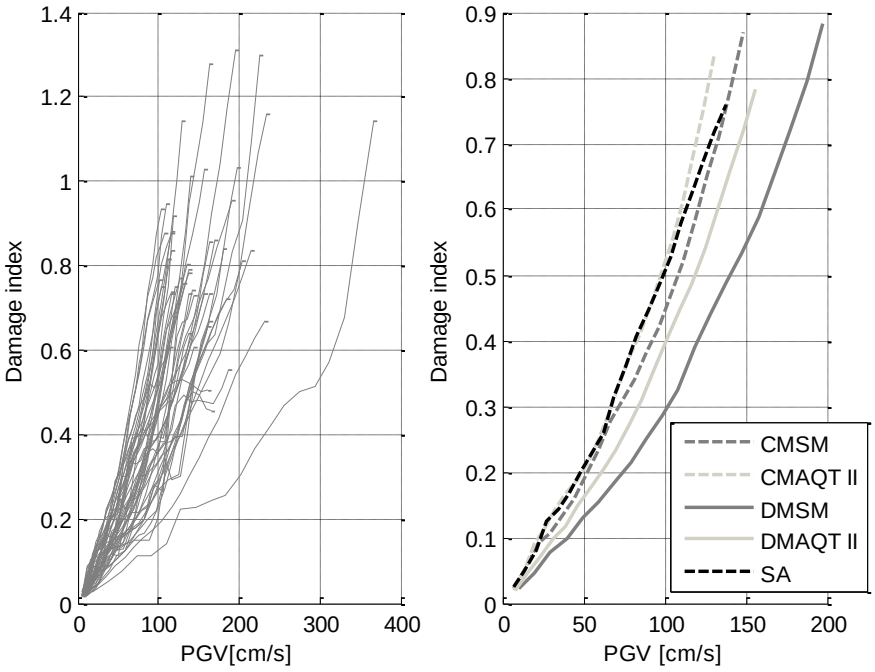

Figure 3.4.12. (a) IDA curves (DI vs. PGV) for all artificial earthquakes (b) Average IDA curves (DI vs. PGV) by approach

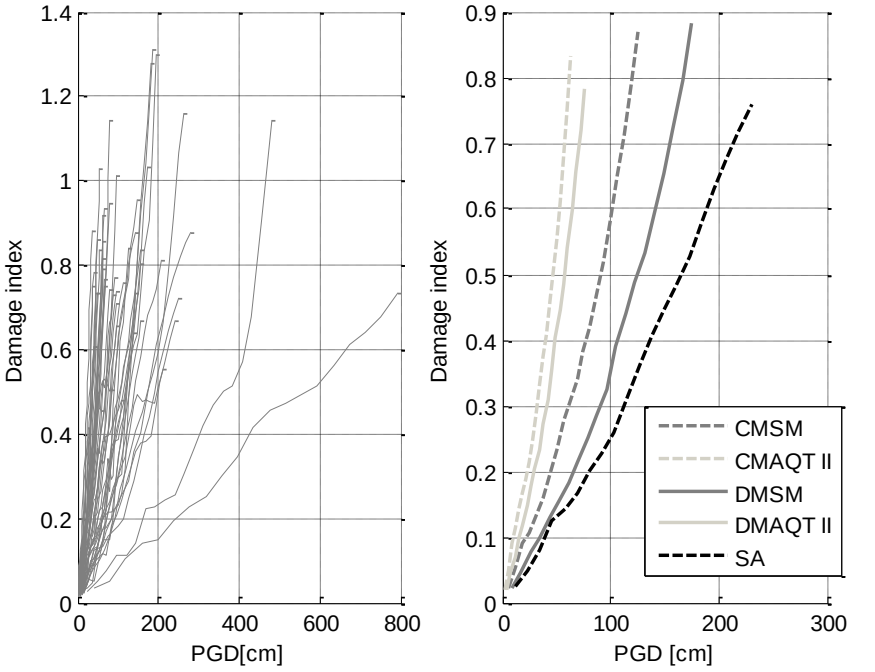

Figure 3.4.13. (a) IDA curves (DI vs. PGD) for all artificial earthquakes (b) Average IDA curves (DI vs. PGD) by approach

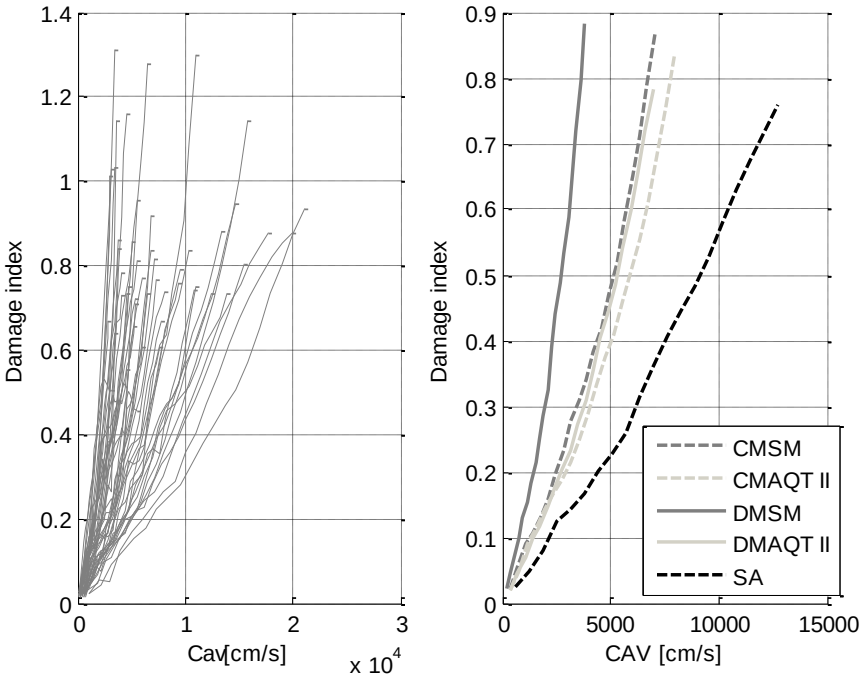

Figure 3.4. 14. (a) IDA curves (DI vs. CAV) for all artificial earthquakes (b) Average IDA curves (DI vs. CAV) by approach

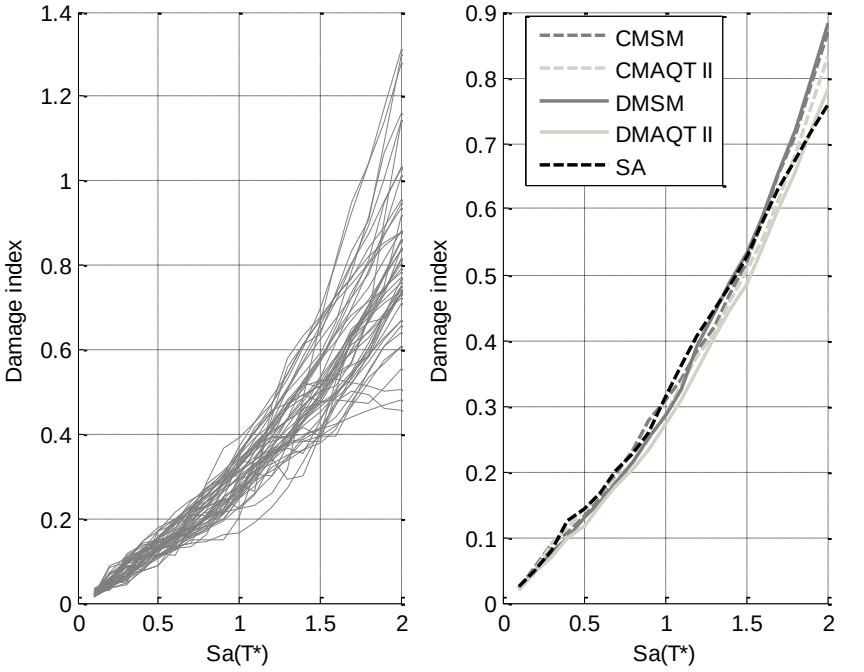

Figure 3.4. 15. (a) IDA curves (DI vs. Sa(T*))for all artificial earthquakes (b) Average IDA curves (DI vs. Sa(T*)) by approach

Based on an initial observation of the results obtained, it can be concluded that the IDA curves generated using Sa(T*) and PGA as IM (Figures 3.4.6, 3.4.10, 3.4.11 and 3.4.15) exhibited the smaller dispersion, in both the ductility and DI results. This means that these two parameters are better suited to be used as DMs in this particular case. Largest dispersions in the curves were observed when PGD and CAV were used as IMs. In an effort to quantify the scatter in the results obtained for each IM evaluated, COVs at key response values are calculated in the next section.

3.4.3 Coefficients of variation (COV)

In this section COVs are calculated for all the IMs and earthquakes sets for: (1) a peak displacement ductility of 4 and, (2) a damage index (DI) of 0.5. These values were selected because they are representative of the expected seismic serviceability level of the structure. The results are presented in Figures 3.4.16 and 3.4.17 for the displacement ductility and DI parameters respectively. It can be seen that the Sa(T*) followed by the PGA exhibited the lowest COV for the ductility and DI at each record suite and for the whole set of records. The IMs with the largest COVs were the CAV and the PGD. From these, the PGD exhibited the largest values of COV. This was expected from the results in Chapter 2 where it was shown that the displacements histories and PGD values of some of the records were unrealistically high. In terms of the records suites, the largest COVs were exhibited by the frequency domain records (SeismoArtif –SA). This value was also somehow expected due to the unrealistic characteristics displayed by these records (Chapter 2). From the approaches using seeds records it can be said that the lowest COVs are obtained when closed match records (CM) are used and for the CWT

approach (ArtifQuakeLet II). Nevertheless, the difference in the COV values obtained for these four suites of records (CMSM, CMAQT II, DMSM, CMAQT II) is not significant.

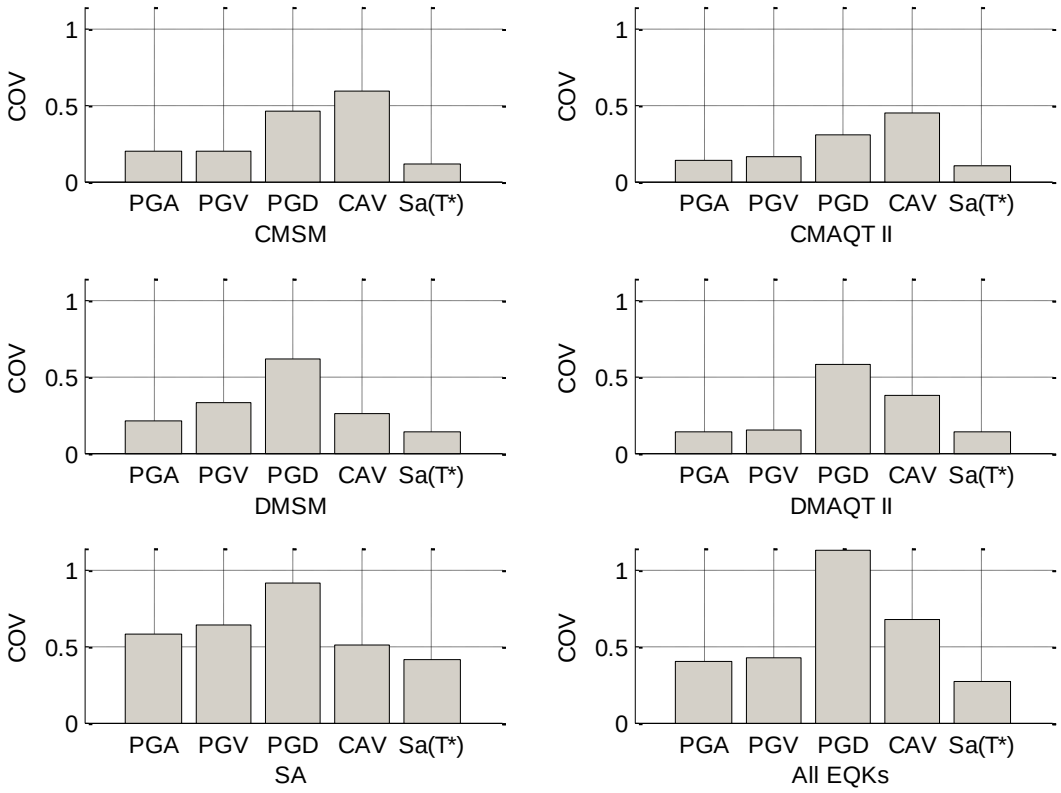

Figure 3.4.16. Coefficient of variation (COV) for displacement ductility of 4 as IMs

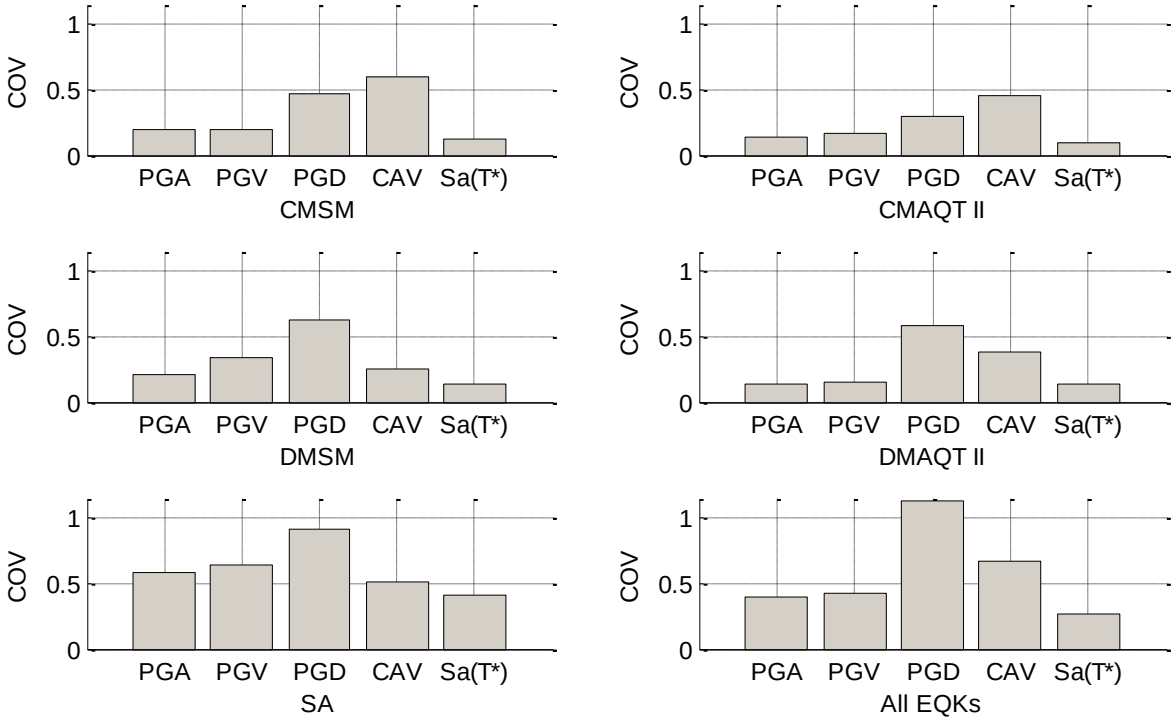

Figure 3.4.17. Coefficient of variation (COV) for 0.5 damage index (DI) as IMs

3.5 Influence of other earthquake record parameters

In the past sections several earthquake parameters were analyzed as intensity measures (IM). Each one of those parameters haves something in common: all of them change their values when the earthquakes are scaled. However, there are some parameters which not necessary change their values when the earthquake are scaled. These parameters are analyzed in this section. The mean period (T_m) and the significant duration (Sd) were the parameters presented in Chapter 2 that present this behavior. Additional to these earthquake characteristics, NRC recommends some parameters as criteria for developing spectrum compatible time histories (NRC, 2007). These are the ratios PGV/PGA and (PGA*PGD)/PGV^2, where PGA, PGV and PGD are peak ground acceleration, peak ground velocity and peak ground displacement respectively.

In order to examine the behavior of these parameters through different levels of seismic intensity and inelastic demand, four scale factors were selected: 0.8, 1.2, 1.6 and 2.0 (Figures 3.5.1 to 3.5.8). It is seen that with exception of the significant duration that exhibited a weak correlation with DI (Figure 3.5.6), neither of the additional parameters evaluated correlate well with the DMs.

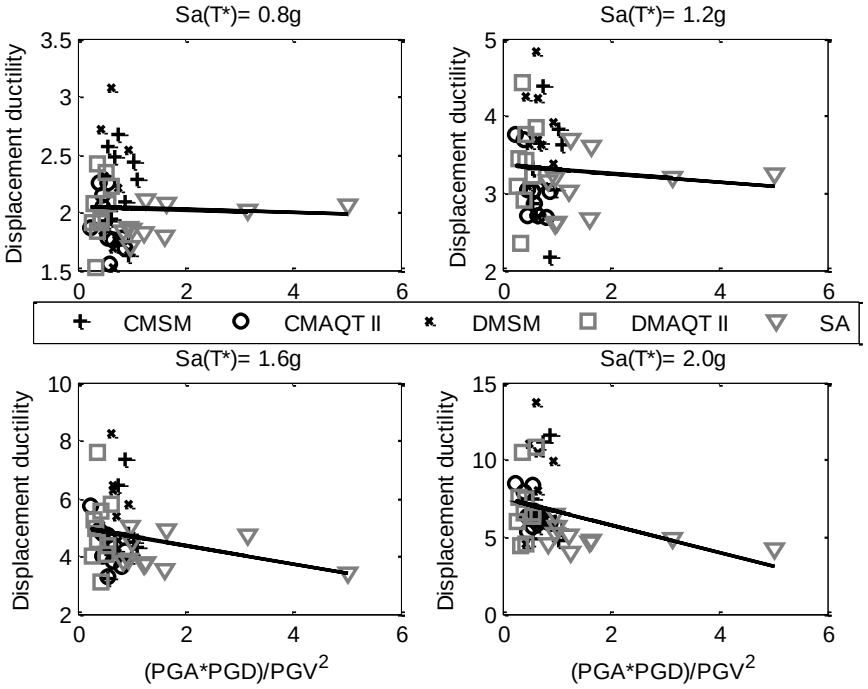

Figure 3.5. 1 PGA*PGD/PGV² plots for displacement ductility as damage measure

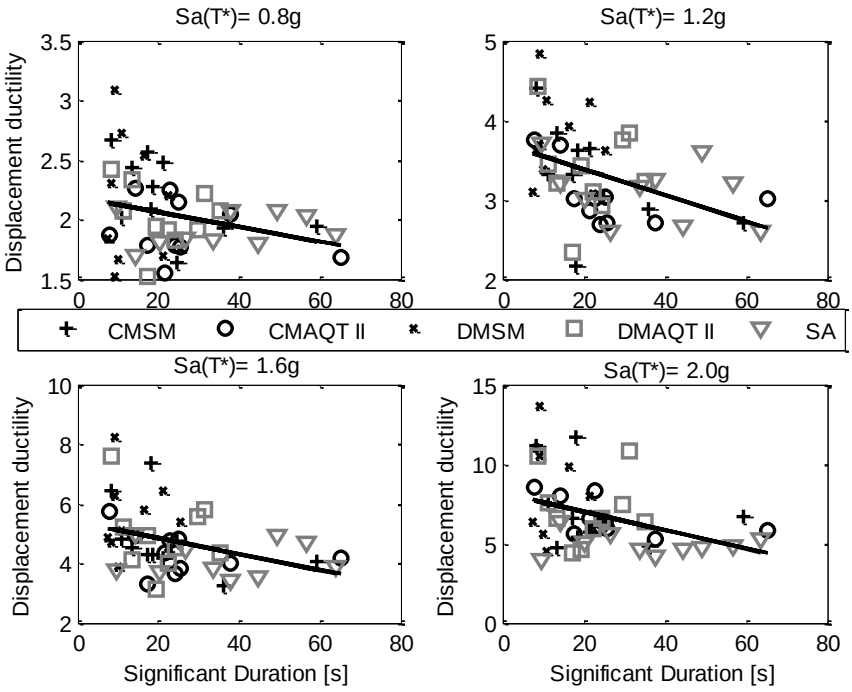

Figure 3.5.2. Significant duration plots for displacement ductility as damage measure

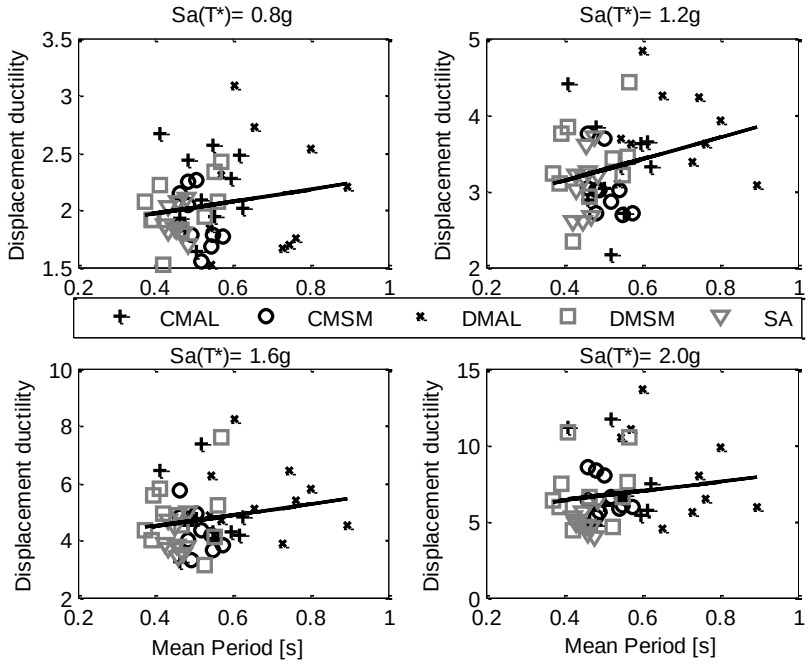

Figure 3.5.3 Mean period plots for displacement ductility as damage measure

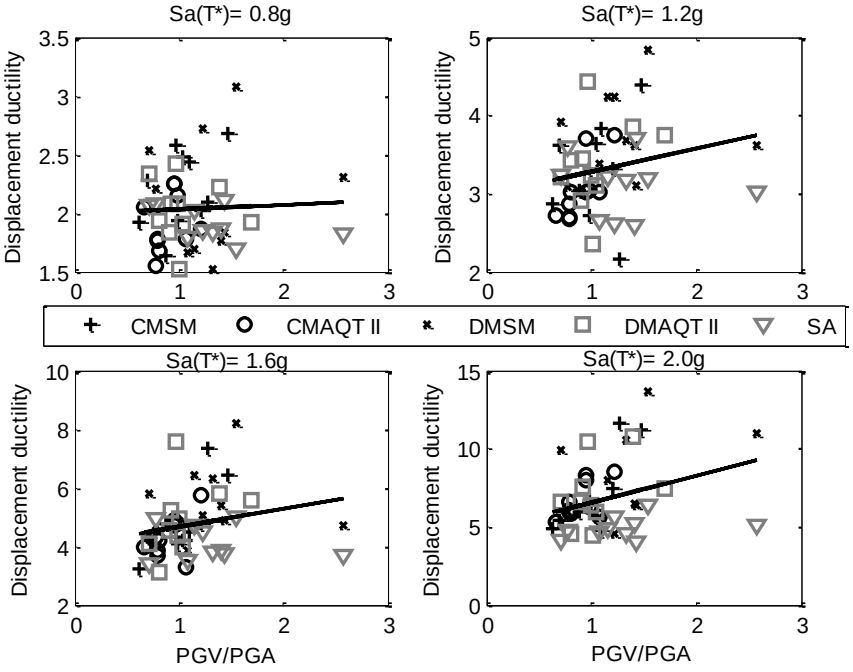

Figure 3.5.4 PGV/PGA plots for displacement ductility as damage measure

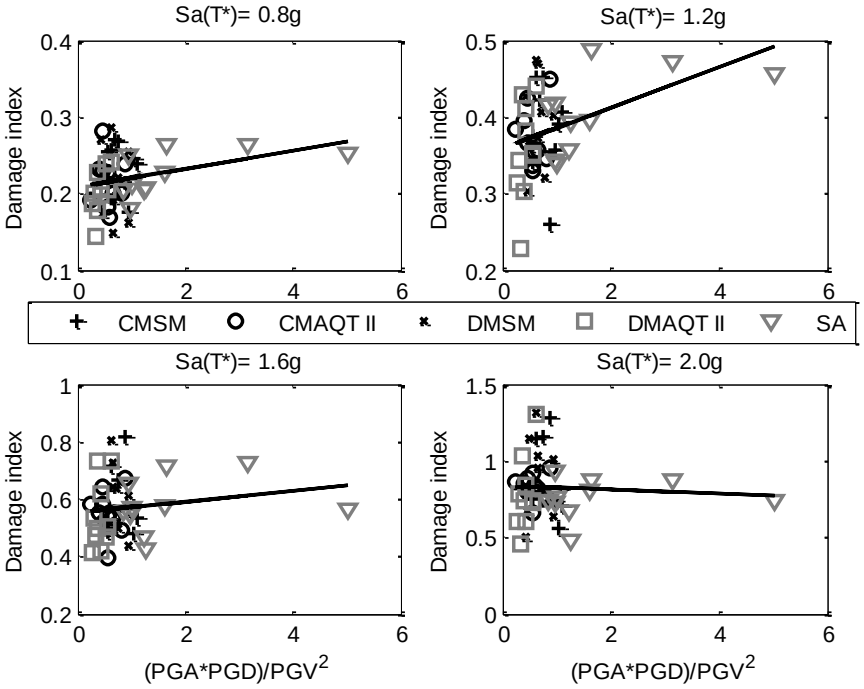

Figure 3.5.5 PGA*PGD/PGV² plots for damage index as damage measure

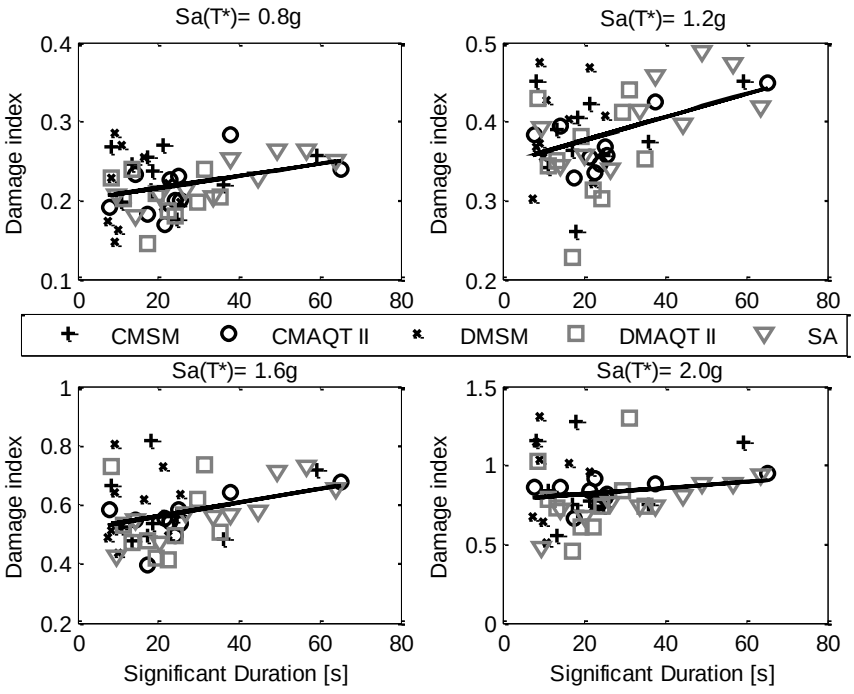

Figure 3.5.6. Significant duration plots for damage index as damage measure

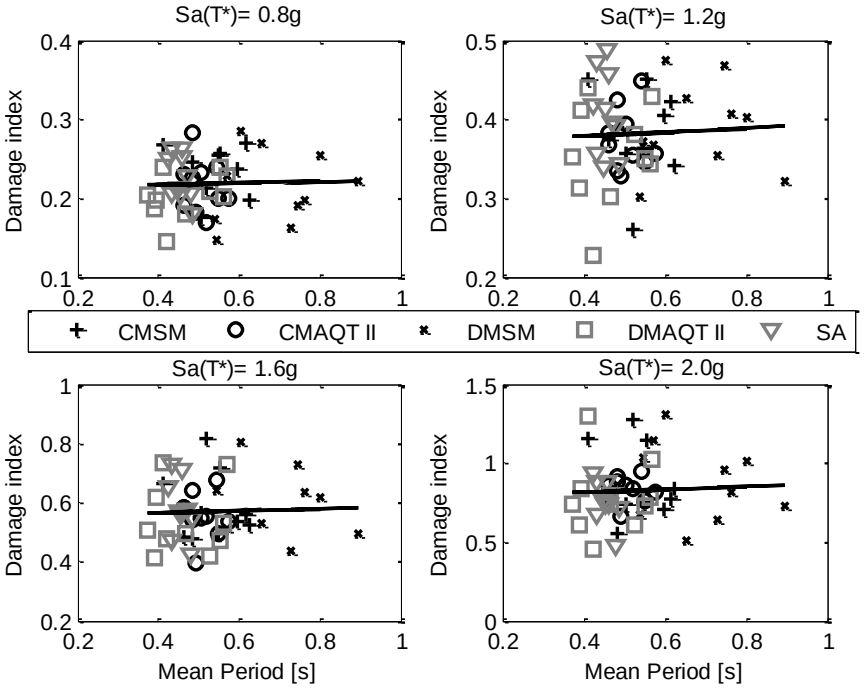

Figure 3.5.7. Mean period plots for damage index as damage measure

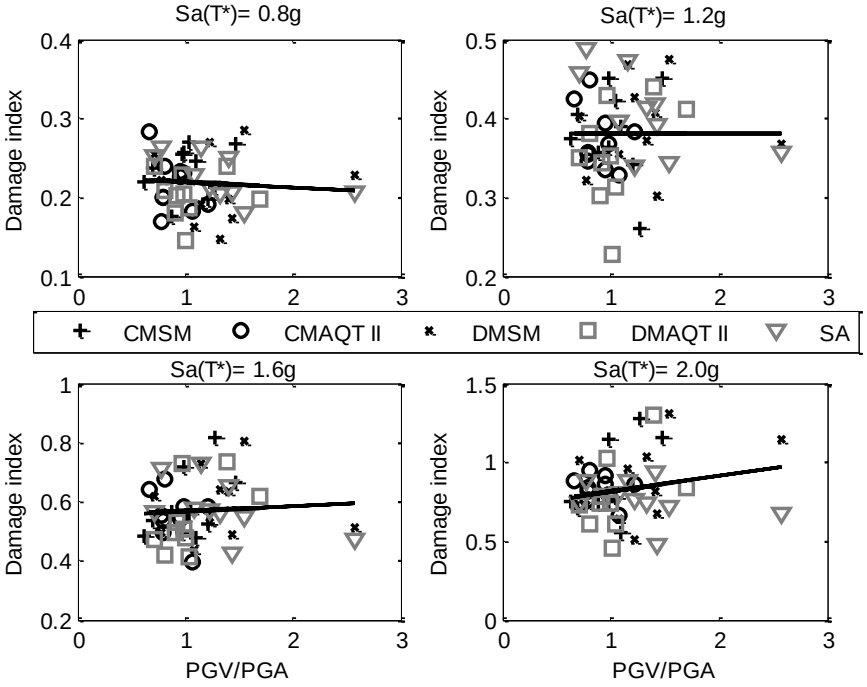

Figure 3.5.8. PGV/PGA plots for damage index as damage measure

3.6 Conclusions

- The records generated using the frequency domain approach as coded in the software SeismoArtif exhibited the largest dispersion in the results of the Incremental Dynamic Analysis (IDA). These records also exhibited a tendency to induce less inelastic demand in the structure as measured by the peak ductility. However, in terms of the Damage Index (DI) the results obtained are similar for all the suites of records.
- The largest inelastic demand as measured by the peak ductility was induced by the records generated using the Wavelet approach (SeismoMatch) when the seed records spectra differs from the target spectrum. However, when the seed records are selected based on the initial spectra compatibility, the results of the IDA when using spectrum compatible records generated by either of the approaches evaluated (Wavelets and CWT) are similar.
- In terms of the intensity measures (IMs), the parameter that better correlates with the damage measures (DMs) evaluated is the spectral acceleration Sa(T*) at the structural period at ductility 1 , followed by the peak ground acceleration (PGA).
- Additional parameters (like strong motion duration) that do not change when the record is scaled were also evaluated to try to explain the scatter in the IDA curves. However, no conclusive correlations were found.

Note that these conclusions apply only to structures like the one examined, i.e. ductile detailed structures with a very dominant mode of vibration. Next Chapter will examine the effect of changing the fundamental natural period of the structure.

3.7 References

Aguirre, D. A. and Montejo, L. A. (2013) "*Damping and Frequency Changes Induced by Increasing Levels of Seismic Inelastic Demand on Reinforced Concrete Structu*res," Submitted for publication

Bertero, V. V. (1977) "Strength and Deformation Capacities of Building under Extreme Environment*", Structural Engineering and Structural Mechanics,* 211-215

Coleman, J., Spacone, E., (2001). "Localization Issues in Nonlinear Force-Based Frame Elements", ASCE *Journal of Structural Engineering*, v 127, 1257-1265.

Cornell, C., Jalayer, F., Hamburger, R. and Foutch, D. (2002). "Probabilistic Basis for 2000 SAC Federal Emergency Management Agency Steel Moment Frame Guidelines." *Journal of Structural Engineering*, v128, Special Issue: Steel Moment Frames after Northridge- Part II, 526-533.

Mander, J. B., Priestly, M. J. N. and Park, R. (1988). "Theorical Stress-Strain Model for Confined Concrete", *ASCE Journal of Structural Engineering*, v114 (8), 1804-1826.

Mohle J. and Kunnath S. "Reinforcing steel. OpenSees User's Manual, 2006

http://opensees.berkeley.edu

Montejo, L. A. (2008). *"*Seismic Behavior of Reinforced Concrete Bridge Columns at Sub-Freezing Temperatures*"*, PhD dissertation, North Carolina State University, NC.

Schoettler, M.J., Restrepo, J.I., Guerrini, G., Duck, D.E., Carrera, F. (2012). "A full-scale, single-column bridge bent tested by shake-table excitation". Center for Civil Engineering Earthquake Research, Department of Civil Engineering, University of Nevada.

Scott, M. H. and Fenves, G. L. (2006). "Plastic Hinge Integration Methods for Force-Based Beam-Column Elements", *ASCE Journal of Structural Engineering*, v 132, 244-252.

Park, Y. J. and Ang, A. H. S. (1985). "Mechanistic Seismic Damage Model for Reinforced Concrete," *Journal Structural Engineering*, v 111, 722-739.

USNRC Regulatory Guide 1.208, "A Performance- Based Approach to Define the Site-Specific Earthquake Ground Motion" Rev. 0, March 2007.

Vamvatsikos, D. and Cornell, C. (2002) "Incremental Dynamic Analysis," *Engineering Structural Dynamics*, v 32, 491-514.

CHAPTER 4

4. Effect of spectrum compatible records on the seismic demand of RC bridge columns with different natural periods

4.1 Introduction

Chapter 3 presented the effect of spectrum compatible records on the inelastic demand of a civil structure. The structure used to achieve this analysis was a full scale reinforced concrete (RC) bridge column, which was part of an experiment conducted at the University of California San Diego. This chapter extends the analysis performed in Chapter 3 by analyzing the behavior of four RC bridge columns with different periods of vibration. To achieve this, the sectional dimensions and reinforcement details of the columns remain exactly as the original column, but the cantilever length was changed to obtain columns with aspect ratios (L/D) of 3.4, 4.2,6 and 8. Just as in Chapter 3, the spectrum compatible records were normalized at the periods exhibited by the structures at ductility 1. The main objective remains to identify if there are any significant differences in the inelastic demand imposed in the structure by the spectrum compatible records, this time taking into account also the natural period of the structure. Due to the changes in dimensions of the columns, new periods for ductility 1 were obtained as well as different scale factors to run the IDA analyses using the compatible records.

4.2 Cases descriptions

The structures to analyze are modified versions of the full scale reinforced concrete (RC) bridge column used in the previous chapter. A total of four columns will be analyzed. The

majority of the structural parameters remain with the same values as the original case. The only parameter that changes is the length of the column, which begins at 4.2 m (case 1) until 9.6 m (case 4). The main reason for this change is obtain different fundamental periods of vibration so that each structure fits under different regions of the design spectrum, as shown in Figure 4.2.1. Table 4.1 shows the column lengths for each one of the cases, the original natural period and the expected period of vibration at ductility 1

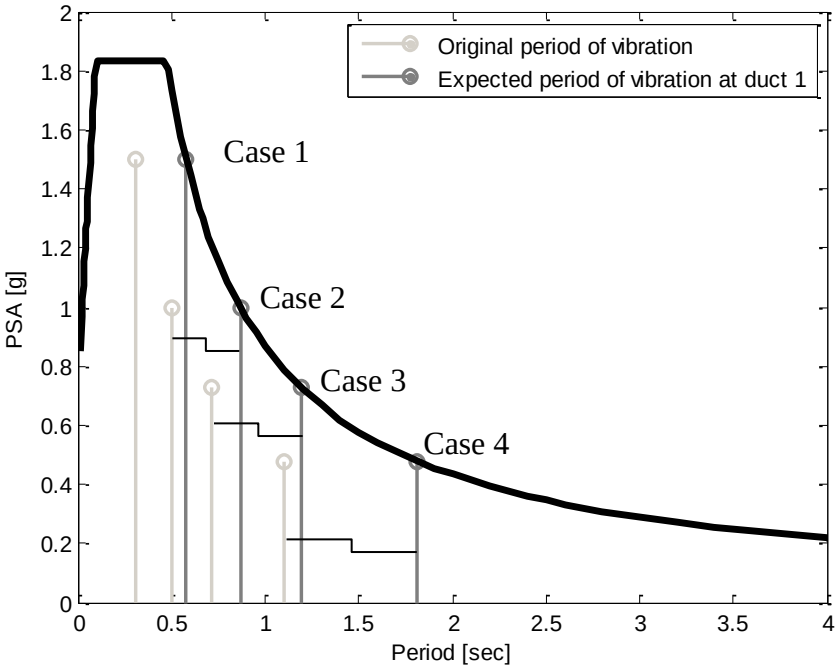

Figure 4.2. 1 Design spectrum and periods of vibration for all the cases

Table 4. 1 Length, diameter, original period of vibration and expected period of vibration at ductility 1

Case	L (m)	D (m)	L/D	T [sec]	T* [sec]
1	4.2	1.2	3.5	0.31	0.57
2	5.76	1.2	4.8	0.50	0.87
3	7.2	1.2	6	0.71	1.19
4	9.6	1.2	8	1.10	1.81

A distributed plasticity fiber based finite element model was developed in OpenSees for all the cases. The confined and unconfined concrete fibers are modeled with the OpenSees *Concrete 01* material and the reinforced bars are modeled with the *ReinforcedSteel* material, the same material used for the previous chapter. Figure 4.2.2 presents the hysteric force displacement response obtained after a symmetric cyclic pushover load history is applied to each of the specimens. As expected the larger shear demand is exhibited by the shorter column (case 1), and as the length of the column increases the p-delta effect becomes more significant.

To obtain the period at displacement ductility 1 and further characterize the behavior of each column, plots of period vs. displacement ductility are generated. These particular curves were generated after a cyclic pushover was applied to the each column. Different displacement ductilities values were specified as target displacements to run the cyclic pushover. The periods shown correspond to the first natural period of the structure after a cycle at a given ductility is completed and the structure is back at displacement zero. These plots are presented in Figure 4.2.3. It is seen that the pattern is the same for the four cases: the largest shifts in the periods of vibration occur when the structure reaches ductility 1. From this point forward the changes in period is almost linear and at much lower the rate despite the increasing in inelastic demand. The next significant shift in the period of vibration is observed when rupture of the longitudinal rebar occurs. Case 3 coincides with the original UCSD experiment and this particular plot also shows the periods obtained based on the experimental data. When compared with the results obtained with the fiber model the periods are close and the pattern remains the same, i.e. this data serves as validation of the models.

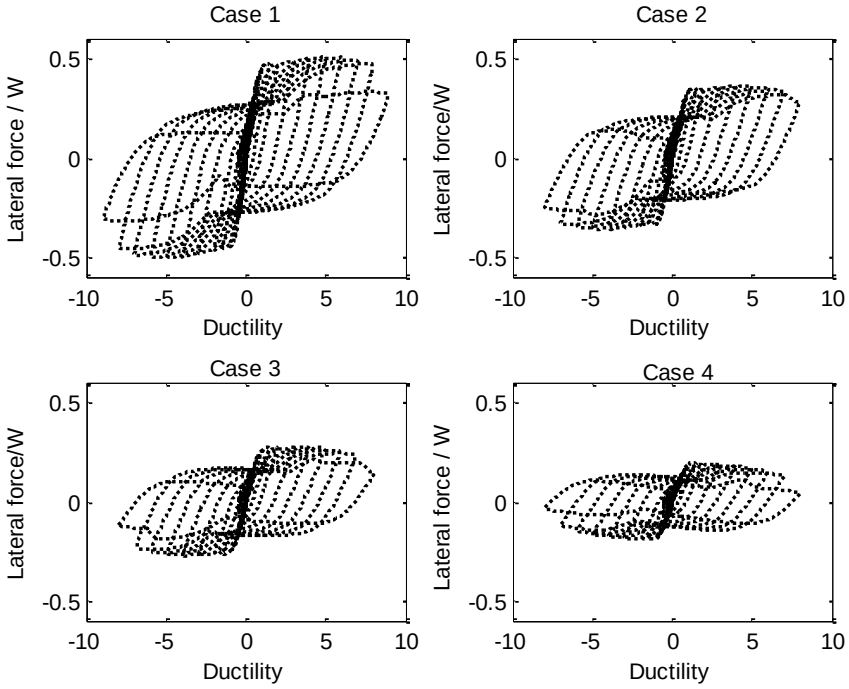

Figure 4.2.2. Hysteretic behavior for all cases

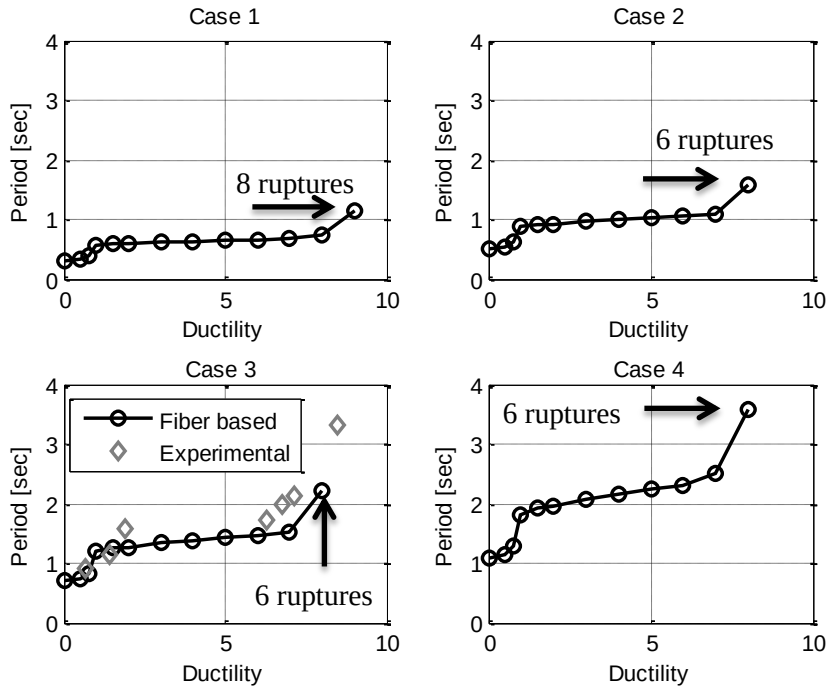

Figure 4.2.3. Period vs. Ductility plots for all cases

4.3 IDA - Sa(T*) as IM

As described in Chapter 3 the incremental dynamic analysis (IDA) is a method that allow us to study the structural response under a variety of ground motion intensities. The intensity measure (IM) for this section is the spectral acceleration Sa(T*) at T*. This IM was the most accurate in the last chapter and therefore it is the first option we evaluated in this chapter.

The damage measures (DM) used in this section are the displacement ductility and the damage index developed by Park and Ang. Figures 4.3.1 to 4.3.8 present the IDA curves for all cases. Using the same configuration as in the last chapter, the left figure presents the mean IDA curve obtained for each earthquake set and the right figure presents the coefficient of variation (COV) curves for each one of the approaches. Case 2 exhibited in average the largest ductility demands, followed by case 1, case 3 and case 4. In terms of damage index (DI) the behavior was almost the opposite, with case 3 presenting the highest values followed by the case 4, case 2 and case 1.It is important to notice that not all the columns were subjected to the same level of earthquake intensities. Moreover, for each column the earthquakes were normalized to the spectral amplitude Sa(T*) at the period of vibration that correspond to ductility 1. The earthquakes were scaled between Sa(T*) = 0.1g until the largest value possible before rebar ruptures occurs; this value was different for each column.

The largest dispersion among the average IDA curves was exhibited by the more flexible column (case 4). This may be a direct consequence of the second order effects which makes the structure more sensible to the characteristics of the input motions. When the dispersion for different DMs are compared, the damage index (DI) presented the lowest one.

It is noticed a tendency of the DMSM (distant match SeismoMatch) records to impose the largest ductility demand in the two more rigid columns (case 1 and 2), where these records also exhibited the largest COVs. However, such tendency disappears as we move toward the more flexible columns (cases 3 and 4).

The SA (SeismoArtif, frequency domain approach) records consistently exhibited the lowest ductility demand and this was especially evident in the two extreme cases (1 and 4). In terms of the COV, the records generated with the SeismoMatch approach using distant match records exhibited the highest values (DMSM). The lower COVs were display by the ArtifQuakeLet and SeismoMatch approaches when close match records (CMSM and AQT II) are used as seeds.

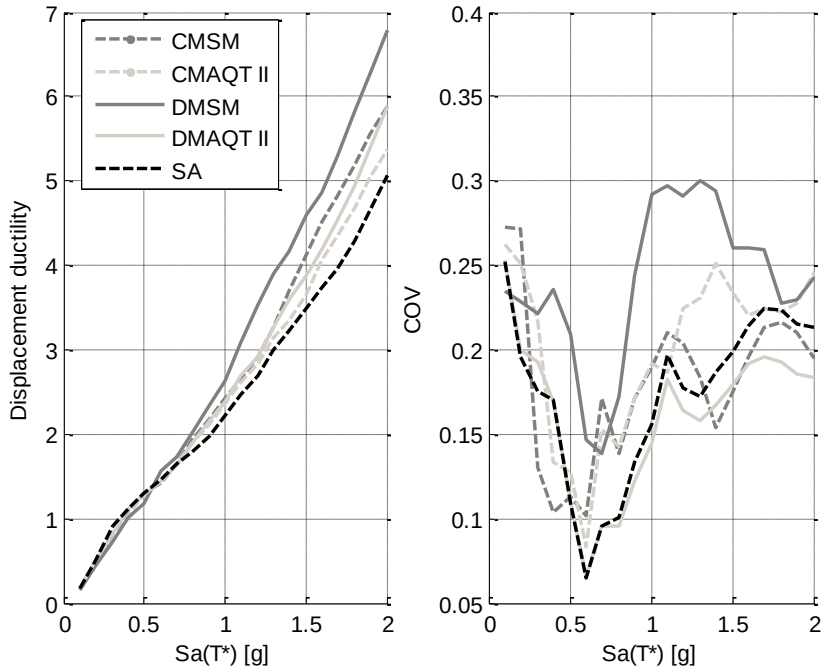

Figure 4.3. 1. Average IDA curves (left) and COVs (right) using Sa(T*) as IM and peak displacement ductility as damage measure for case 1

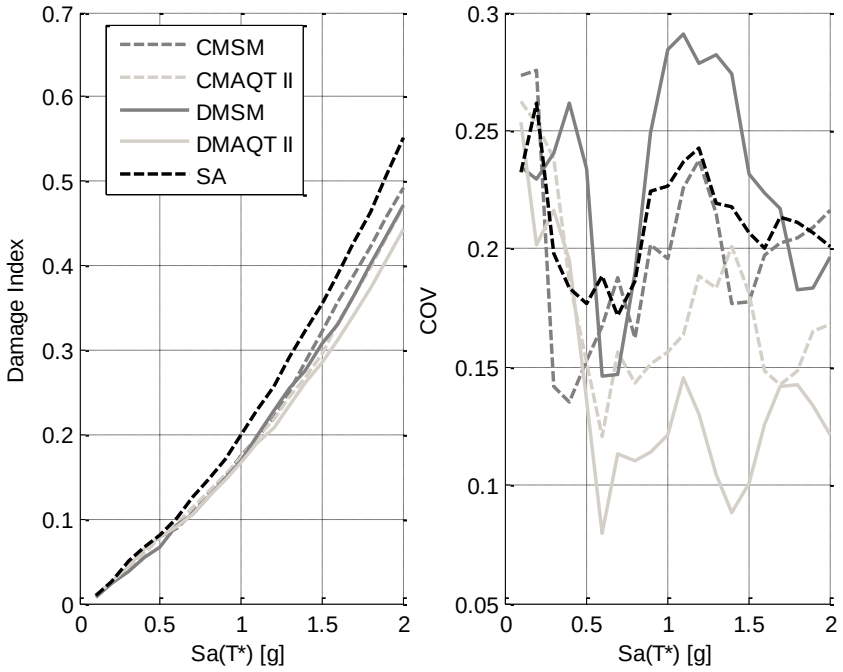

Figure 4.3.2 Average IDA curves (left) and COVs (right) using Sa(T*) as IM and damage index (DI) as damage measure for case 1

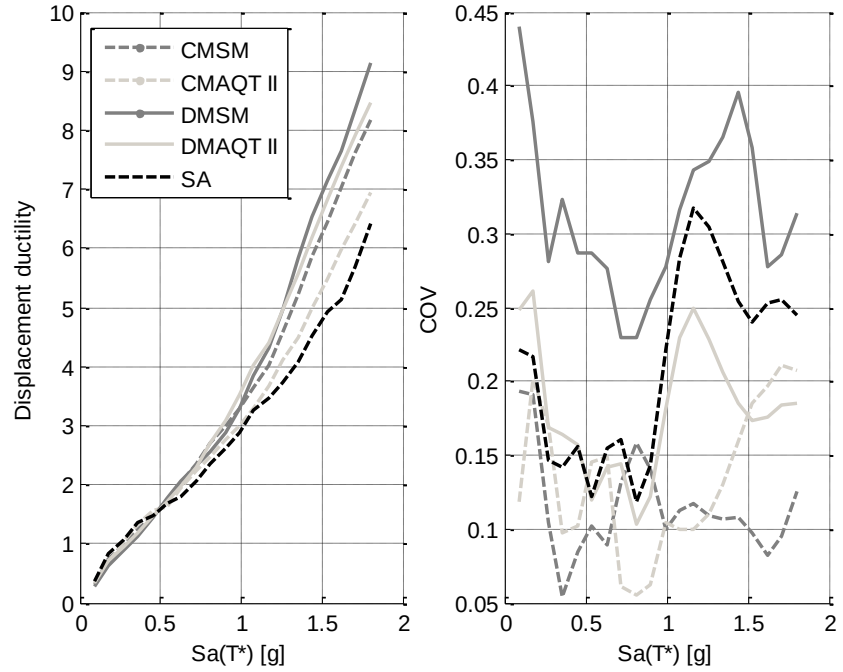

Figure 4.3.3 Average IDA curves (left) and COVs (right) using Sa(T*) as IM and peak displacement ductility as damage measure for case 2

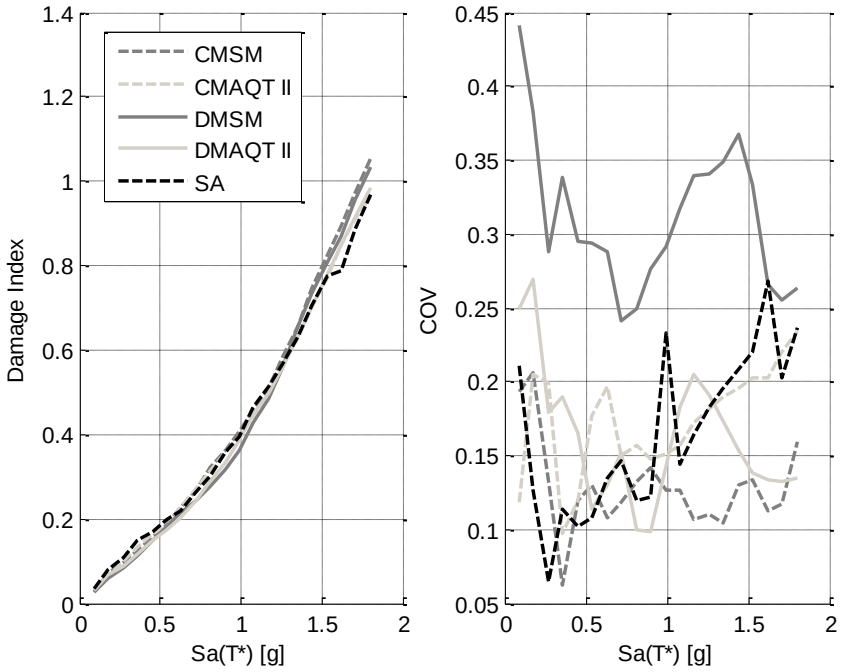

Figure 4.3. 4. Average IDA curves (left) and COVs (right) using Sa(T*) as IM and damage index (DI) as damage measure for case 2

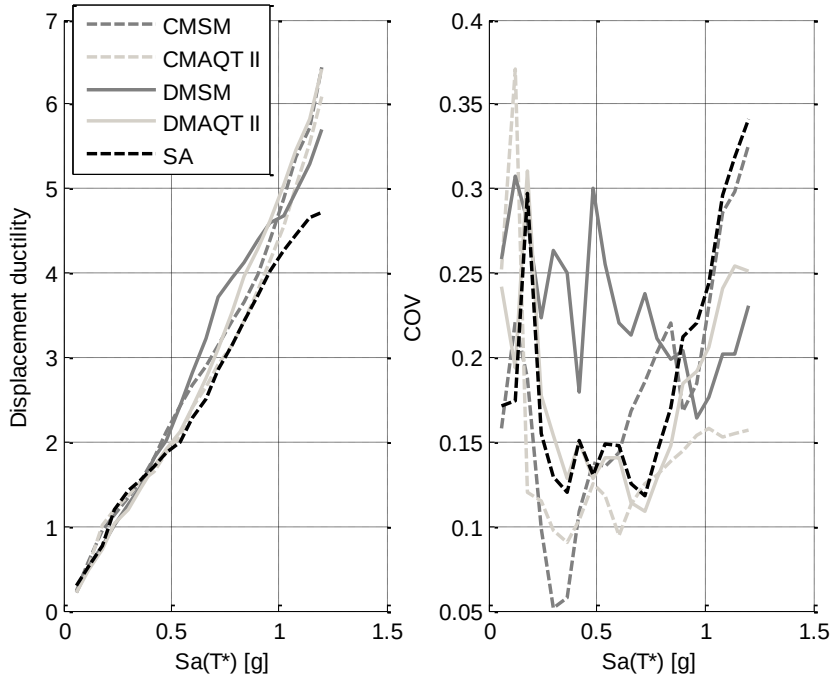

Figure 4.3.5. Average IDA curves (left) and COVs (right) using Sa(T*) as IM and peak displacement ductility as damage measure for case 3

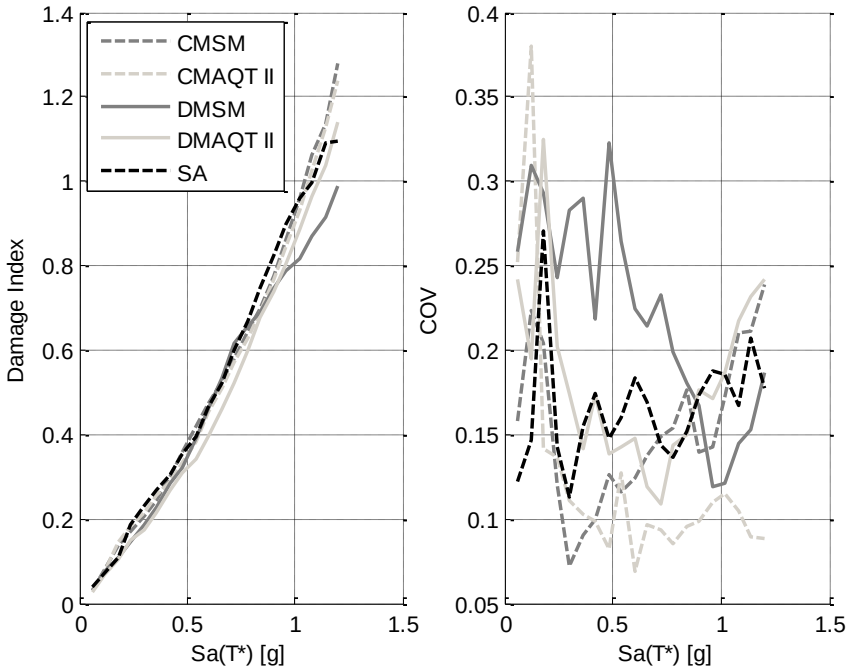

Figure 4.3.6. Average IDA curves (left) and COVs (right) using Sa(T*) as IM and damage index (DI) as damage measure for case 3

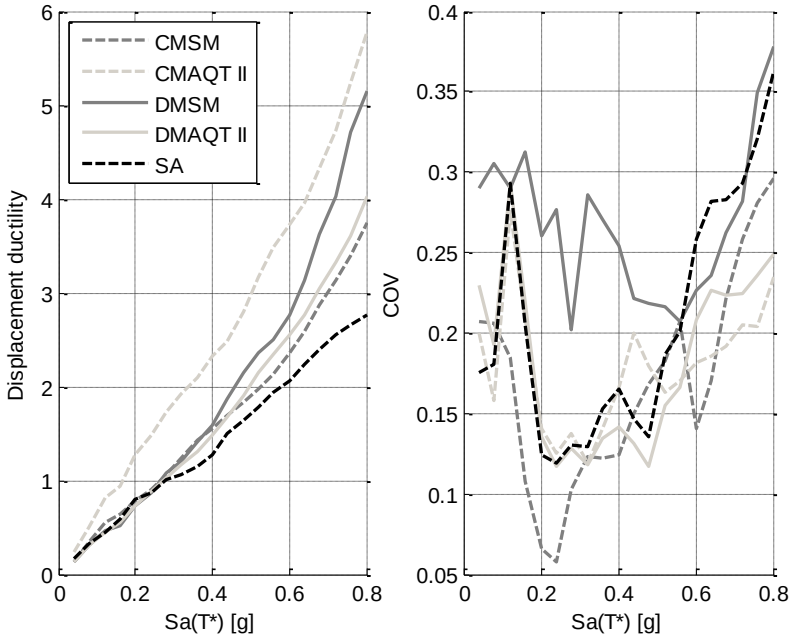

Figure 4.3.7. Average IDA curves (left) and COVs (right) using Sa(T*) as IM and peak displacement ductility as damage measure for case 4

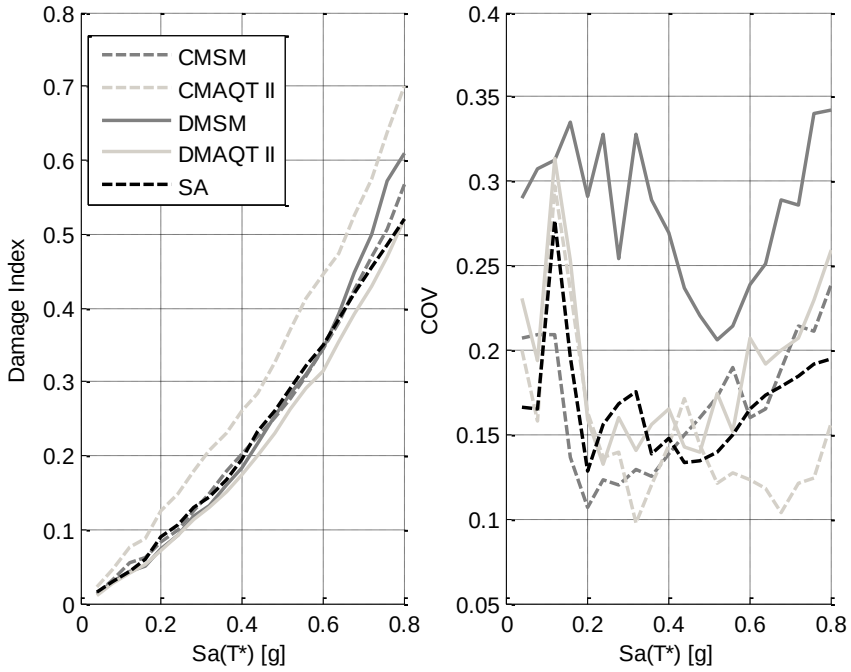

Figure 4.3. 8. Average IDA curves (left) and COVs (right) using Sa(T*) as IM and damage index (DI) as damage measure for case 4

4.4 CAV and AI as IM

For this section the cumulative absolute velocity (CAV) and the Arias intensity (AI) were selected as IMs. Figure 4.4.1 through Figure 4.4.16 present the IDA curves for each one of the cases. The plot in the left shows the curves for each one of the records (50) and the right plot shows the average IDA curves for every earthquake set. The results obtained are in agreement with the obtained in Chapter 3 for a single column: the dispersion in both DMs (ductility and damage index) using the two IMs evaluated (CAV and AI) are quite large when compared to the dispersion obtained using Sa(T*). Plots with PGA, PGV and PGV as IM can be seen in Appendix E. The results obtained are similar to the presented in the previous chapter.

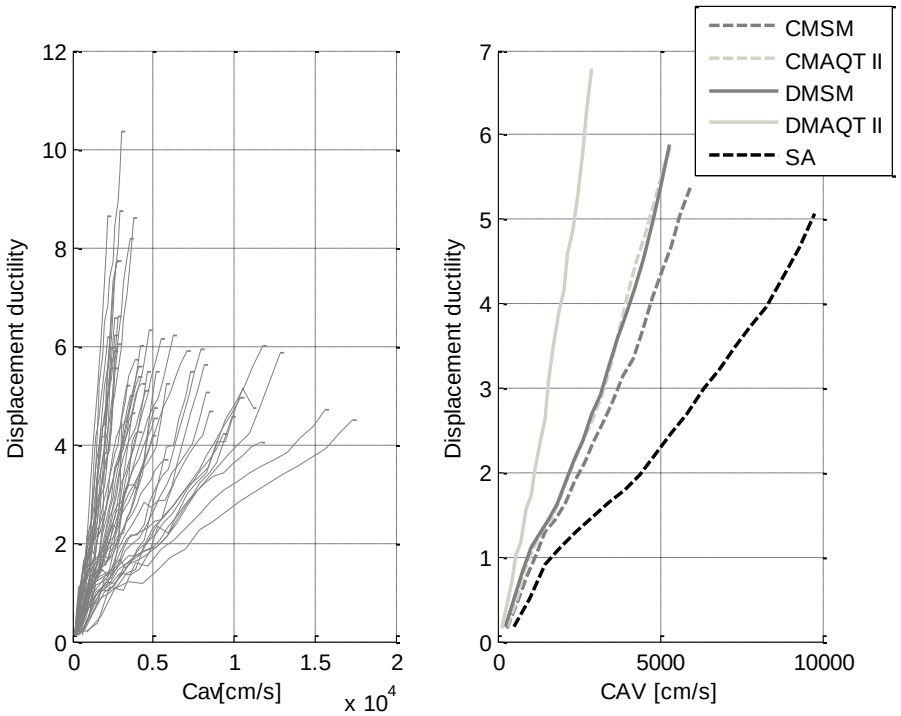

Figure 4.4.1 (a) IDA curves (Ductility vs. CAV) for all artificial earthquakes (b) Average IDA curves (Ductility vs. CAV) by approach for case 1

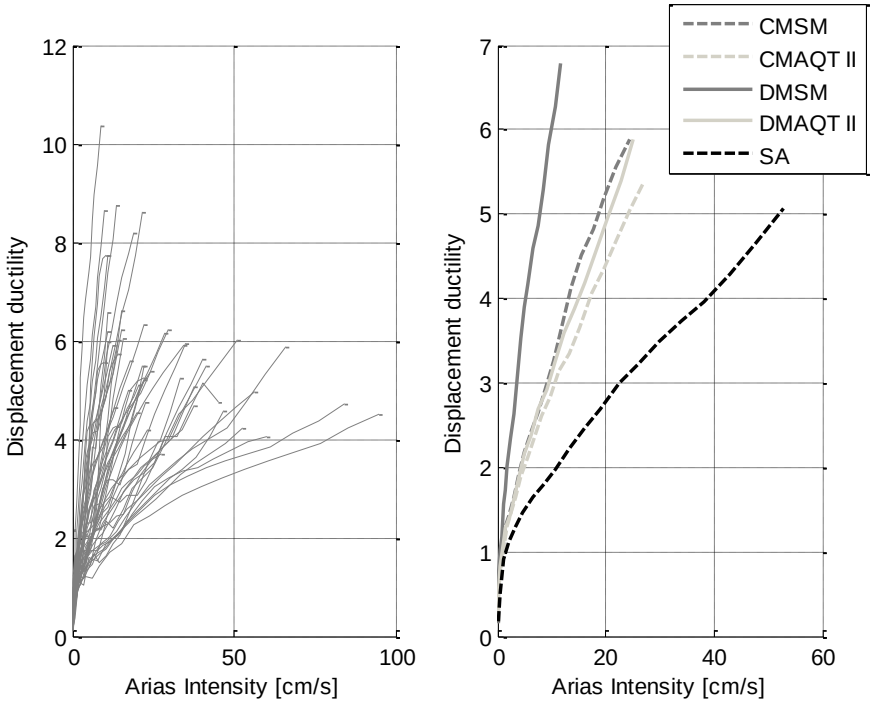

Figure 4.4. 2. (a) IDA curves (Ductility vs. AI) for all artificial earthquakes (b) Average IDA curves (Ductility vs. AI) by approach for case 1

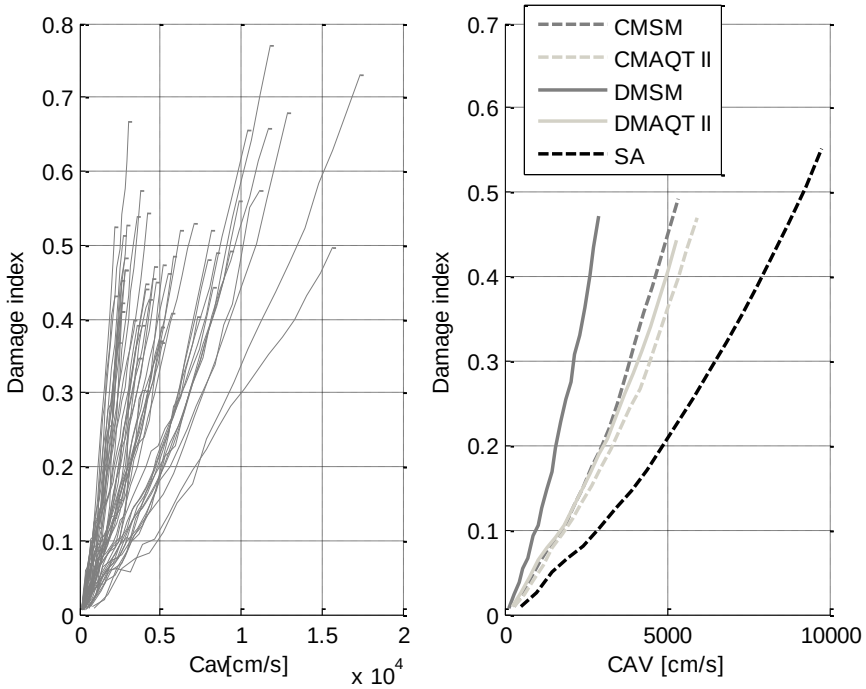

Figure 4.4. 3. (a) IDA curves (DI vs. CAV) for all artificial earthquakes (b) Average IDA curves (DI vs. CAV) by approach for case 1

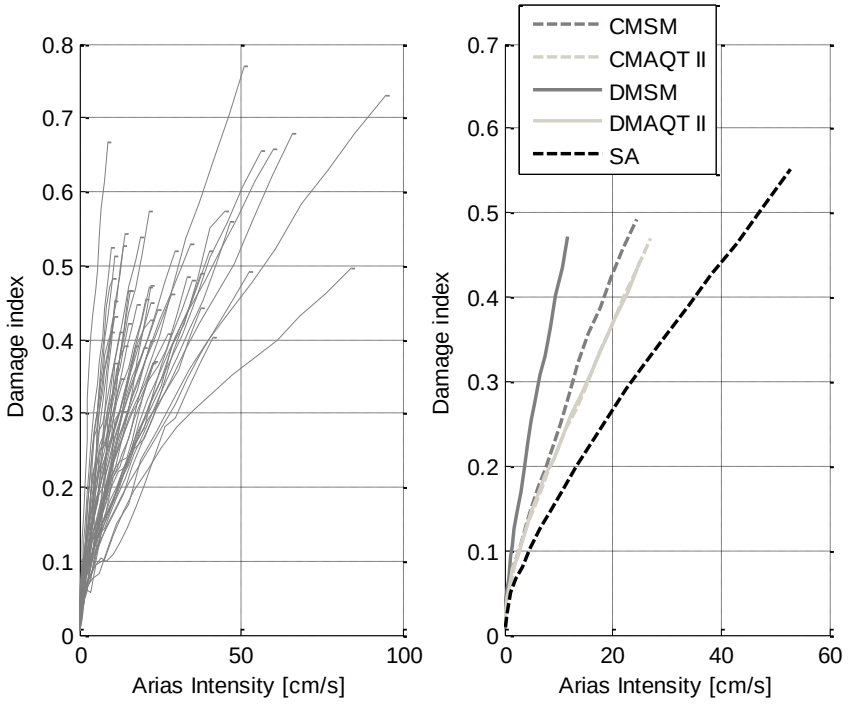

Figure 4.4.4. (a) IDA curves (DI vs. AI) for all artificial earthquakes (b) Average IDA curves (DI vs. AI) by approach for case 1

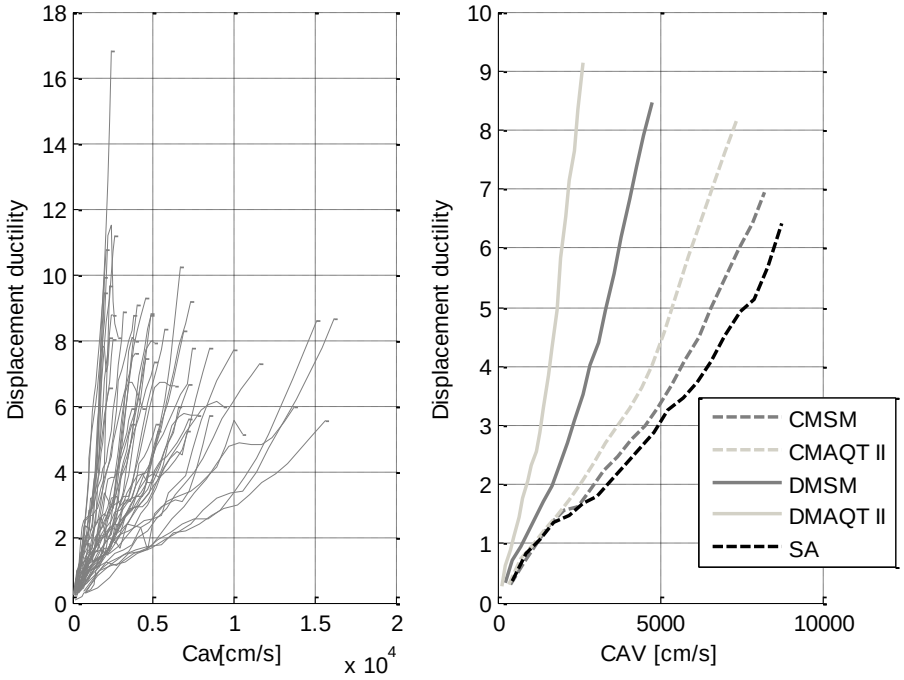

Figure 4.4.5. (a) IDA curves (Ductility vs. CAV) for all artificial earthquakes (b) Average IDA curves (Ductility vs. CAV) by approach for case 2

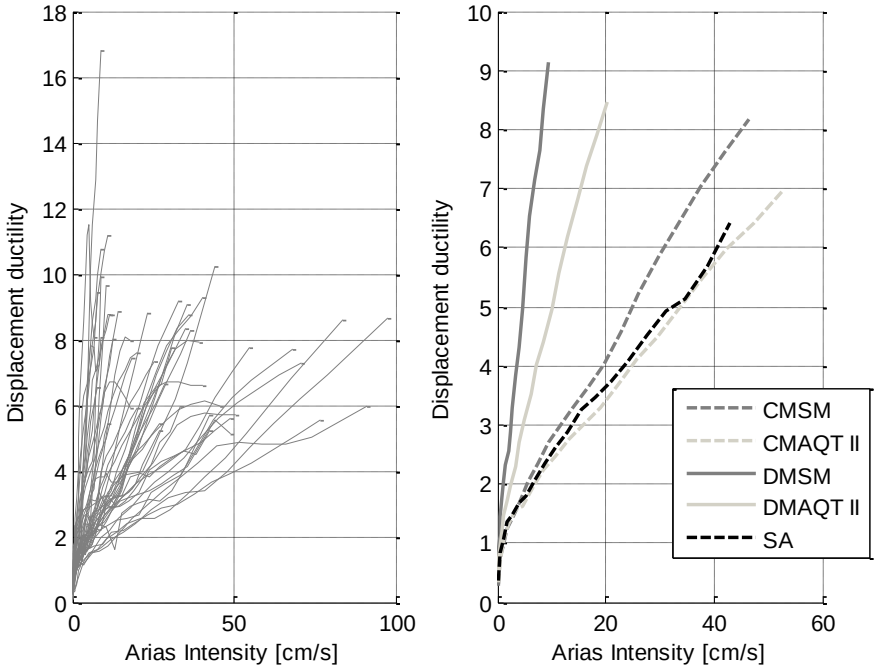

Figure 4.4.6. (a) IDA curves (Ductility vs. AI) for all artificial earthquakes (b) Average IDA curves (Ductility vs. AI) by approach for case 2

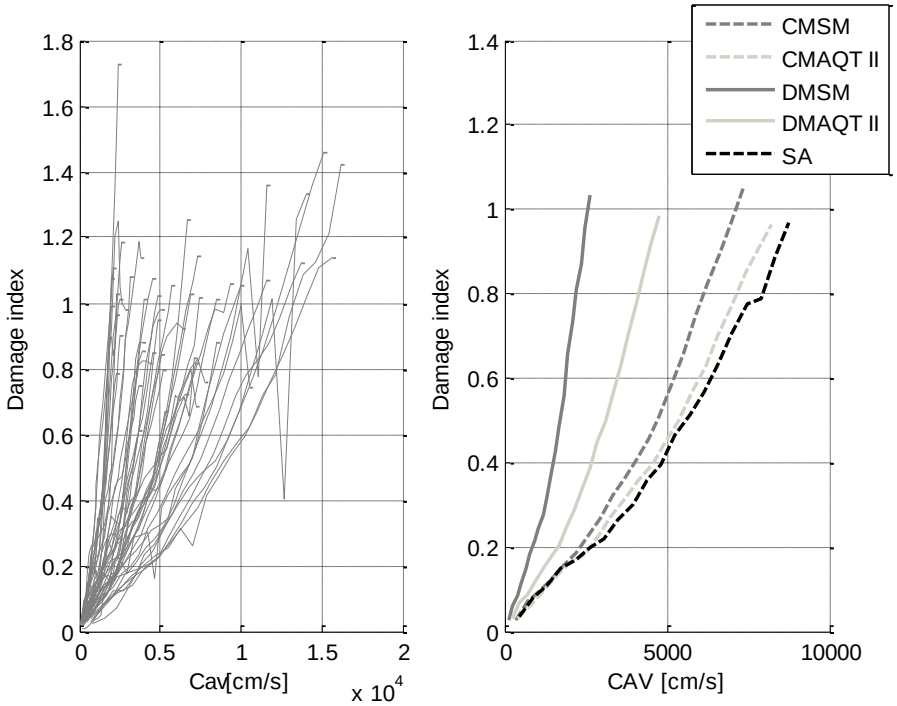

Figure 4.4. 7. (a) IDA curves (DI vs. CAV) for all artificial earthquakes (b) Average IDA curves (DI vs. CAV) by approach for case 2

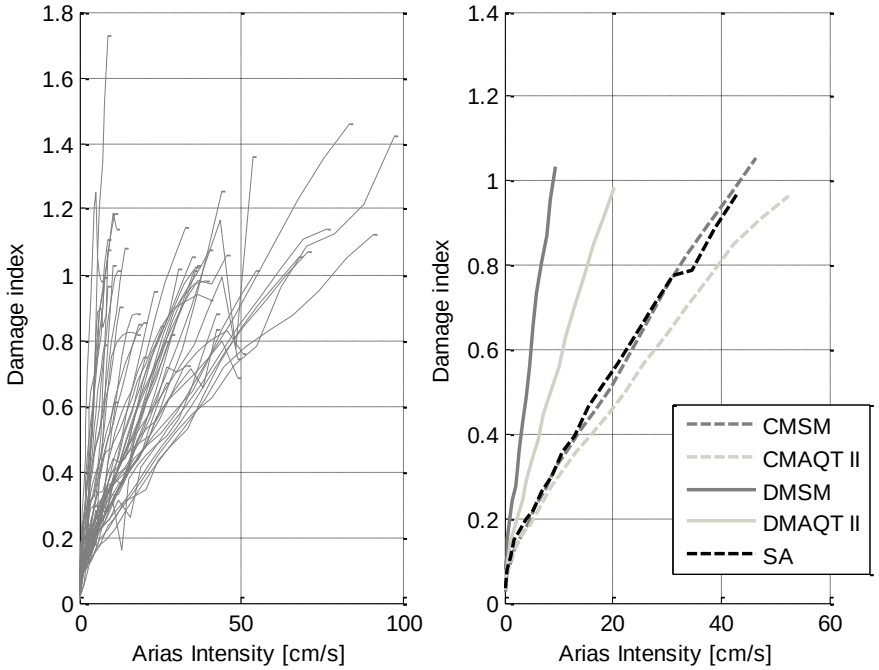

Figure 4.4. 8. (a) IDA curves (DI vs. AI) for all artificial earthquakes (b) Average IDA curves (DI vs. AI) by approach for case 2

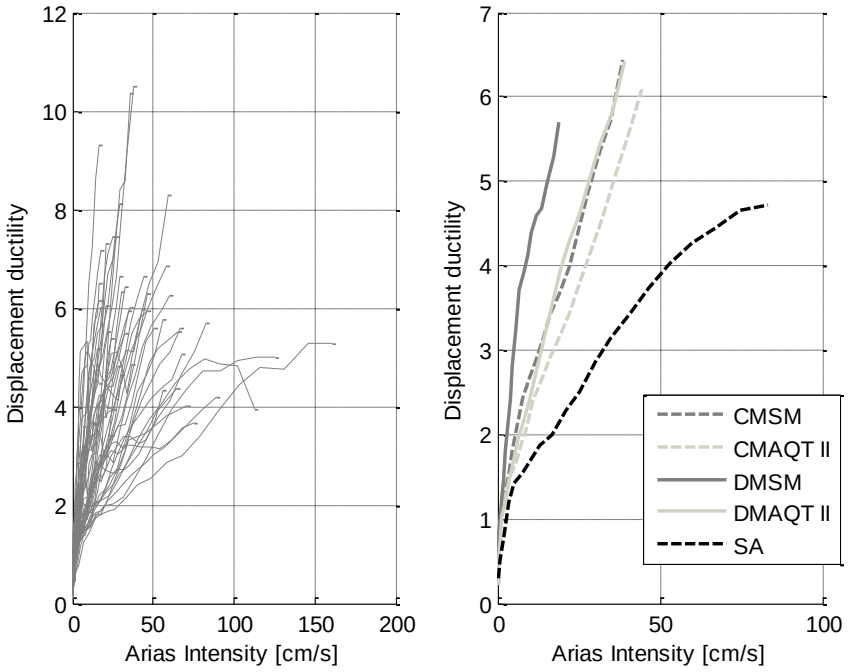

Figure 4.4.9. (a) IDA curves (Ductility vs. CAV) for all artificial earthquakes (b) Average IDA curves (Ductility vs. CAV) by approach for case 3

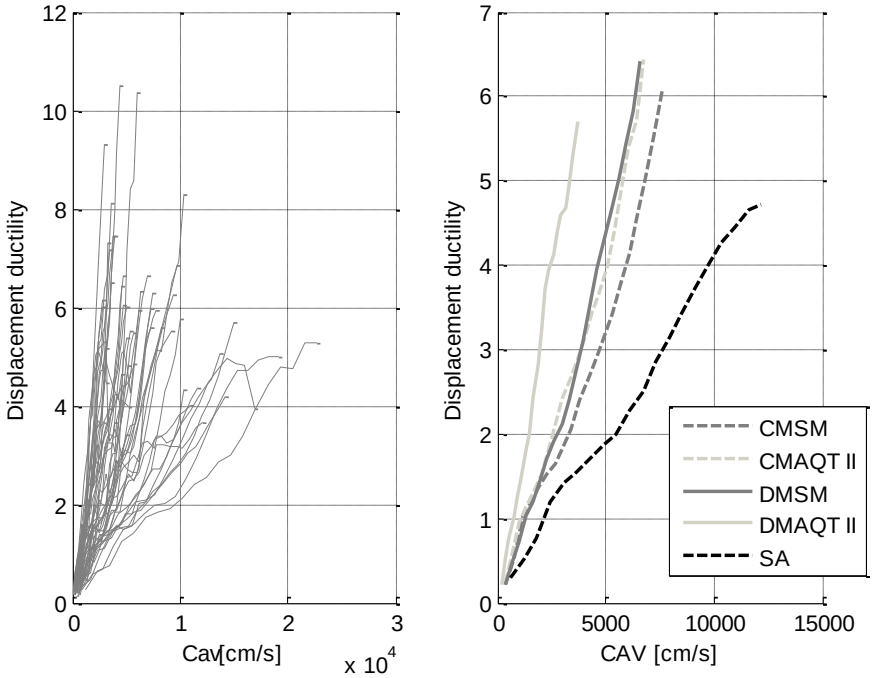

Figure 4.4. 10. (a) IDA curves (Ductility vs. AI) for all artificial earthquakes (b) Average IDA curves (Ductility vs. AI) by approach for case 3

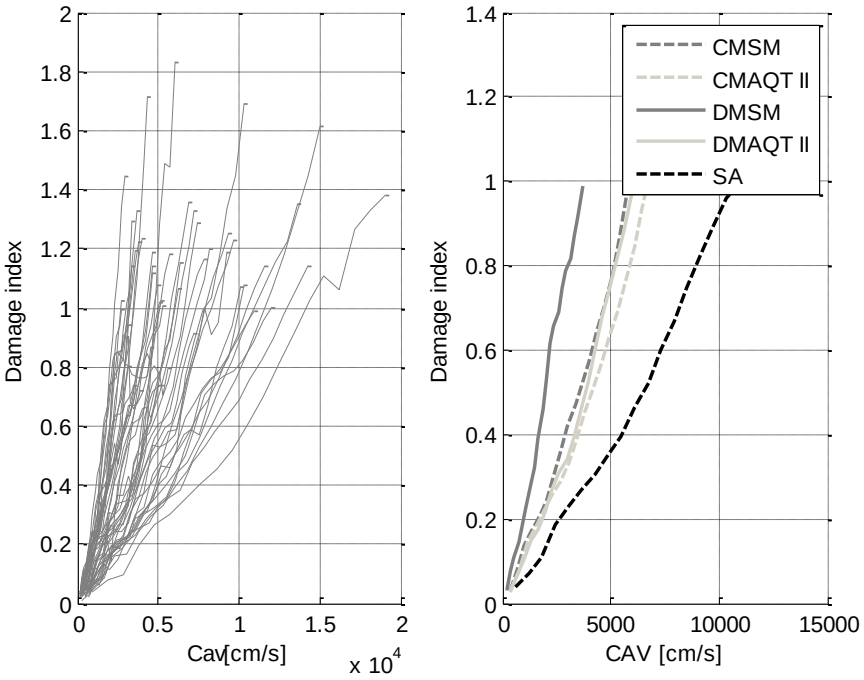

Figure 4.4.11. (a) IDA curves (DI vs. CAV) for all artificial earthquakes (b) Average IDA curves (DI vs. CAV) by approach for case 3

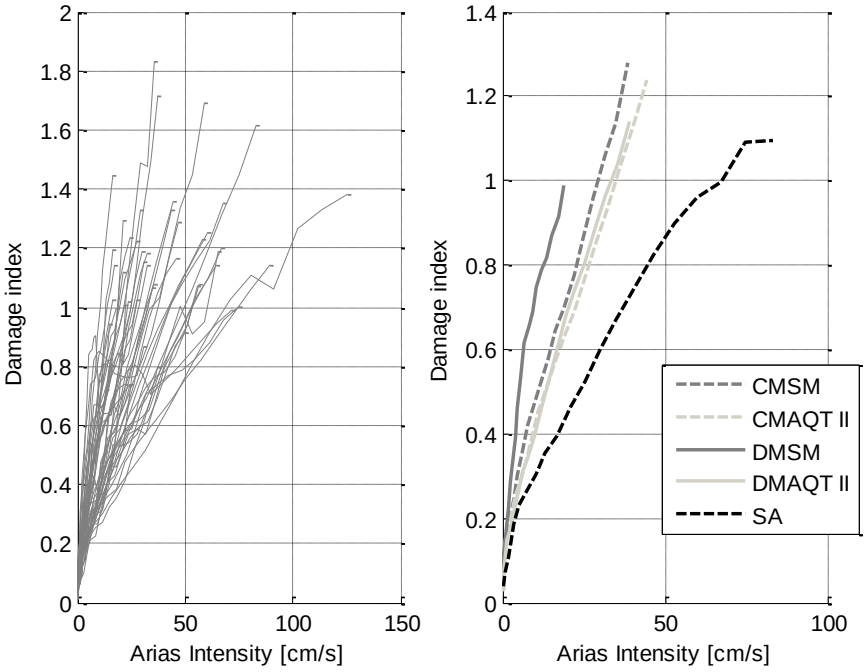

Figure 4.4. 12. (a) IDA curves (DI vs. AI) for all artificial earthquakes (b) Average IDA curves (DI vs. AI) by approach for case 3

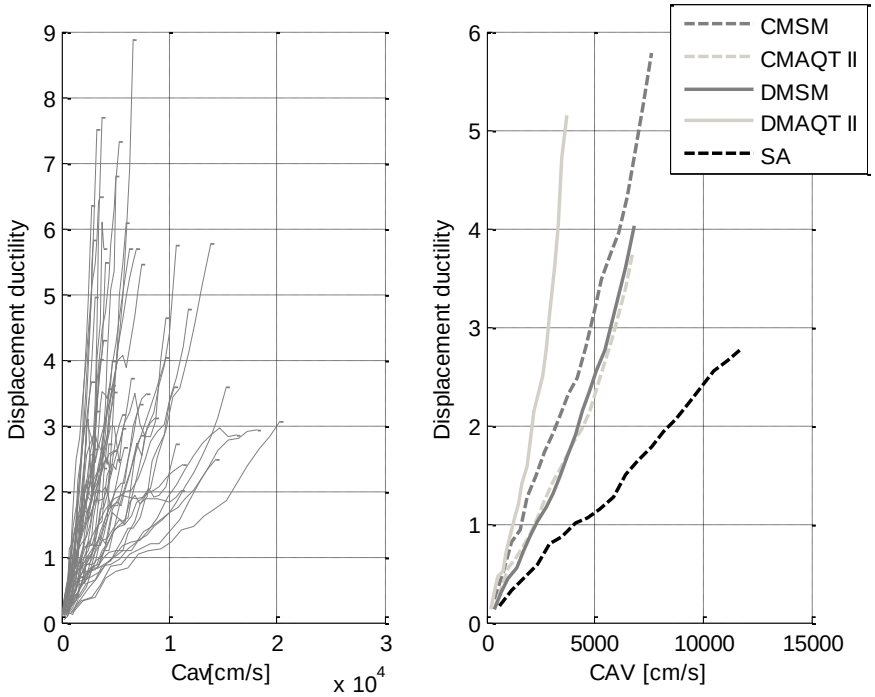

Figure 4.4.13. (a) IDA curves (Ductility vs. CAV) for all artificial earthquakes (b) Average IDA curves (Ductility vs. CAV) by approach for case 4

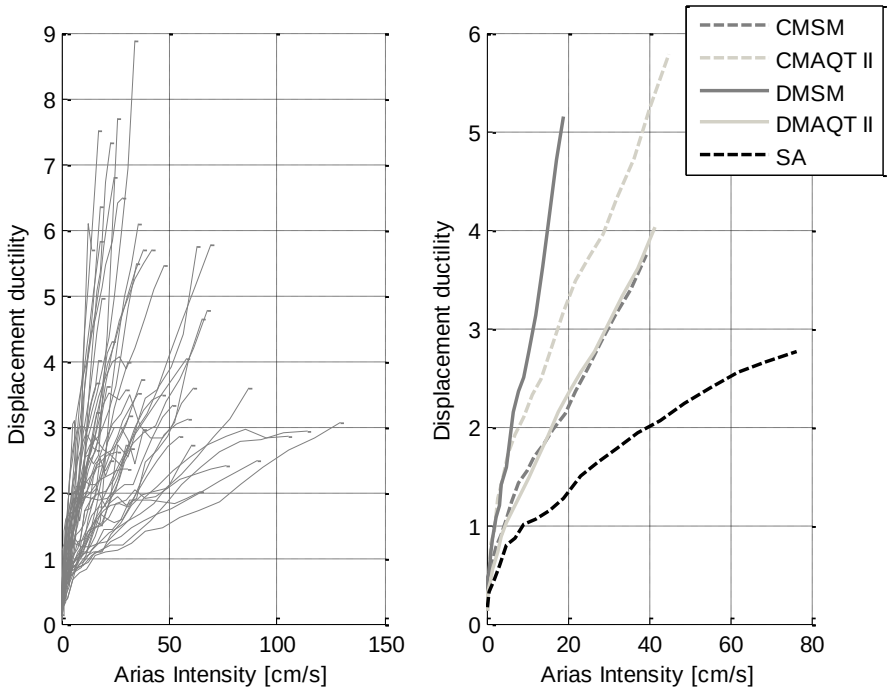

Figure 4.4. 14. (a) IDA curves (Ductility vs. AI) for all artificial earthquakes (b) Average IDA curves (Ductility vs. AI) by approach for case 4

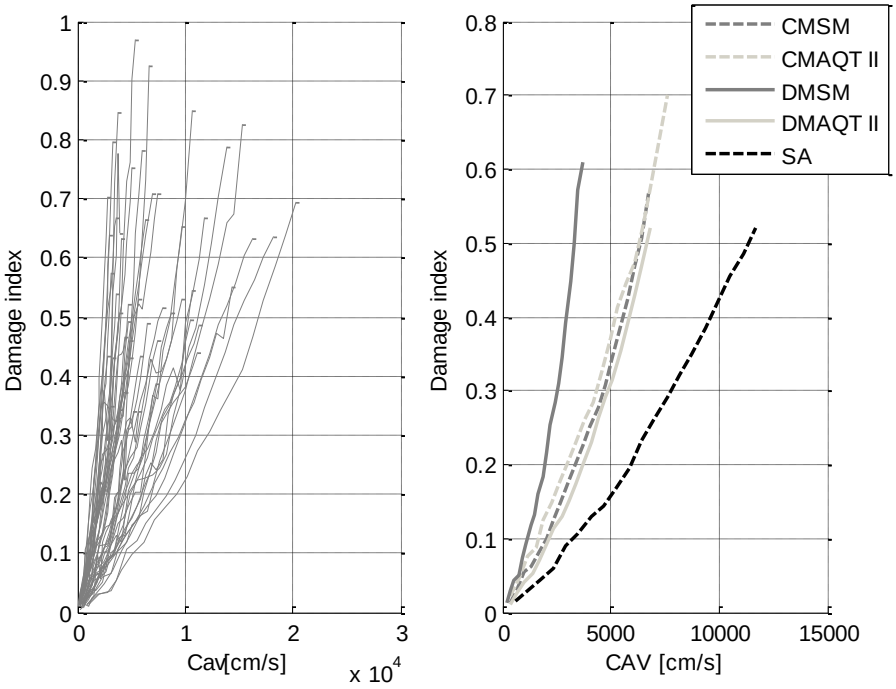

Figure 4.4. 15. (a) IDA curves (DI vs. CAV) for all artificial earthquakes (b) Average IDA curves (DI vs. CAV) by approach for case 4

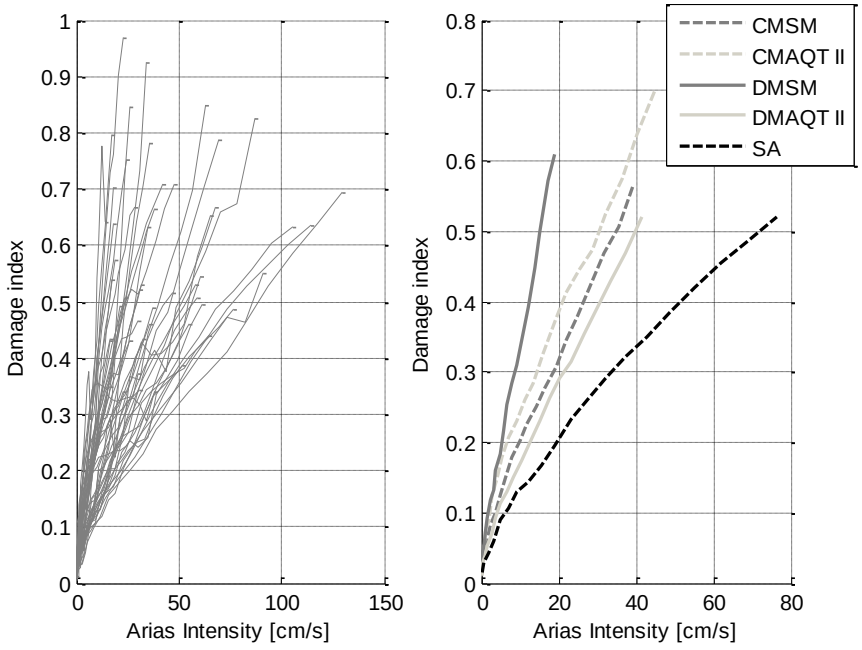

Figure 4.4. 16 (a) IDA curves (DI vs. AI) for all artificial earthquakes (b) Average IDA curves (DI vs. AI) by approach for case 4

4.5 Coefficients of Variation (COV's)

This section presents the coefficient of variation (COV) for all the IMs and earthquake sets for damage index of 0.35 (Figure 4.5.1) and displacement ductility of 2.5 (Figure 4.5.2). These values were the maximum values that can be used to account for all 50 records in the analysis, i.e. these are the smallest of the maximum values reached by the structure on a single record basis. The smaller variations of the intensity measures (IMs) in all cases for both damage measures (ductility and DI) were obtained for Sa(T*) followed by PGA. Then, with significant larger variations we have PGV, CAV, AI and PGD. Comparing the overall results obtained for both DMs evaluated, the DI exhibited less dispersion than the ductility. Looking now at the effect of the initial level of matching of the seed record, it is noticed that less dispersion in the structural response is obtained when the seed motions exhibit some compatibility with the target spectrum; this applies for both methodologies (Wavelet and CWT). Nevertheless, when the distant match records are compared, the IMs generated with the CWT methodology (DMAQT II) exhibit less dispersion in the structural response than those generated based on the addition of wavelets (DMSM).

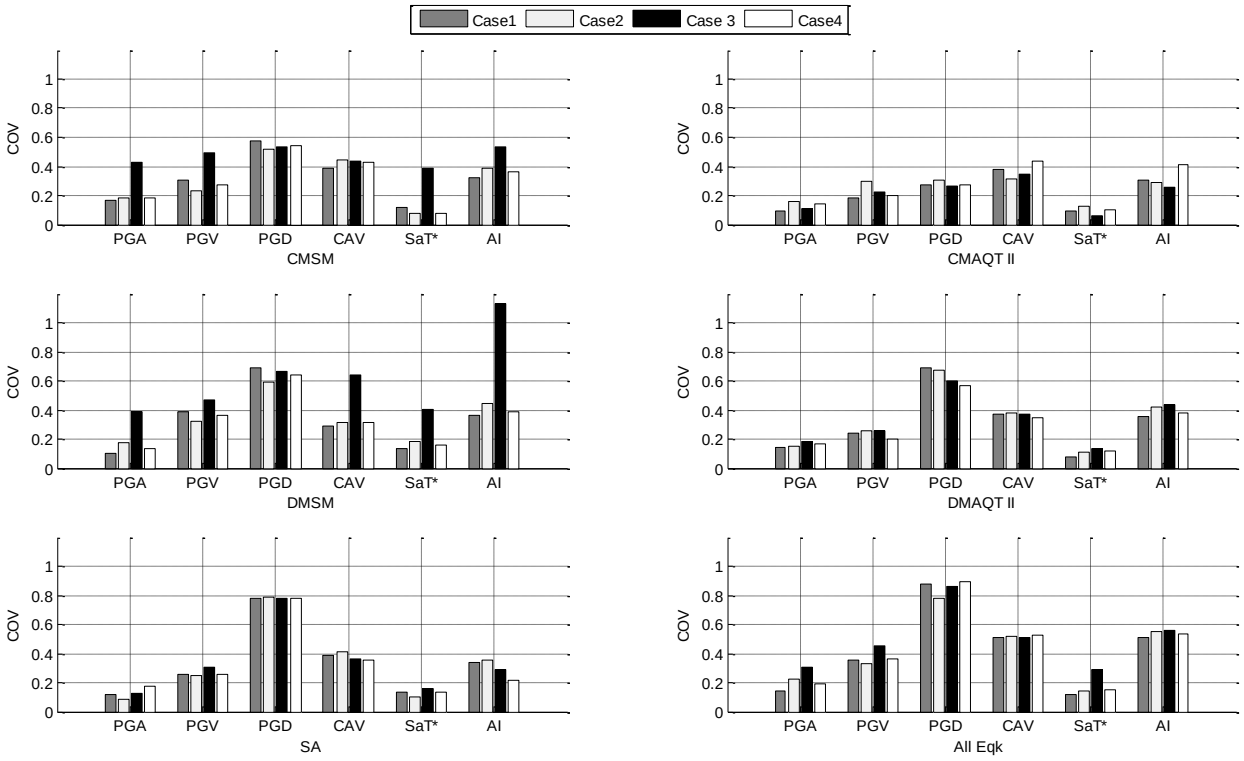

Figure 4.5.1. Coefficient of variation (COV) of the Intensity Measures for 0.35 damage index (DI)

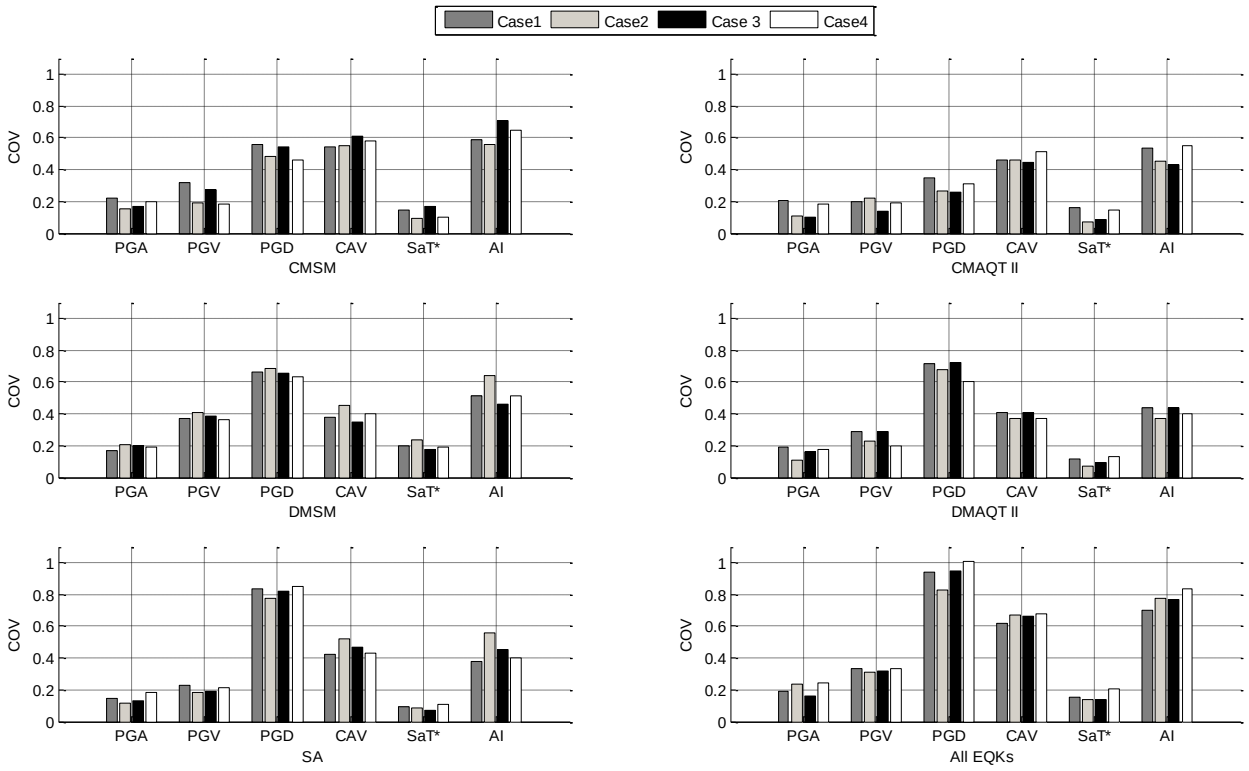

Figure 4.5.2 Coefficient of variation (COV) of the Intensity Measures for displacement ductility of 2.5

4.6 Influence of strong motion duration

As presented in section 3.5 of Chapter 3, there are some parameters which not necessarily change its value when the earthquake is scaled. The influence of significant duration is further investigated in this section, as it was the only one of these factors to exhibit some positive correlation in Chapter 3. Figures 4.6.1 to 4.6.8 present the significant duration plots for displacement ductility and damage index for all the cases scaled at different factors. Because neither case was scaled with the same factor, there are four different sets of scaled factors. It is seen that no positive correlation was obtained with displacement ductility in any of the four cases. However, a positive correlation is noticed with the Ang and Park damage index (DI), especially for the shorter period columns.

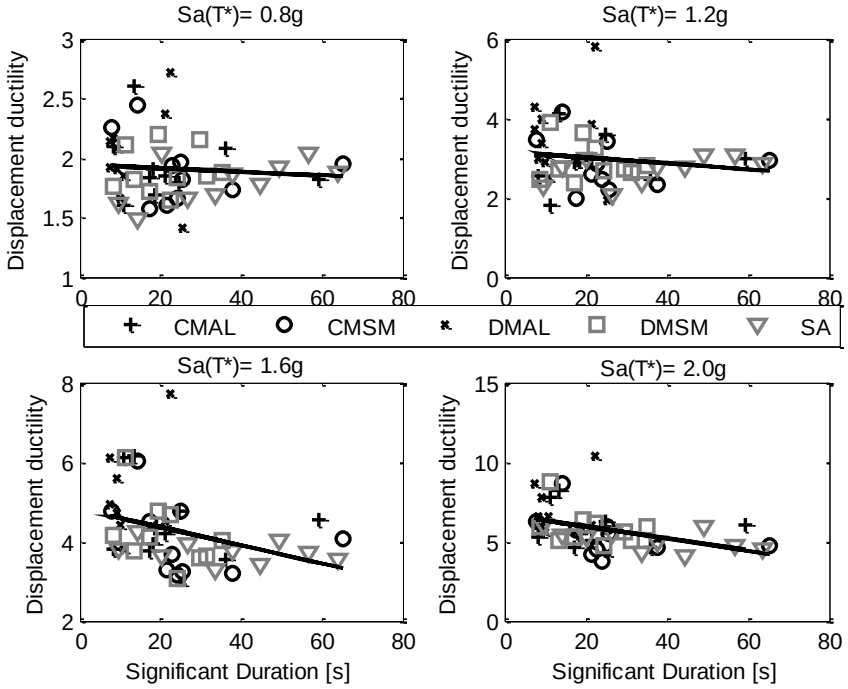

Figure 4.6. 1 Significant duration plots for displacement ductility for case 1

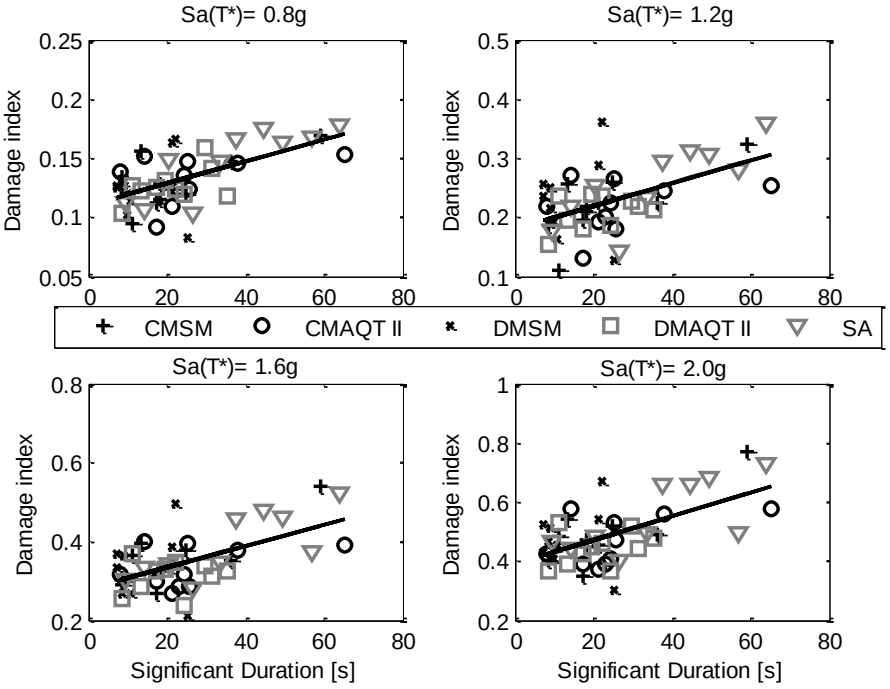

Figure 4.6.2 Significant duration plots for damage index for case 1

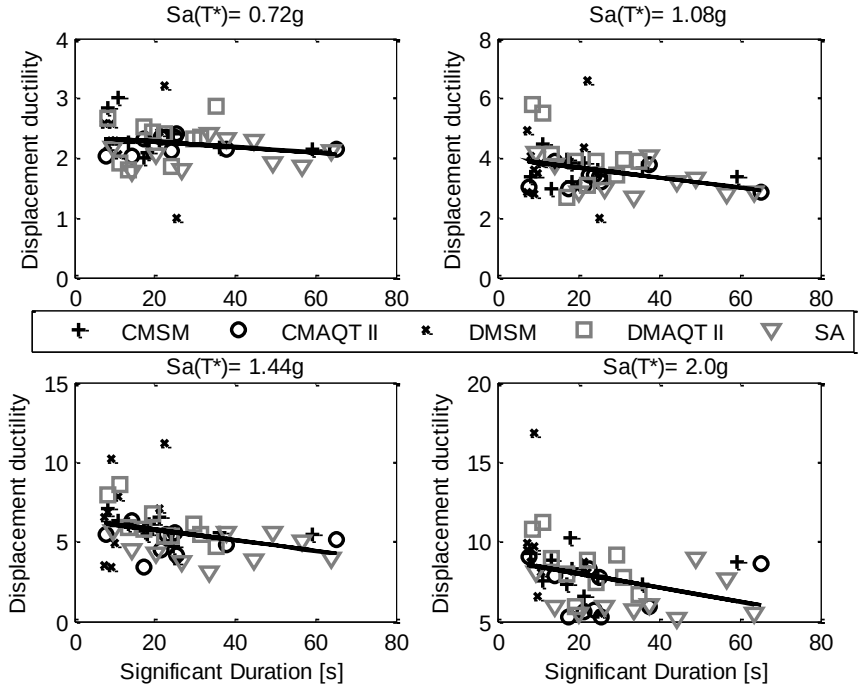

Figure 4.6.3.Significant duration plots for displacement ductility for case 2

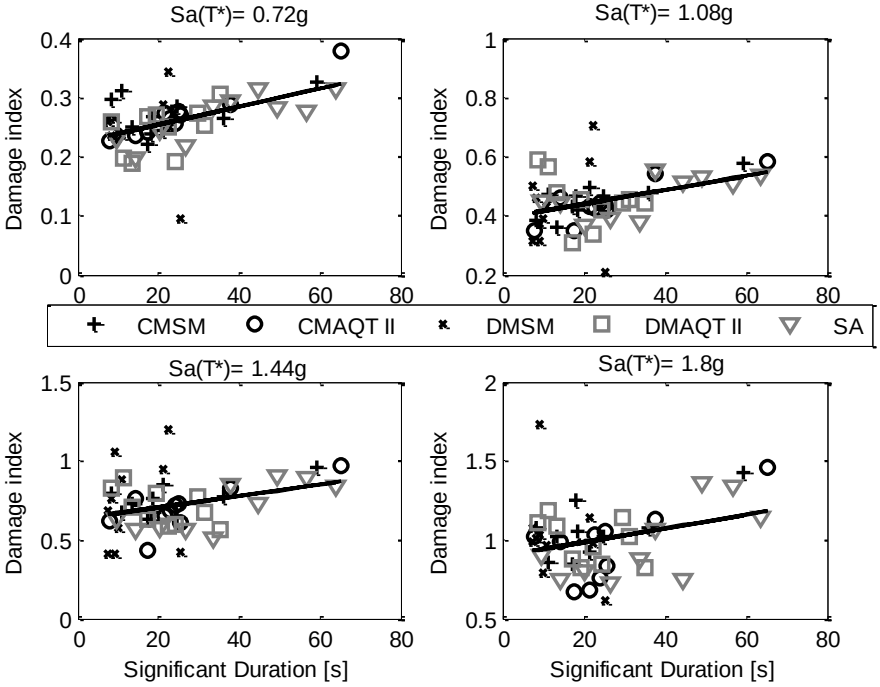

Figure 4.6.4.Significant duration plots for damage index for case 2

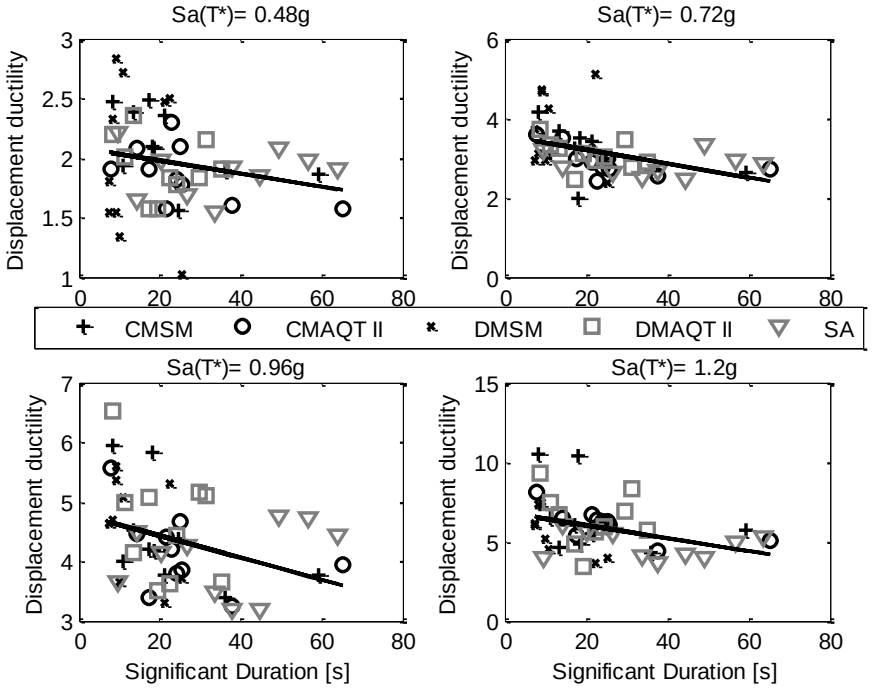

Figure 4.6.5. Significant duration plots for displacement ductility for case 3

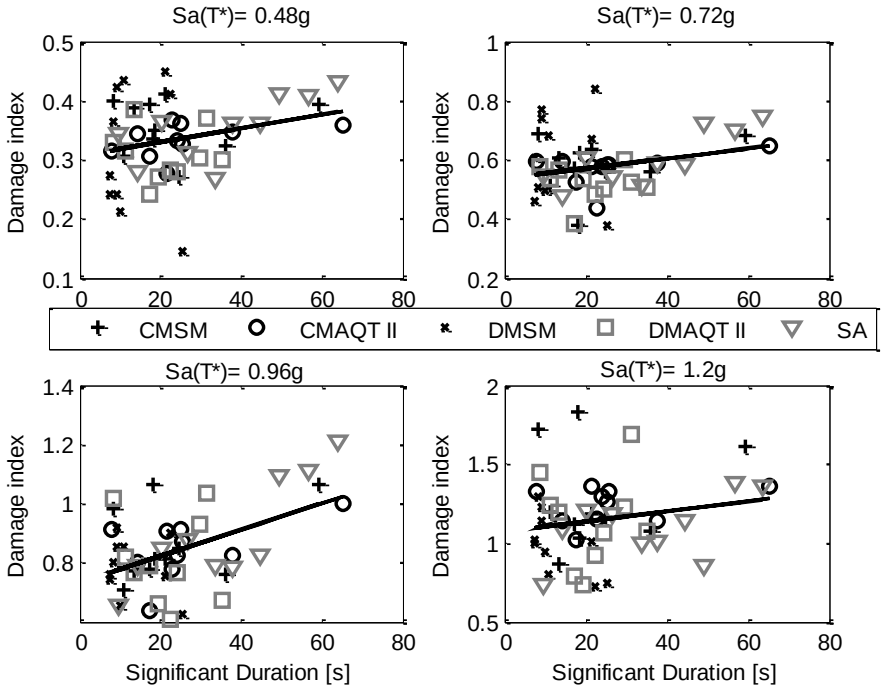

Figure 4.6.6. Significant duration plots for damage index for case 3

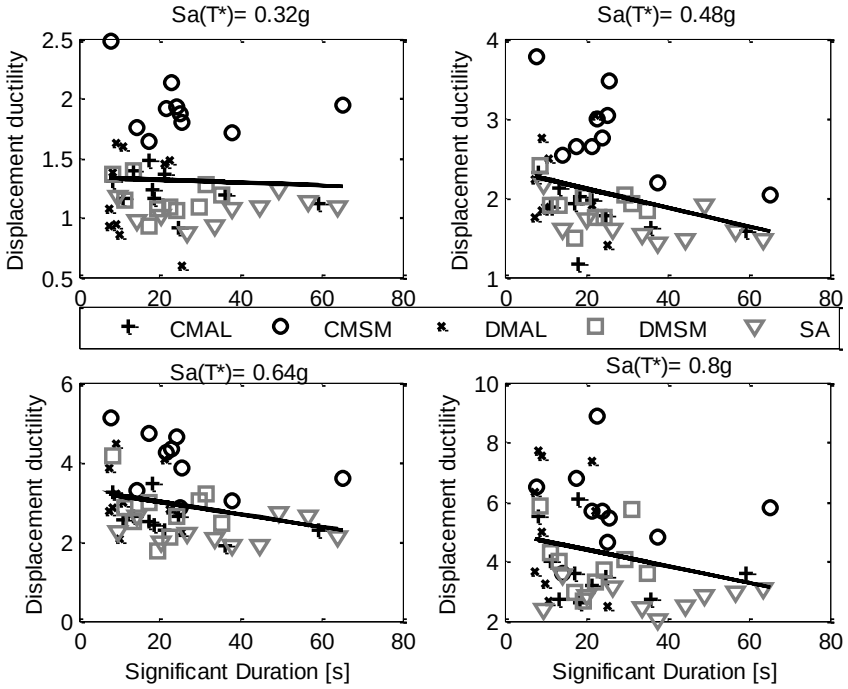

Figure 4.6.7 Significant duration plots for displacement ductility for case 4

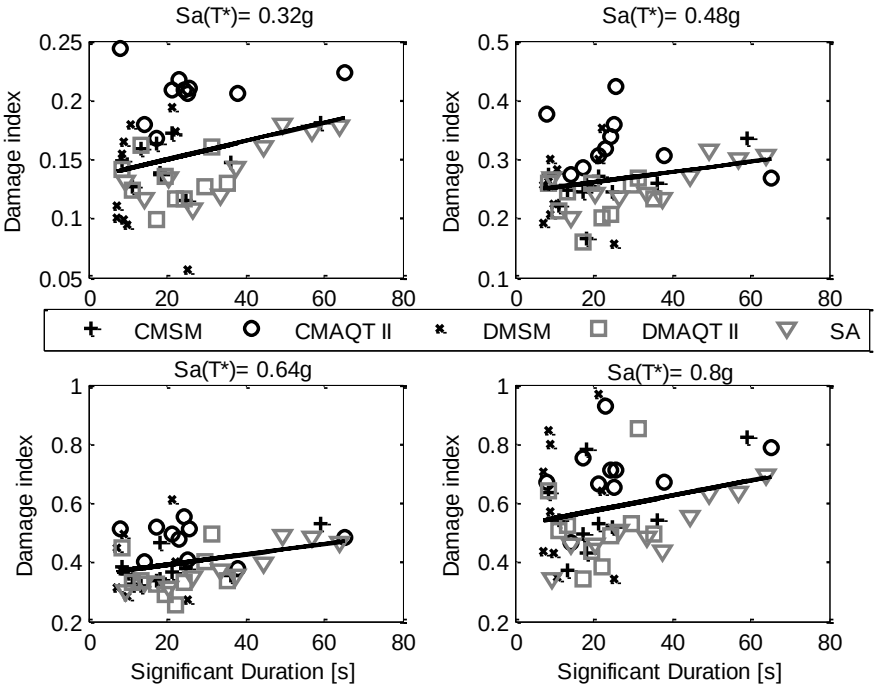

Figure 4.6. 8.Significant duration plots for damage index for case 4

4.7 Conclusions

- The SeismoArtif records continue to exhibit a tendency to induce less inelastic demand in the structure as measured by the peak ductility. However, in terms of the Damage Index (DI) the results obtained are similar for all the suites of records.
- The largest inelastic demand was induced by the records generated by the wavelet approach (SeismoMatch), using seed records with response spectra that largely differ from the target spectrum.
- Compatible records generated with seed records whose response spectral shapes are close to the target spectrum exhibited less dispersion on the structural response of the bridge columns than the records generated from seed records with response spectra that largely differ from the target spectrum. This independent of the methodology used for the record generation (wavelet or CWT).
- Some positive correlation was found between the strong motion duration and the Ang and Park damage index, and this correlation was more noticeable in the shorter period columns. This is in agreement with the results obtained by other researchers (e.g. Hancock and Bommer in 2006 and 2007, Montejo and Kowalsky in 2008).

4.8 References

Hancock, J., Bommer, J.J, (2006),” A State-of-Knowledge Review of the Influence of Strong-Motion Duration on Structural Damage”, *Earthquake Spectra,* v 22, 827-847

Hancock, J., Bommer, J. J., (2007), "Using Spectral Matched Records to Explore the Influence of Strong- Motion Duration on Inelastic Structural Response", *Soil Dynamics and Earthquake Engineering*, v 27, 291-299

Montejo, L. A. and Kowalsky, M. J., (2008), "Estimation of Frequency Dependent Strong Motion Duration via Wavelets and its Influence in Nonlinear Seismic Response." *Computer Aided Civil and Infrastructure Engineering*, v 3, 253-264

CHAPTER 5

5. Conclusions and recommendations

5.1 Summary

This study aimed to evaluate the influence of spectrum compatible records on the inelastic behavior of a reinforced concrete structure. Three methodologies were used to generate a total of 50 spectrum compatible records. One of the methods use a time domain adjustment by adding wavelets to an original time history to generate a compatible record (SeismoMatch), other adjusts the wavelet coefficients of a seed record via CWT (ArtifQuakeLet II) and the last one use a frequency domain modification of an initial random signal to obtain a compatible record. The structure analyzed was a full scale reinforced concrete (RC) bridge column subjected to strong motions in a shaking table at the University of California San Diego. With the experimental data from this test a distributed plasticity fiber based finite element model was developed in OpenSees. In addition to the original case, some length modifications were made in order to obtain structures with different periods of vibration so that each model falls under different regions of the design spectrum. To evaluate the influence of the spectrum compatible records over a wide range of inelastic demand, incremental dynamic analyses (IDA) were performed.

5.2 Conclusions

- In general, all three methodologies were successful generating acceleration series with a response spectrum that matches a prescribed design spectrum. The compatible records with the best match were those generated using a frequency domain approach (SeismoArtif), followed by the CWT based approach (ArtifQuakeLet II) and the Wavelets approach (SeismoMatch).
- For the methodologies working with seeds records it was found that the initial level of match does not significantly affect the level of match that can be attained by the final compatible record. However, the characteristics of the seed records are much better preserved in the compatible records when the initial spectral match is close.
- The frequency domain approach (SeismoArtif) records exhibited unrealistic strong motion characteristics and a constant tendency to induce less inelastic demand in the structure (same for all cases) as measured by the peak ductility.
- The largest inelastic demand was induced by the records generated using the Wavelet approach (SeismoMatch) when the seed records spectra differ from the target spectrum (DM). However, when the seed records are selected based on the initial spectra compatibility, the results of the IDA when using spectrum compatible records generated by either of the approaches evaluated (Wavelets and CWT) are similar.
- Compatible records generated based on seed records with response spectra shapes close to the target spectrum exhibited less dispersion on the structural response of the bridge columns than the records generated from seed records whose response spectra largely differ from the target spectrum, independent of the methodology used for the record generation (Wavelets or CWT).

- The most appropriate Intensity Measure for the Incremental Dynamic Analyses performed was the spectral acceleration at the natural period of which the structure reaches a ductility equal to 1.
- A positive correlation was found between strong motion duration and the Ang and Park damage index and such correlation was more noticeable in the shorter period columns.

5.3 Recommendations for further research

The conclusions of this work are limited to the type of the structure studied, i.e. a well detailed flexural controlled structure with a very dominant mode. Therefore, it is recommended to extend this study to other type of structural systems. Short period structures with substantial stiffness degradation or large multi-story structures with important higher mode contribution, for example, could be more sensitive to different strong motion characteristics. Notice also that all of the compatible records generated were compatible with the same target spectrum (ASCE 7). It is recommended that other type of design spectra be used in further studies.

APPENDIX A

A. Time histories of acceleration, velocity and displacement

A.1 SeismoMatch Close Match

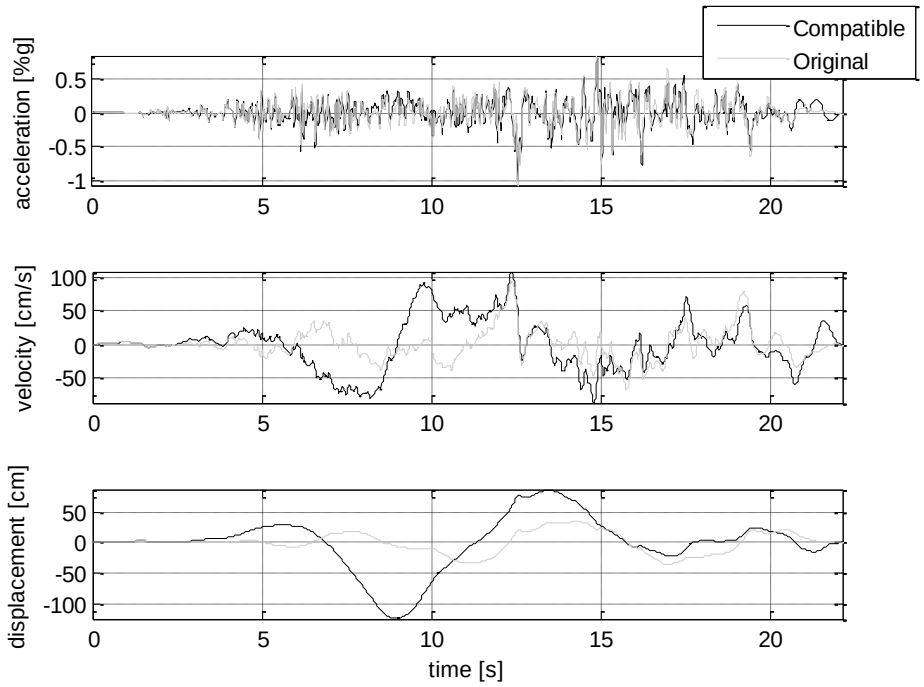

Figure A.1. 1 Time histories of acceleration, velocity and displacement for the scaled seed record and the compatible earthquake record CM1.

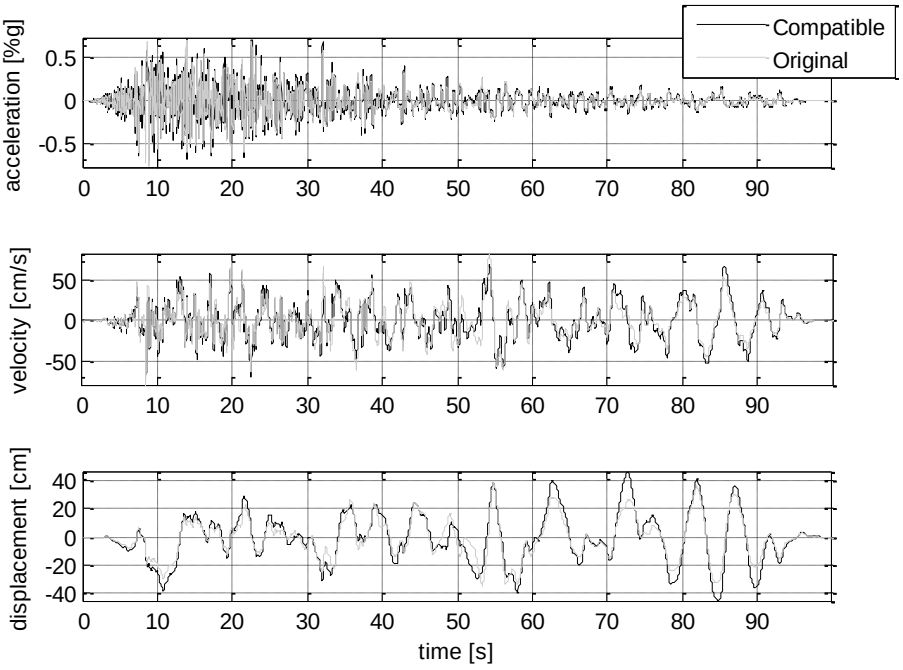

Figure A.1. 2 Time histories of acceleration, velocity and displacement for the scaled seed record and the compatible earthquake record CM2

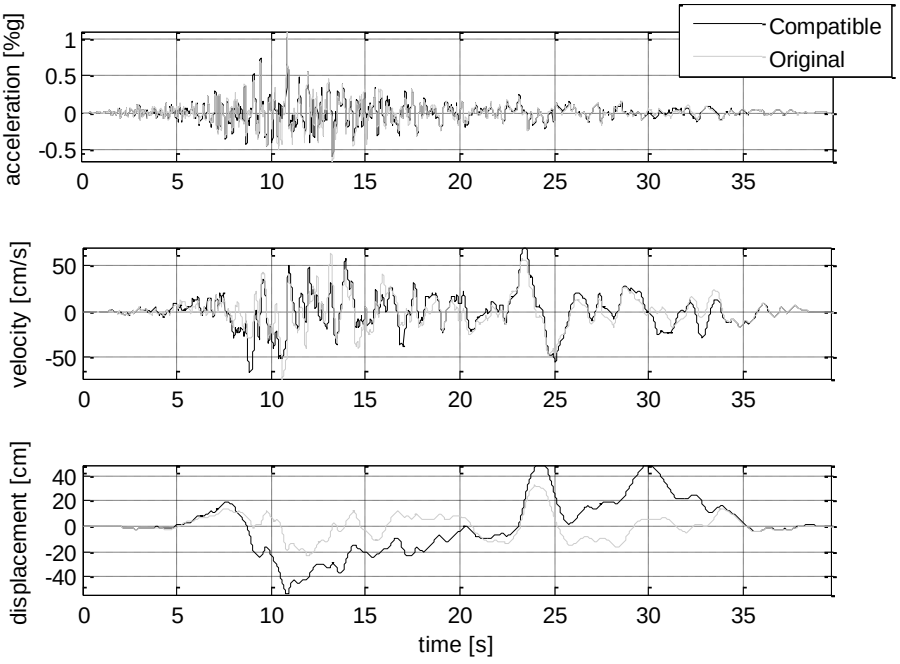

Figure A.1. 3. Time histories of acceleration, velocity and displacement for the scaled seed record and the compatible earthquake record CM3

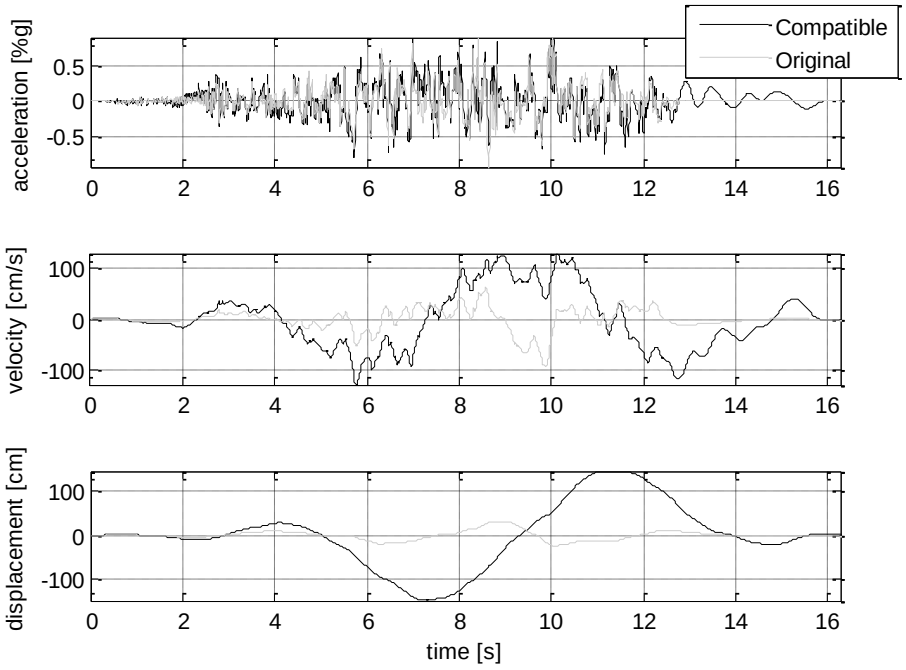

Figure A.1. 4. Time histories of acceleration, velocity and displacement for the scaled seed record and the compatible earthquake record CM4.

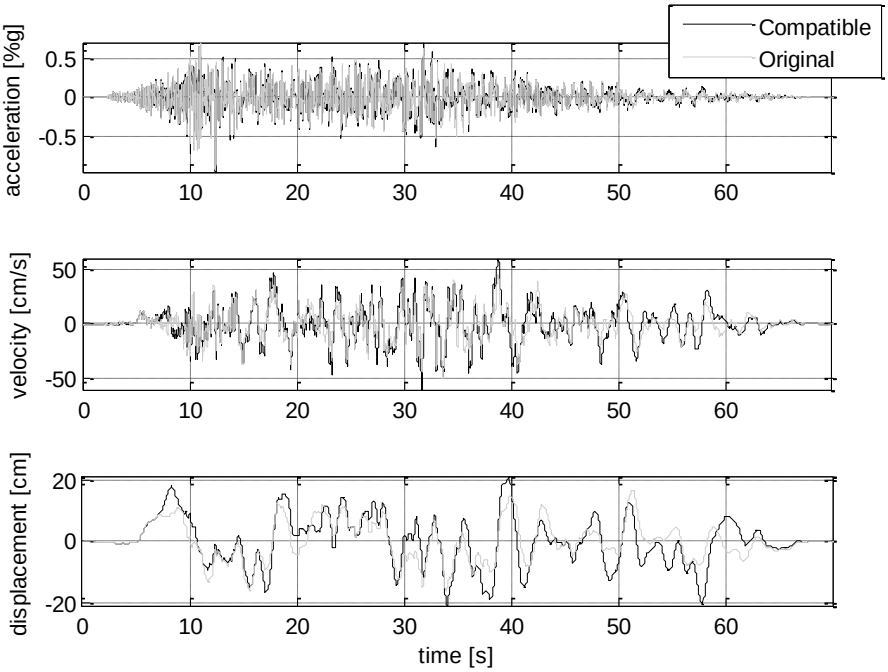

Figure A.1. 5. Time histories of acceleration, velocity and displacement for the scaled seed record and the compatible earthquake record CM5.

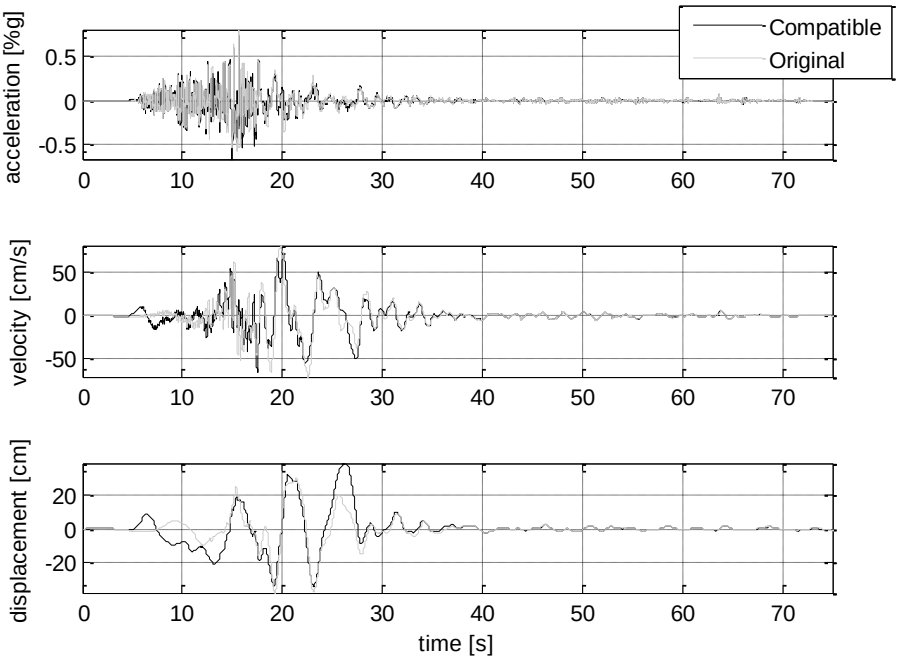

Figure A.1. 6. Time histories of acceleration, velocity and displacement for the scaled seed record and the compatible earthquake record CM6.

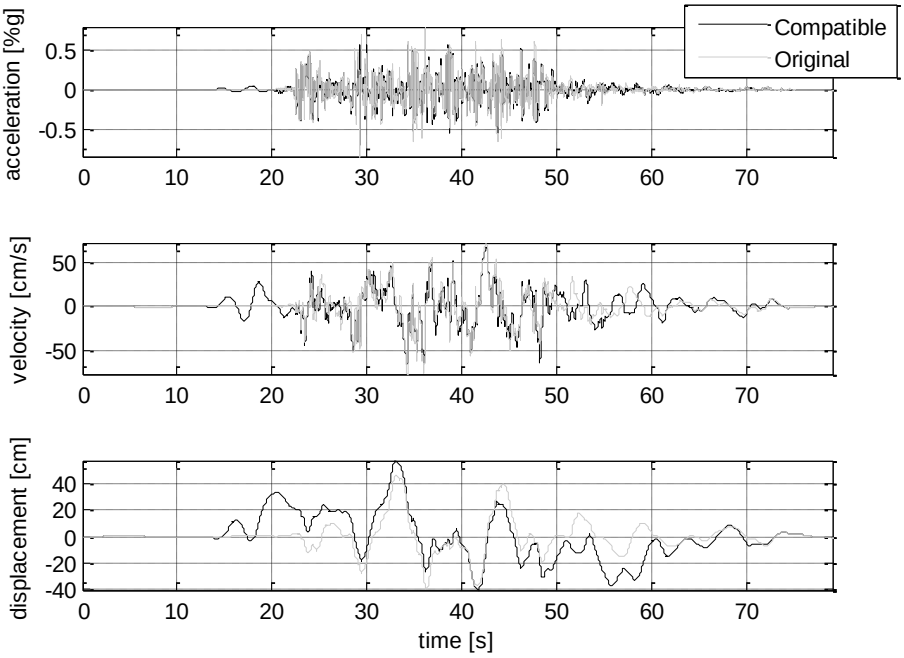

Figure A.1. 7. Time histories of acceleration, velocity and displacement for the scaled seed record and the compatible earthquake record CM7.

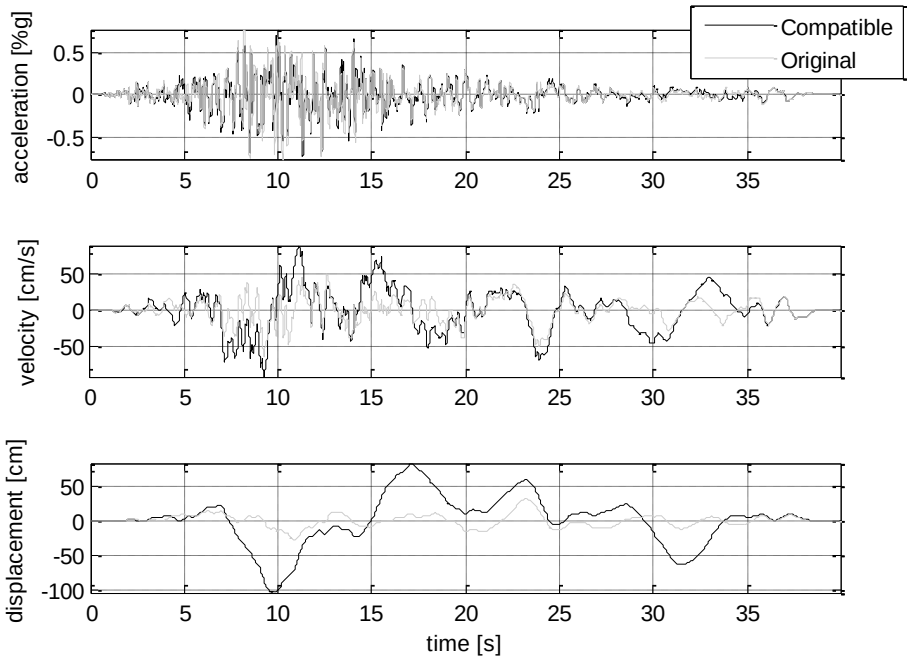

Figure A.1. 8. Time histories of acceleration, velocity and displacement for the scaled seed record and the compatible earthquake record CM8.

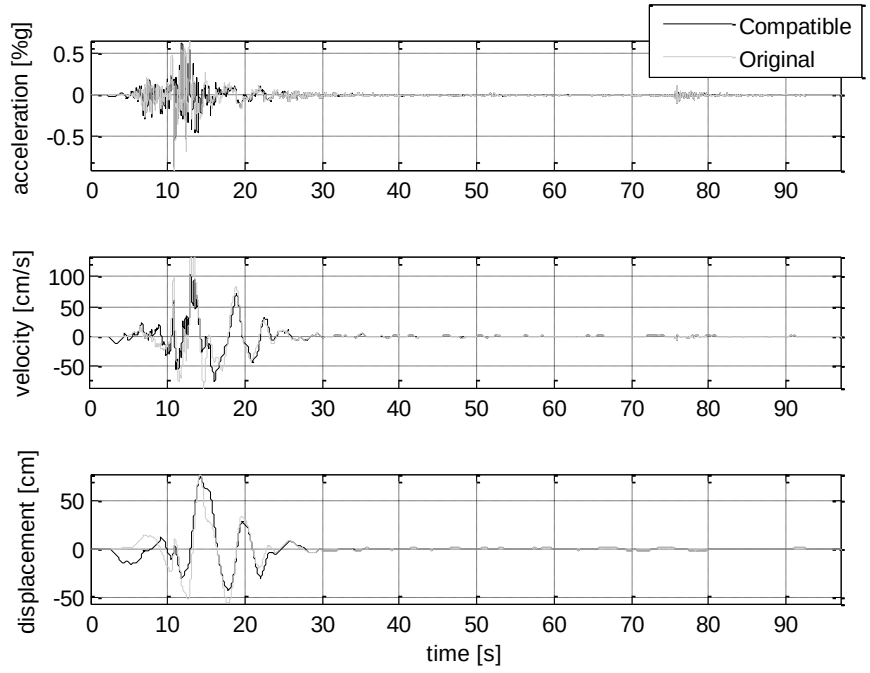

Figure A.1. 9. Time histories of acceleration, velocity and displacement for the scaled seed record and the compatible earthquake record CM9.

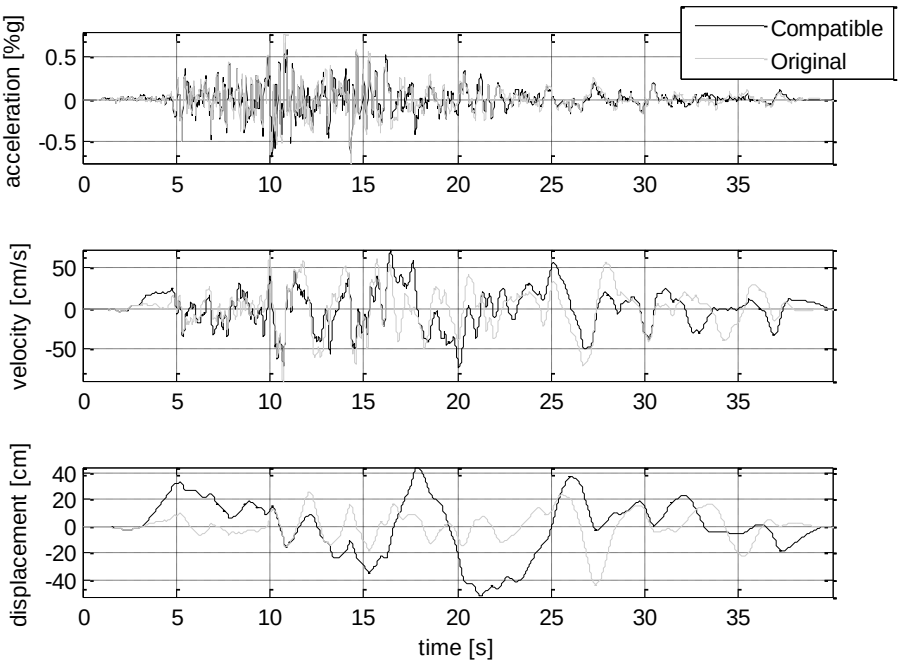

Figure A.1. 10. Time histories of acceleration, velocity and displacement for the scaled seed record and the compatible earthquake record CM10.

A.2. SeismoMatch Distant Match

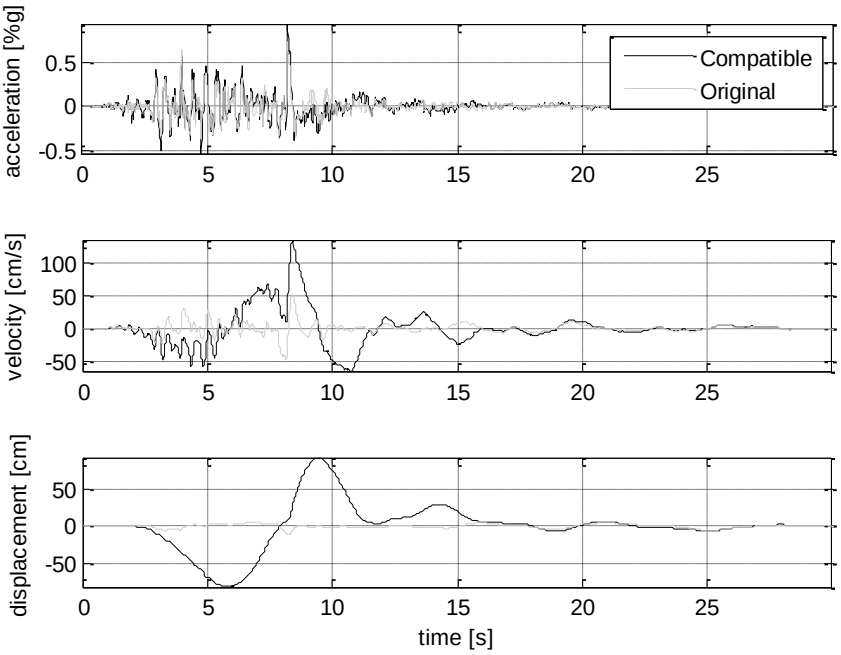

Figure A.2. 1 Time histories of acceleration, velocity and displacement for the scaled seed record and the compatible earthquake record DM1

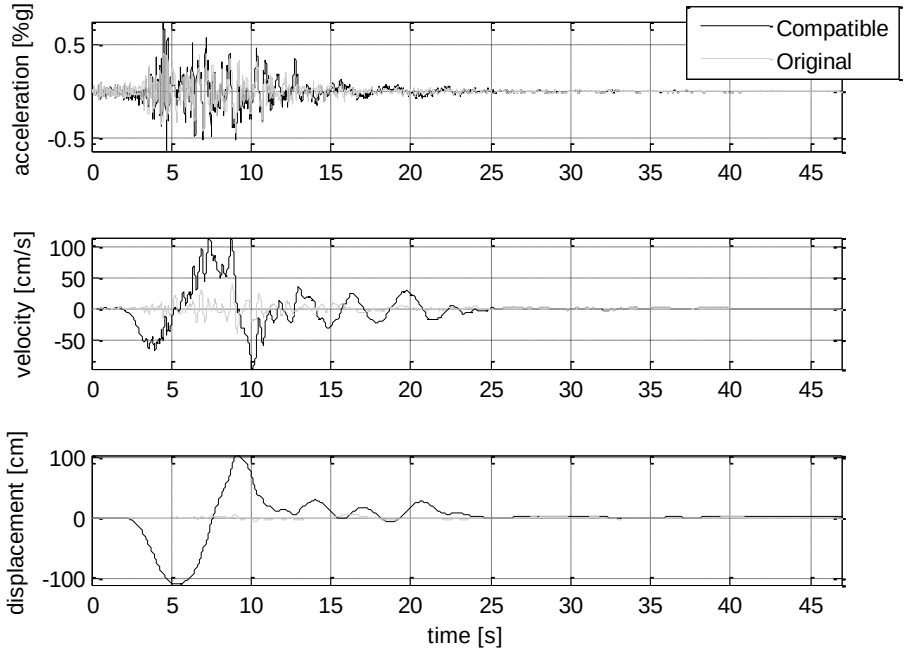

Figure A.2. 2. Time histories of acceleration, velocity and displacement for the scaled seed record and the compatible earthquake record DM2.

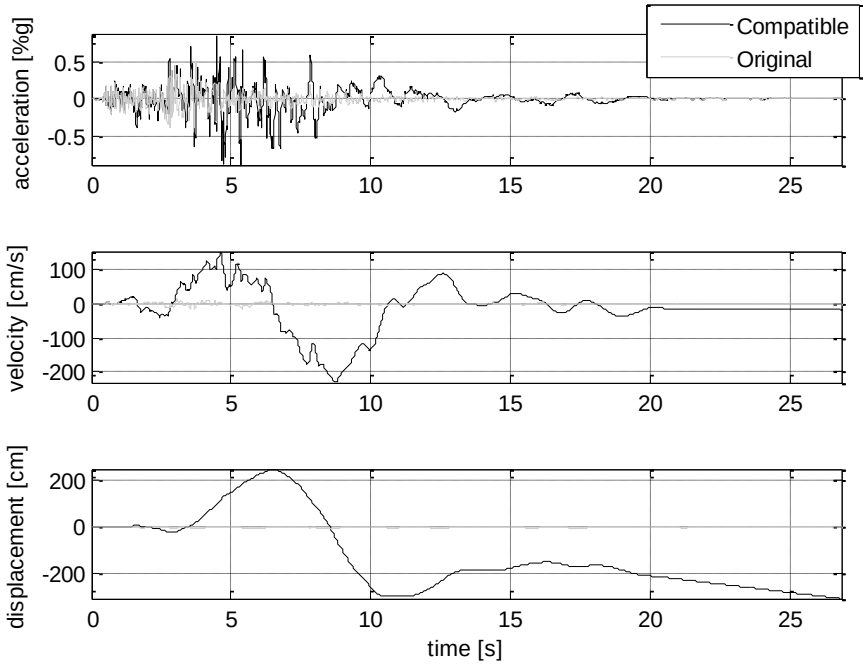

Figure A.2. 3. Time histories of acceleration, velocity and displacement for the scaled seed record and the compatible earthquake record DM3.

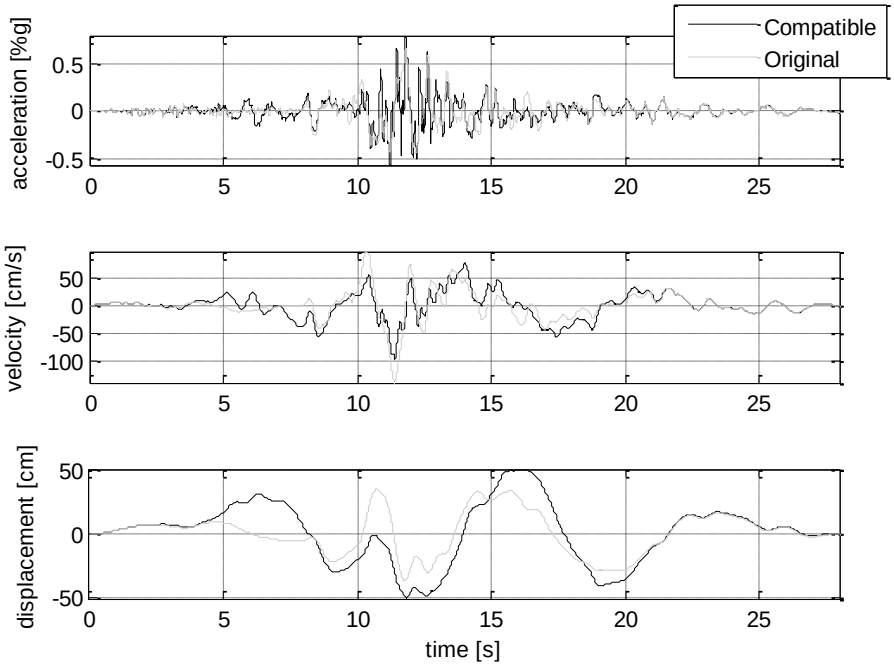

Figure A.2. 4. Time histories of acceleration, velocity and displacement for the scaled seed record and the compatible earthquake record DM4.

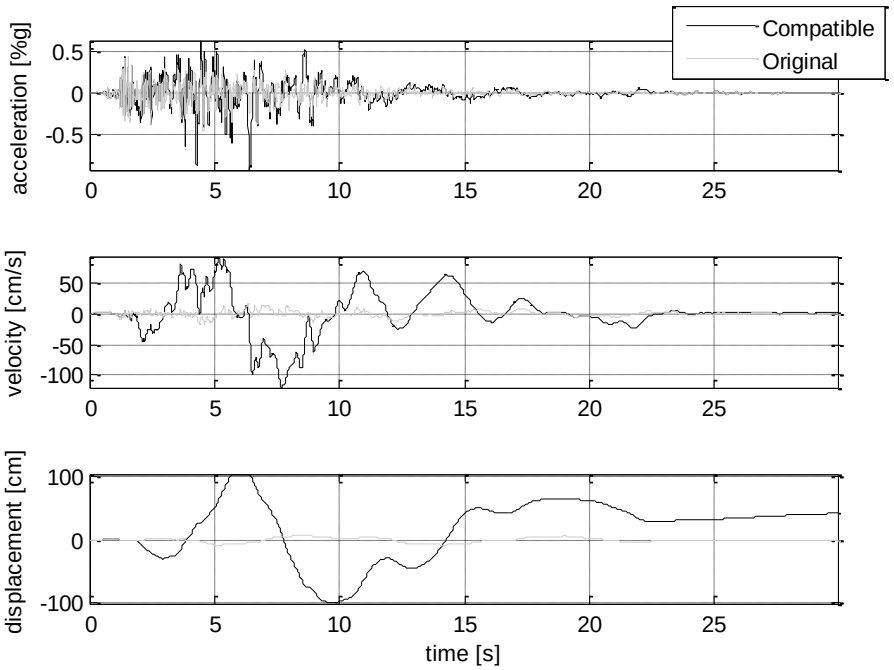

Figure A.2. 5. Time histories of acceleration, velocity and displacement for the scaled seed record and the compatible earthquake record DM5.

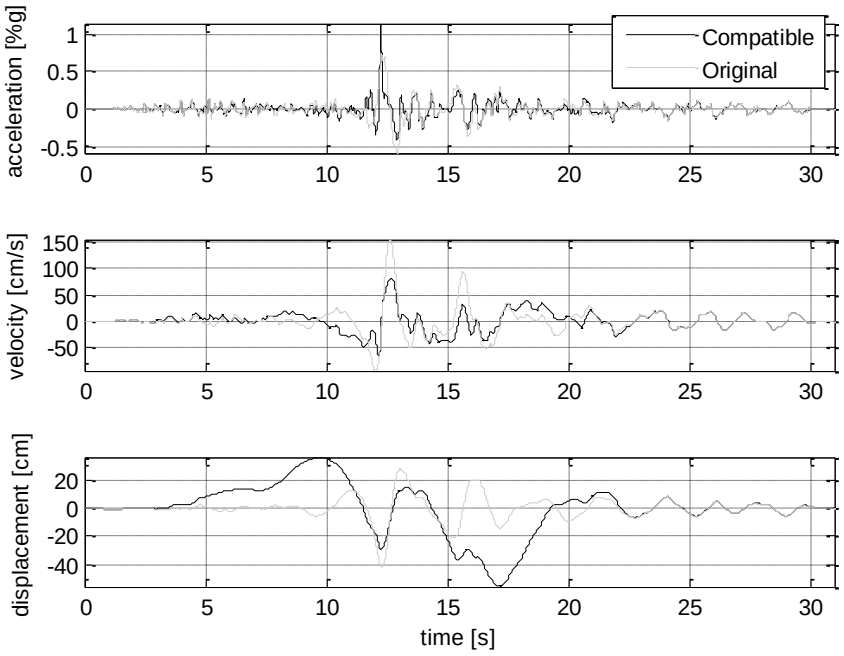

Figure A.2. 6. Time histories of acceleration, velocity and displacement for the scaled seed record and the compatible earthquake record DM6.

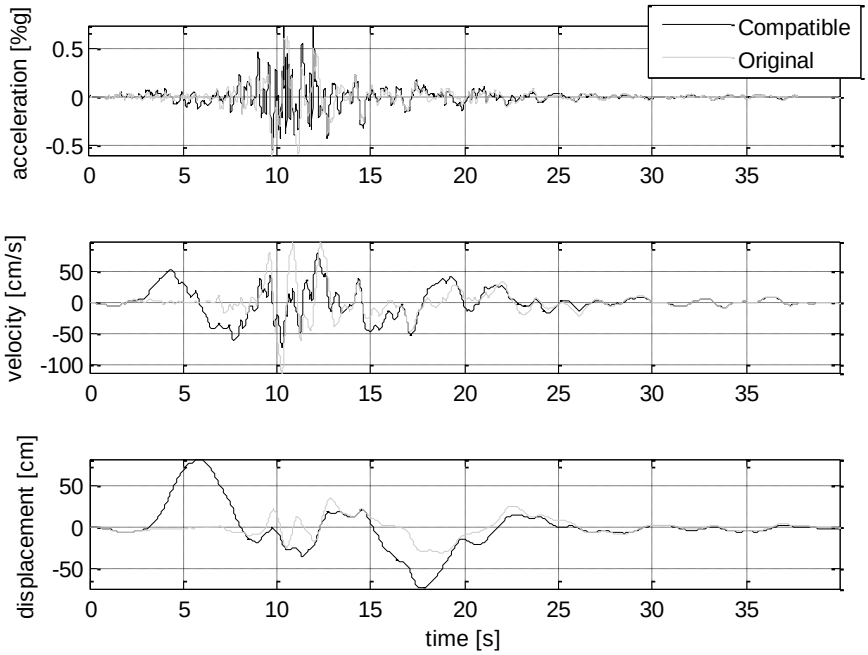

Figure A.2. 7. Time histories of acceleration, velocity and displacement for the scaled seed record and the compatible earthquake record DM7.

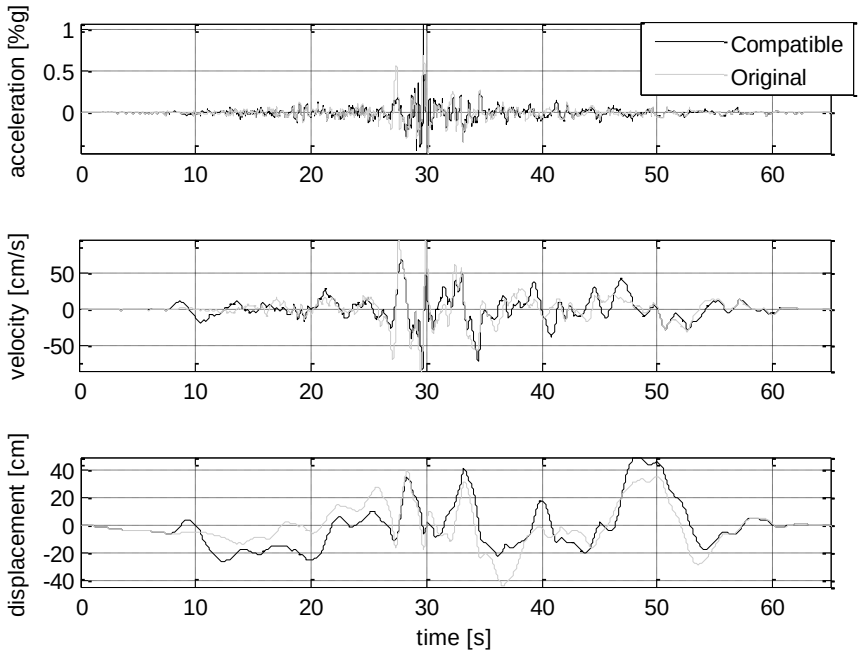

Figure A.2. 8. Time histories of acceleration, velocity and displacement for the scaled seed record and the compatible earthquake record DM8.

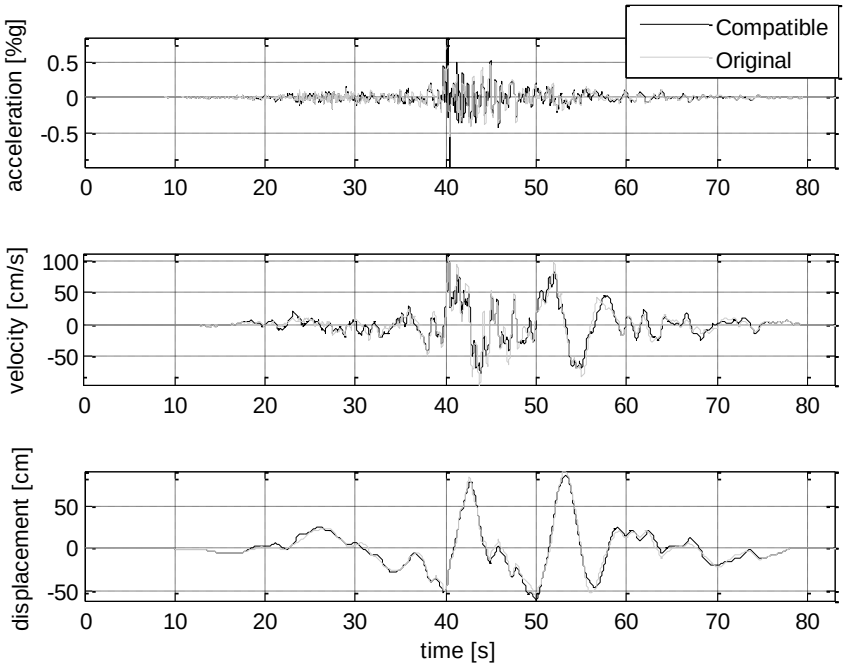

Figure A.2. 9. Time histories of acceleration, velocity and displacement for the scaled seed record and the compatible earthquake record DM9.

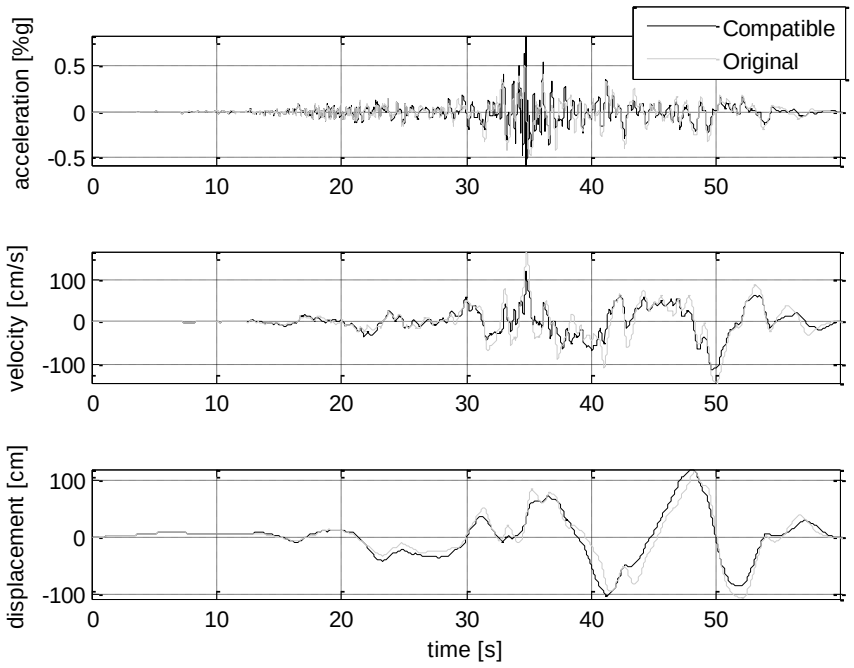

Figure A.2. 10. Time histories of acceleration, velocity and displacement for the scaled seed record and the compatible earthquake record DM10.

A.3 ArtifQuakeLet close match

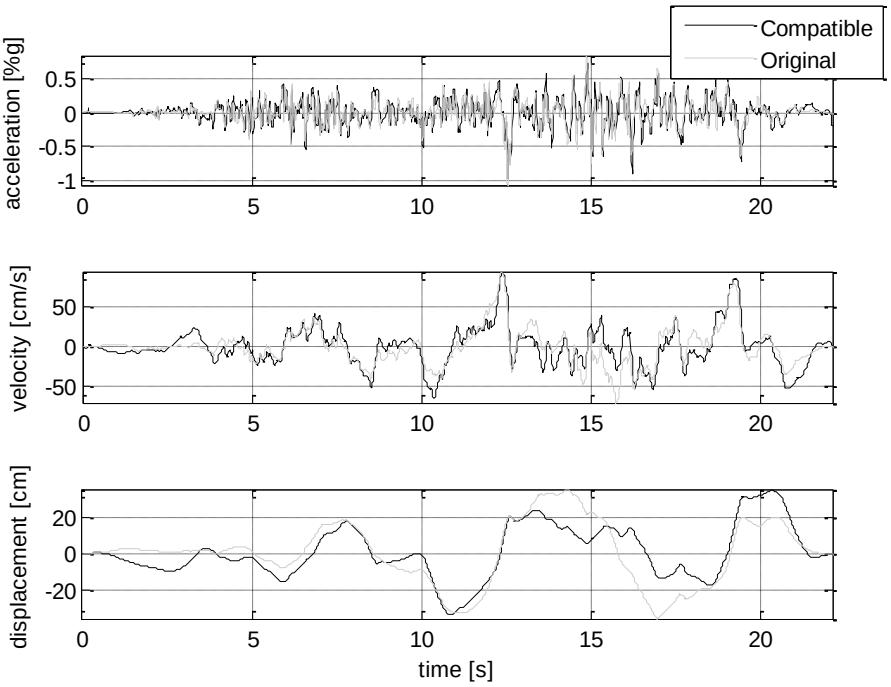

Figure A.3. 1.Time histories of acceleration, velocity and displacement for the scaled seed record and the compatible earthquake record CM1.

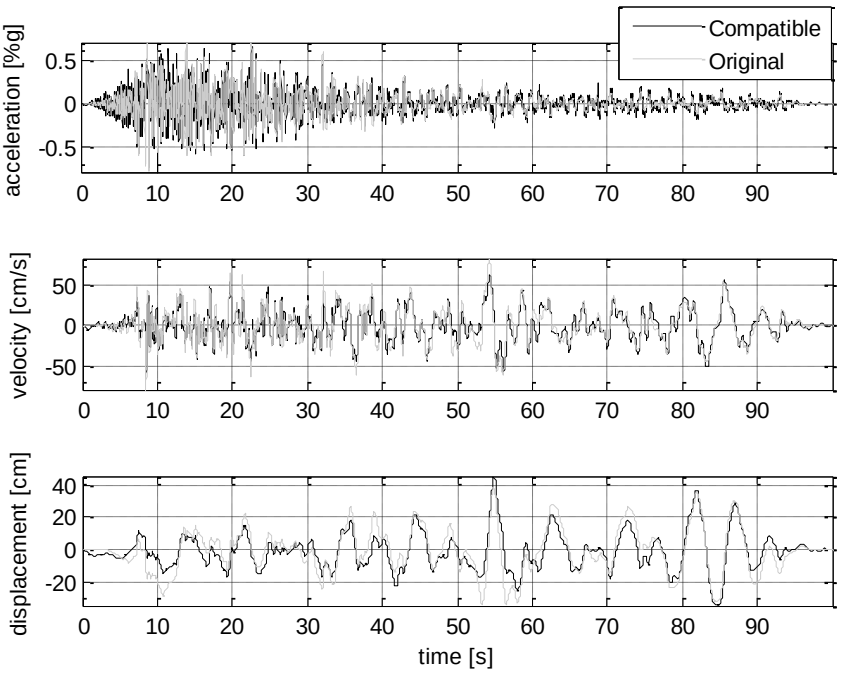

Figure A.3. 2.Time histories of acceleration, velocity and displacement for the scaled seed record and the compatible earthquake record CM2.

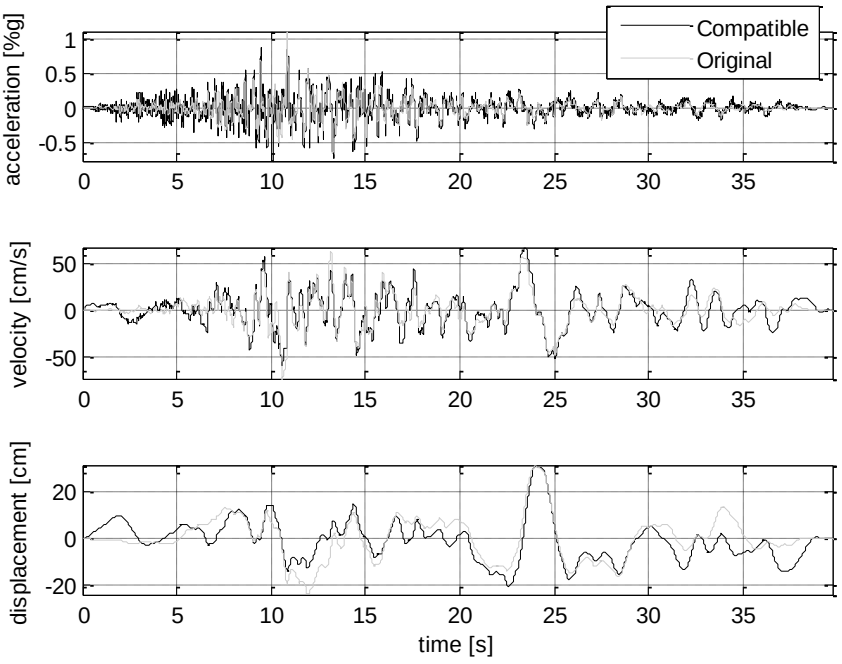

Figure A.3. 3. Time histories of acceleration, velocity and displacement for the scaled seed record and the compatible earthquake record CM3.

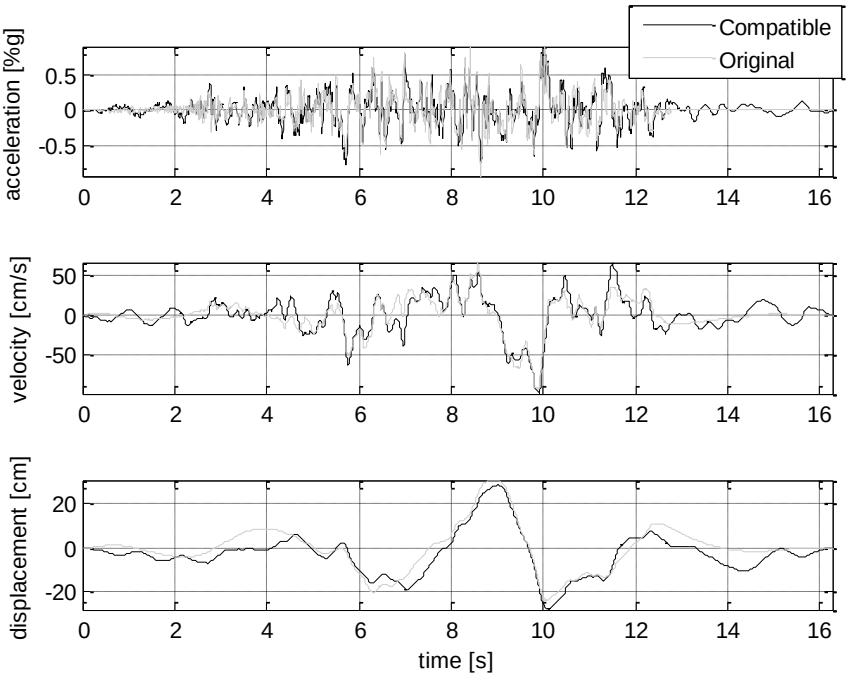

Figure A.3. 4. Time histories of acceleration, velocity and displacement for the scaled seed record and the compatible earthquake record CM4.

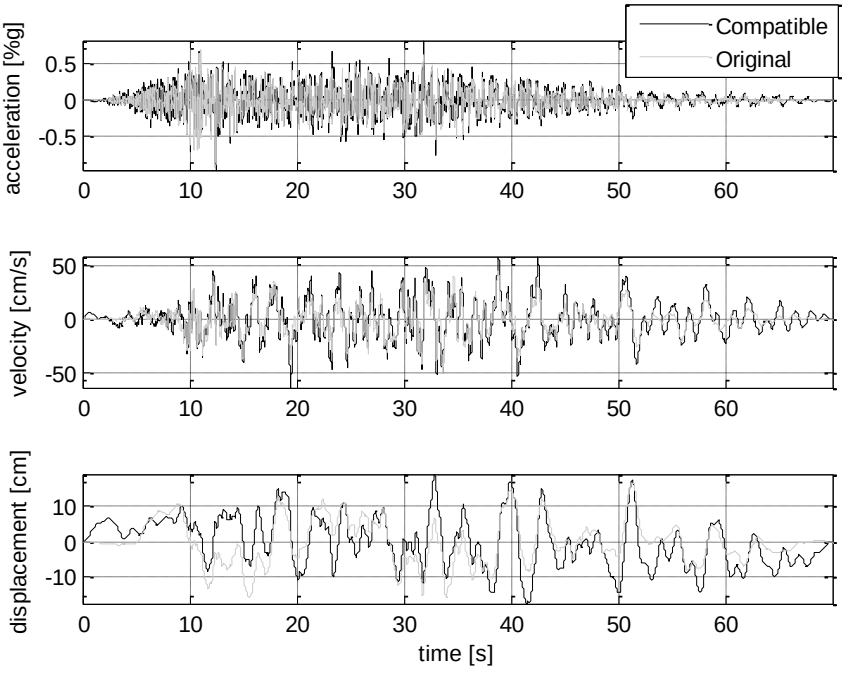

Figure A.3. 5. Time histories of acceleration, velocity and displacement for the scaled seed record and the compatible earthquake record CM5.

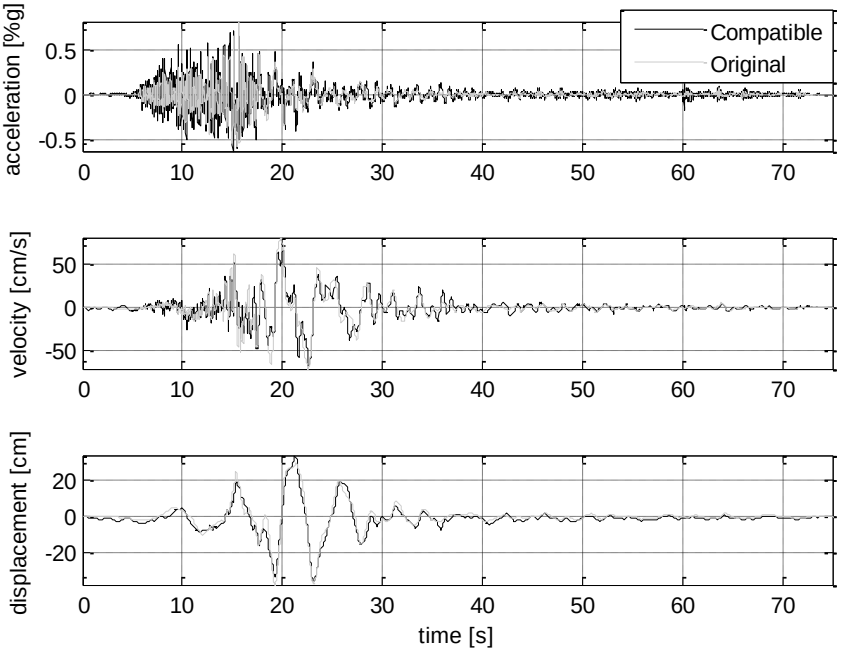

Figure A.3. 6. Time histories of acceleration, velocity and displacement for the scaled seed record and the compatible earthquake record CM6.

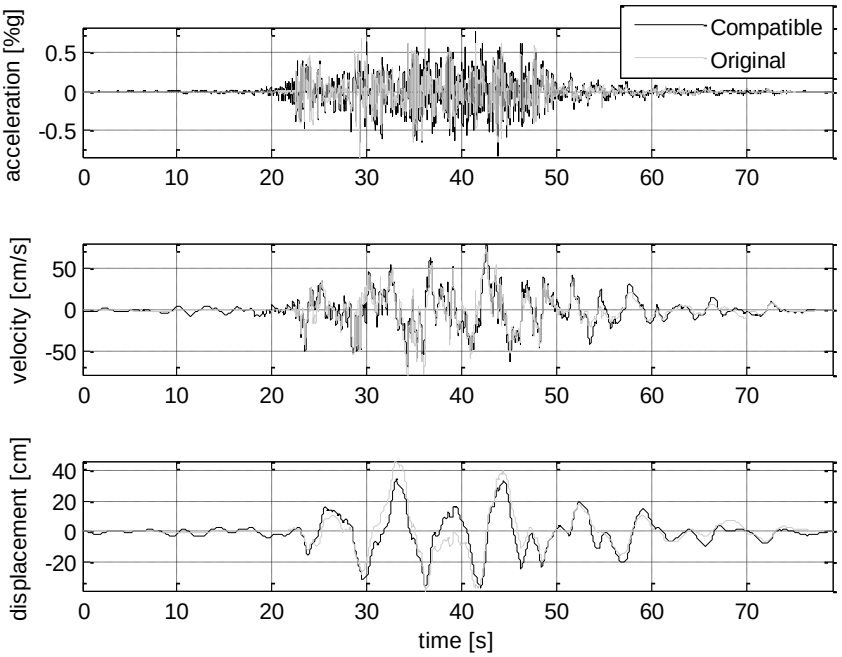

Figure A.3. 7. Time histories of acceleration, velocity and displacement for the scaled seed record and the compatible earthquake record CM7.

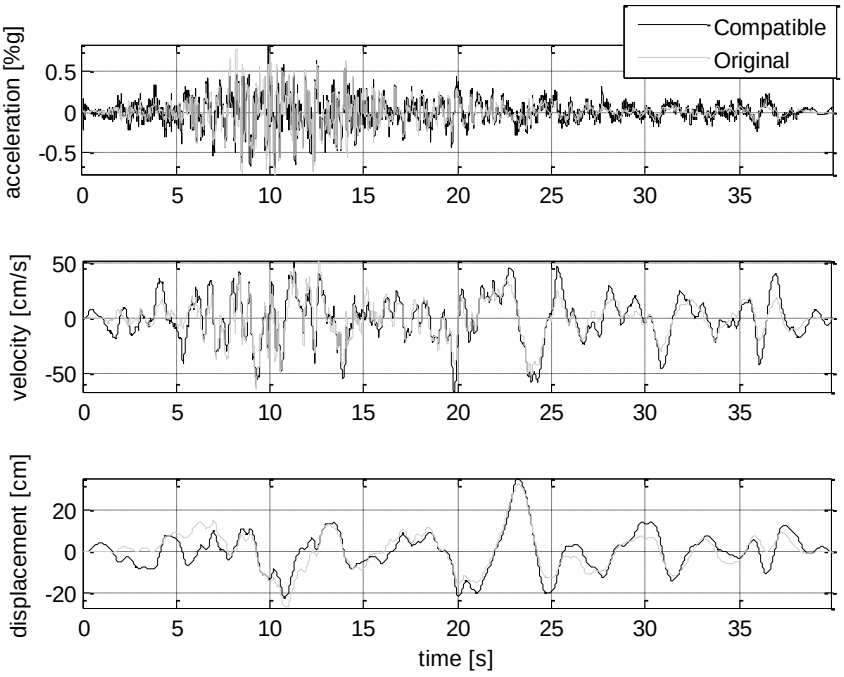

Figure A.3. 8. Time histories of acceleration, velocity and displacement for the scaled seed record and the compatible earthquake record CM8.

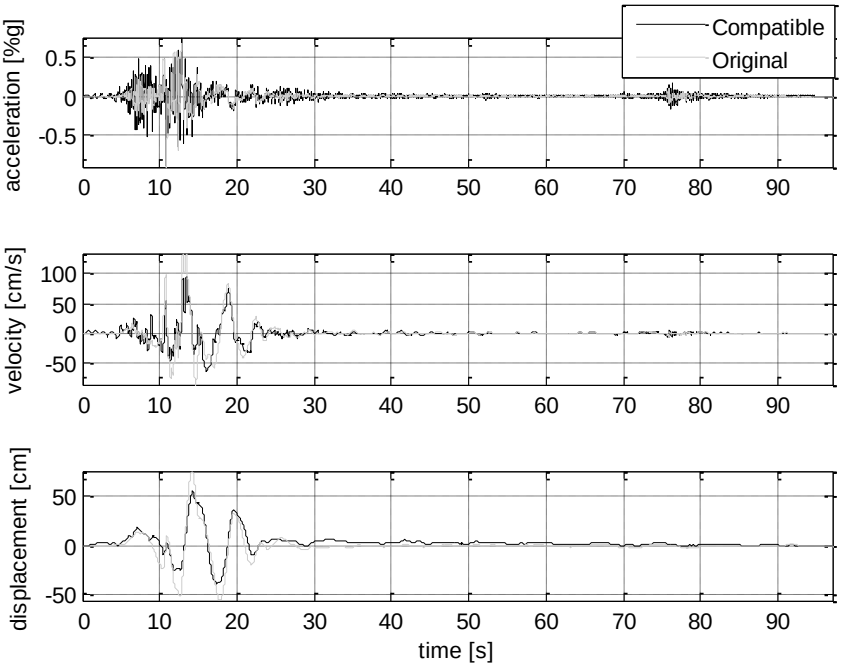

Figure A.3. 9. Time histories of acceleration, velocity and displacement for the scaled seed record and the compatible earthquake record CM9.

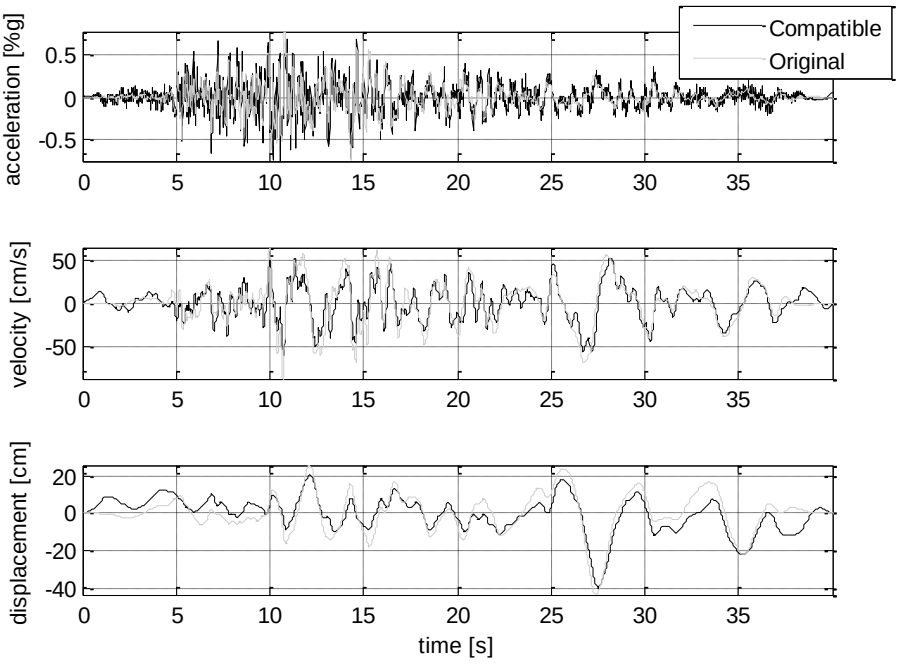

Figure A.3. 10. Time histories of acceleration, velocity and displacement for the scaled seed record and the compatible earthquake record CM10.

A.4 ArtifQuakeLet distant match

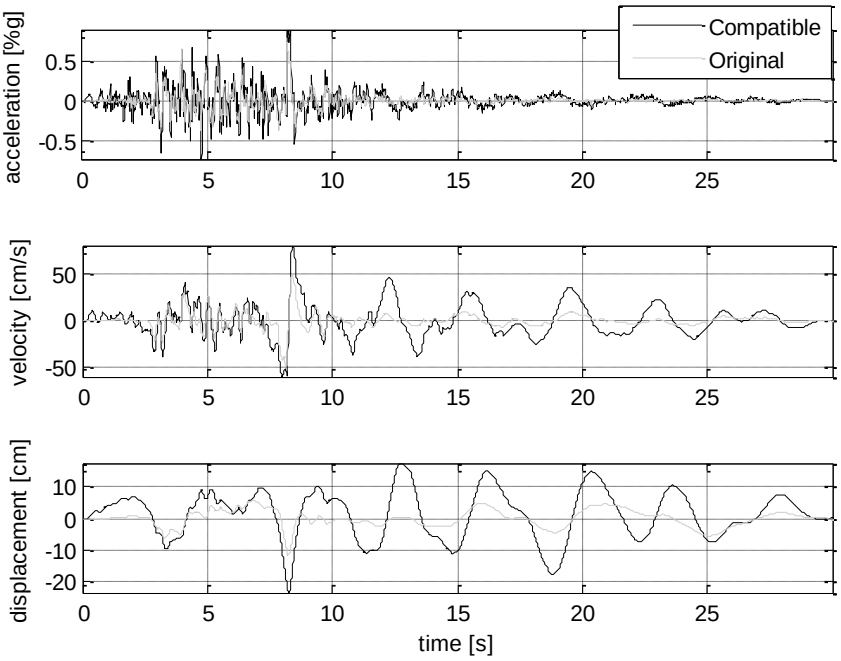

Figure A.4. 1. Time histories of acceleration, velocity and displacement for the scaled seed record and the compatible earthquake record DM1.

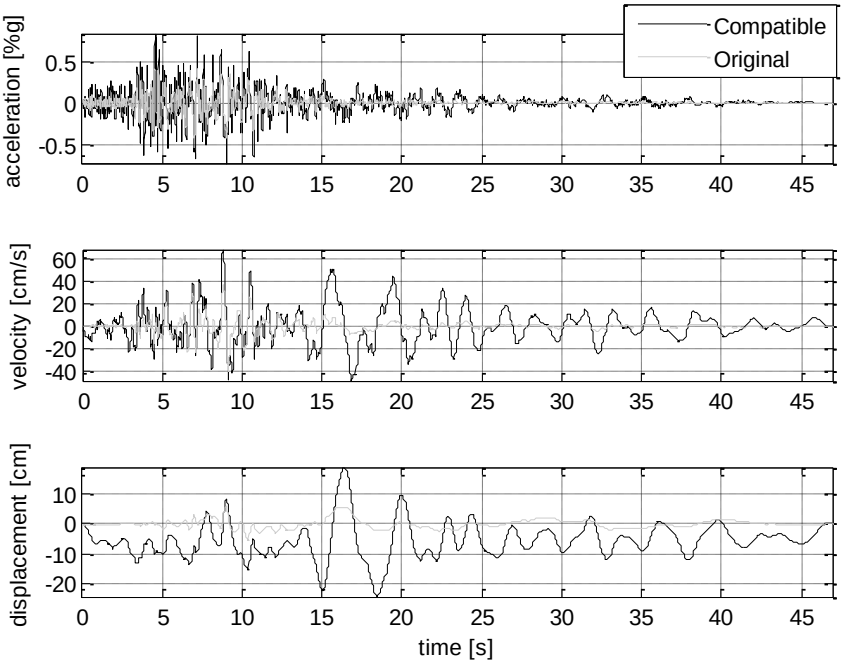

Figure A.4. 2. Time histories of acceleration, velocity and displacement for the scaled seed record and the compatible earthquake record DM2.

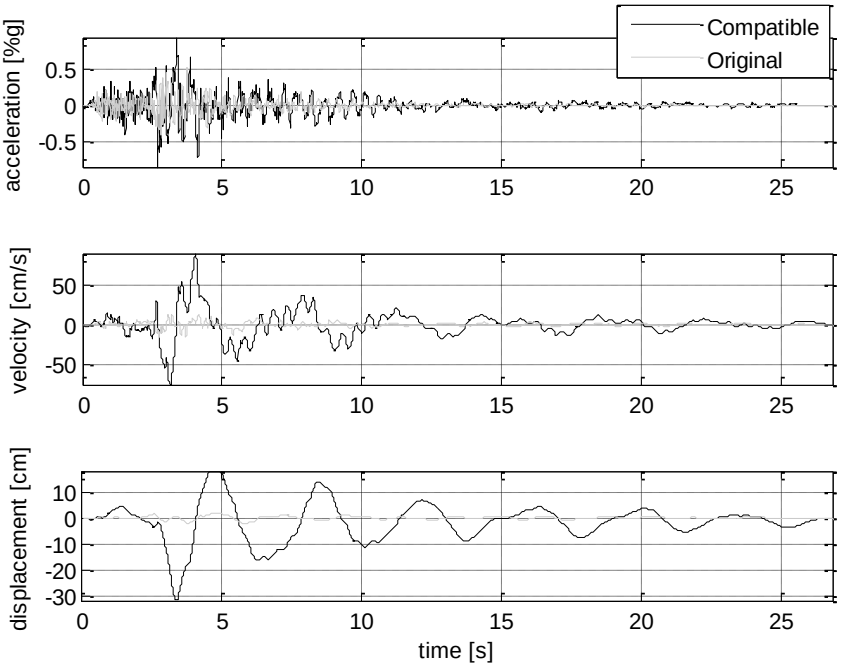

Figure A.4. 3. Time histories of acceleration, velocity and displacement for the scaled seed record and the compatible earthquake record DM3.

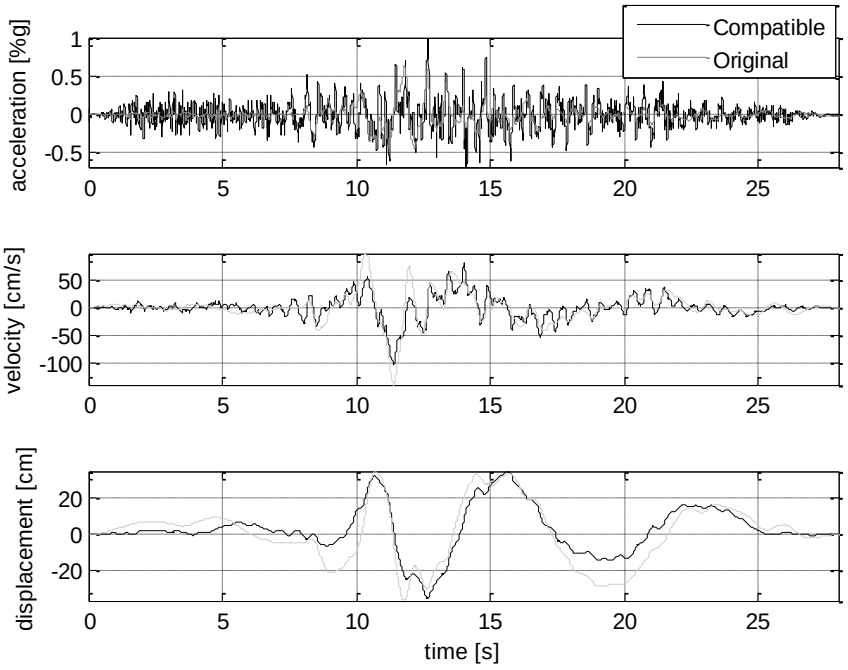

Figure A.4. 4. Time histories of acceleration, velocity and displacement for the scaled seed record and the compatible earthquake record DM4.

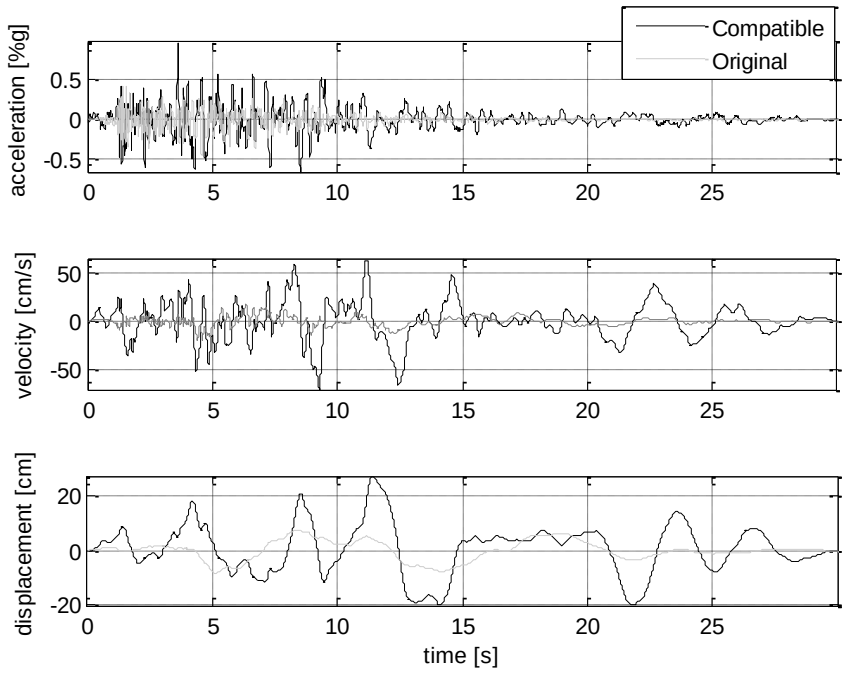

Figure A.4. 5. Time histories of acceleration, velocity and displacement for the scaled seed record and the compatible earthquake record DM5.

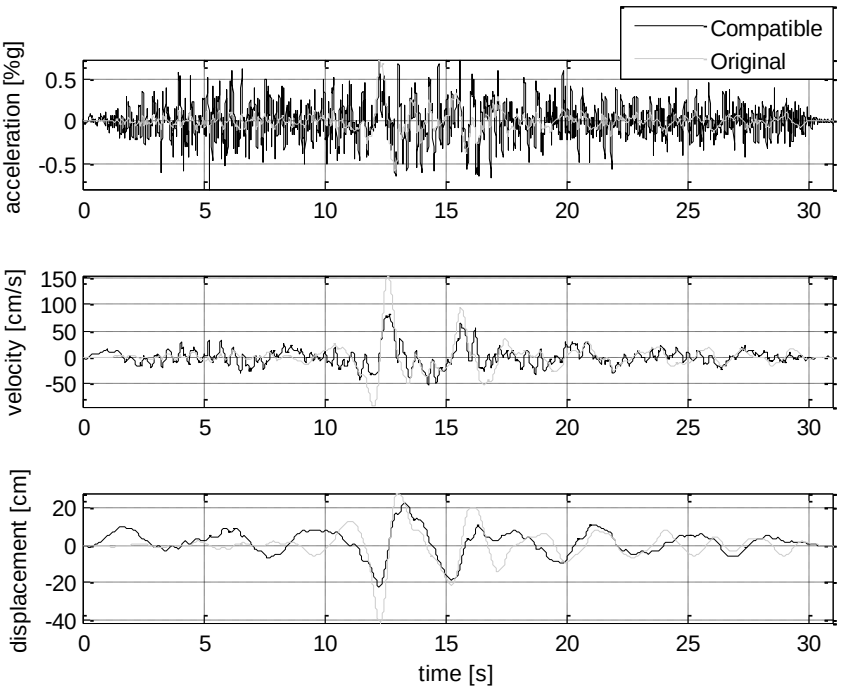

Figure A.4. 6. Time histories of acceleration, velocity and displacement for the scaled seed record and the compatible earthquake record DM6.

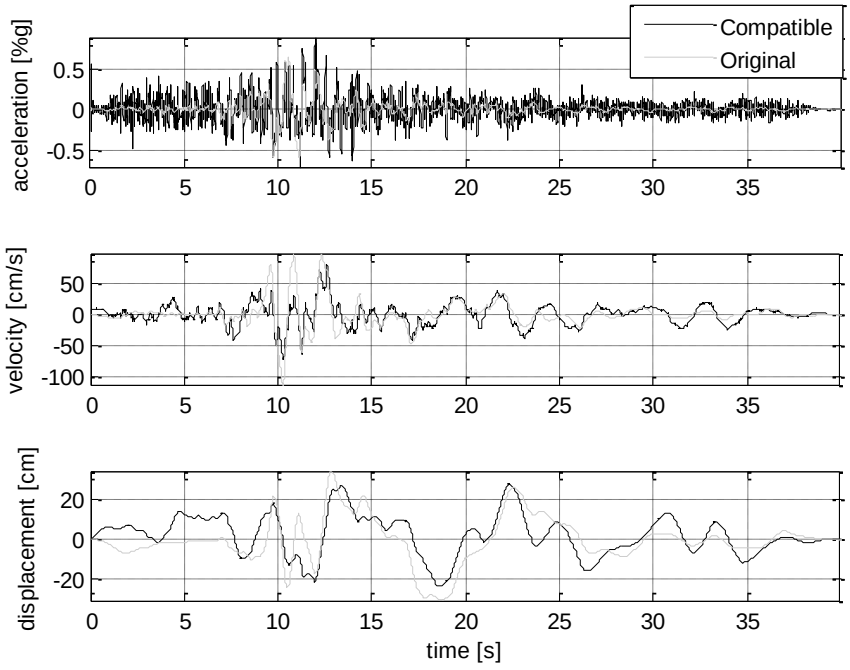

Figure A.4. 7. Time histories of acceleration, velocity and displacement for the scaled seed record and the compatible earthquake record DM7.

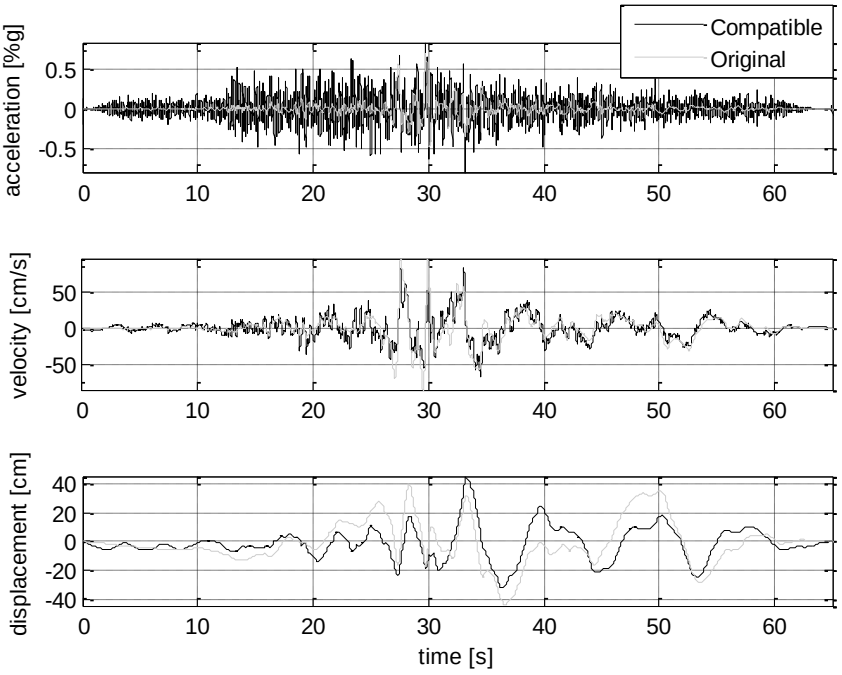

Figure A.4. 8. Time histories of acceleration, velocity and displacement for the scaled seed record and the compatible earthquake record DM8.

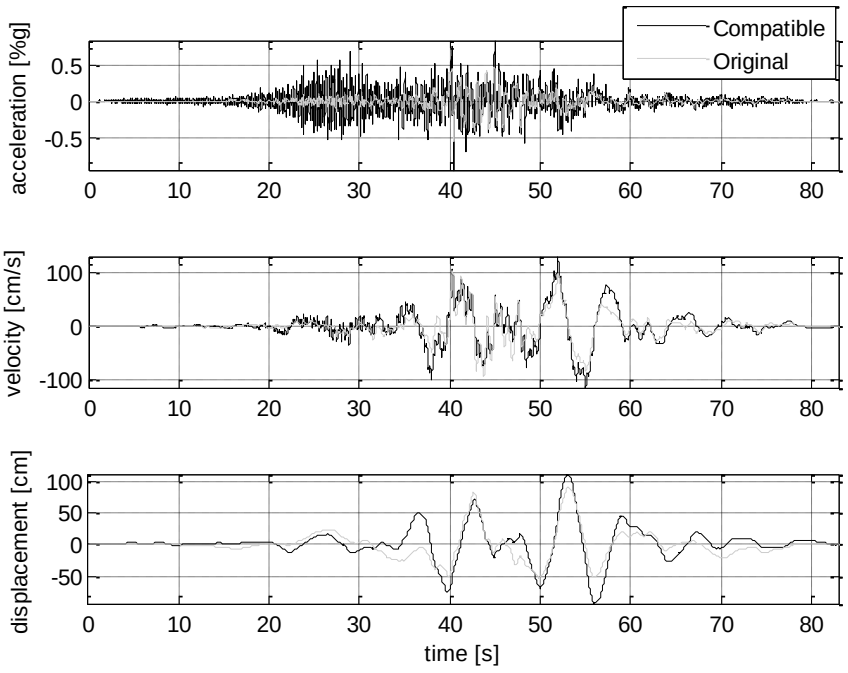

Figure A.4. 9. Time histories of acceleration, velocity and displacement for the scaled seed record and the compatible earthquake record DM9.

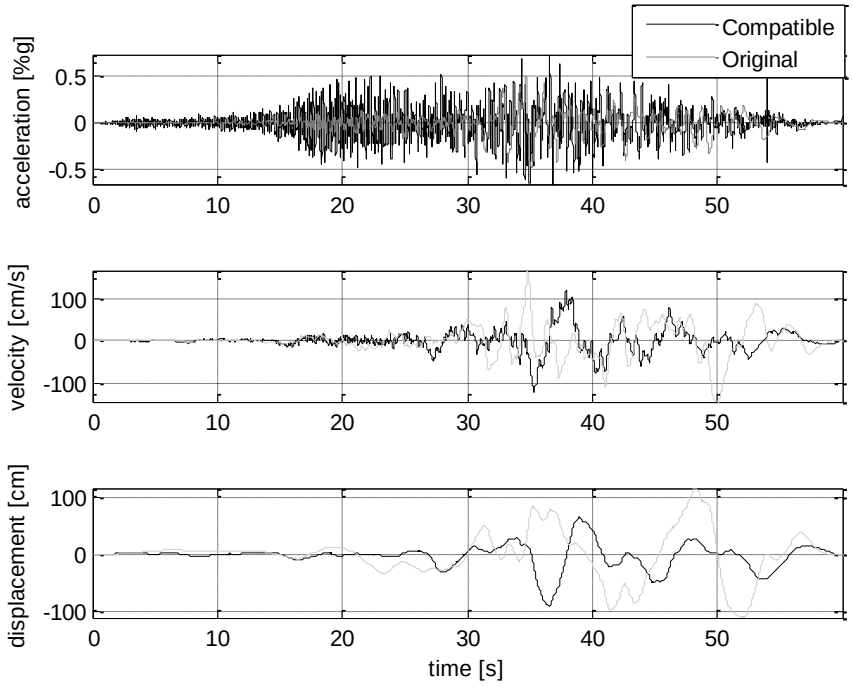

Figure A.4. 10. Time histories of acceleration, velocity and displacement for the scaled seed record and the compatible earthquake record DM10.

A.5 SeismoArtif

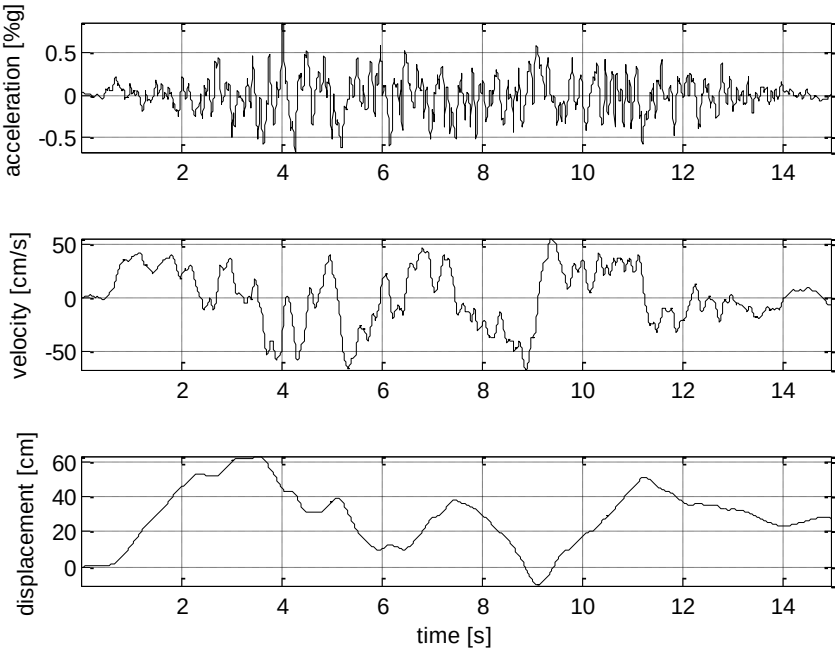

Figure A.5. 1. Time histories of acceleration, velocity and displacement from the artificial earthquake

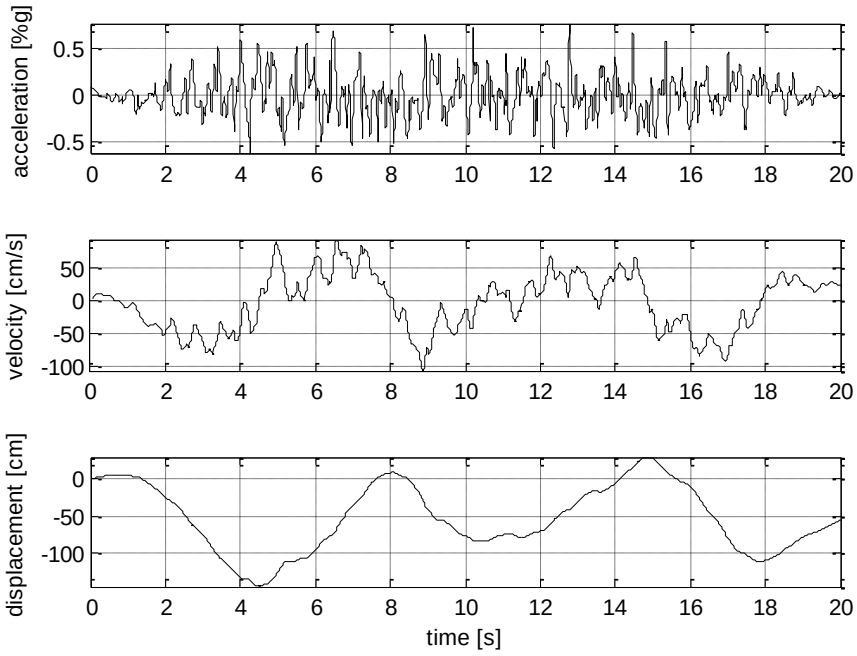

Figure A.5. 2. Time histories of acceleration, velocity and displacement from the artificial earthquake

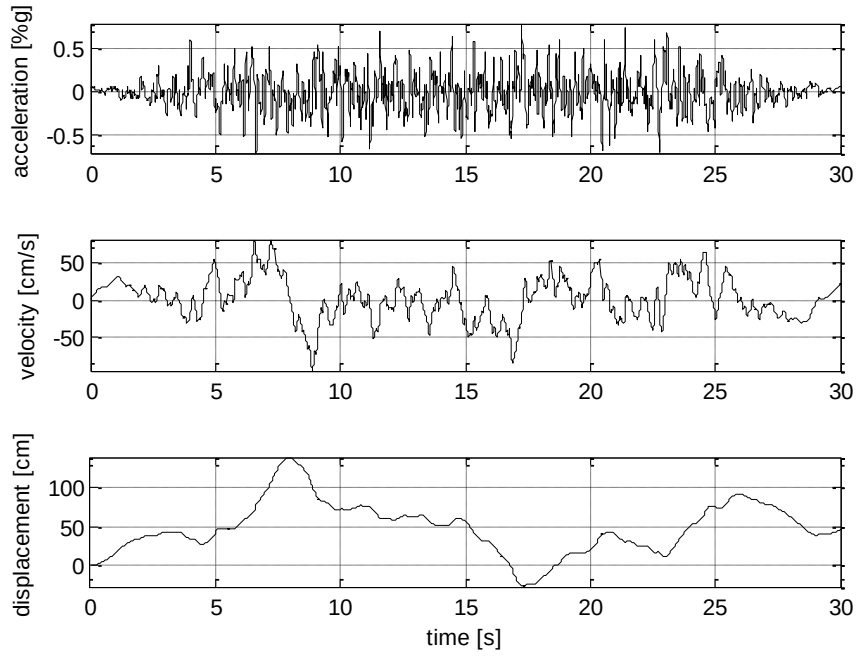

Figure A.5. 3. Time histories of acceleration, velocity and displacement from the artificial earthquake

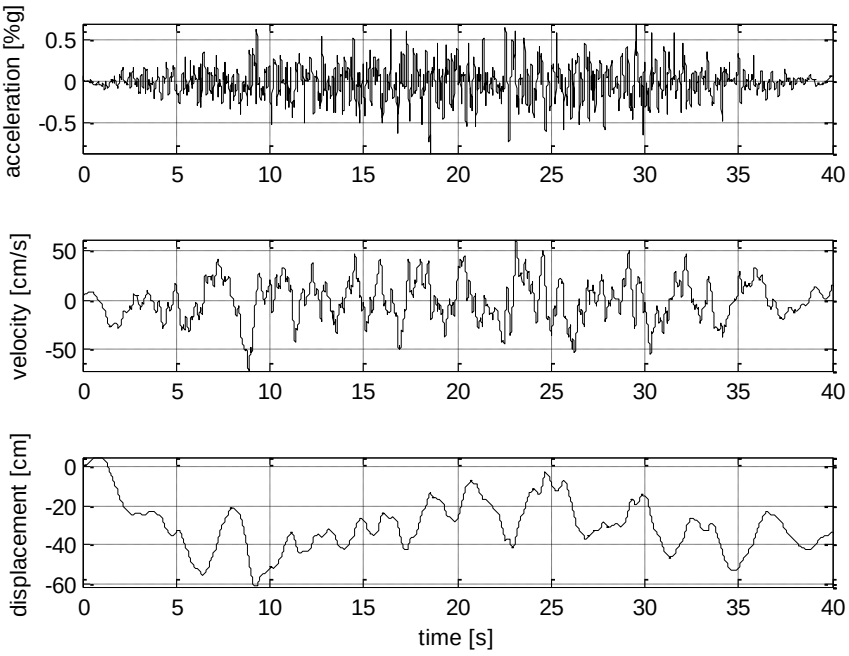

Figure A.5. 4. Time histories of acceleration, velocity and displacement from the artificial earthquake

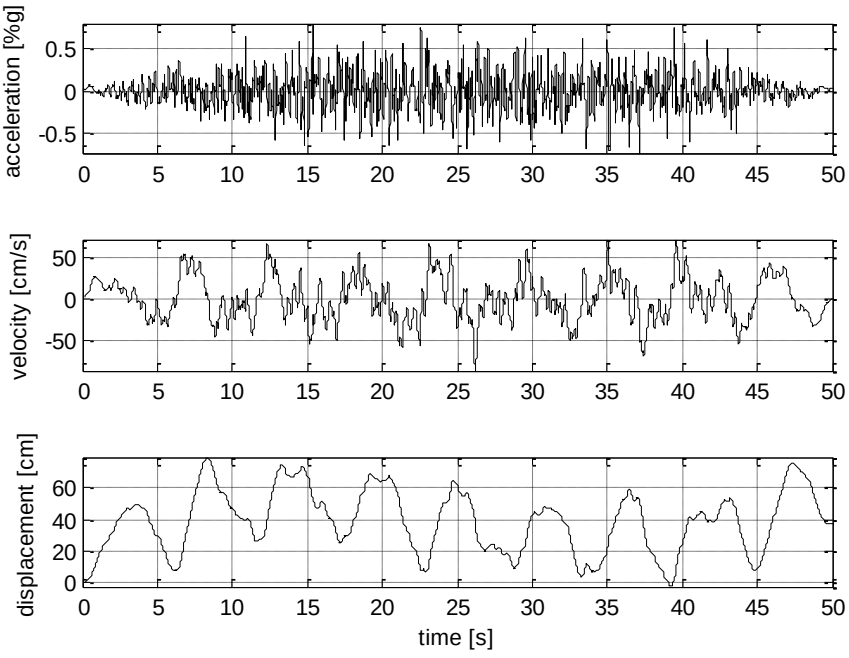

Figure A.5. 5. Time histories of acceleration, velocity and displacement from the artificial earthquake

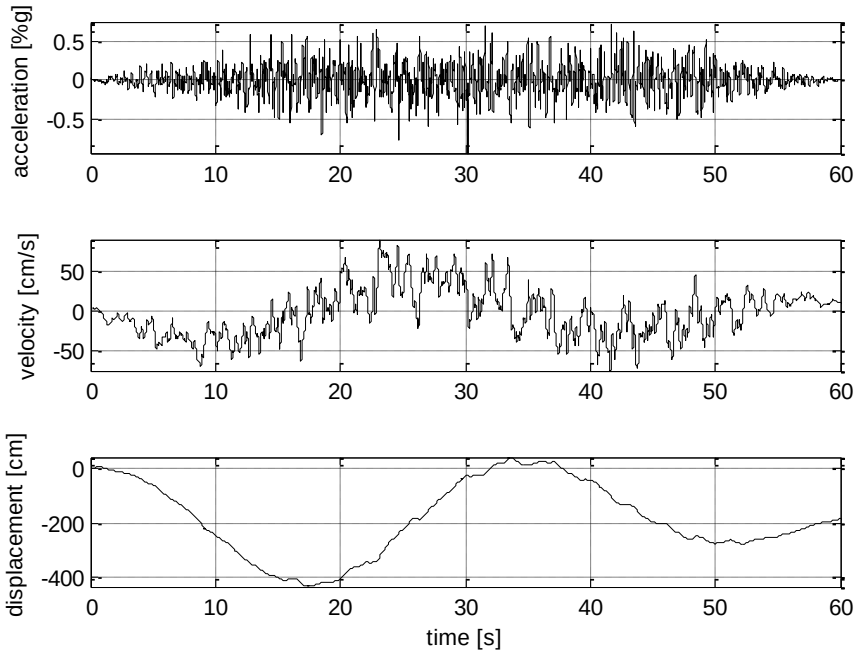

Figure A.5. 6. Time histories of acceleration, velocity and displacement from the artificial earthquake

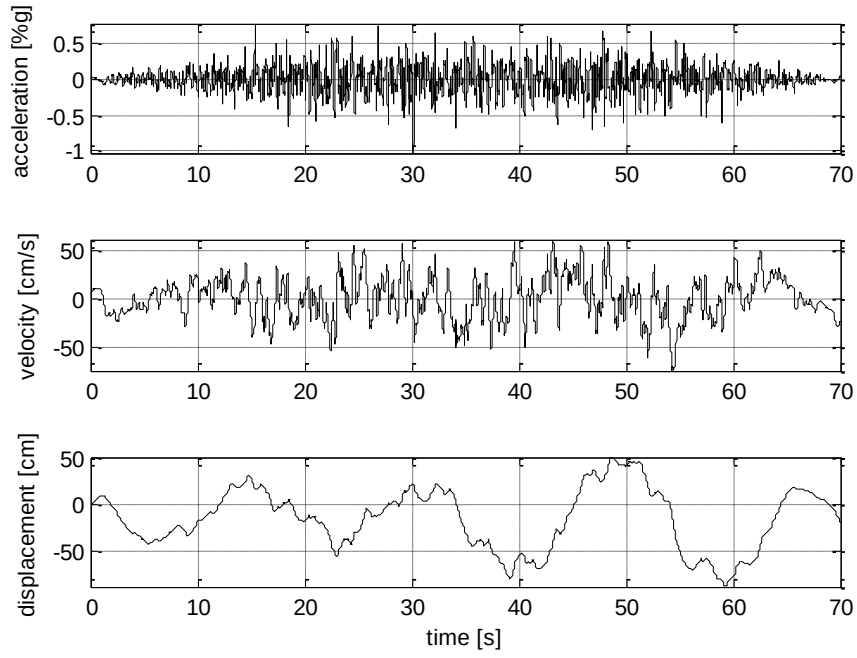

Figure A.5. 7. Time histories of acceleration, velocity and displacement from the artificial earthquake

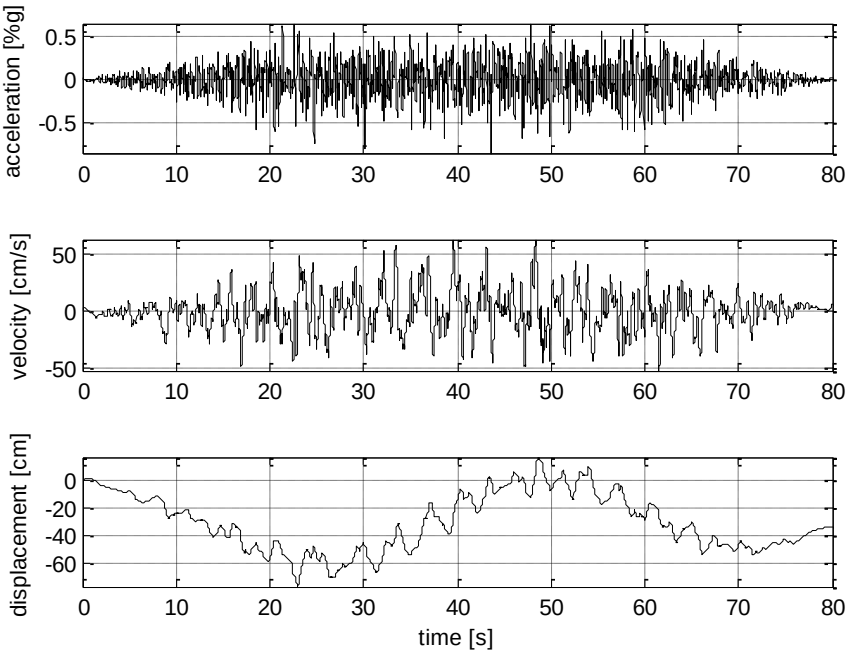

Figure A.5. 8. Time histories of acceleration, velocity and displacement from the artificial earthquake

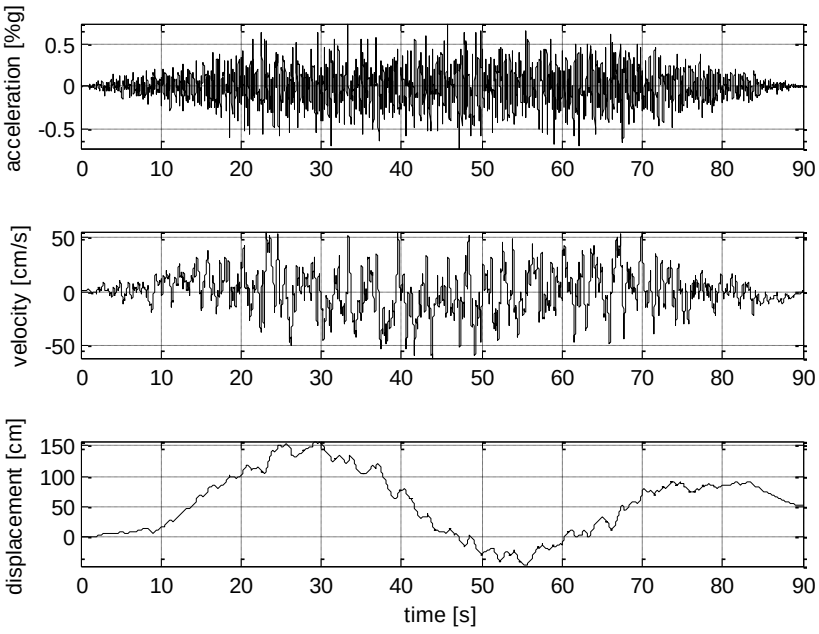

Figure A.5. 9. Time histories of acceleration, velocity and displacement from the artificial earthquake

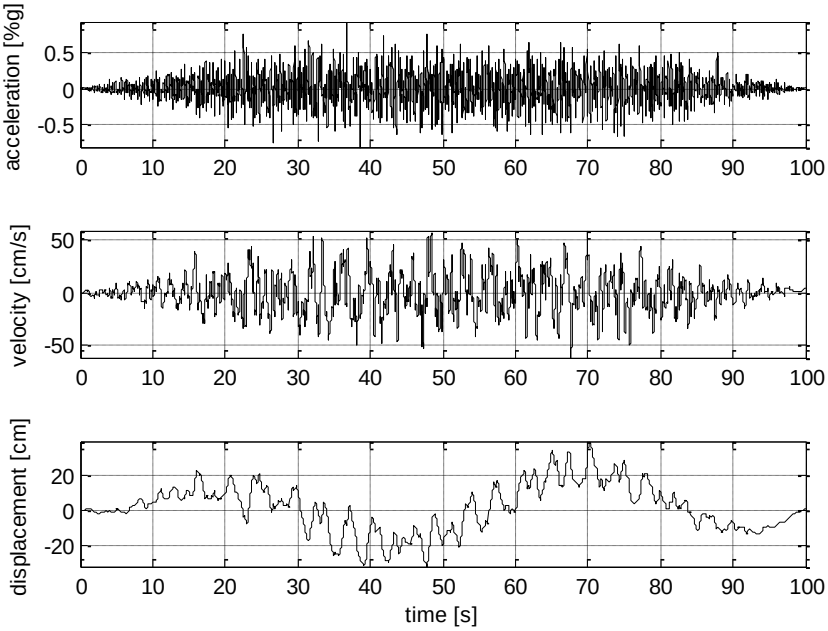

Figure A.5. 10. Time histories of acceleration, velocity and displacement from the artificial earthquake

APPENDIX B

B. Husid plots and significant duration interval

B1. Close Match

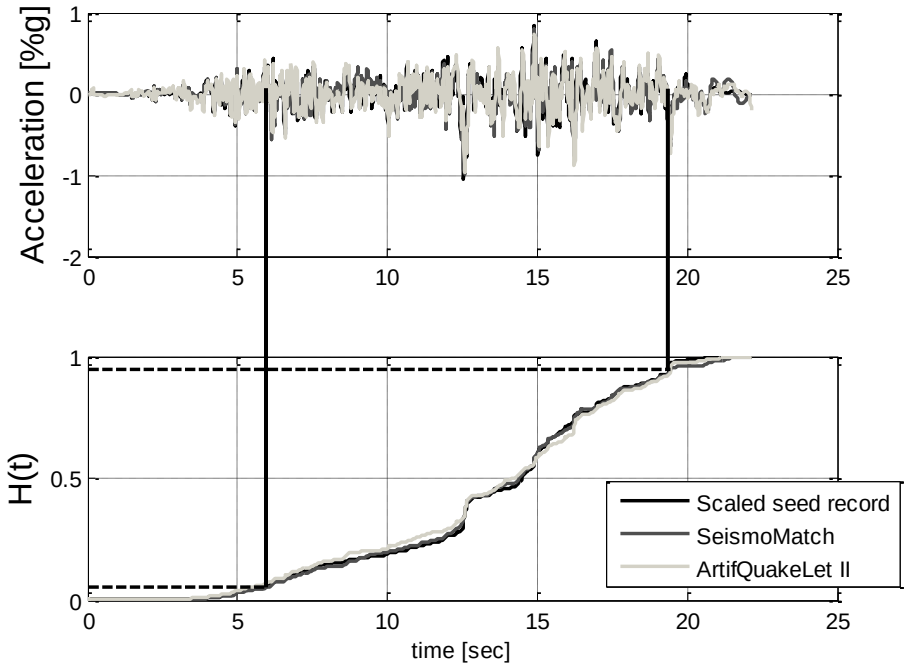

Figure B.1.1 Husid plot and significant duration interval for CM1

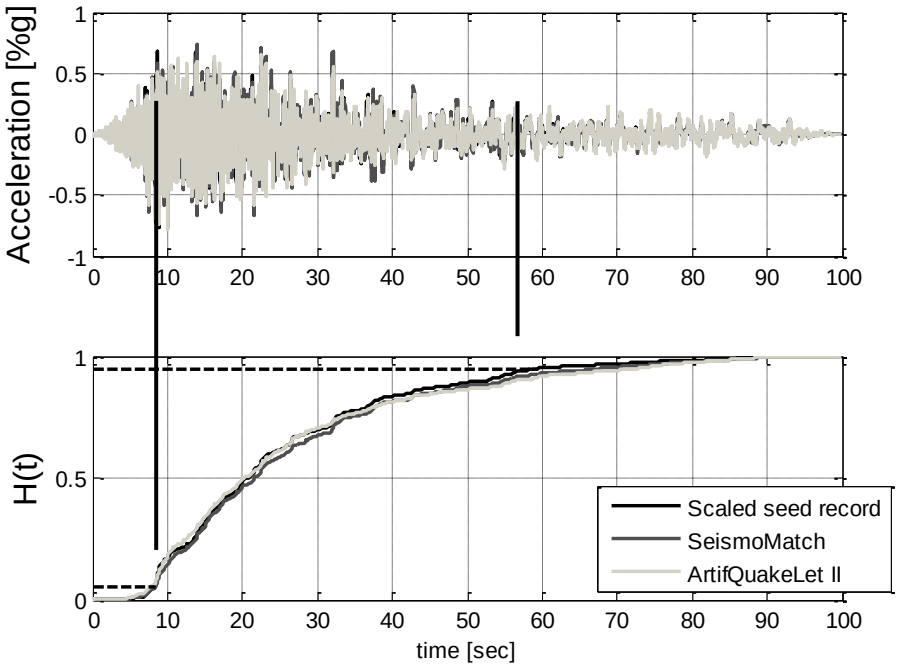

Figure B.1.2. Husid plot and significant duration interval for CM2

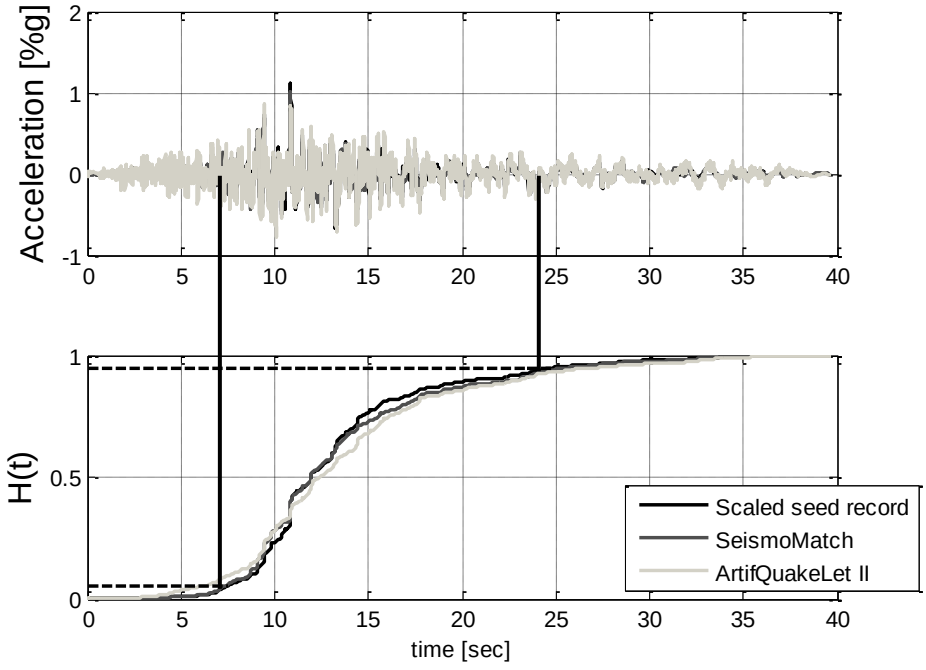

Figure B.1.3. Husid plot and significant duration interval for CM3

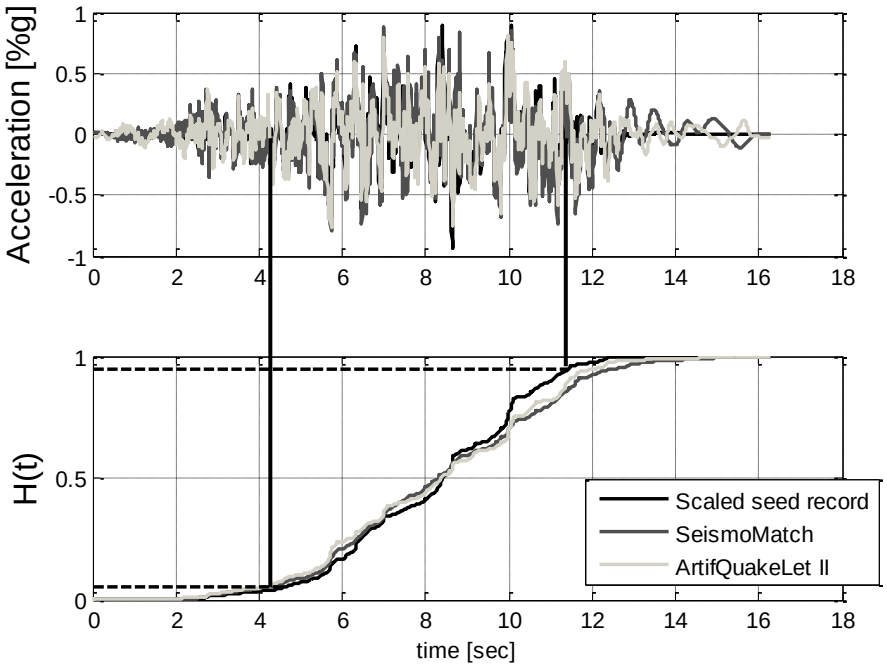

Figure B.1.4. Husid plot and significant duration interval for CM4

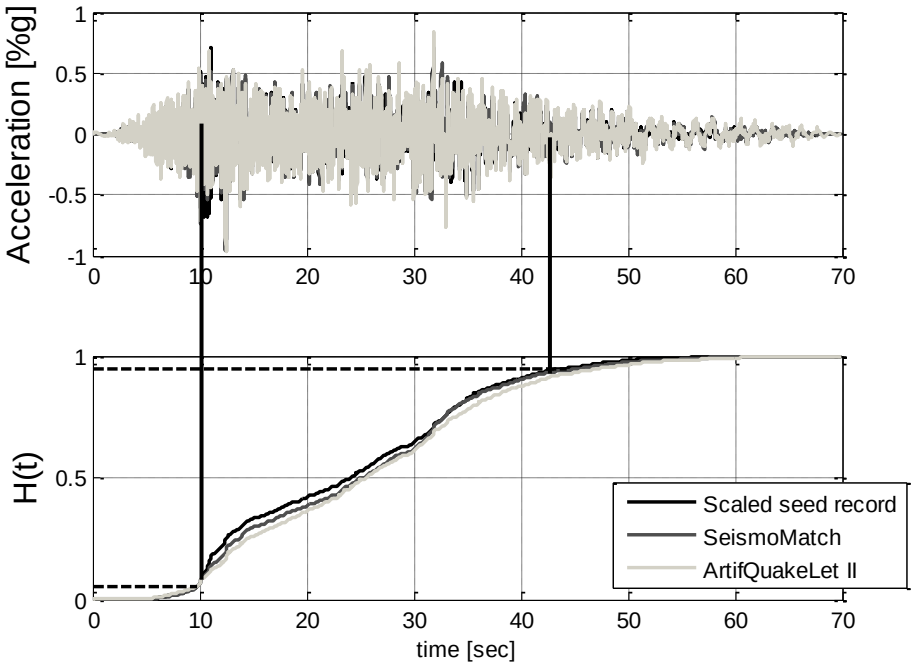

Figure B.1.5. Husid plot and significant duration interval for CM5

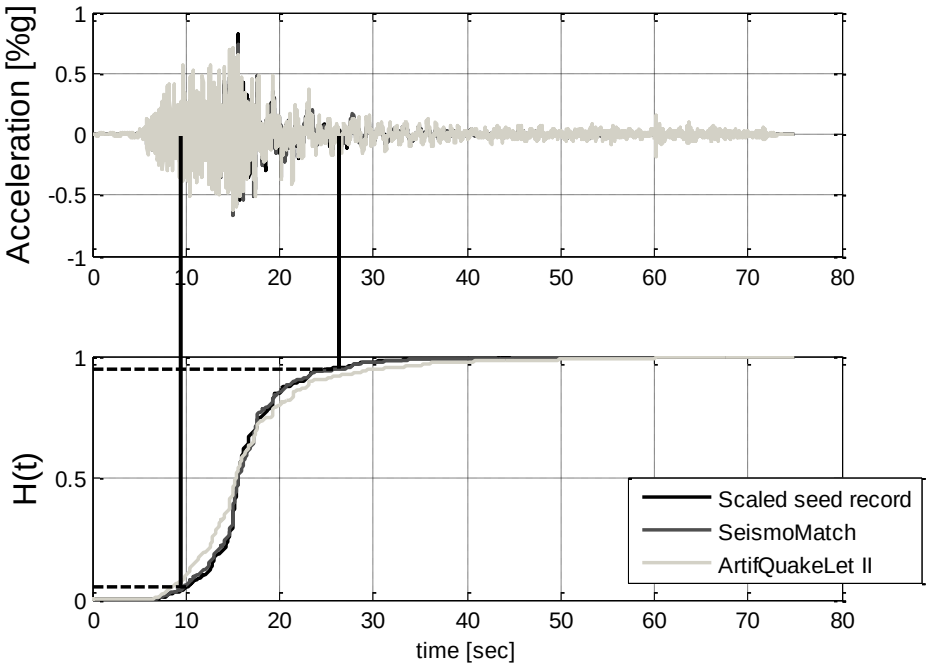

Figure B.1.6. Husid plot and significant duration interval for CM6

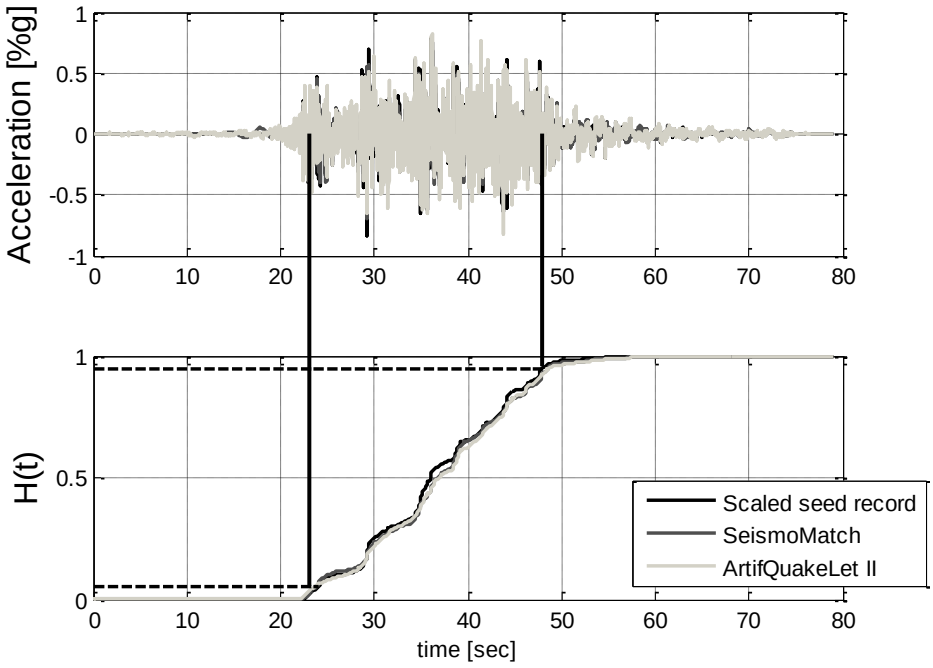

Figure B.1.7. Husid plot and significant duration interval for CM7

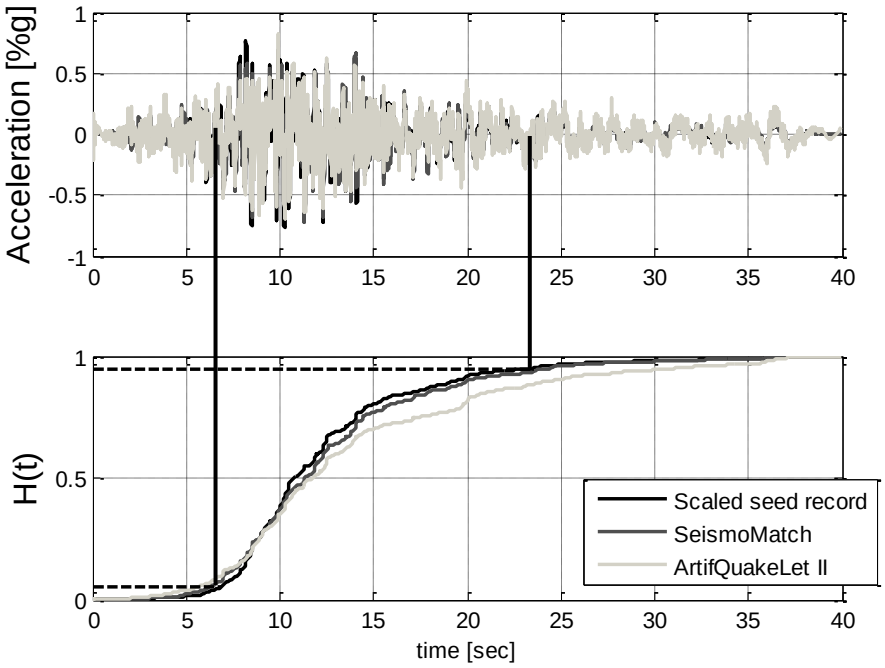

Figure B.1.8. Husid plot and significant duration interval for CM8

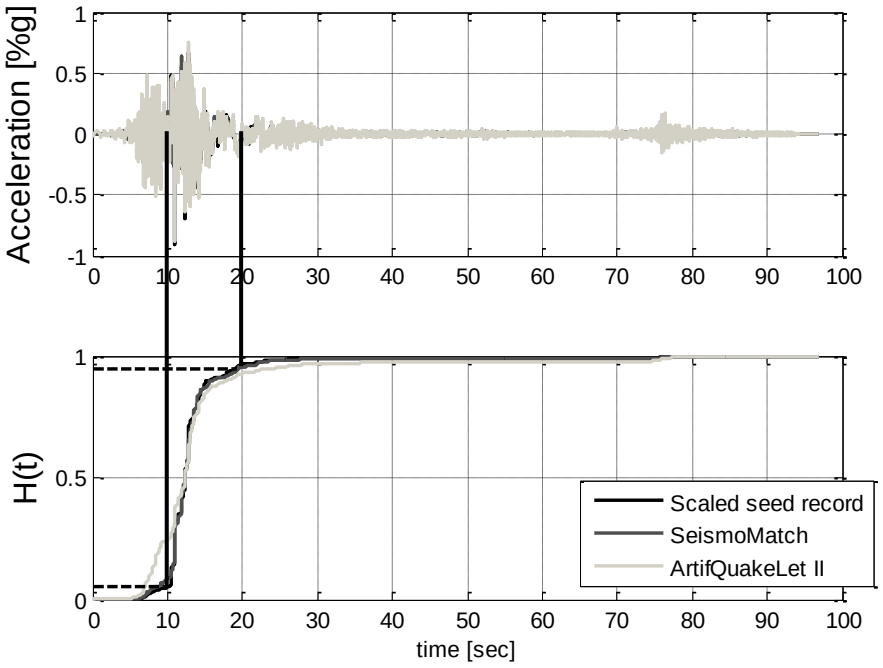

Figure B.1.9. Husid plot and significant duration interval for CM9

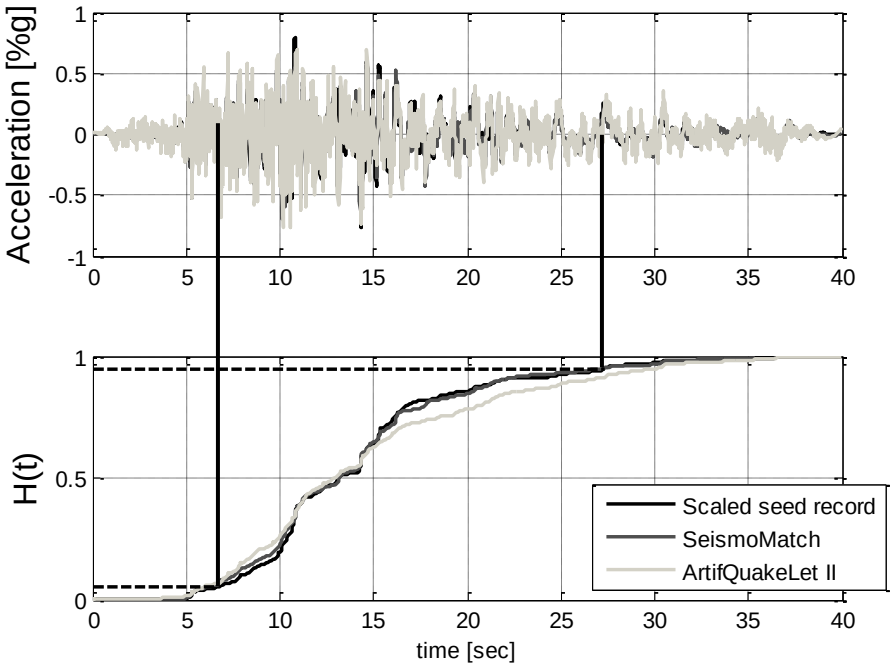

Figure B.1.10. Husid plot and significant duration interval for CM10

B.2 Distant Match

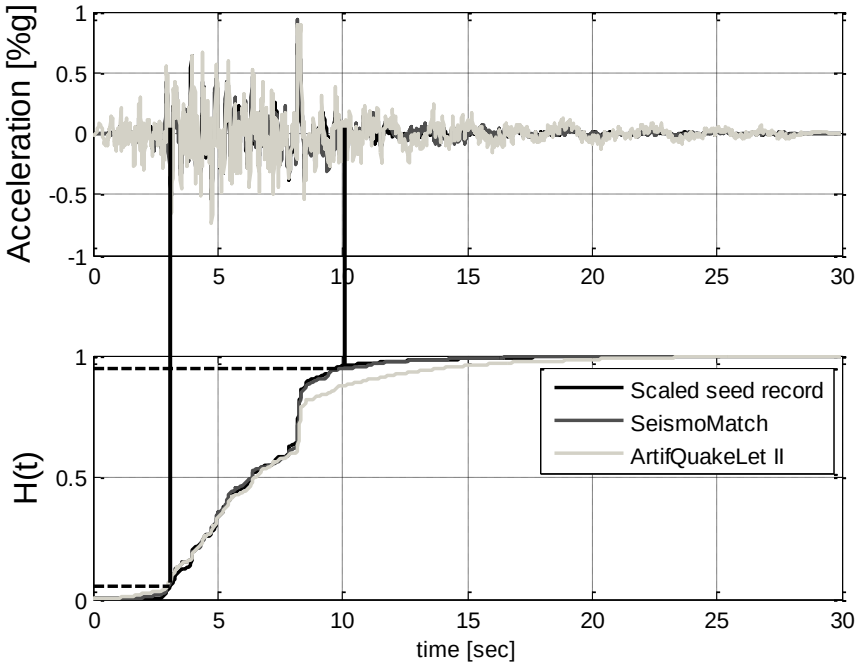

Figure B.2.1 Husid plot and significant duration interval for DM1

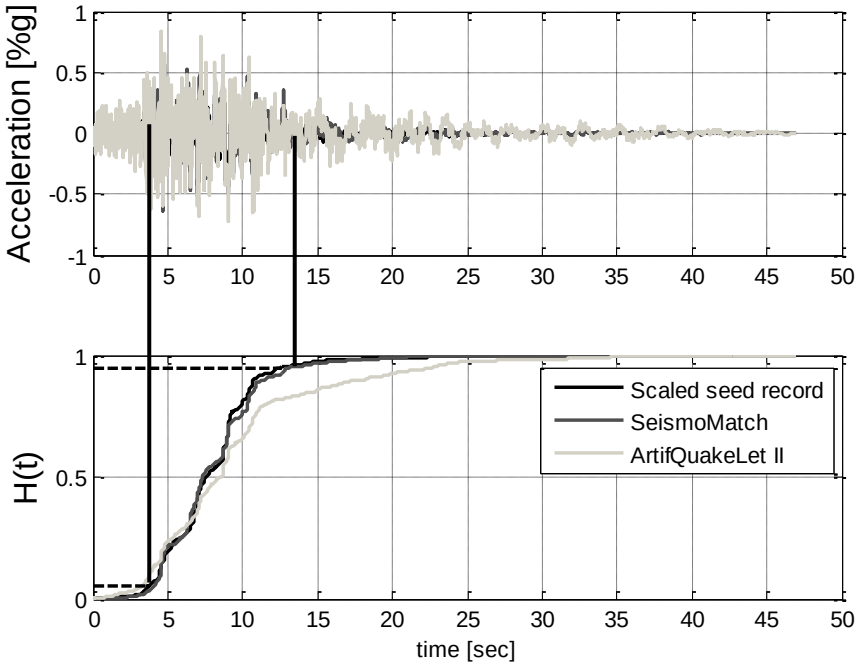

Figure B.2.2. Husid plot and significant duration interval for DM2

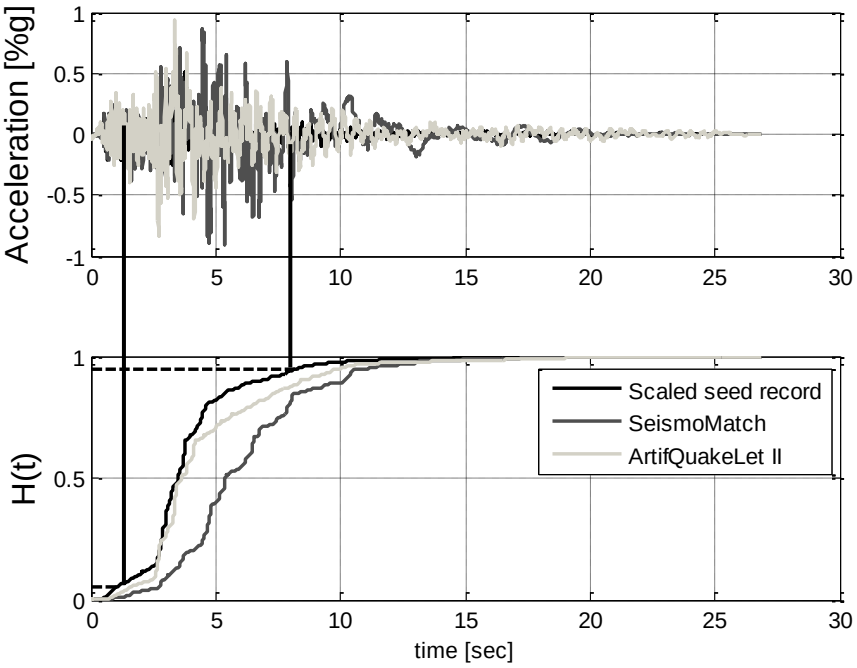

Figure B.2.3. Husid plot and significant duration interval for DM3

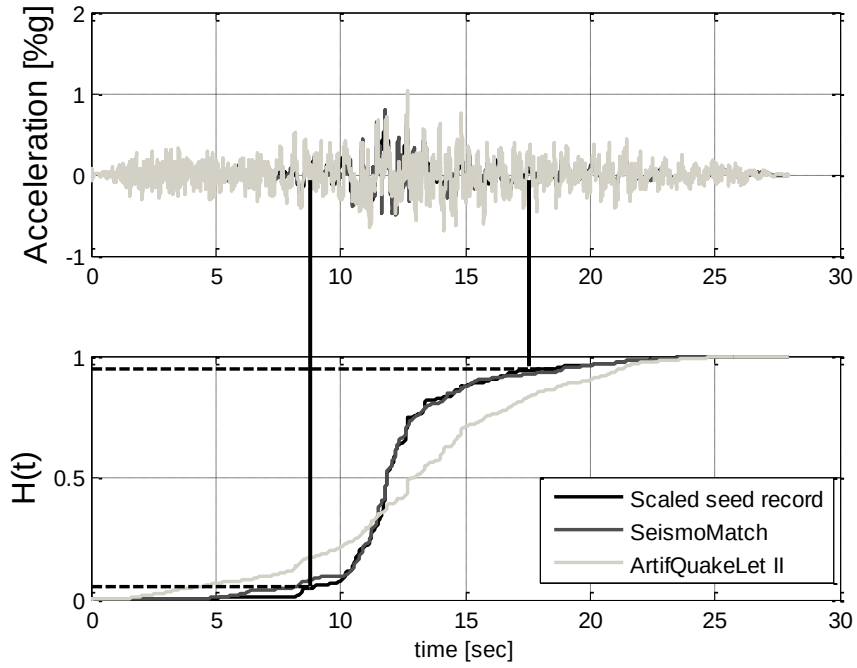

Figure B.2.4. Husid plot and significant duration interval for DM4

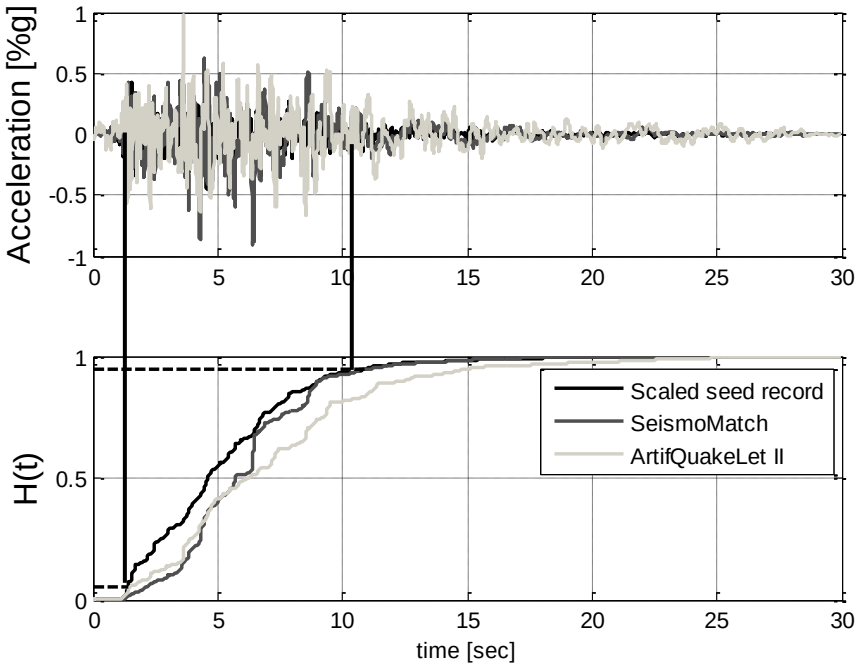

Figure B.2.5. Husid plot and significant duration interval for DM5

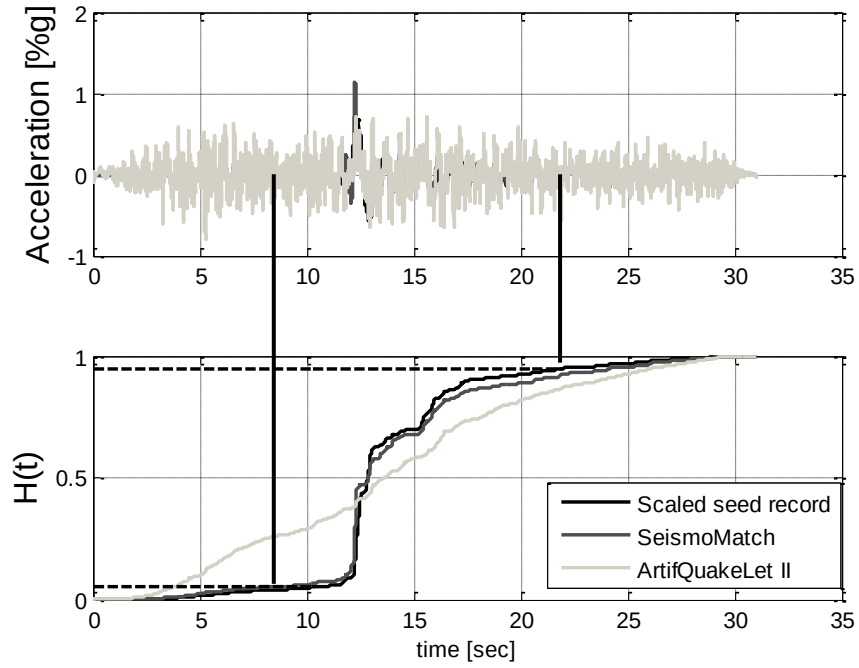

Figure B.2.6. Husid plot and significant duration interval for DM6

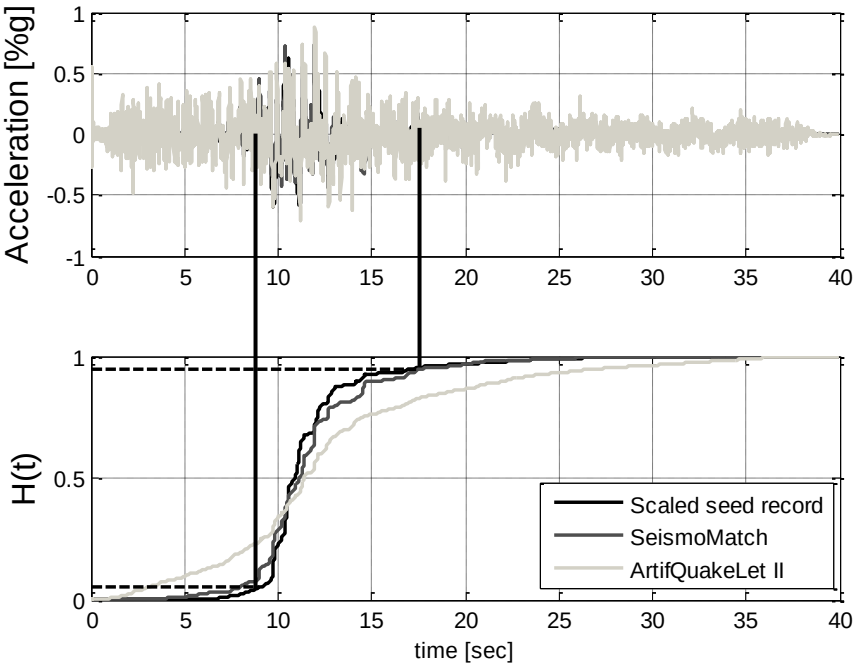

Figure B.2.7. Husid plot and significant duration interval for DM7

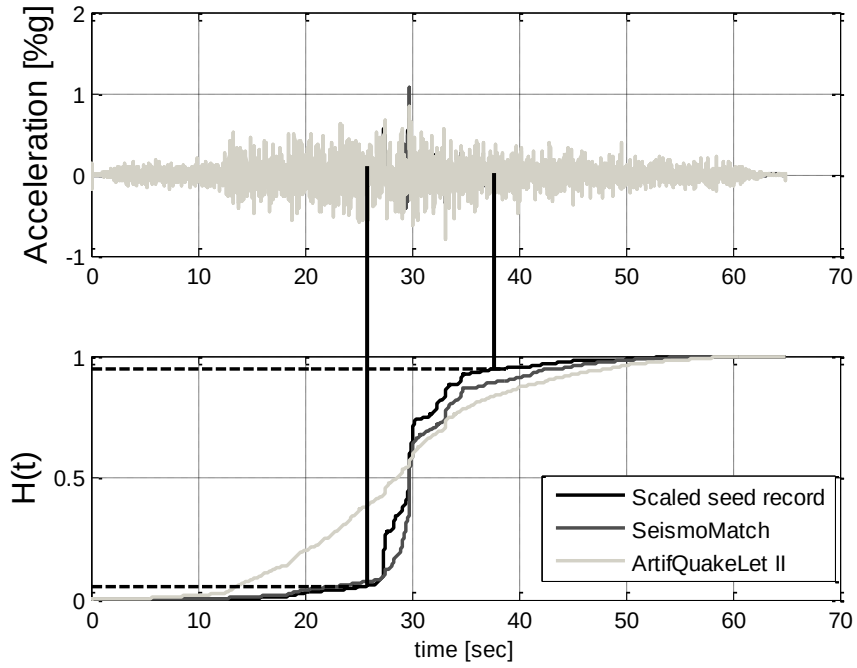

Figure B.2. 8. Husid plot and significant duration interval for DM8

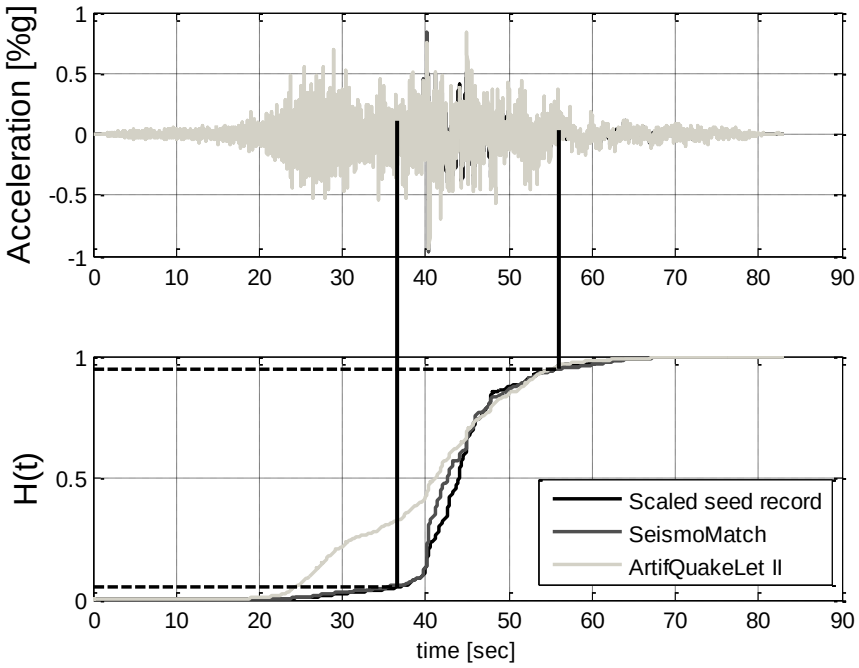

Figure B.2.9. Husid plot and significant duration interval for DM9

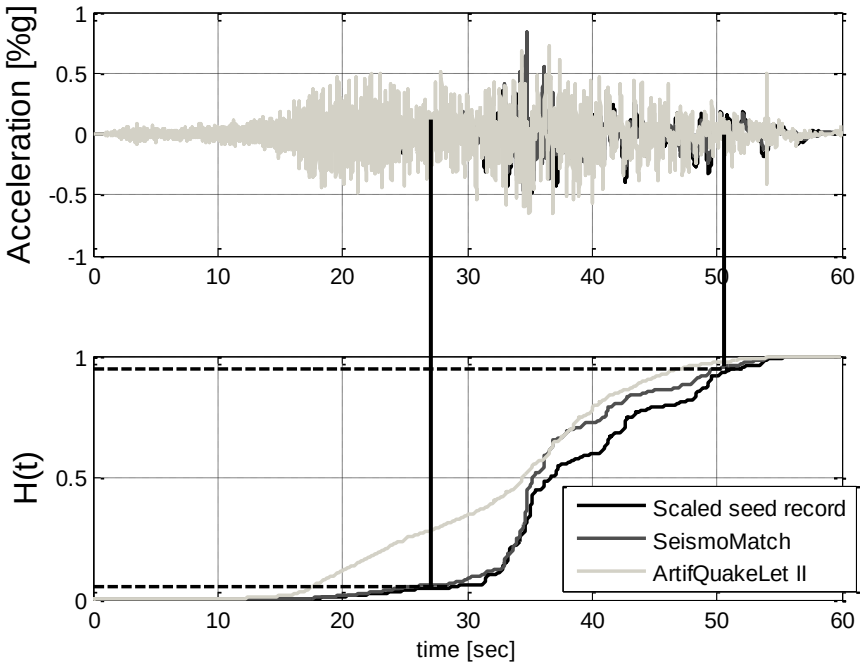

Figure B.2.10. Husid plot and significant duration interval for DM10

B.3 SeismoArtif

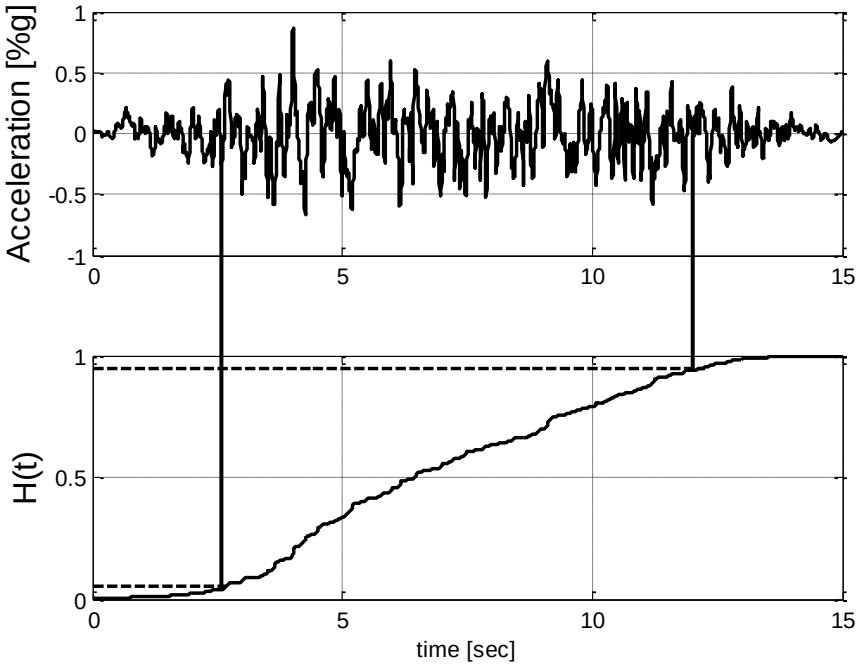

Figure B.3.1 Husid plot and significant duration interval for SA1

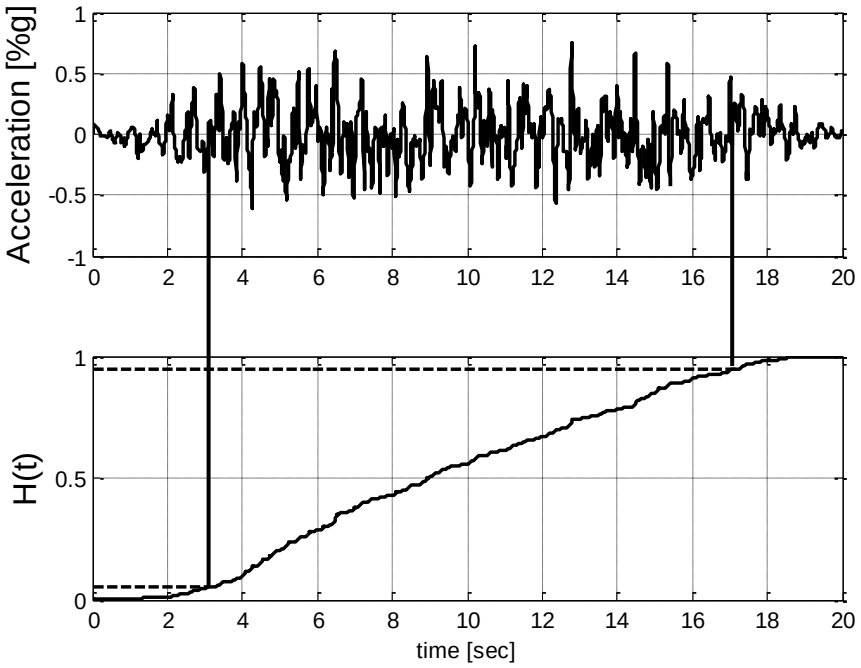

Figure B.3.2. Husid plot and significant duration interval for SA2

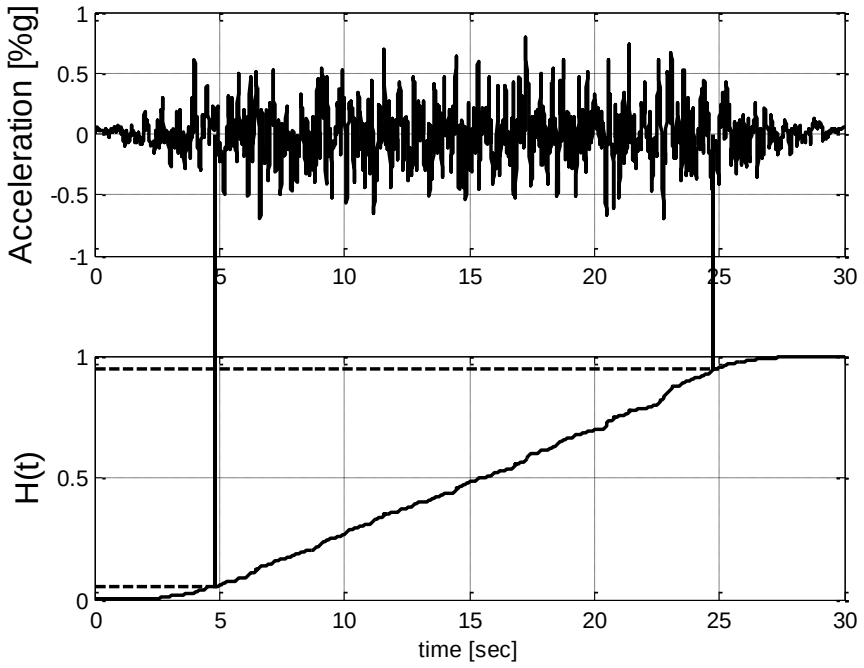

Figure B.3.3. Husid plot and significant duration interval for SA3

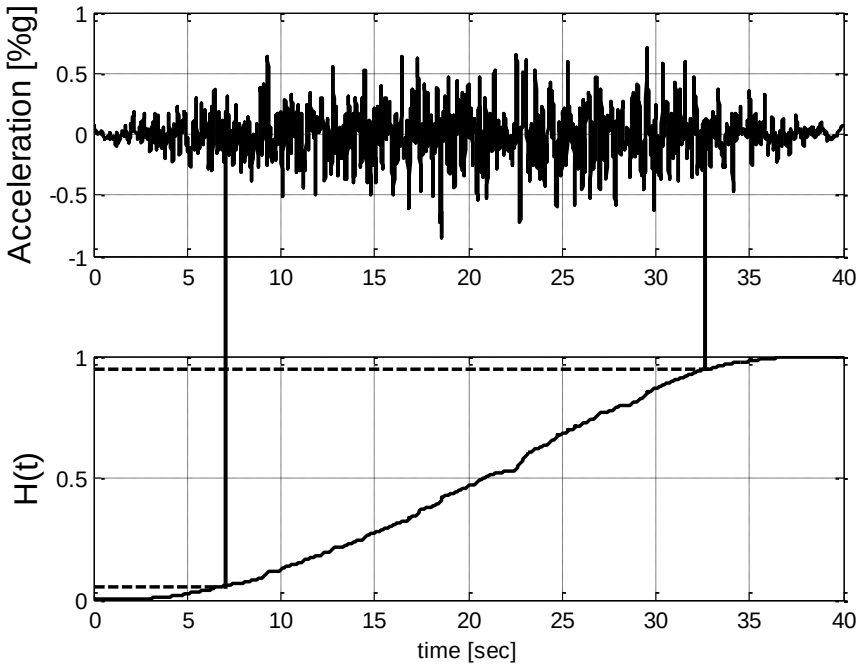

Figure B.3.4. Husid plot and significant duration interval for SA4

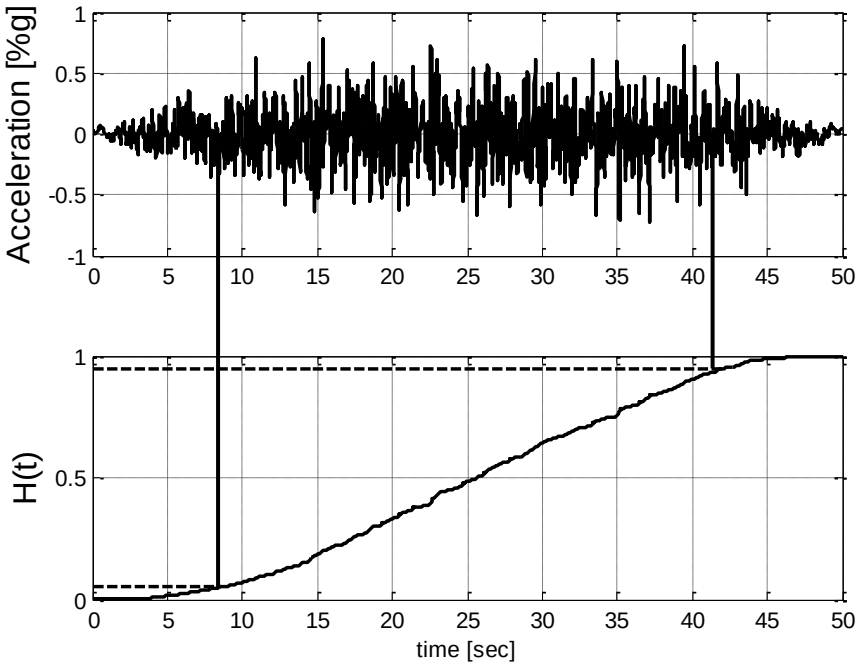

Figure B.3.5. Husid plot and significant duration interval for SA5

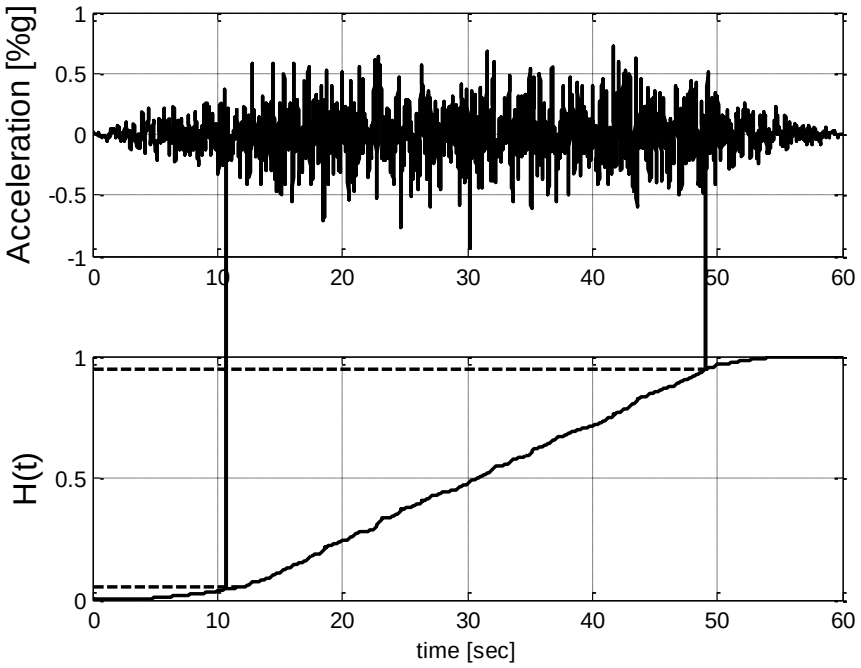

Figure B.3.6. Husid plot and significant duration interval for SA6

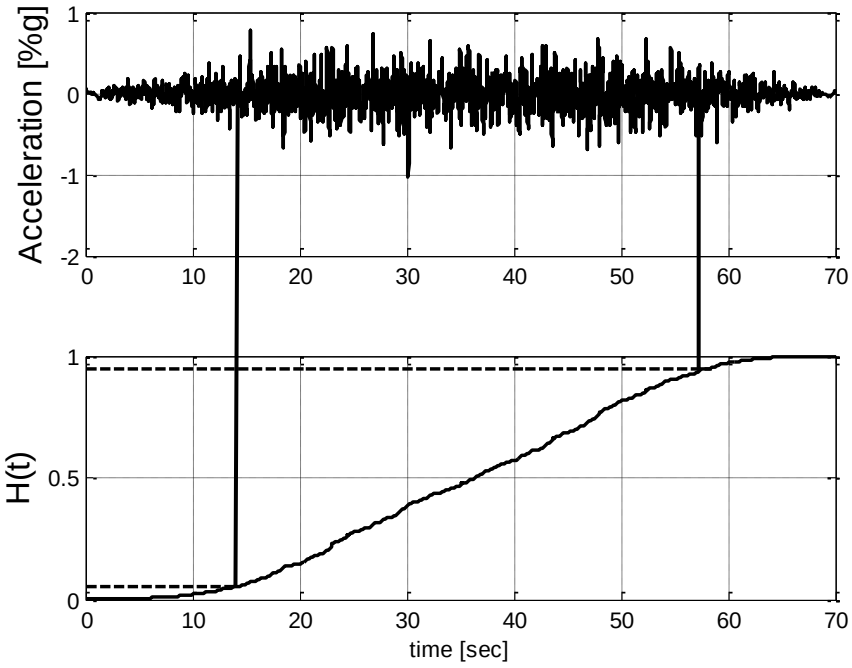

Figure B.3.7. Husid plot and significant duration interval for SA7

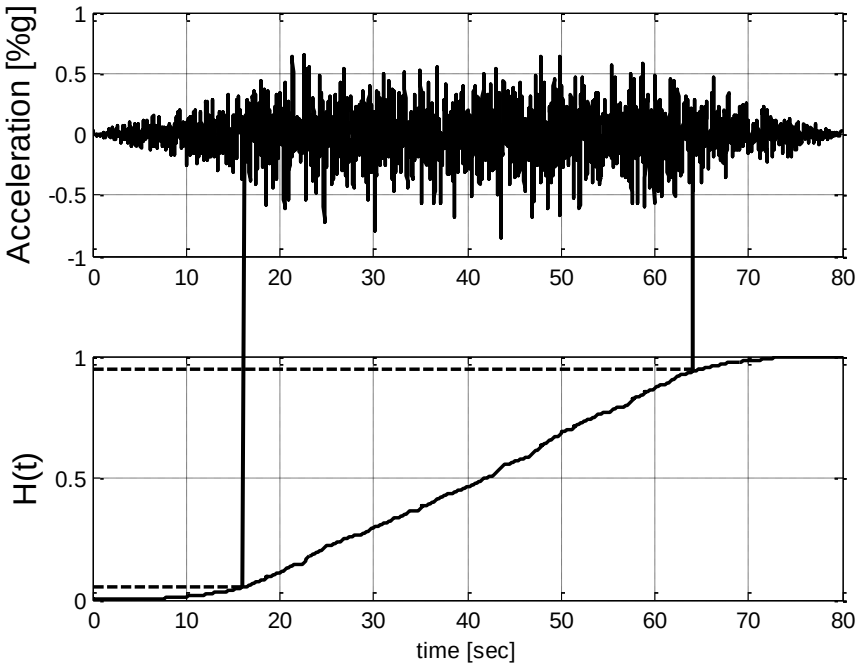

Figure B.3.8. Husid plot and significant duration interval for SA8

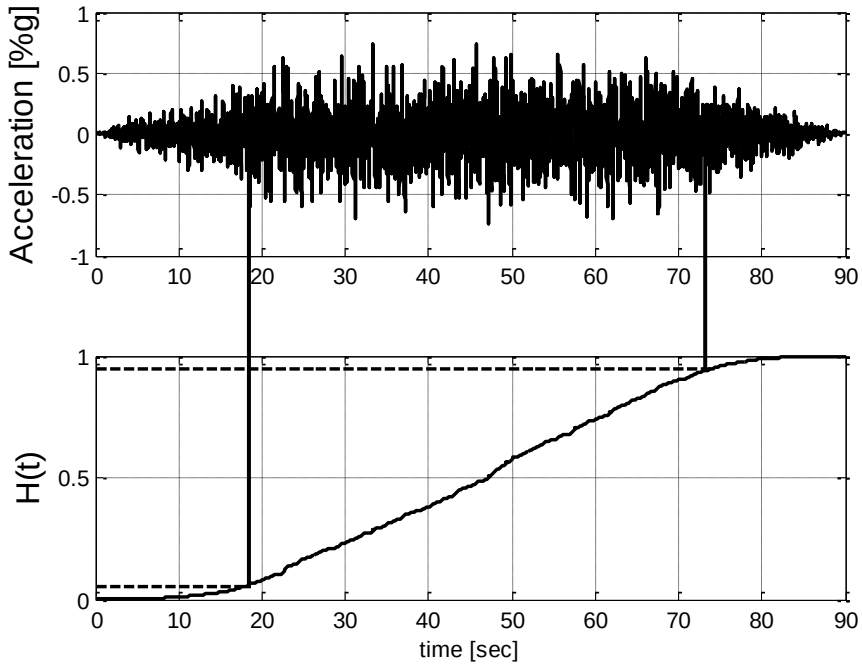

Figure B.3.9. Husid plot and significant duration interval for SA9

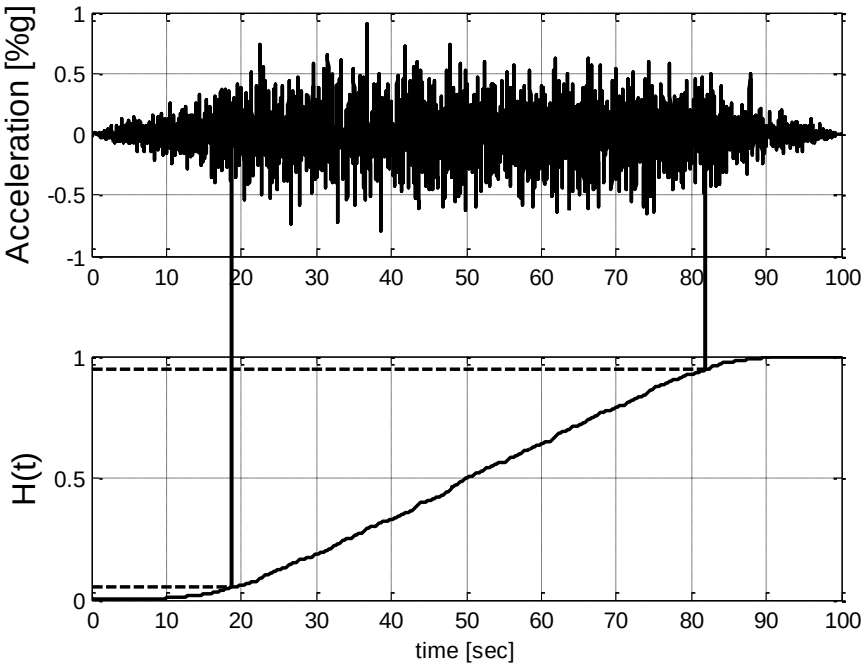

Figure B.3.10 Husid plot and significant duration interval for SA10

APPENDIX C

C. Fourier spectrum and wavelet map

C1. Close Match (CM) scaled seed records

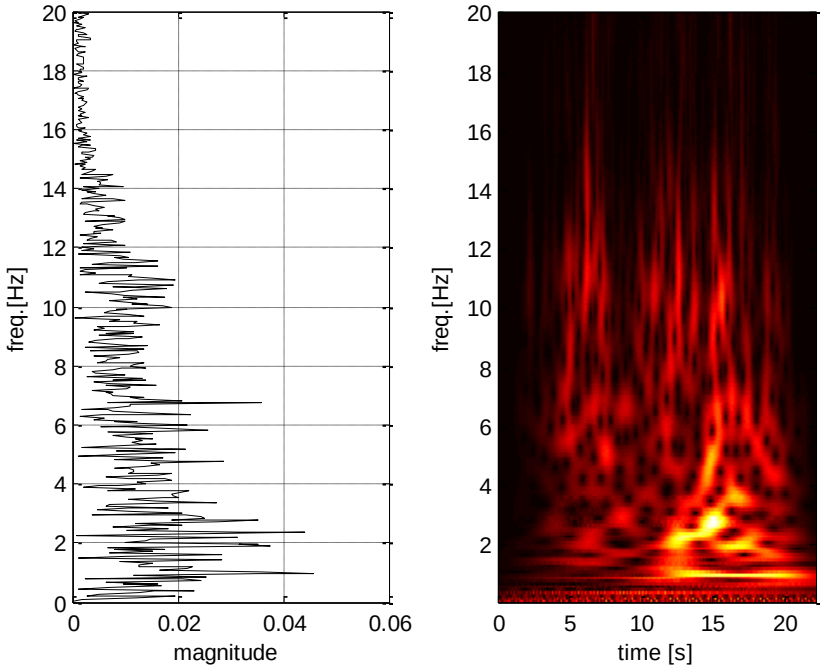

Figure C1.1CM1

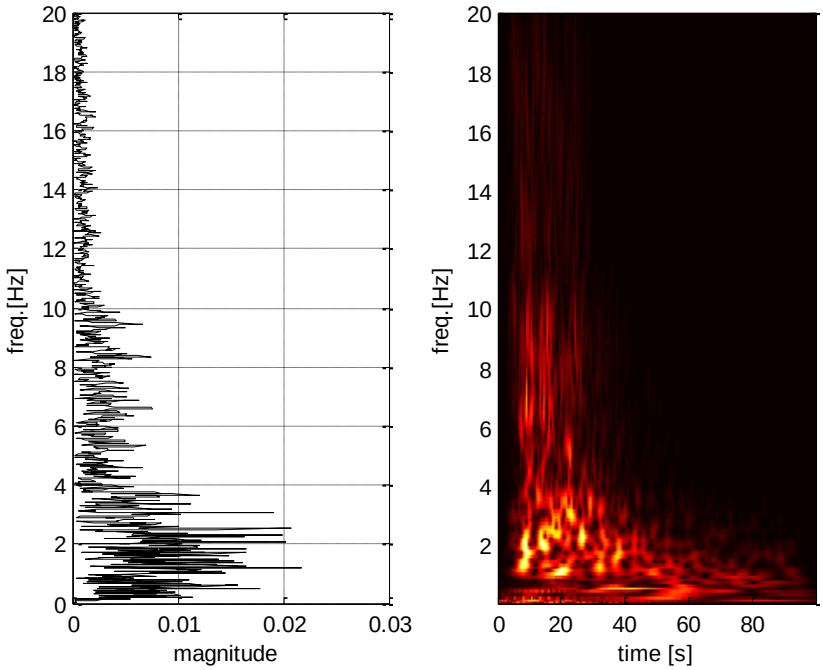

Figure C1.2. CM2

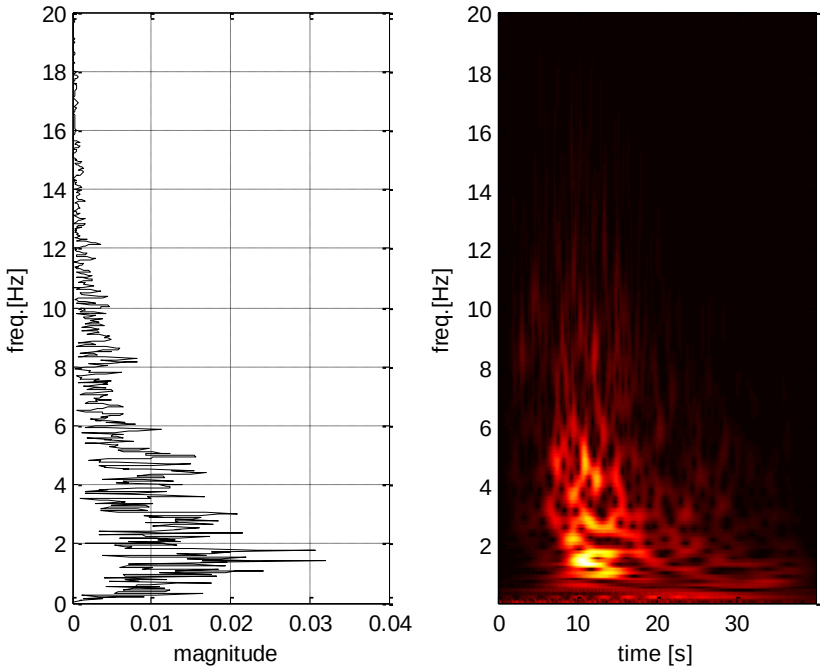

Figure C1.3 CM3

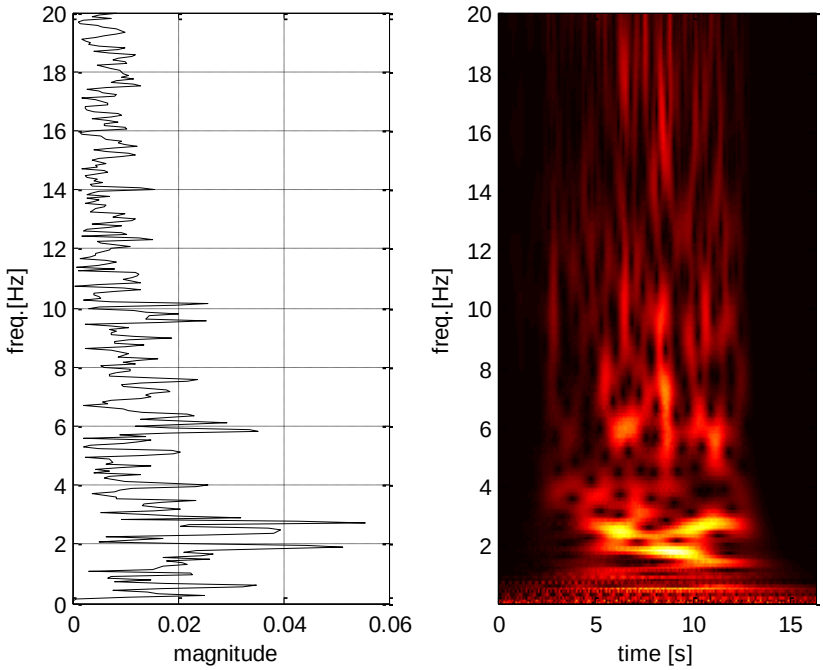

Figure C1.4 CM4

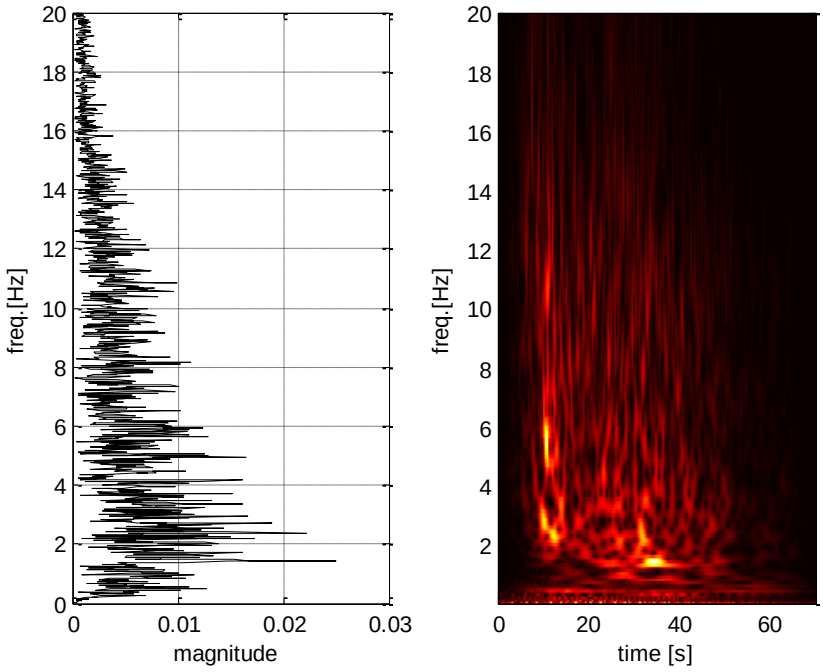

Figure C1.5 CM5

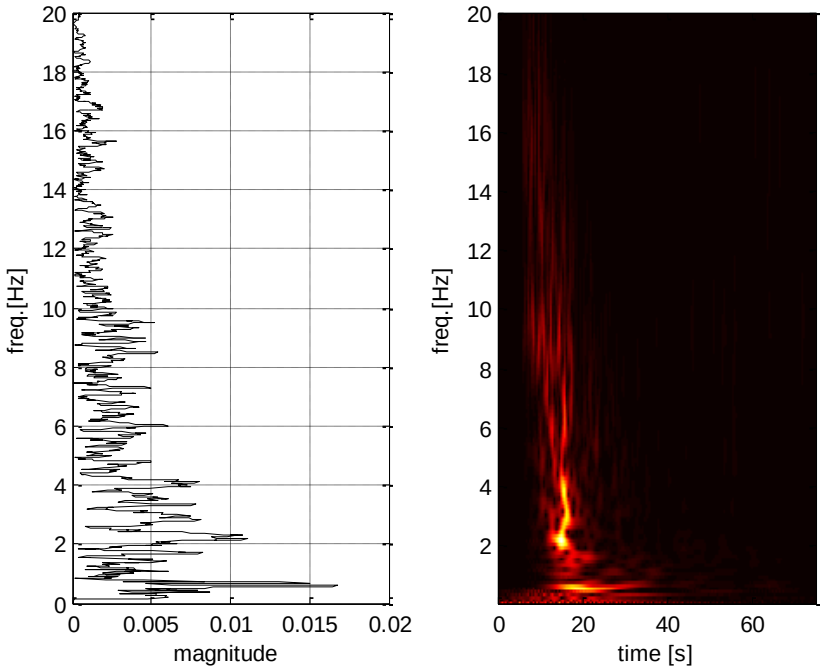

Figure C1.6. CM6

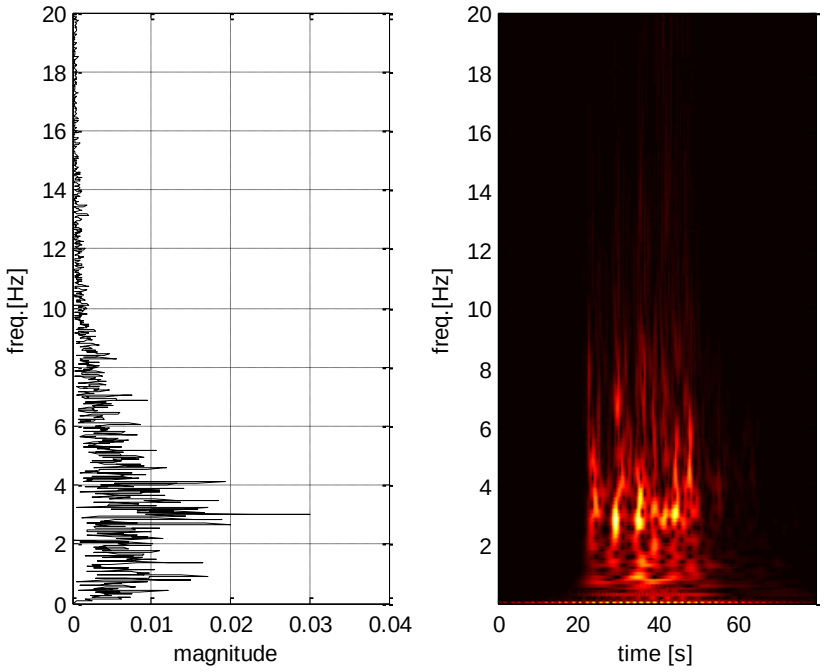

Figure C1.7. CM7

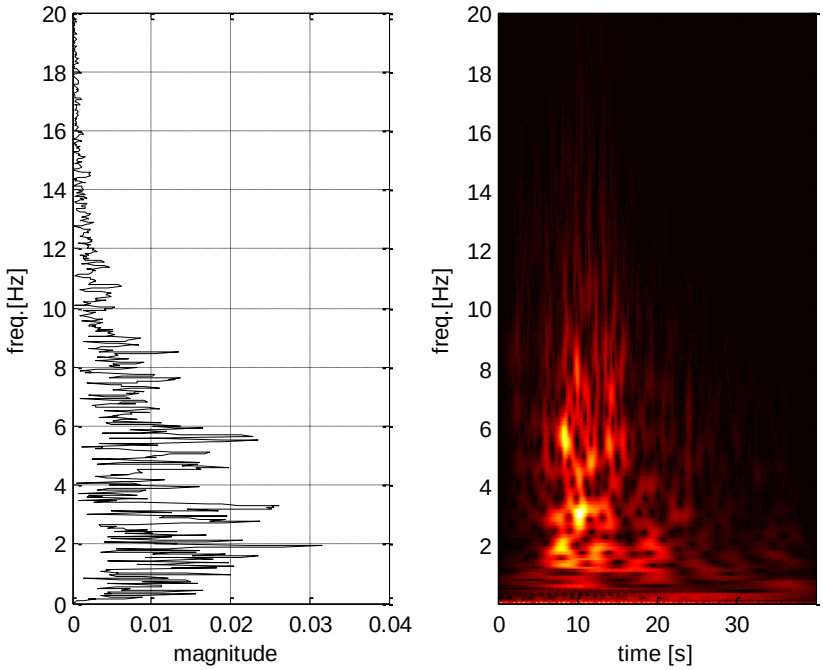

Figure C1.8. CM8

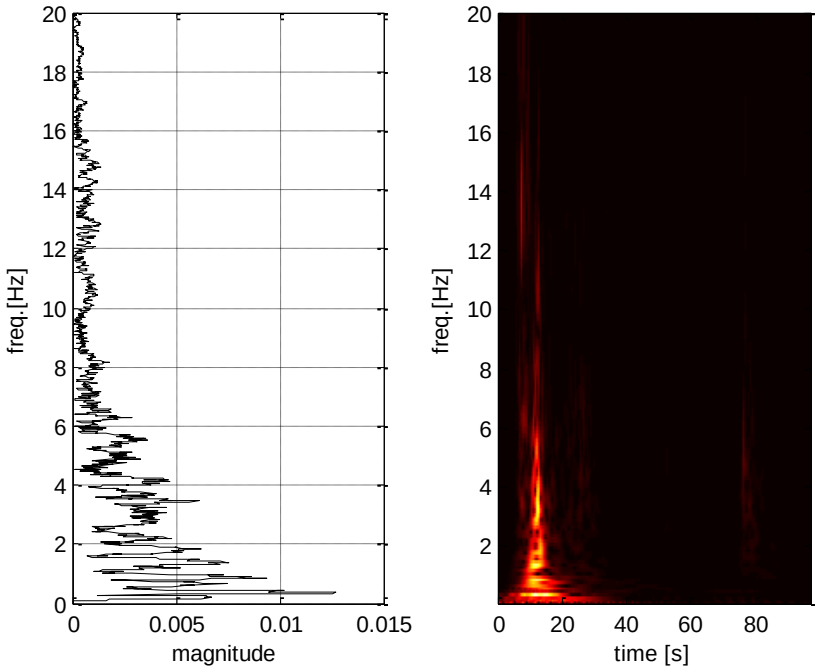

Figure C1.9. CM9

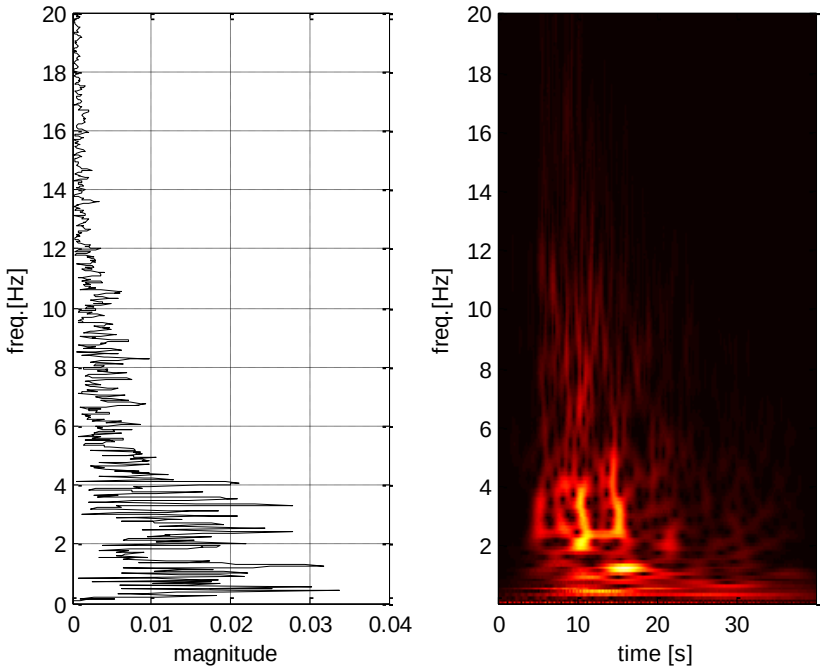

Figure C1.10. CM 10

C2. CM SeismoMatch records

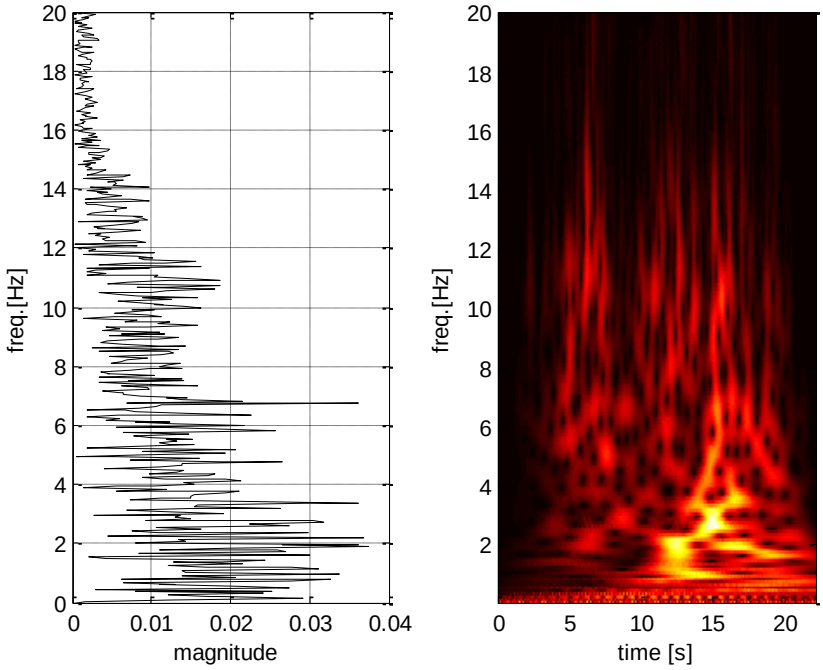

Figure C2.1.CM1

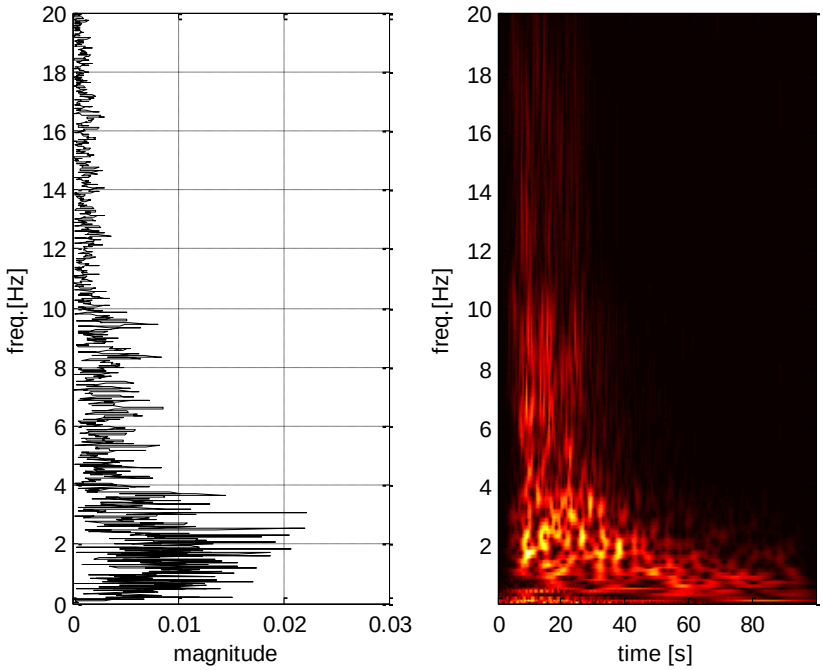

Figure C2.2.CM2

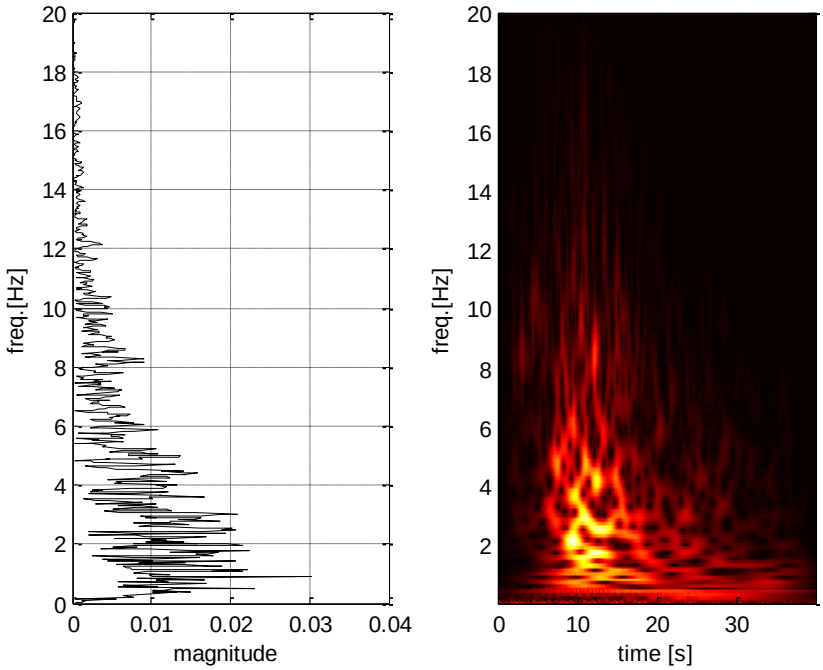

Figure C2.3. CM3

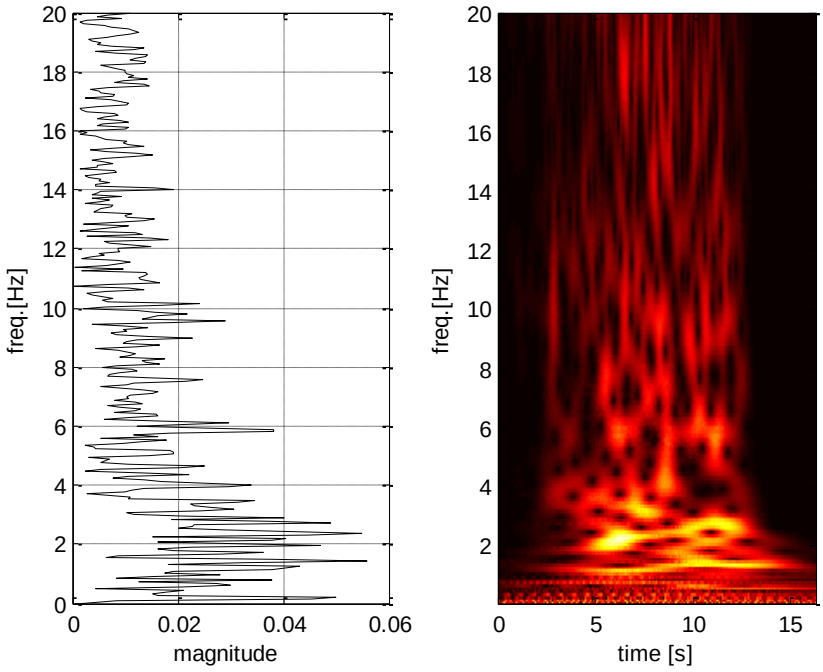

Figure C2.4.CM4

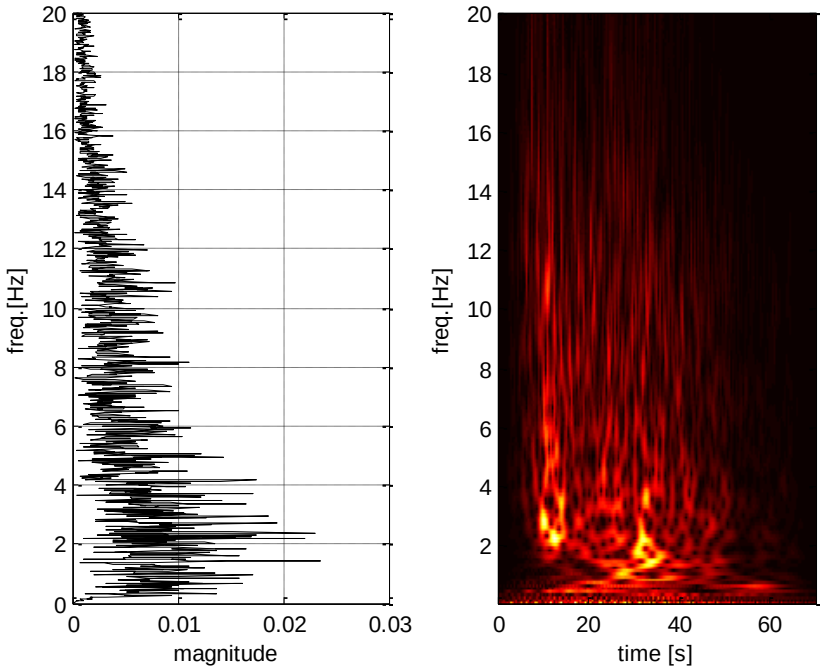

Figure C2.5. CM5

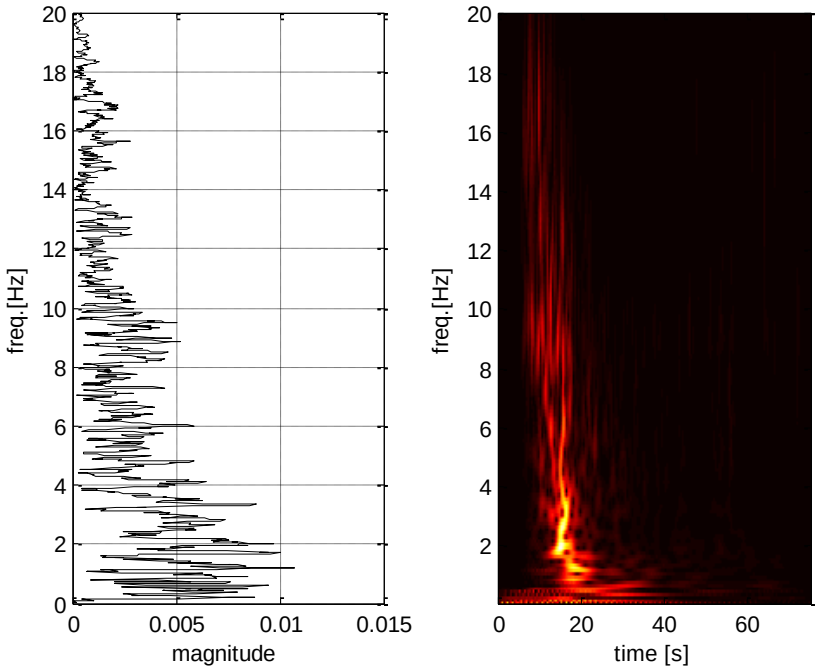

Figure C2.6. CM6

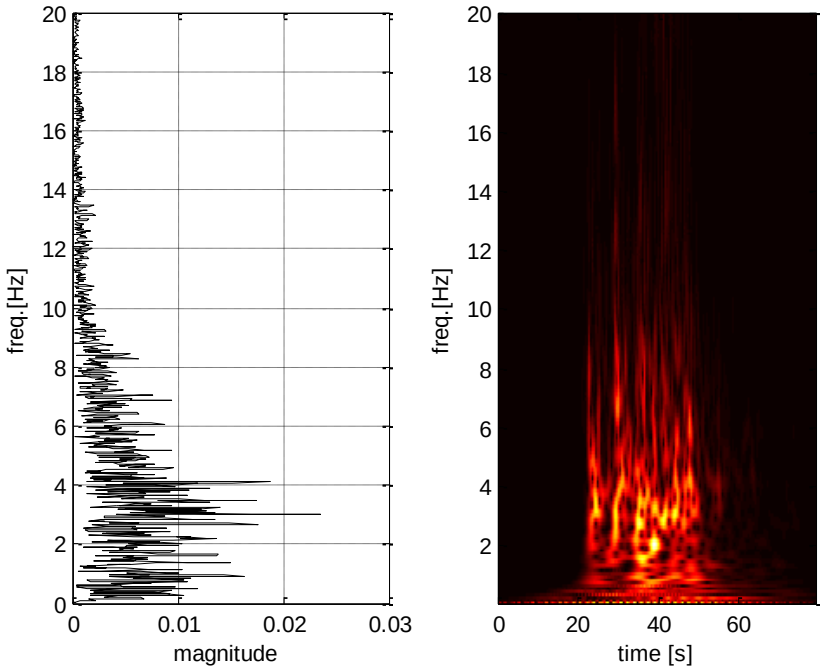

Figure C2.7. CM7

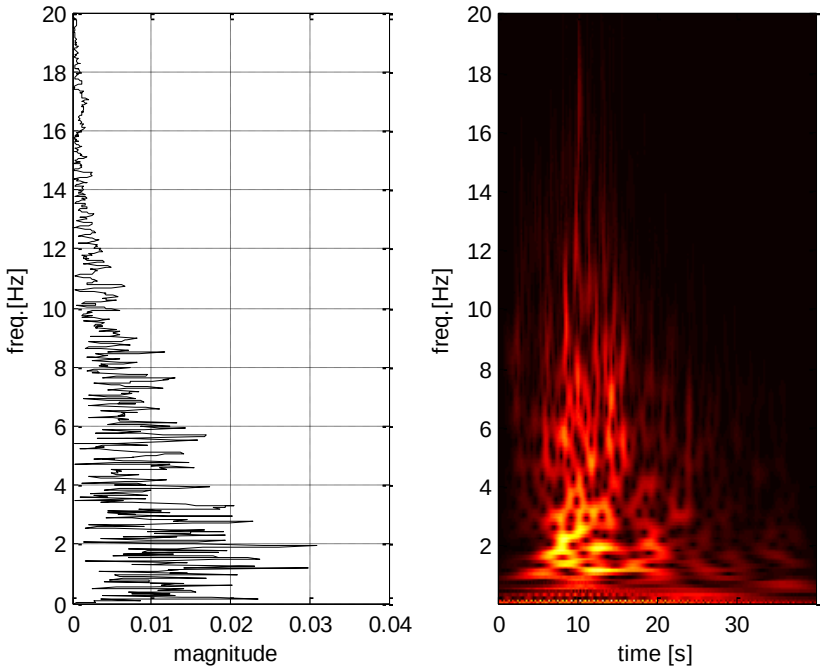

Figure C2.8. CM8

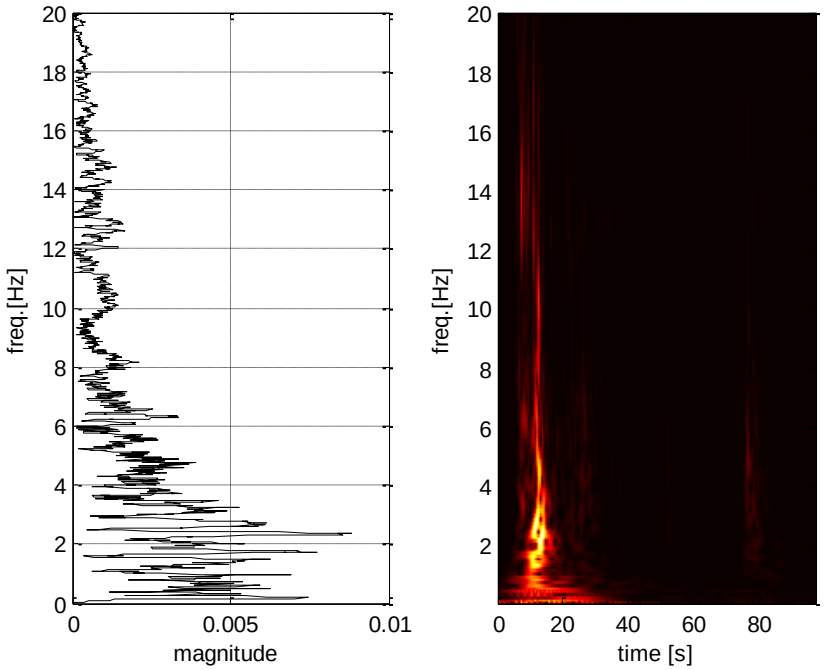

Figure C2.9. CM9

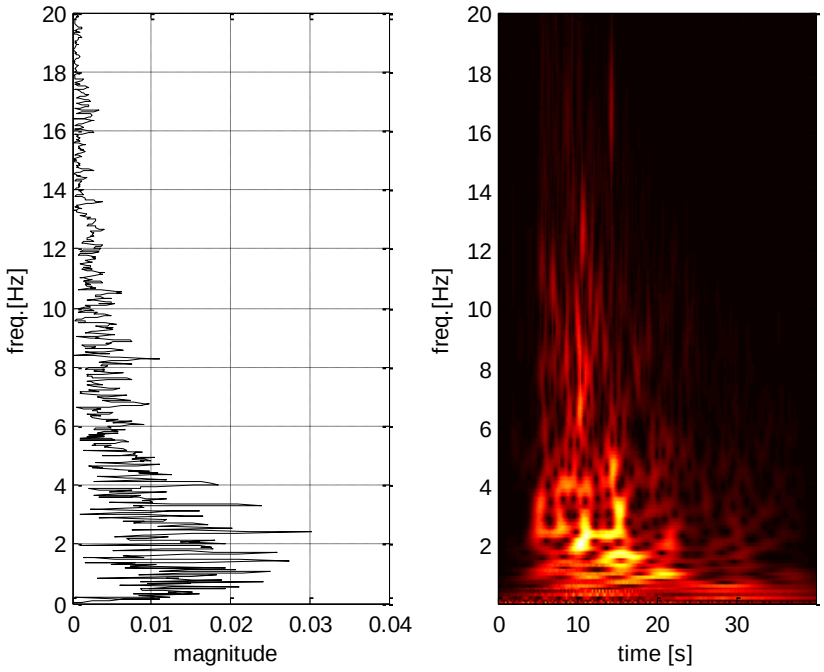

Figure C2.10. CM10

C3. CM AritfQuakeLet II records

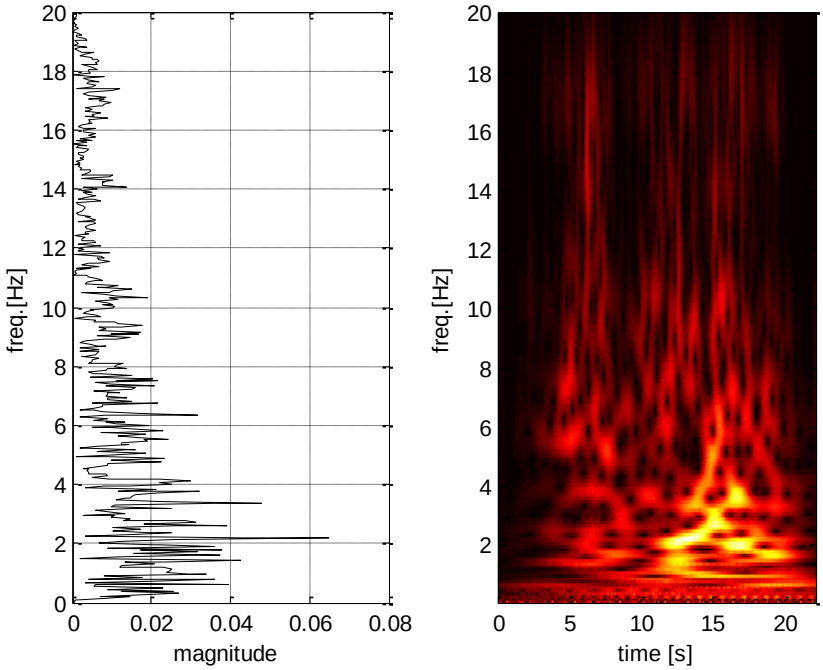

Figure C3. 1.CM1

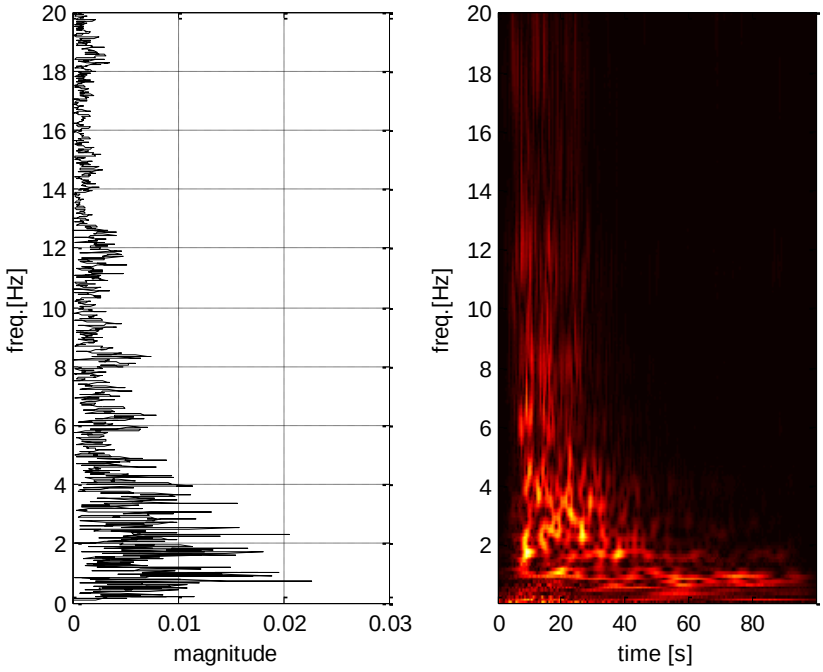

Figure C3.2. CM2

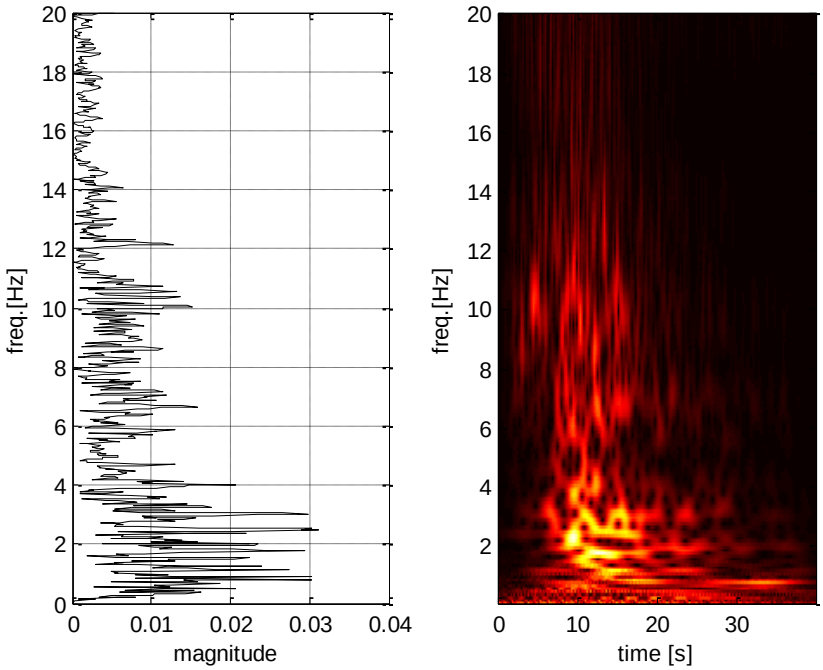

Figure C3. 3. CM3

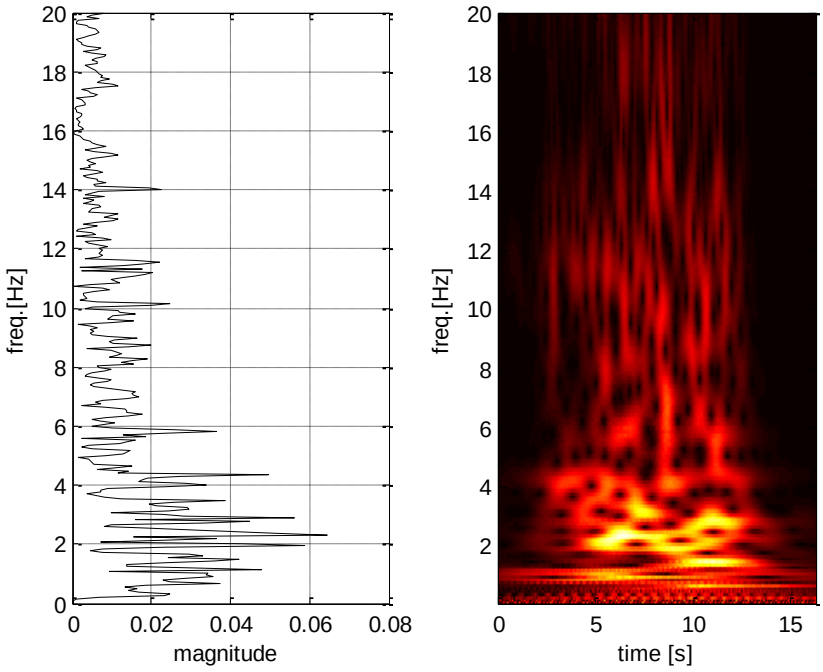

Figure C3. 4. CM4

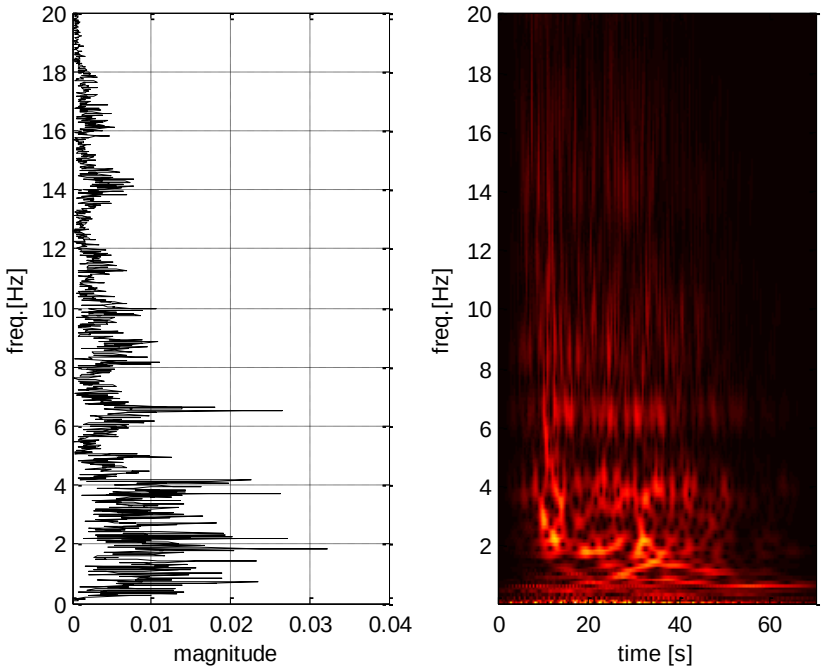

Figure C3. 5. CM5

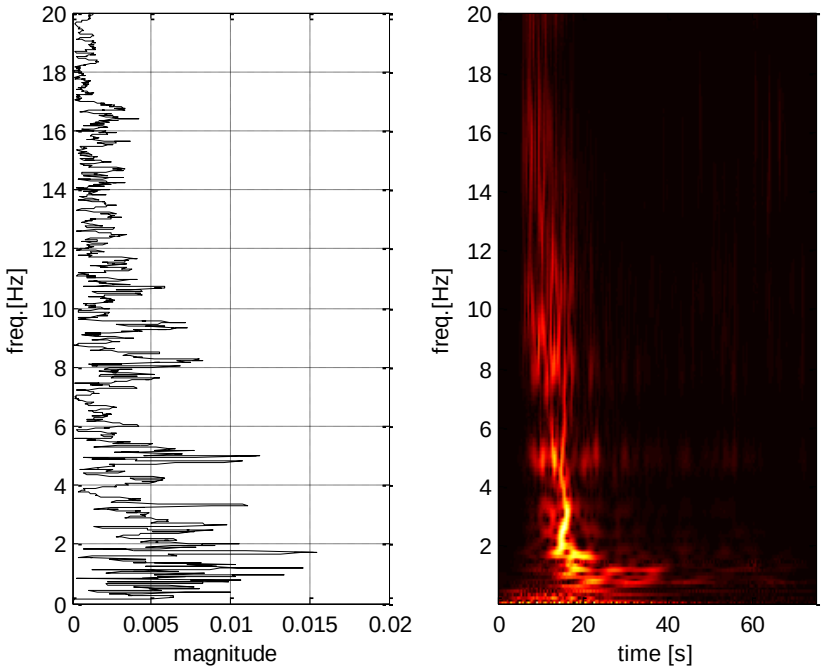

Figure C3. 6. CM6

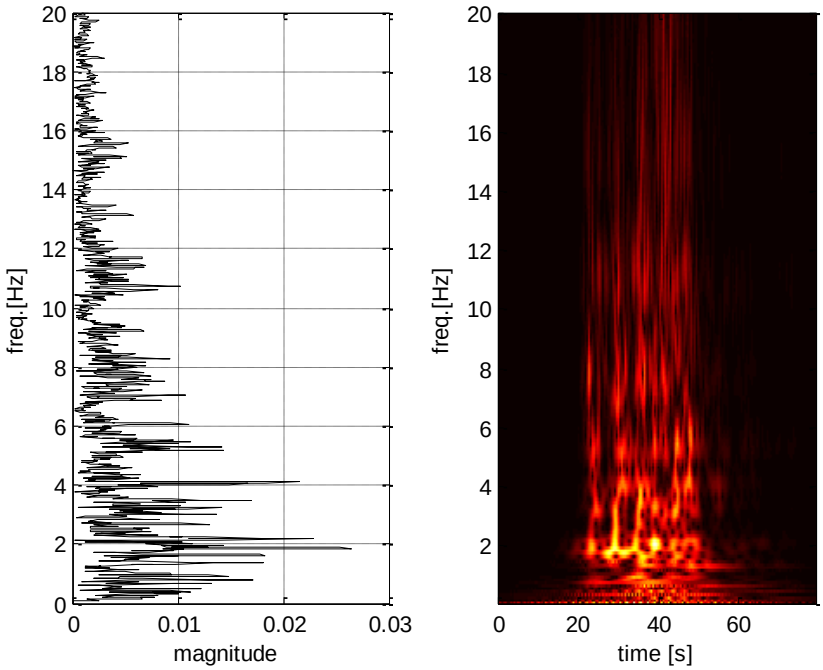

Figure C3. 7. CM7

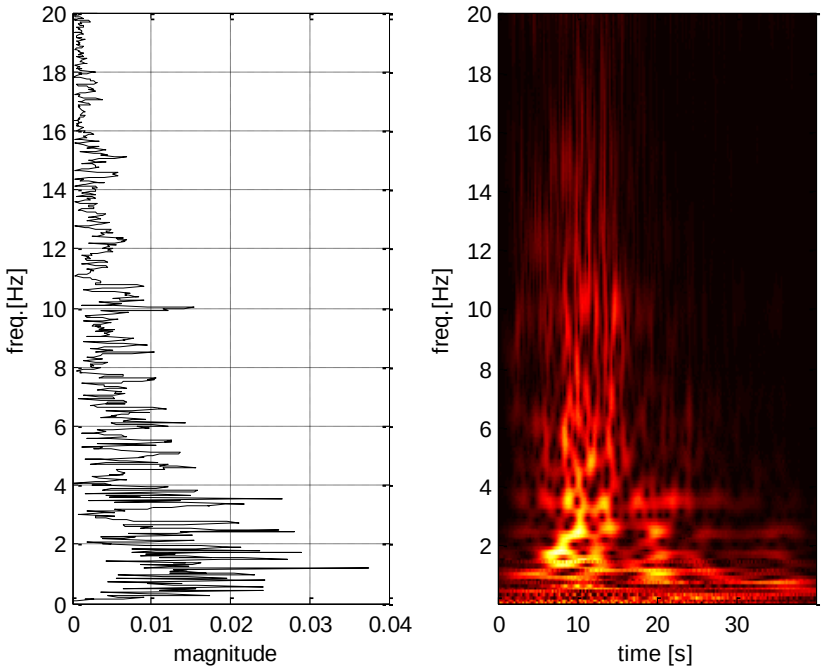

Figure C3. 8. CM8

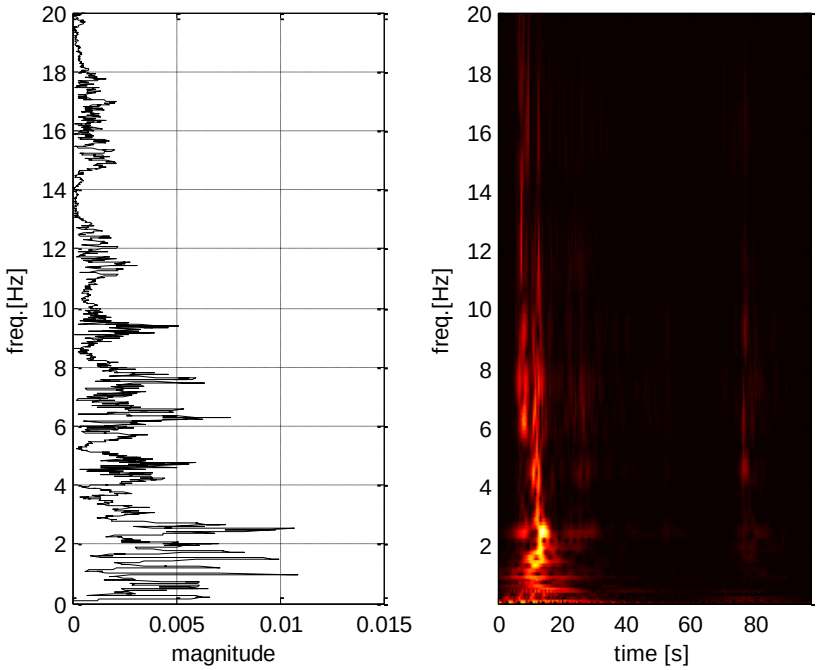

Figure C3. 9. CM9

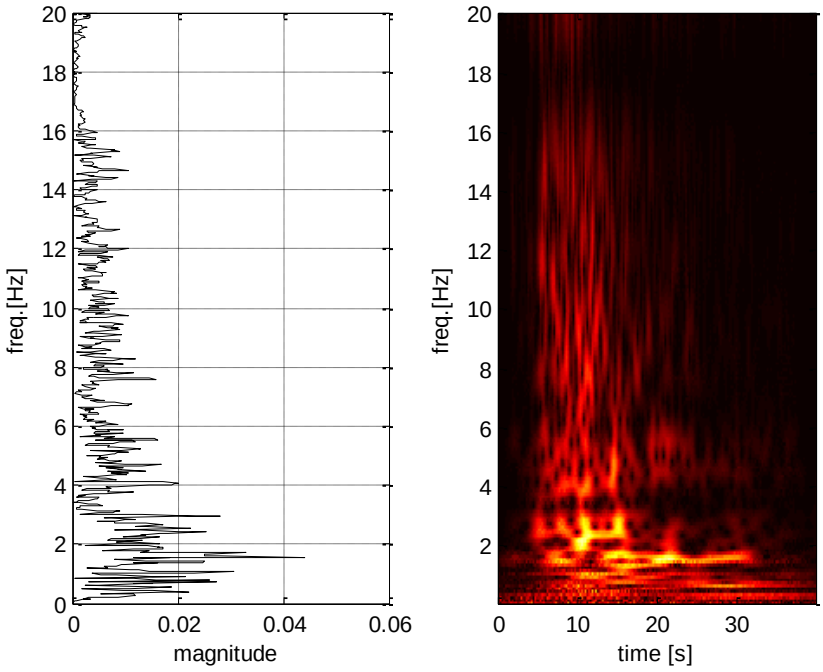

Figure C3. 10. CM10

C4. Distant Match (DM) Scaled seed record

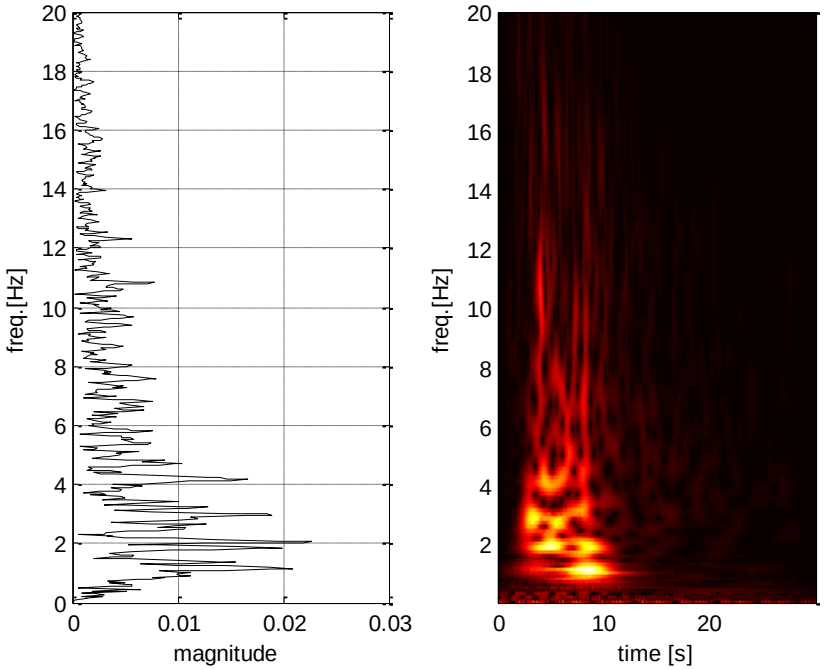

Figure C4. 1 DM1

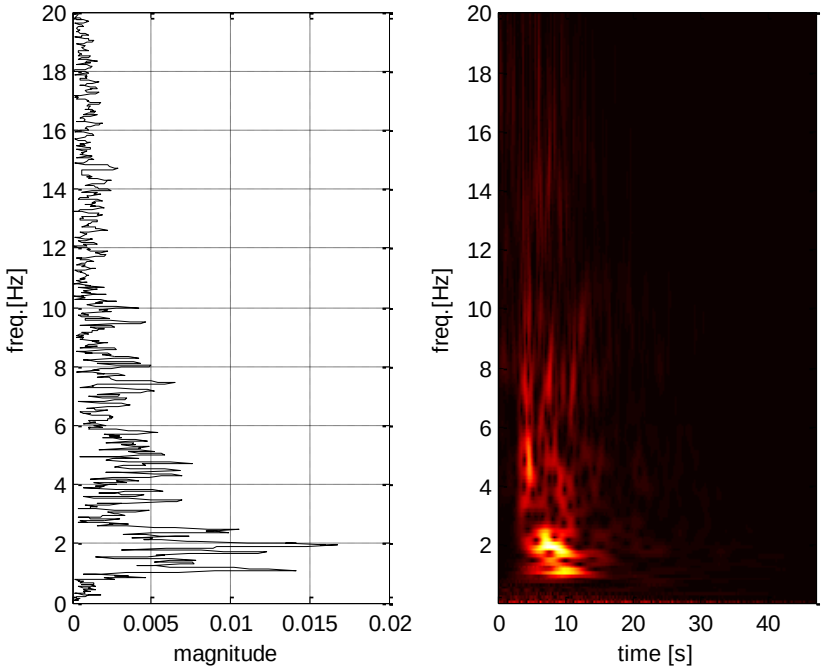

Figure C4. 2.DM2

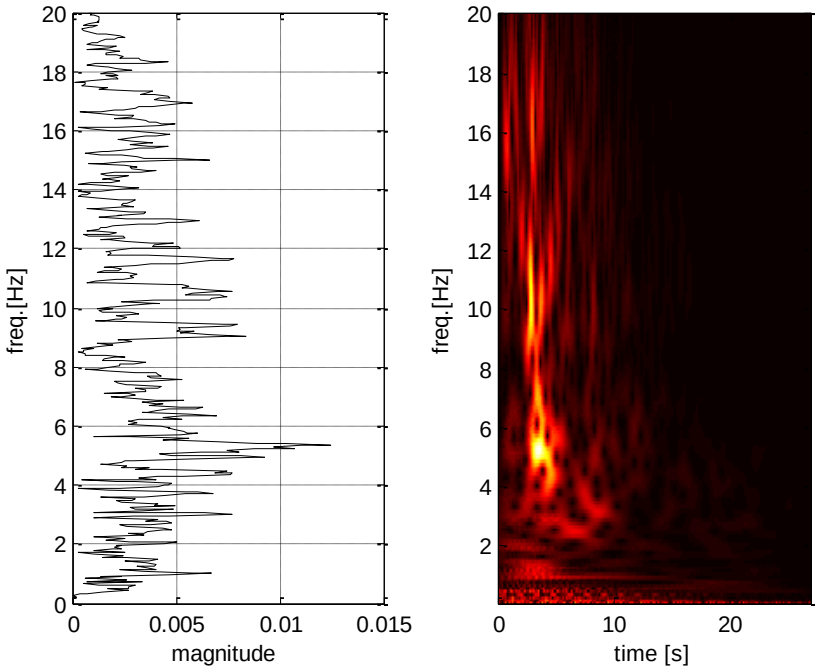

Figure C4. 3. DM3

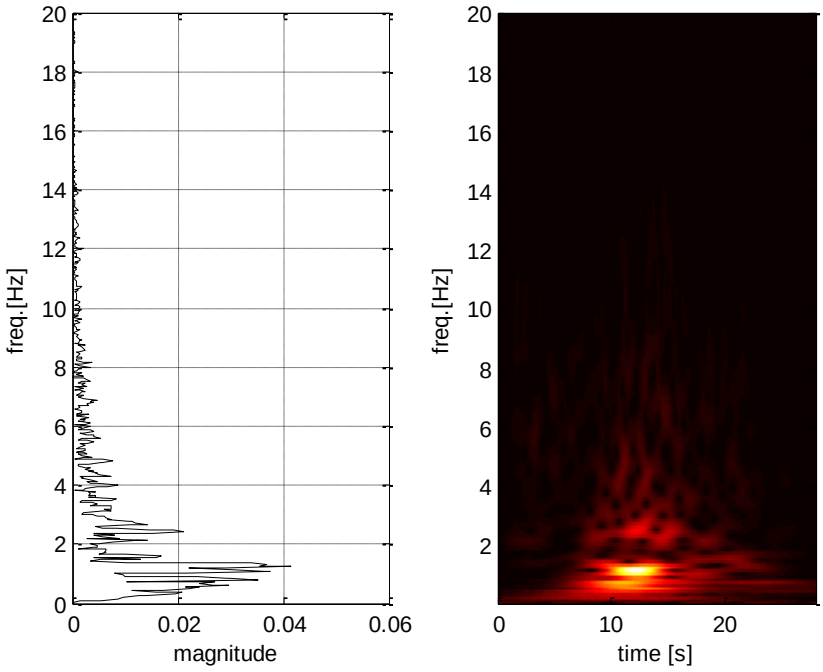

Figure C4. 4. DM4

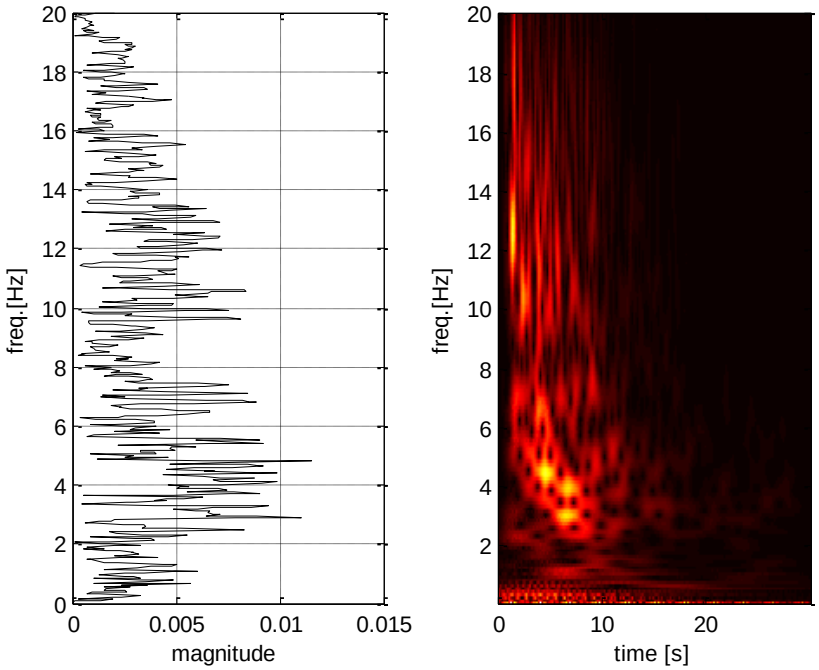

Figure C4. 5. DM5

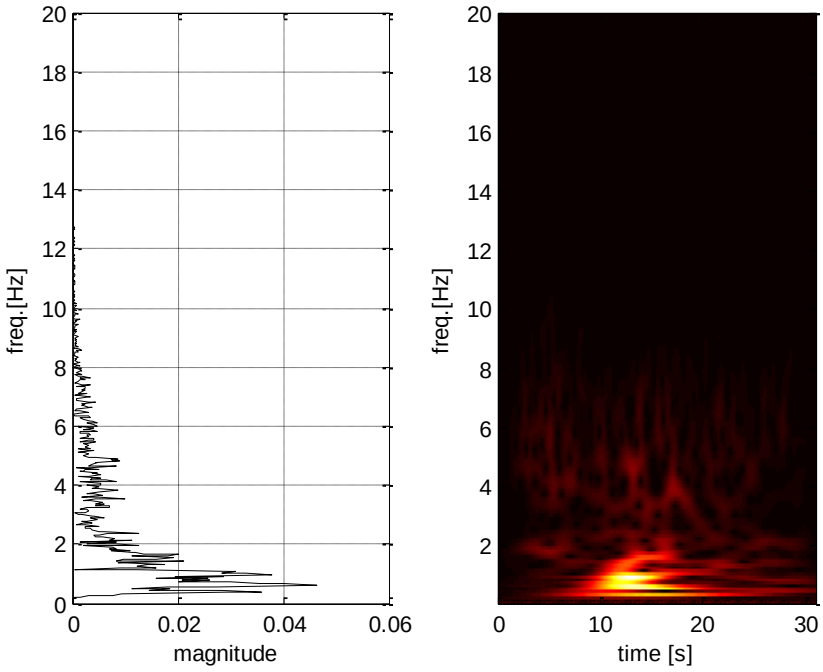

Figure C4. 6. DM6

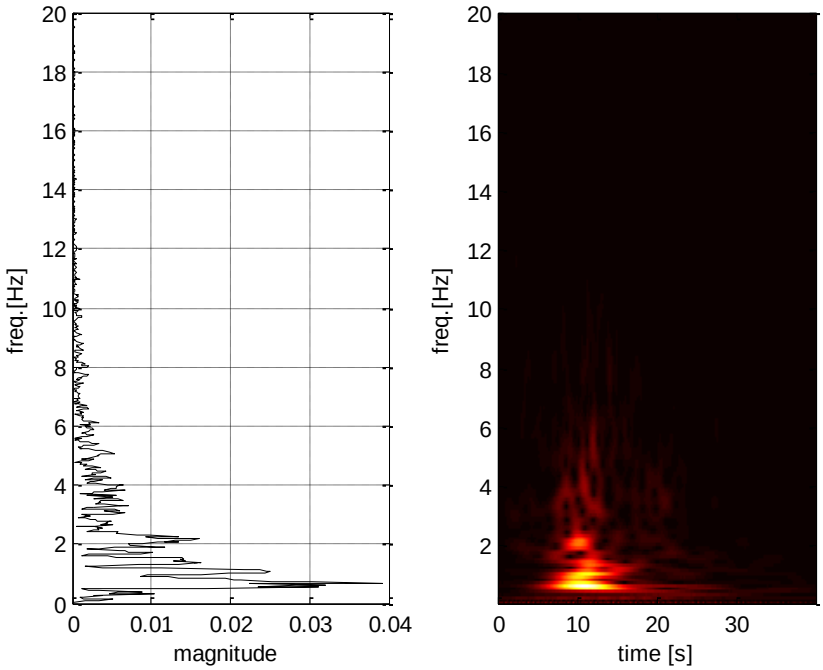

Figure C4. 7. DM7

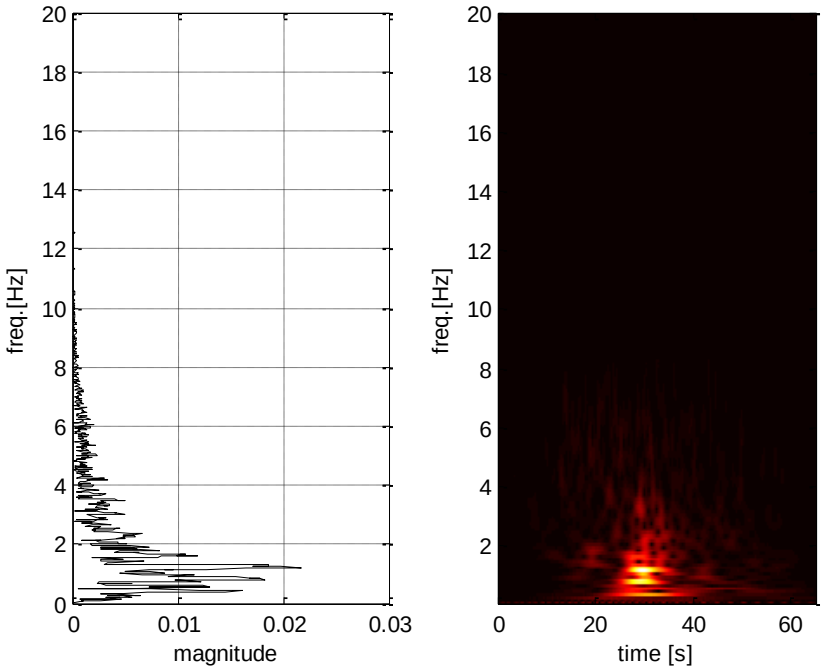

Figure C4. 8. DM8

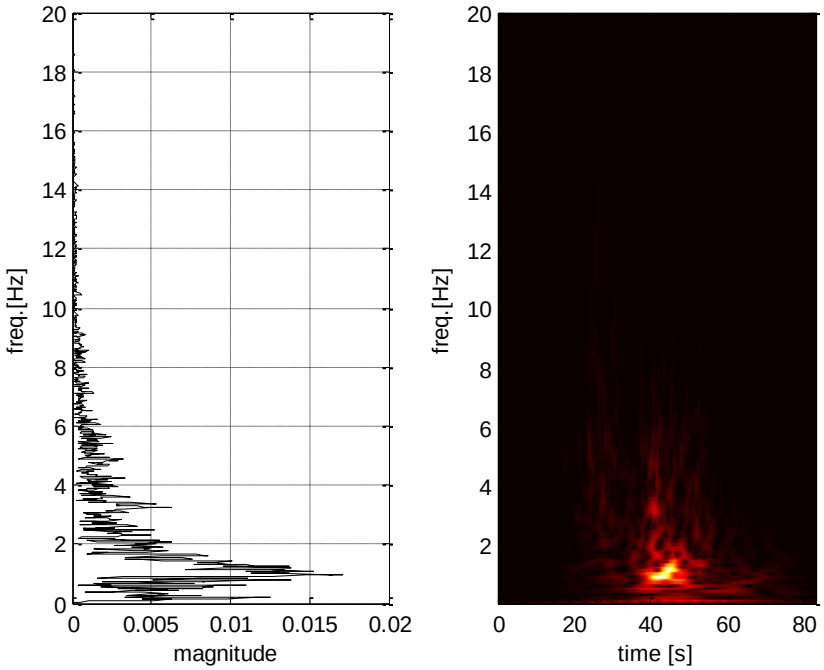

Figure C4. 9. DM9

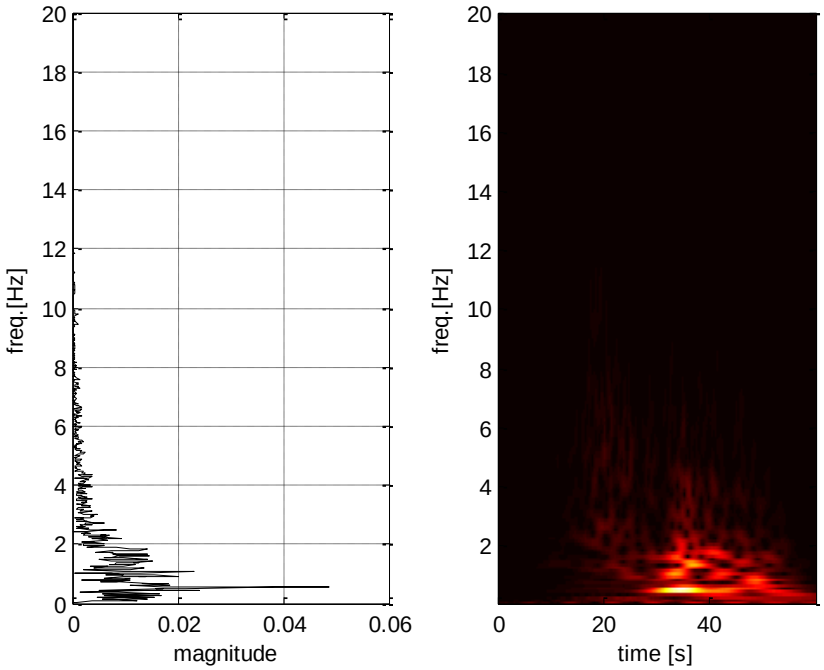

Figure C4. 10. DM10

C5. DM SeismoMatch records

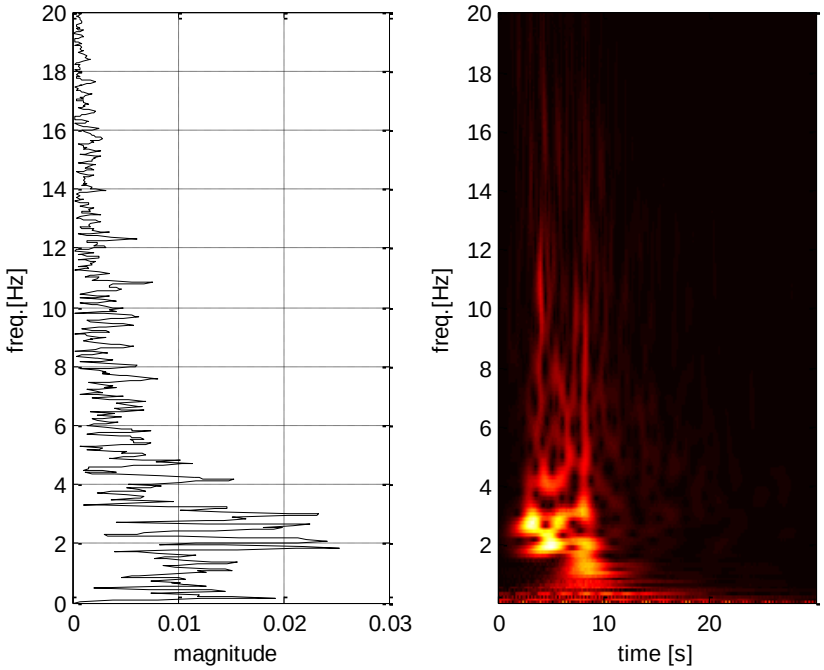

Figure C5. 1. DM1

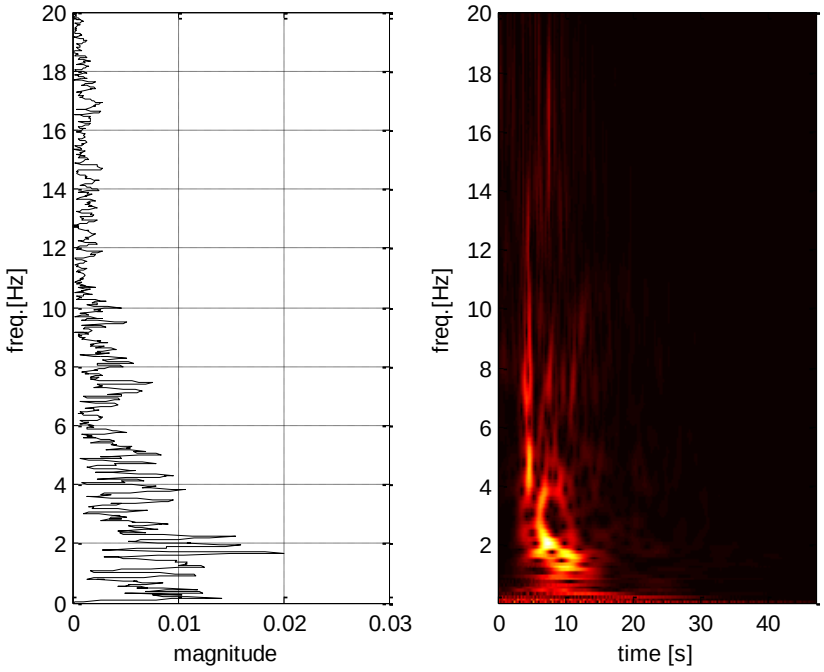

Figure C5. 2. DM2

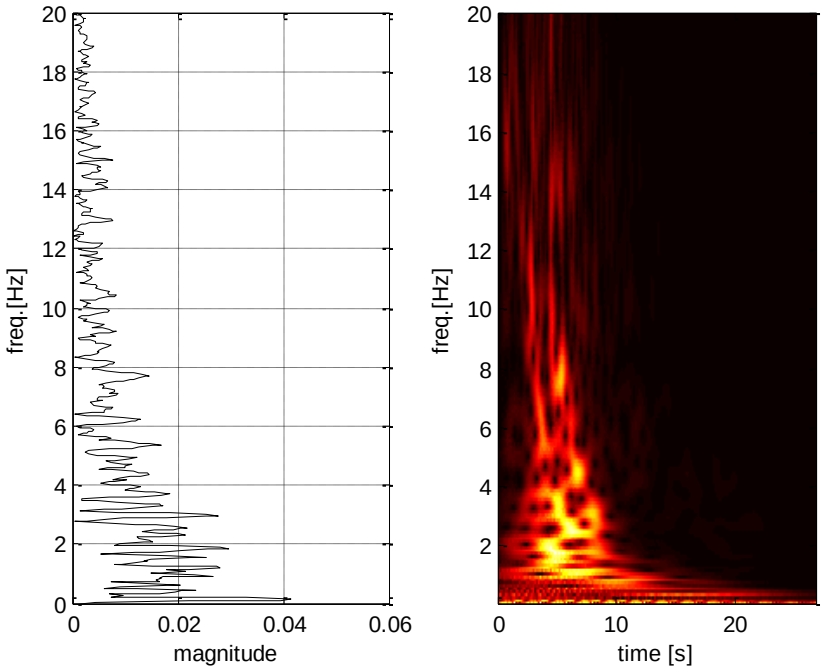

Figure C5. 3. DM3

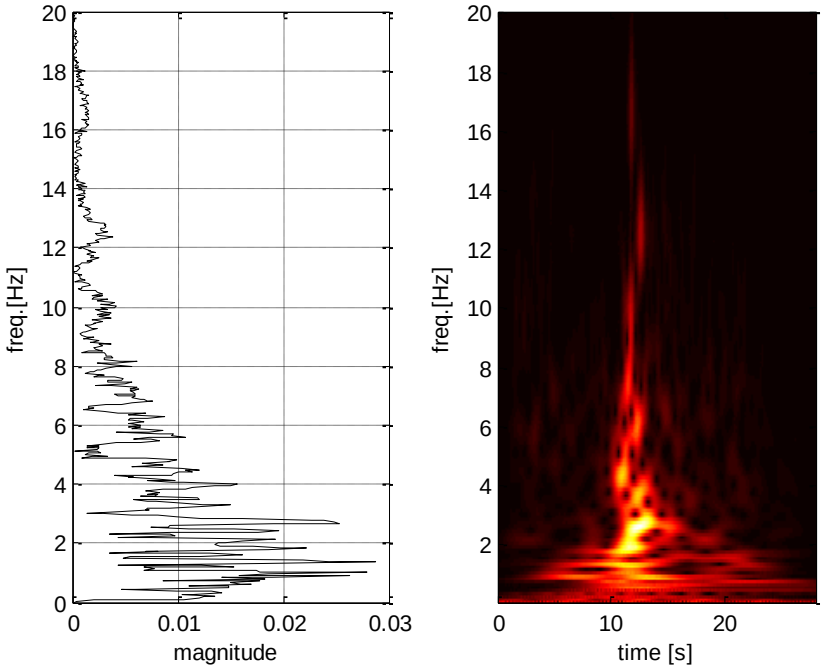

Figure C5. 4. DM4

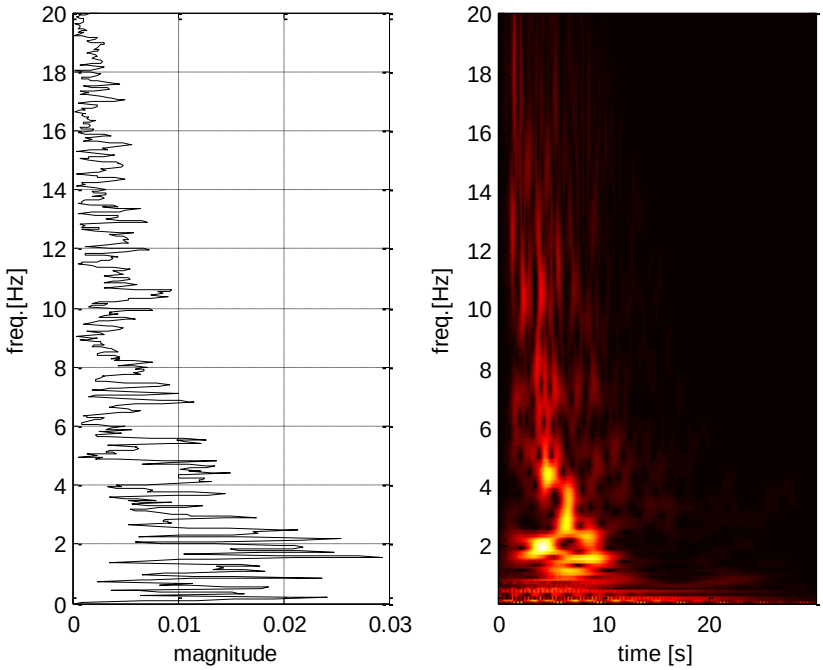

Figure C5. 5. DM5

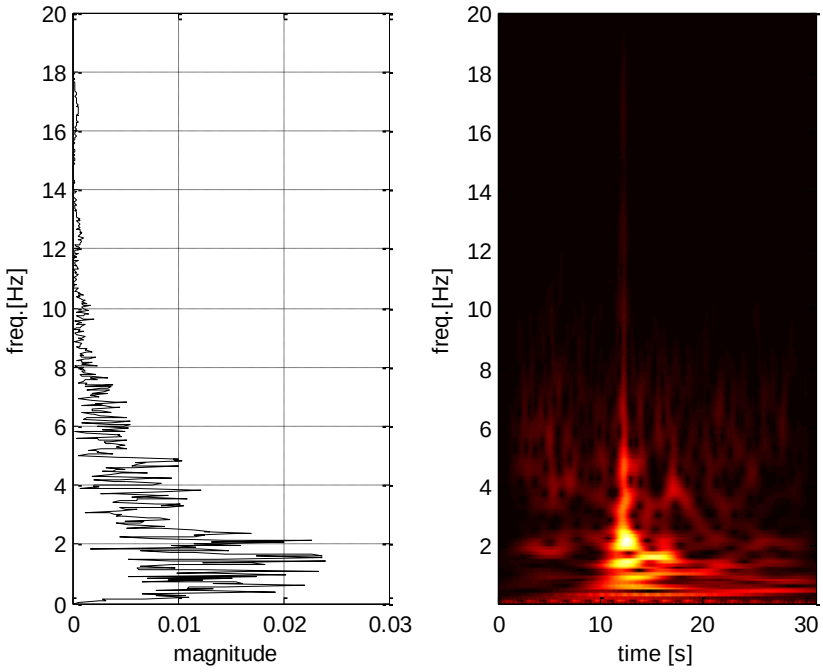

Figure C5. 6. DM6

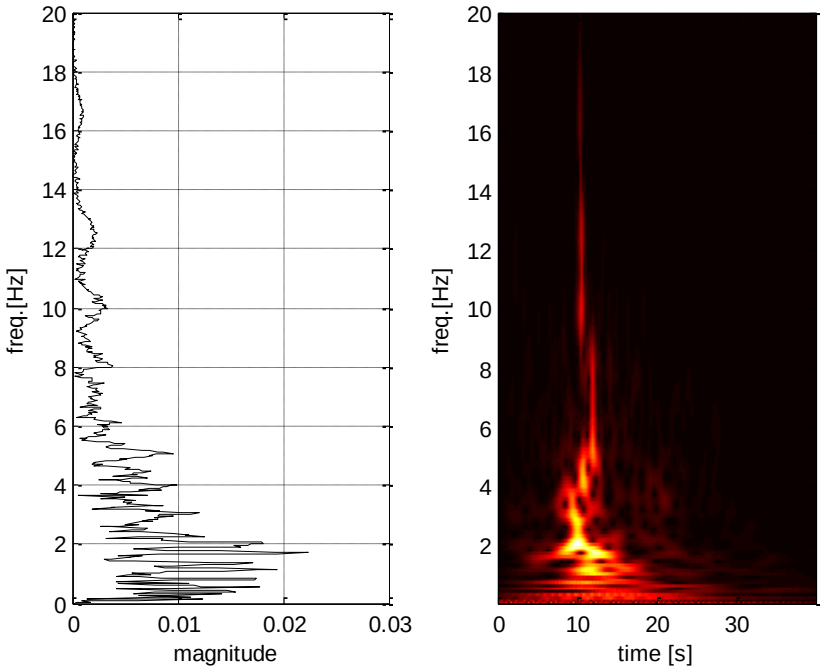

Figure C5. 7. DM7

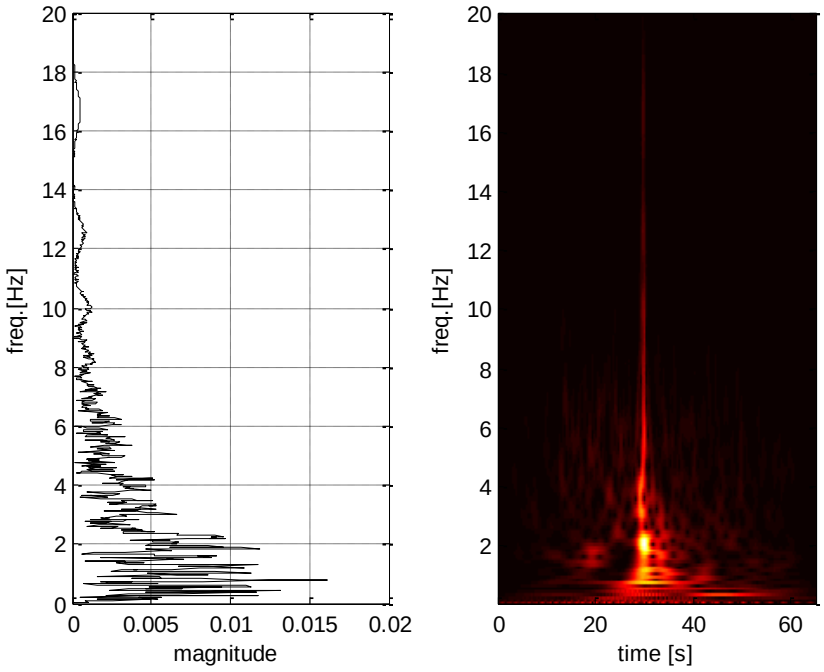

Figure C5. 8. DM8

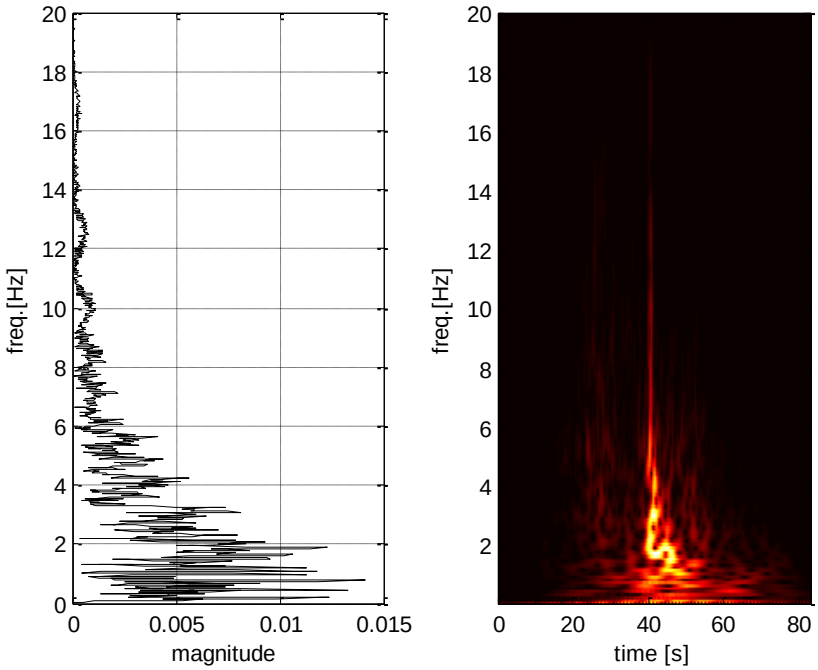

Figure C5. 9. DM9

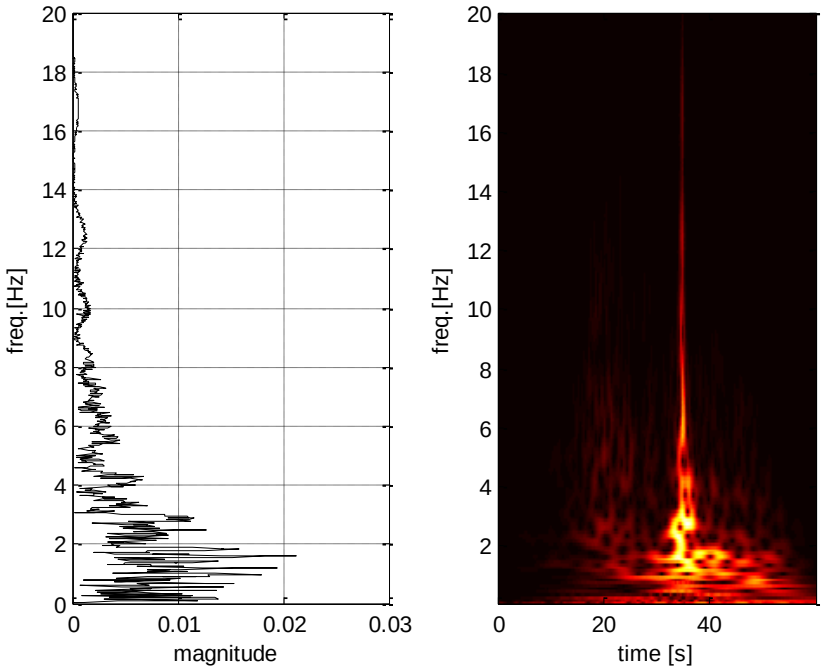

Figure C5. 10. DM10

C6. DM ArtifQuakeLet II records

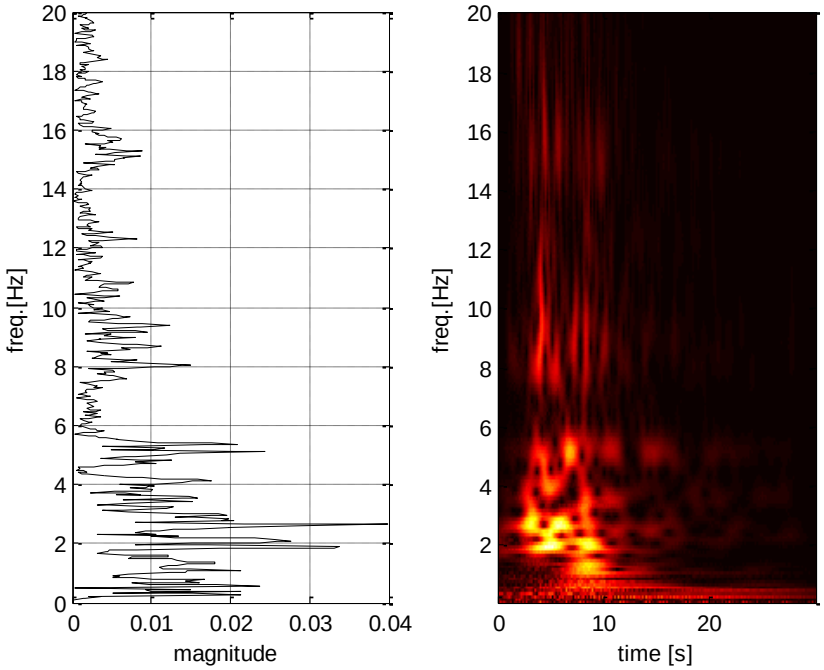

Figure C6. 1. DM1

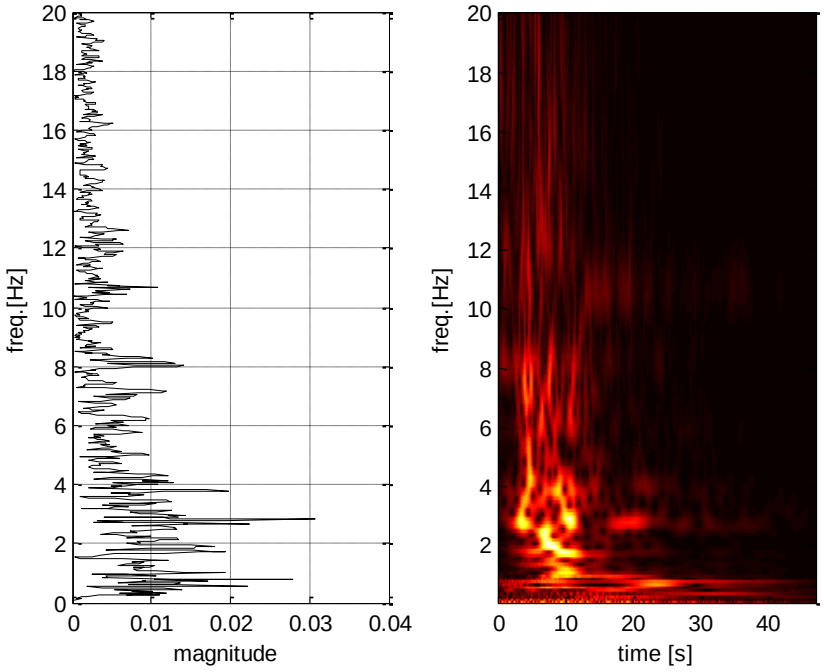

Figure C6. 2. DM2

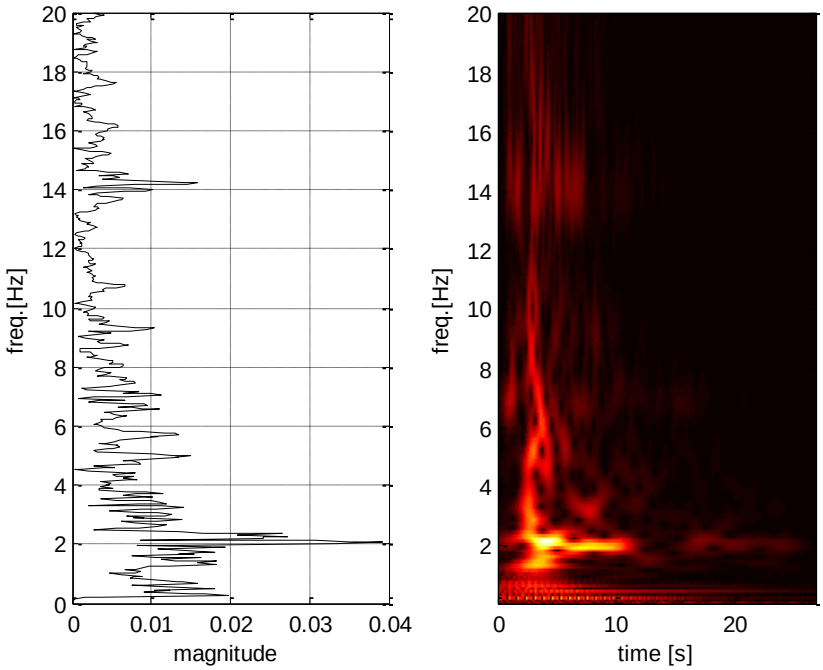

Figure C6. 3. DM3

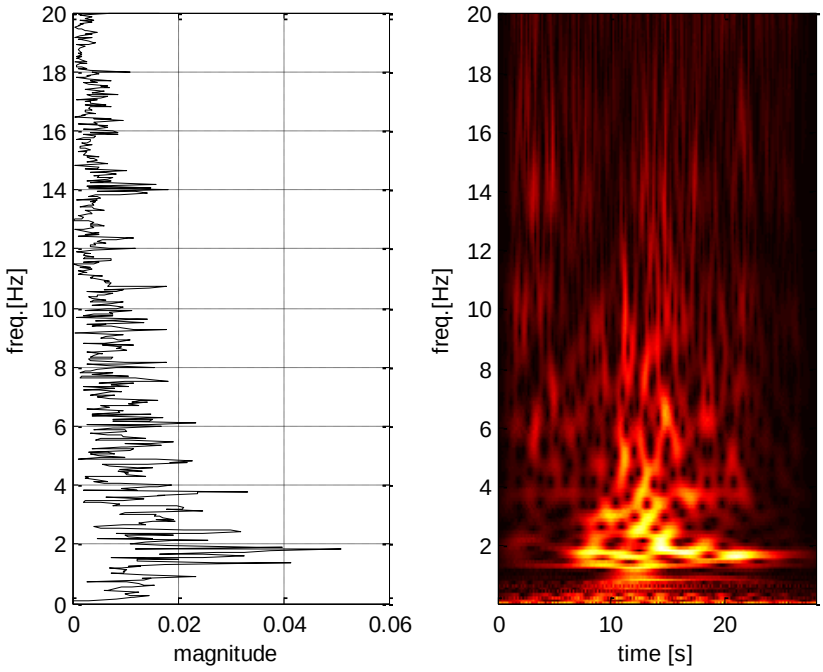

Figure C6. 4. DM4

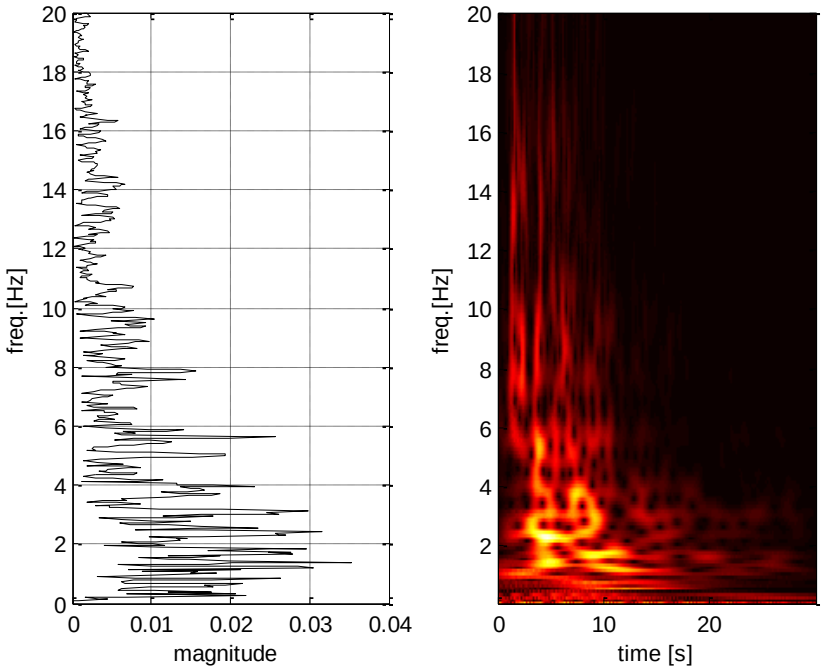

Figure C6. 5. DM5

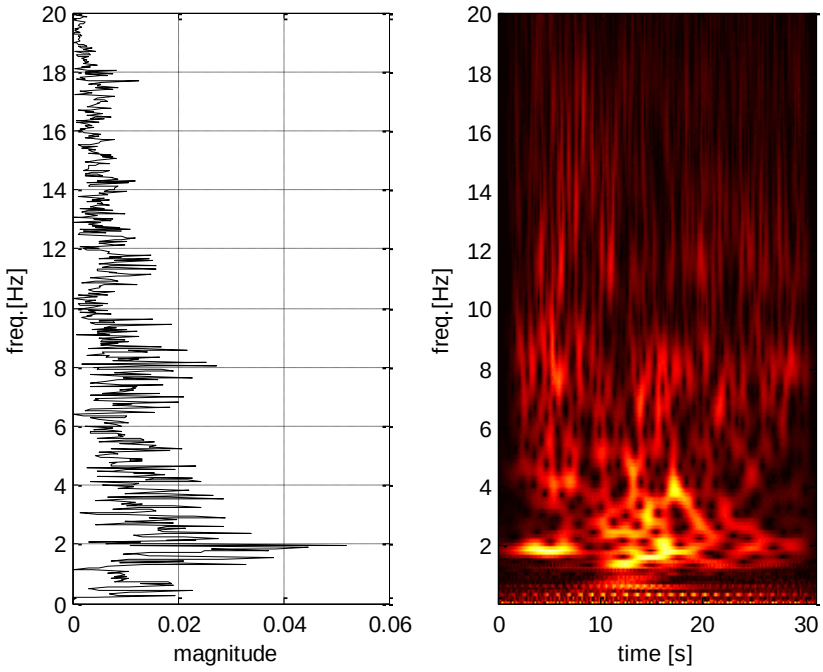

Figure C6. 6. DM6

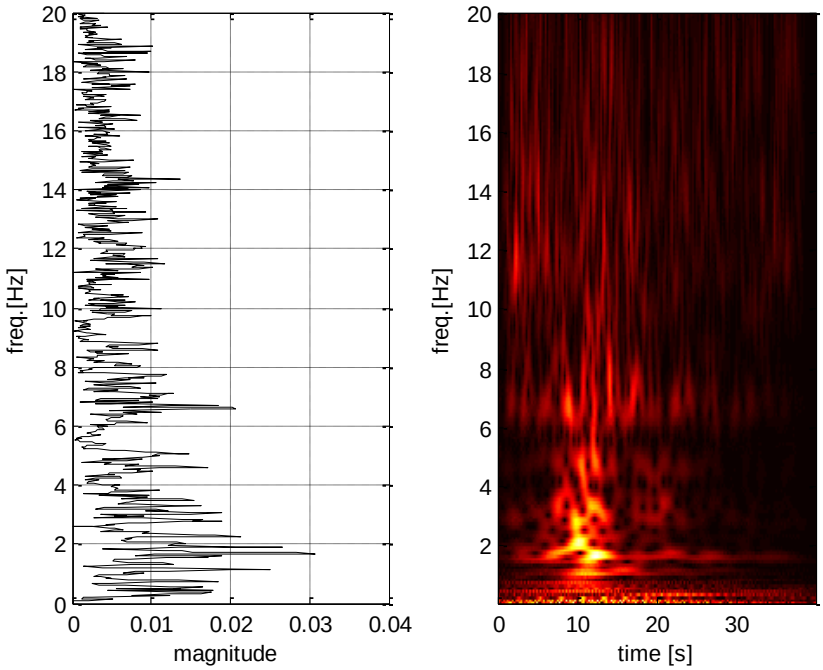

Figure C6. 7. DM7

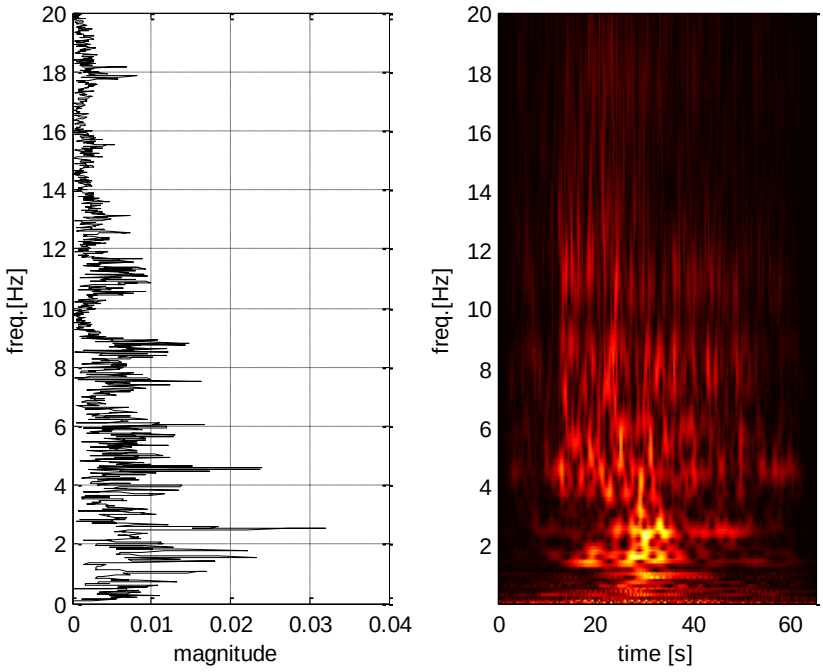

Figure C6. 8. DM8

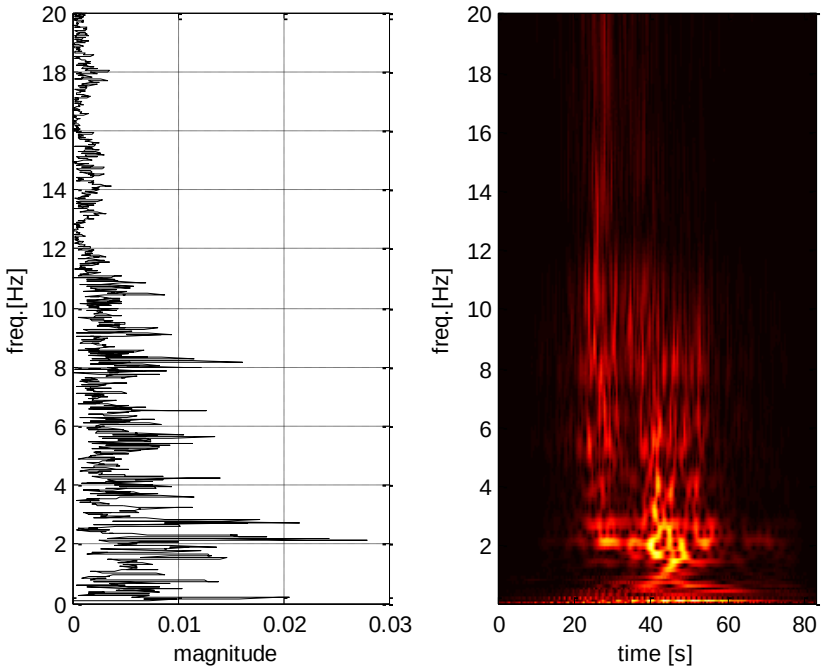

Figure C6. 9. DM9

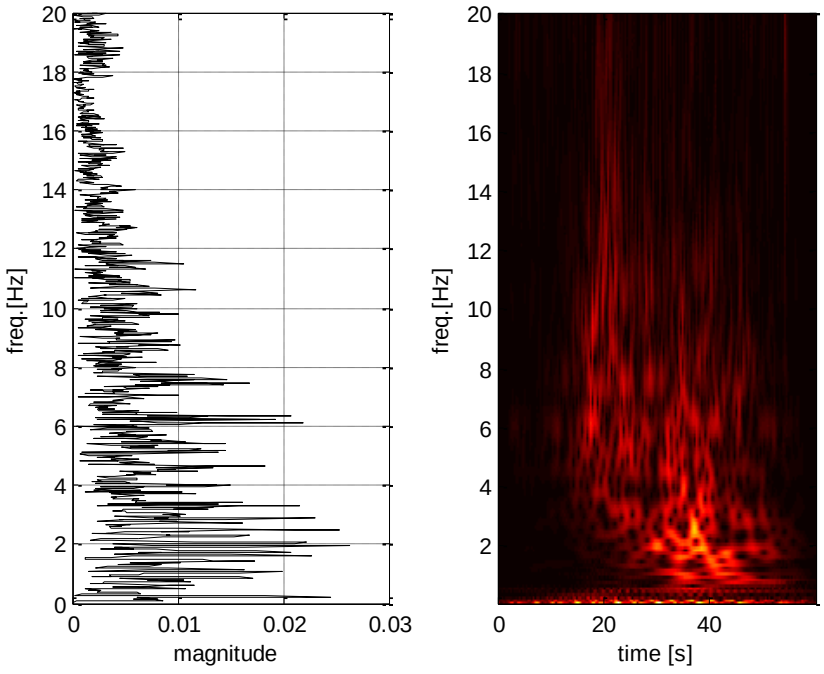

Figure C6. 10. DM10

C7. SeismoArtif records

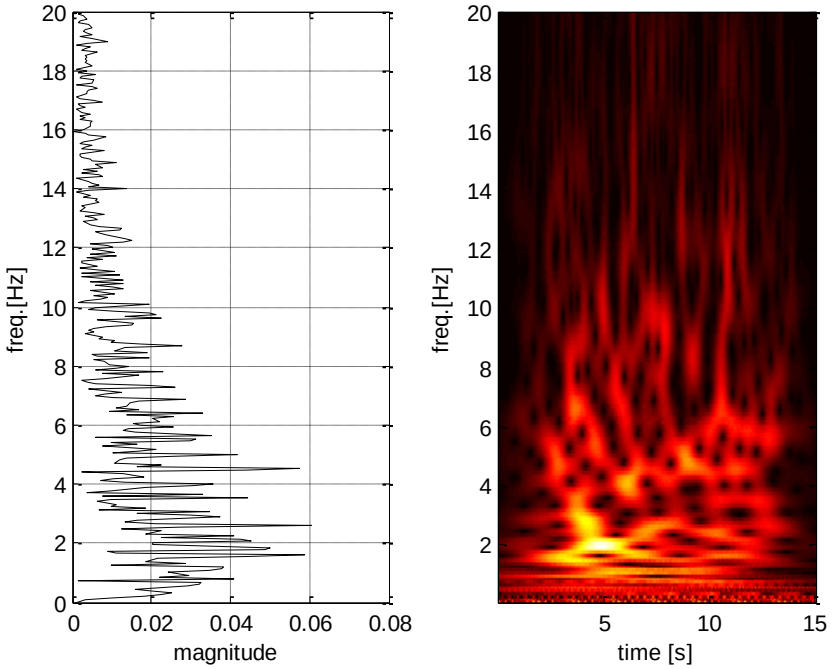

Figure C7.1. SA1

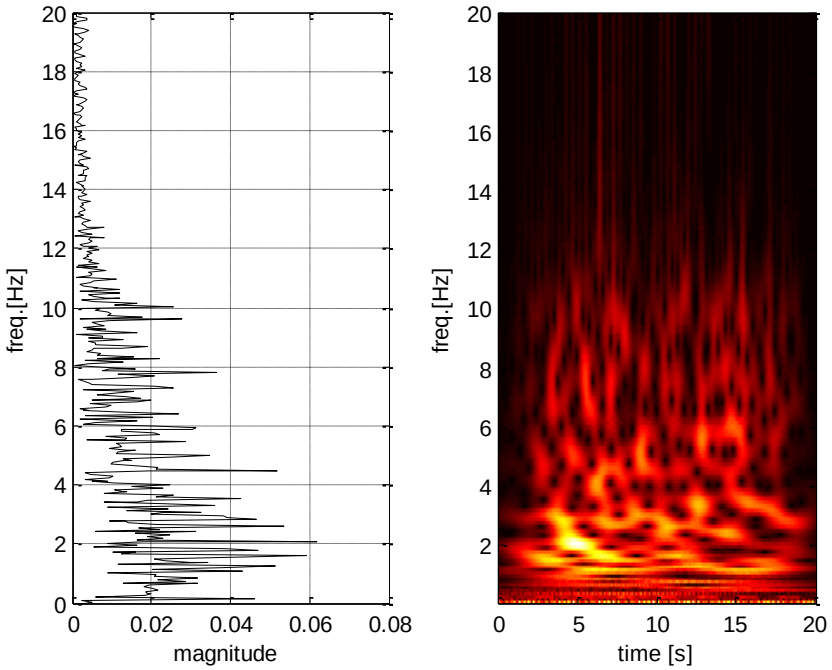

Figure C7. 2. SA2

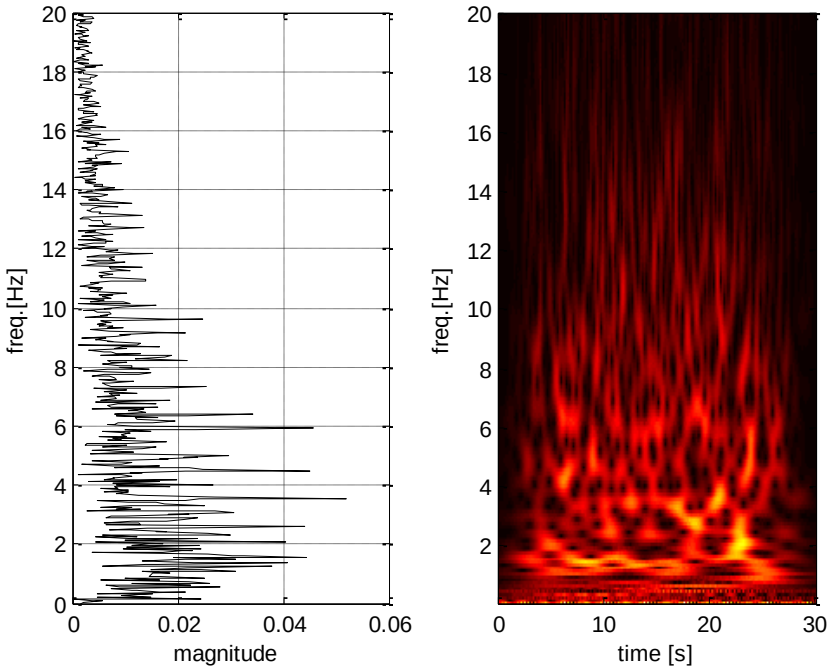

Figure C7. 3. SA3

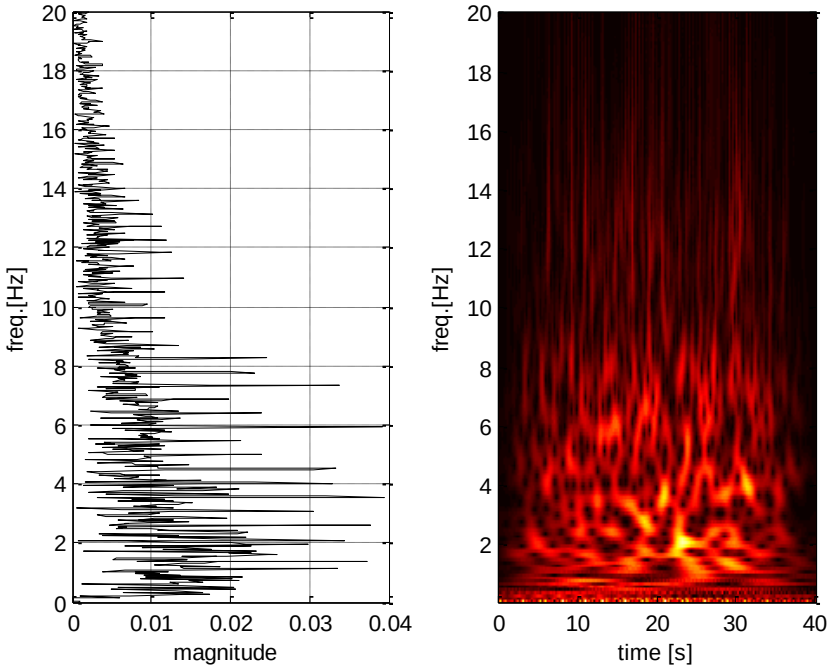

Figure C7. 4. SA4

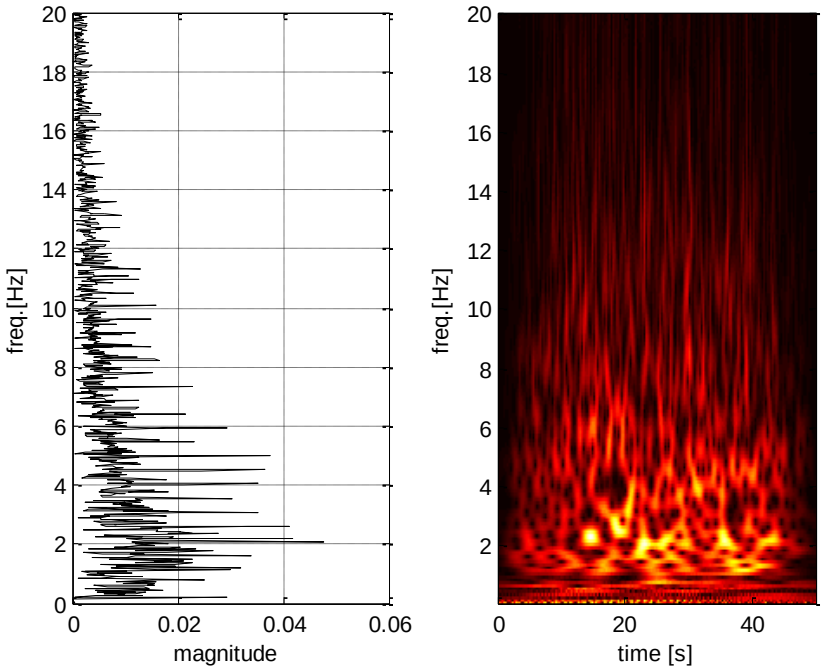

Figure C7. 5. SA5

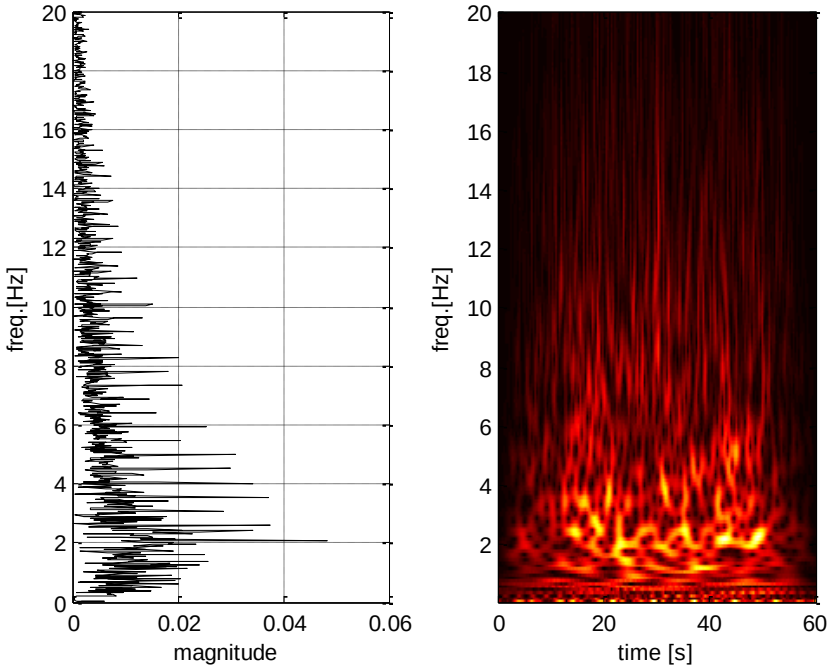

Figure C7. 6. SA6

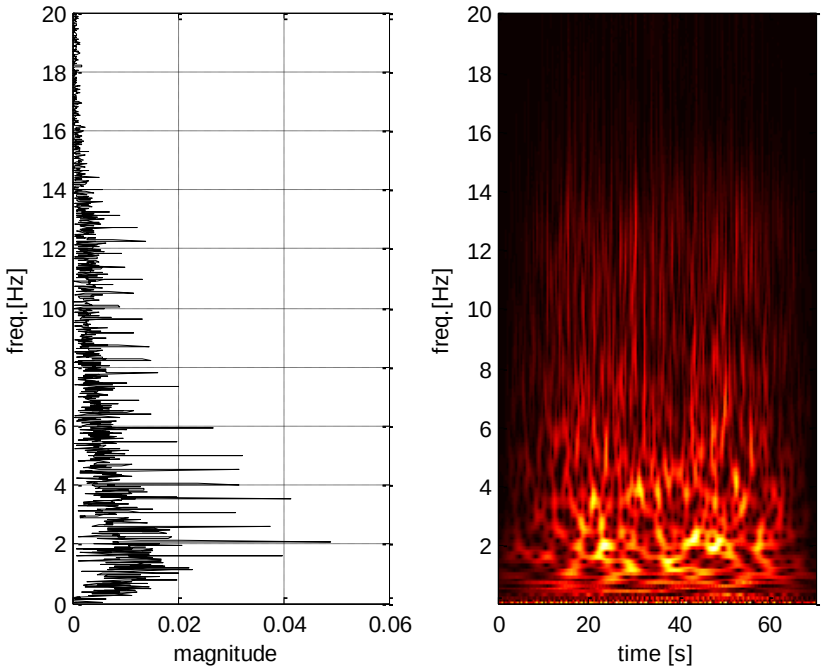

Figure C7. 7. SA7

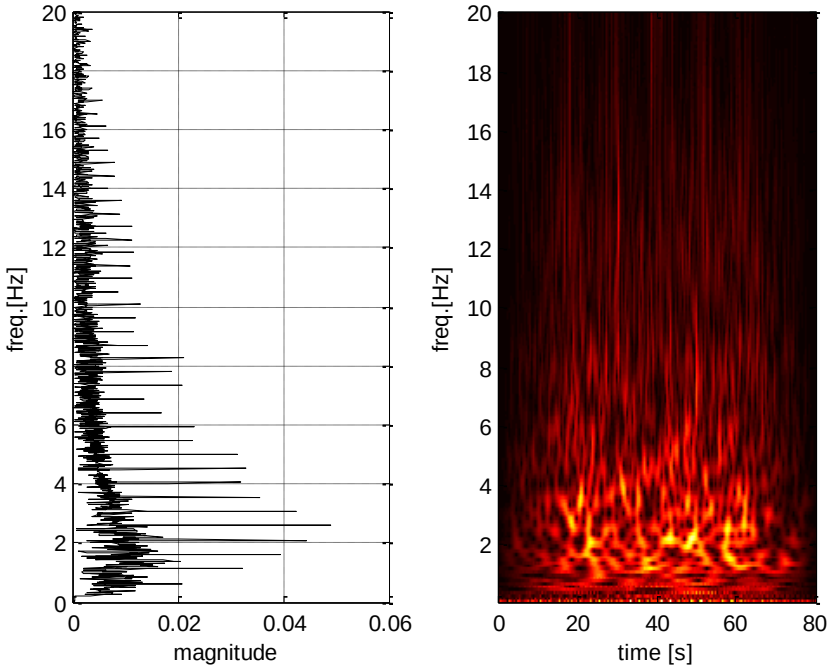

Figure C7. 8. SA8

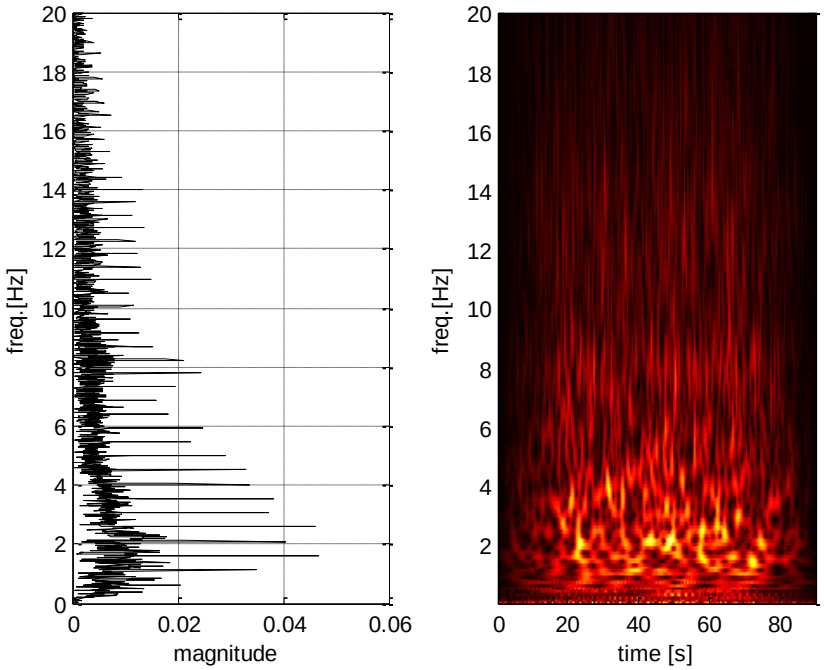

Figure C7. 9. SA9

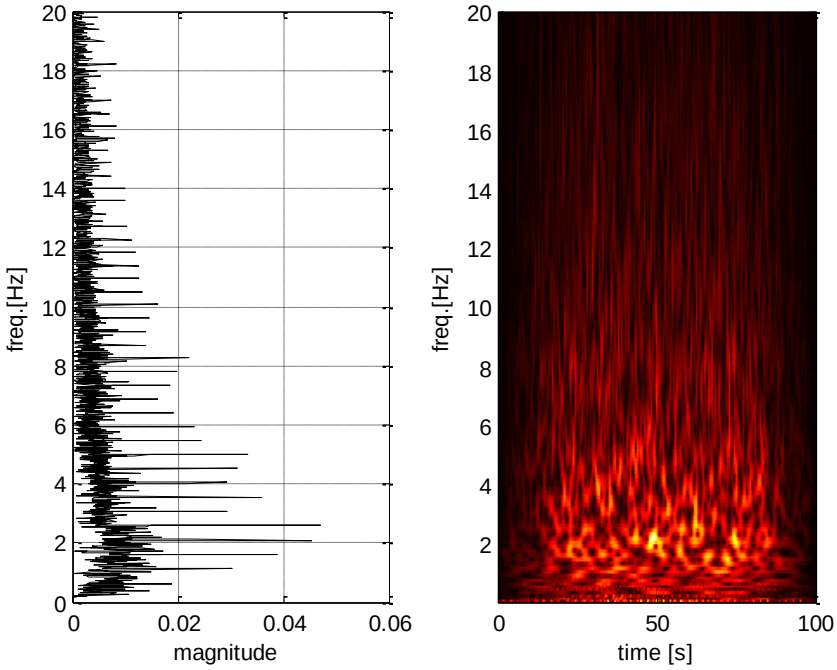

Figure C7. 10. SA10

APPENDIX D

D. IDA CURVES

D1. Sa(T*) as IM

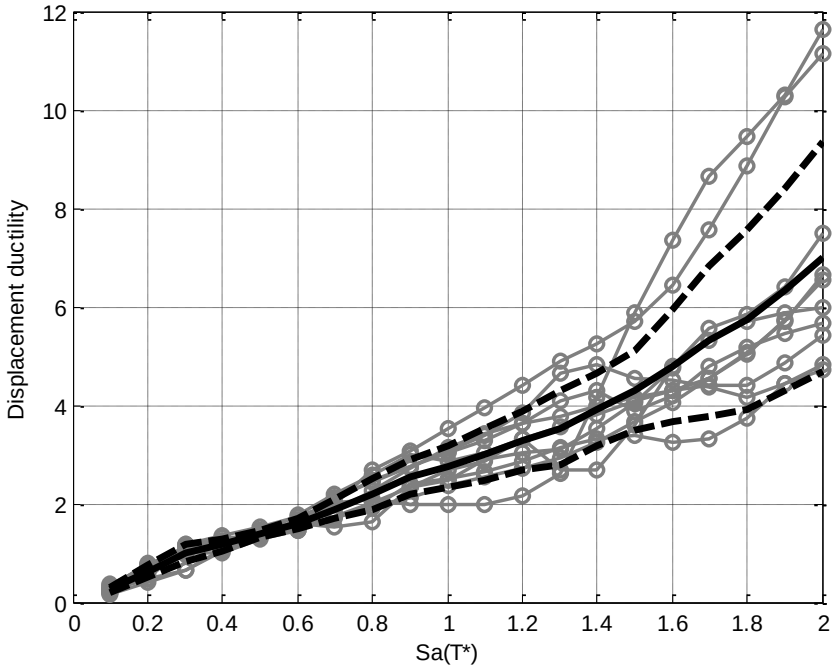

Figure D.1.1.CM SeismoMatch IDA curves peak displacement ductility

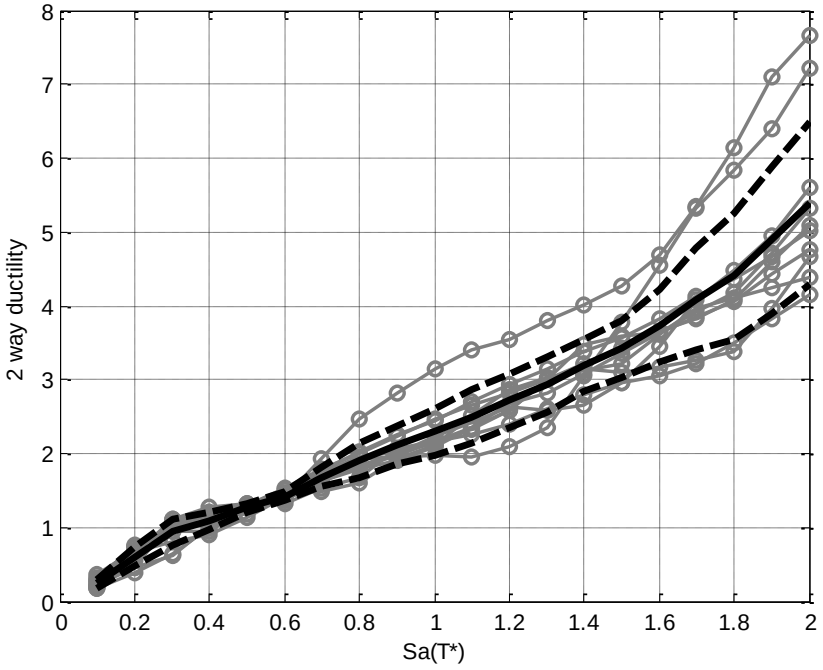

Figure D.1.2. CM SeismoMatch IDA curves 2 way ductility

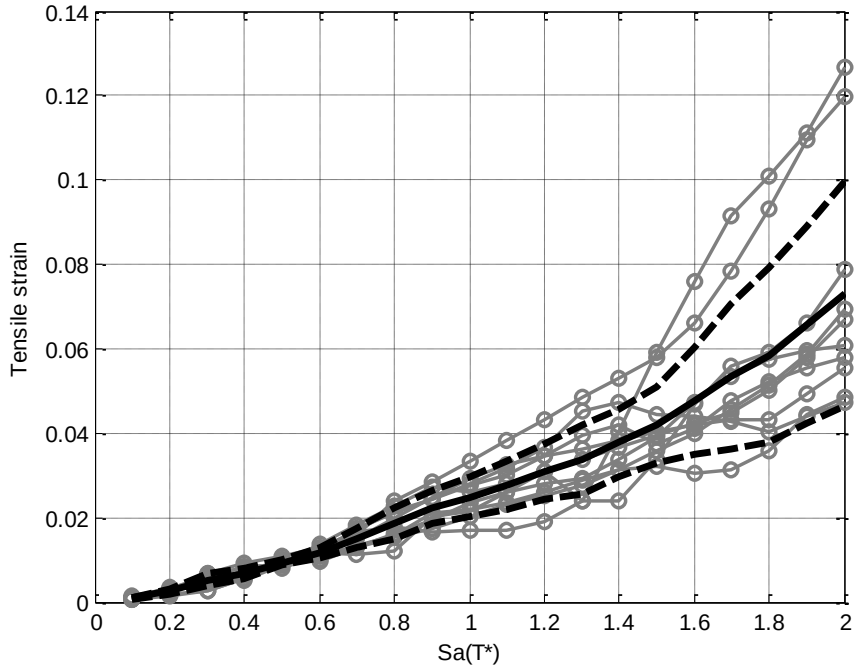

Figure D.1.3.CM SeismoMatch IDA curves bars tensile strain

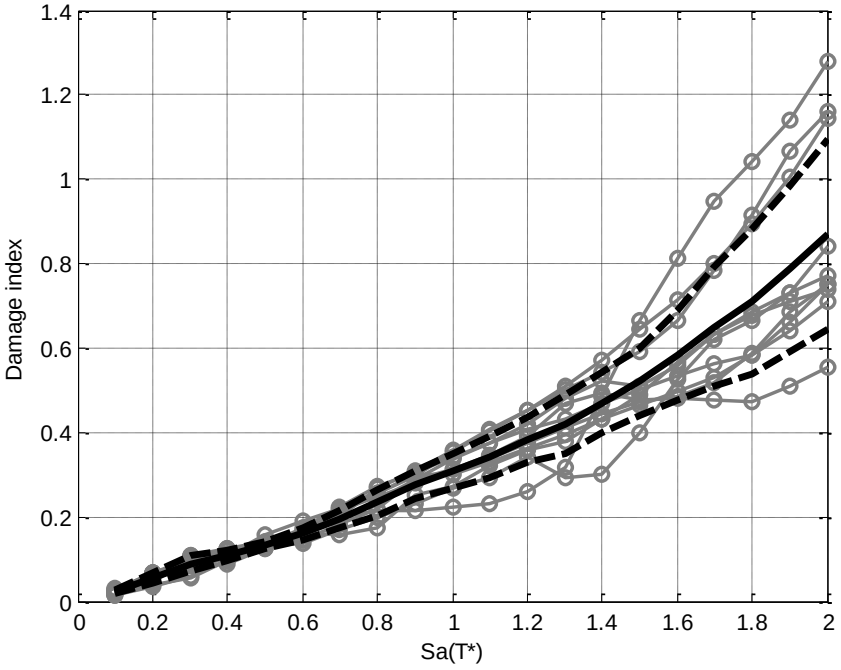

Figure D.1.4. CM SeismoMatch IDA curves damage index

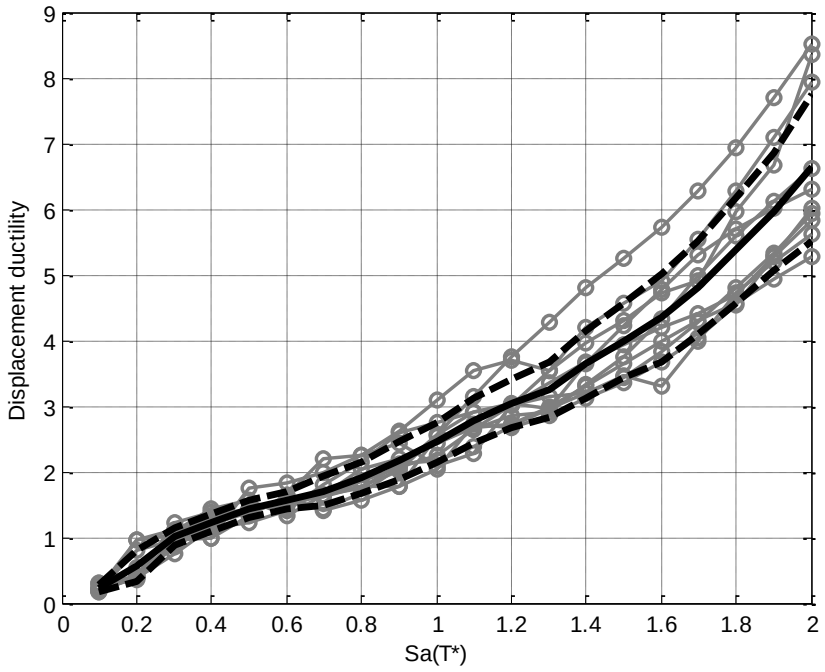

Figure D.1.5. CM ArtifQuakeLet II IDA curves peak displacement ductility

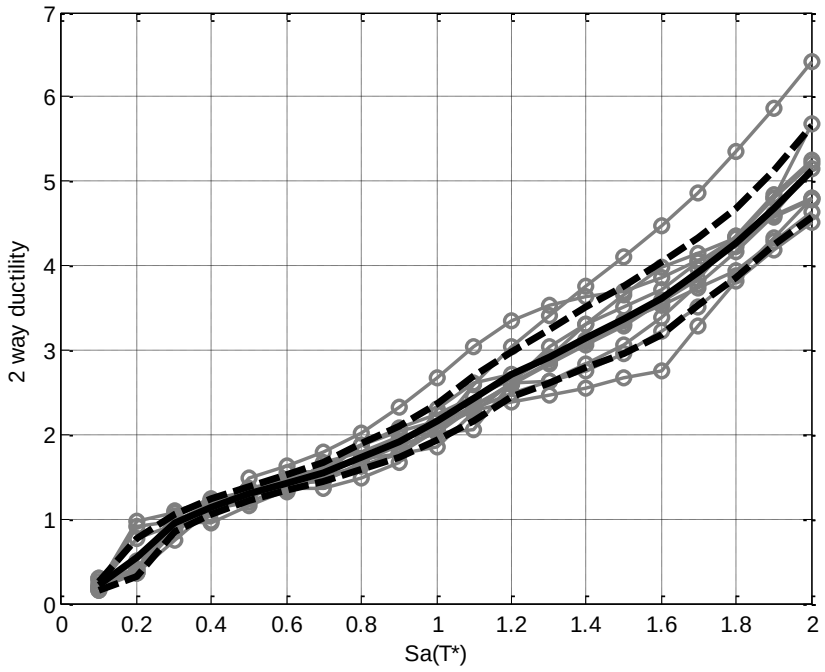

Figure D.1.6. CM ArtifQuakeLet II IDA curves 2 way ductility

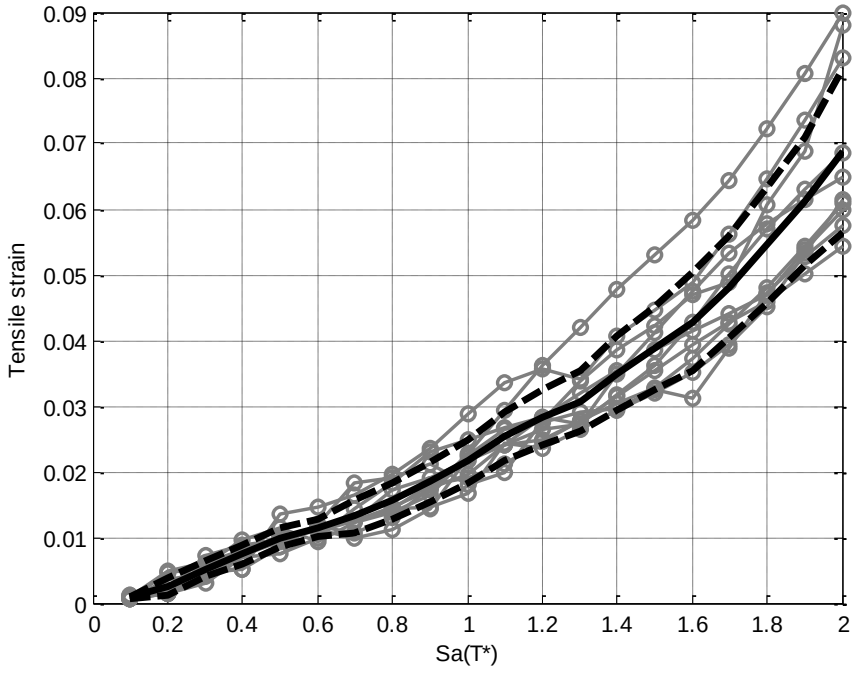

Figure D.1.7. CM ArtifQuakeLet II IDA curves bars tensile strain

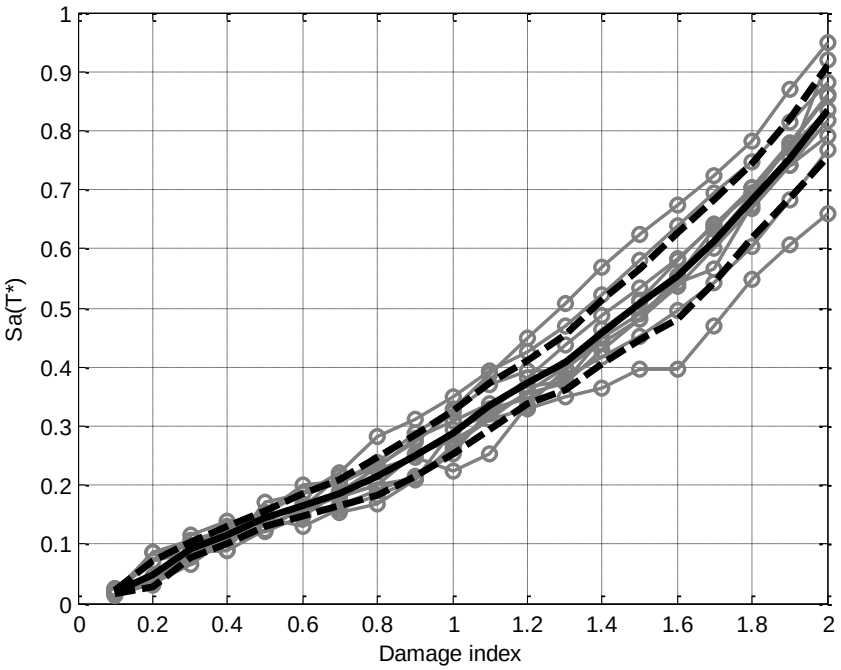

Figure D.1.8. CM ArtifQuakeLet II IDA curves damage index

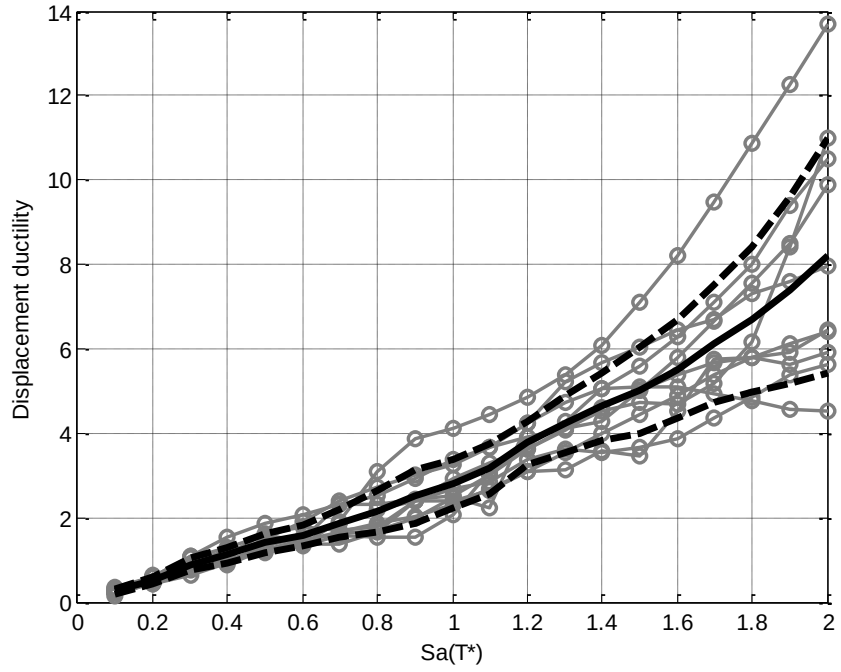

Figure D.1.9. DM SeismoMatch IDA curves peak displacement ductility

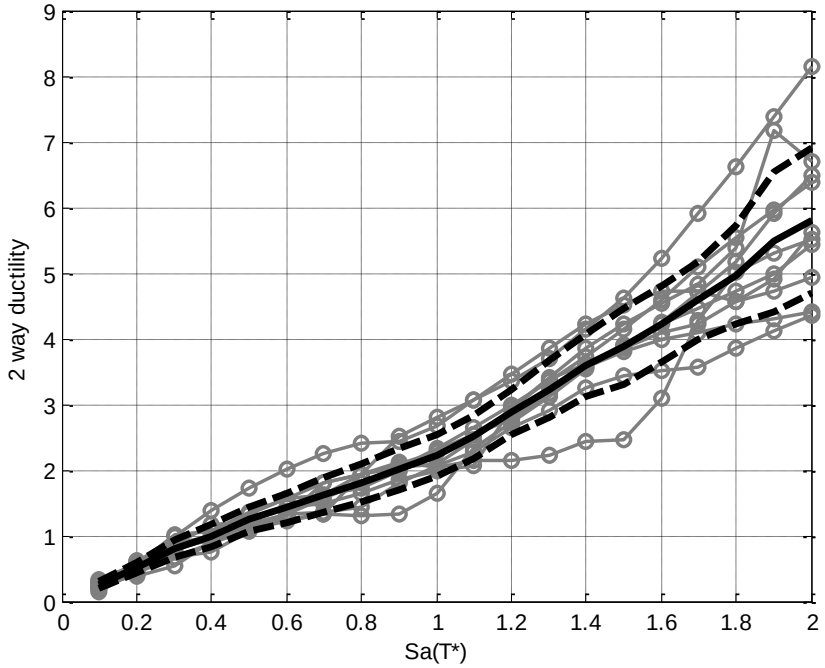

Figure D.1.10. DM SeismoMatch IDA curves 2 way ductility

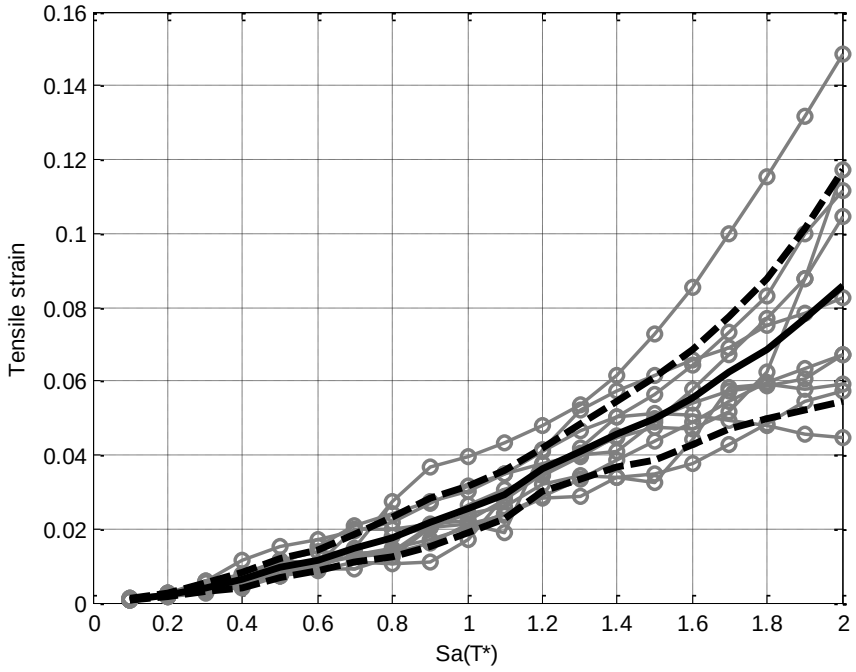

Figure D.1.11. DM SeismoMatch IDA curves bars tensile strain

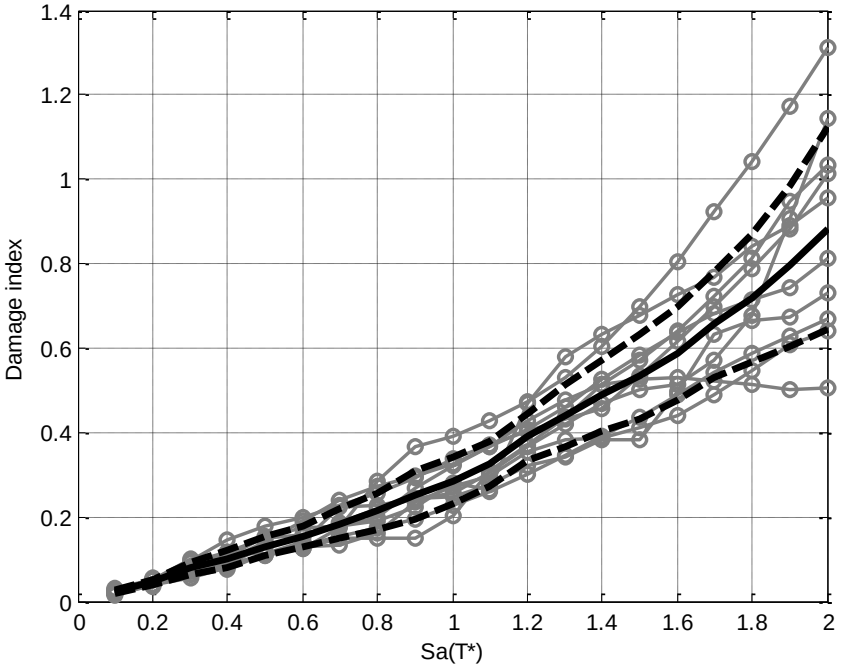

Figure D.1.12. DM SeismoMatch IDA curves damage index

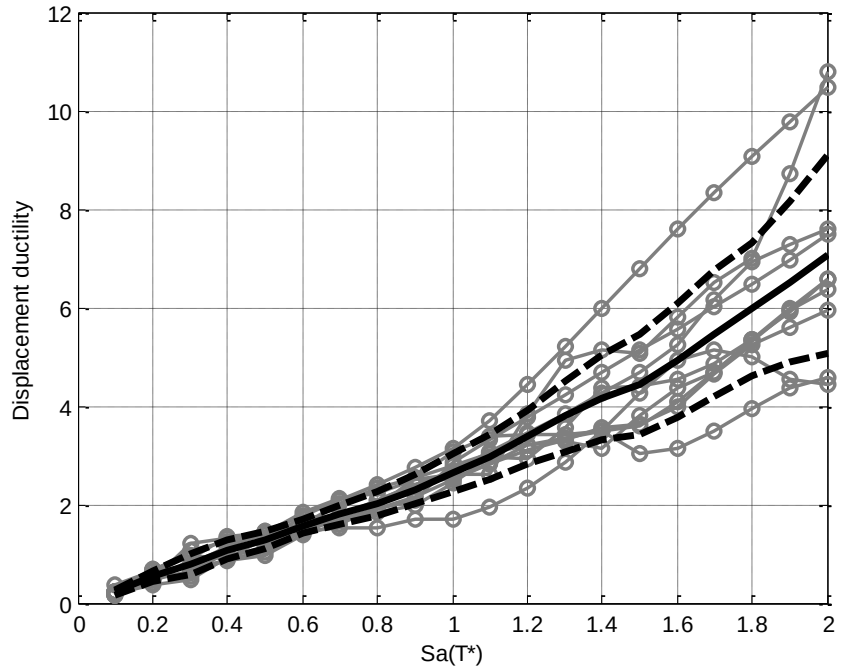

Figure D.1. 13. DM ArtifQuakeLet II IDA curves peak displacement ductility

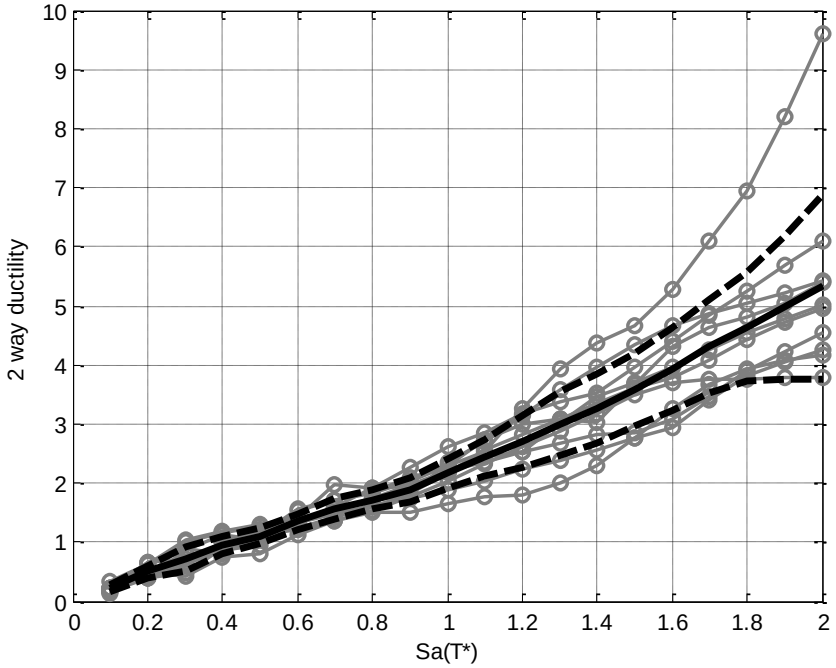

Figure D.1. 14. DM ArtifQuakeLet II IDA curves 2 way ductility

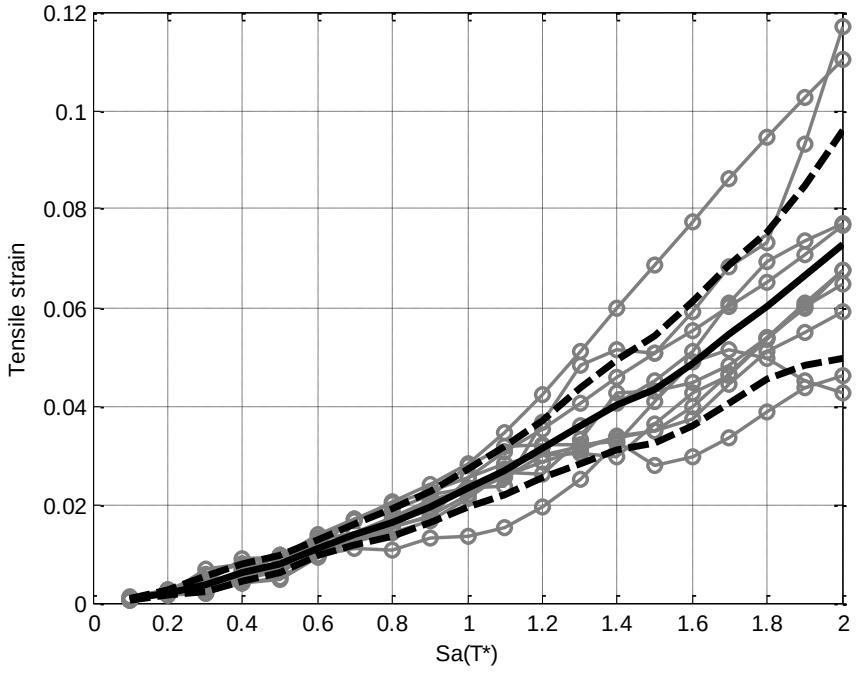

Figure D.1.15. DM ArtifQuakeLet II IDA curves bars tensile strain

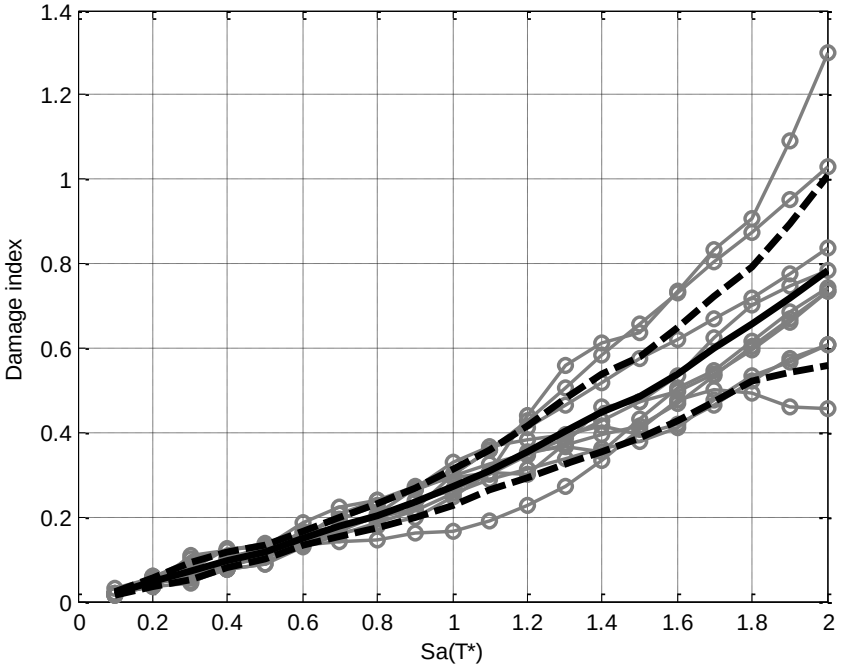

Figure D.1.16. DM ArtifQuakeLet II IDA curves damage index

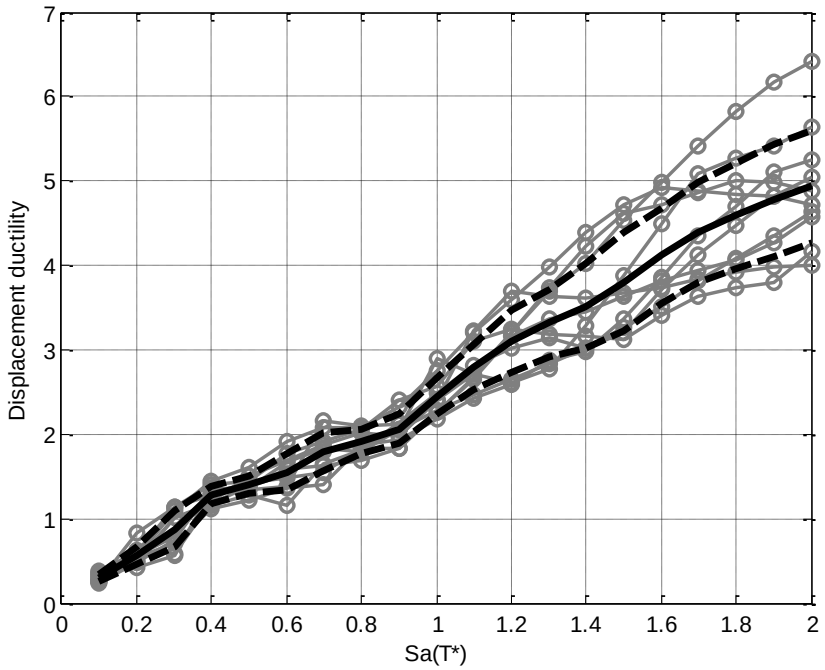

Figure D.1.17. SeismoArtif IDA curves peak displacement ductility

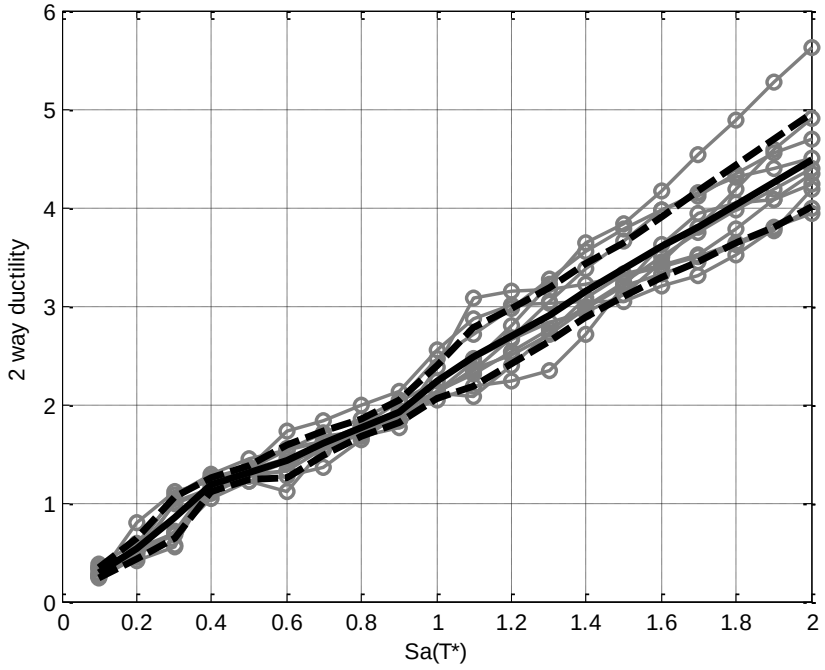

Figure D.1.18. SeismoArtif IDA curves 2 way ductility

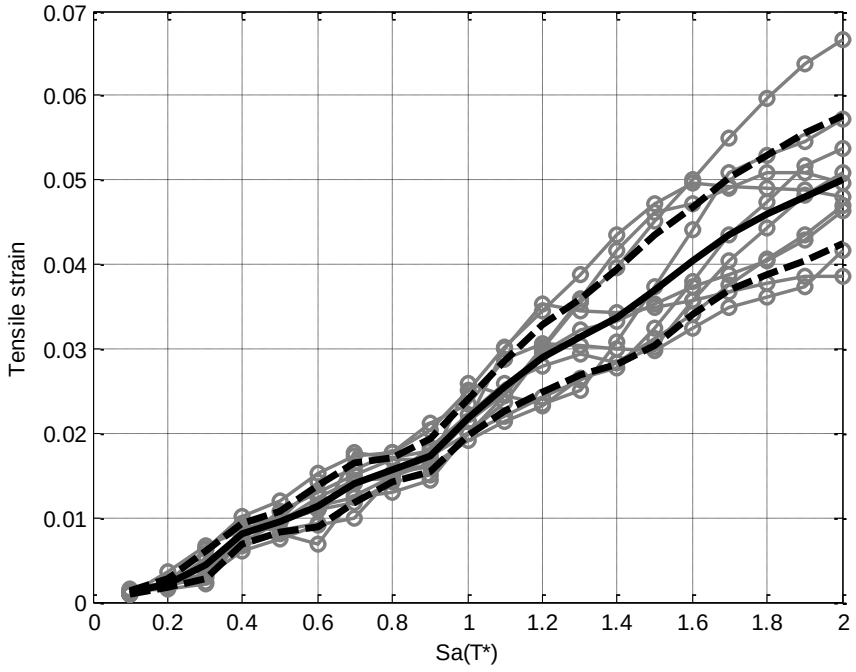

Figure D.1.19. SeismoArtif IDA curves bars tensile strain

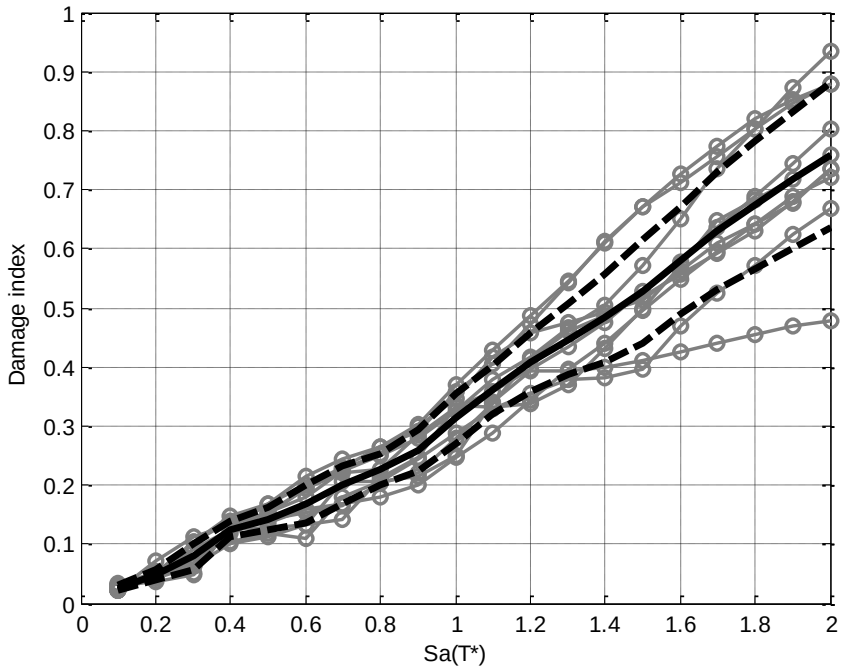

Figure D.1.20. SeismoArtif IDA curves damage index

APPENDIX E

E. IDA Curves PGA, PGV, PGD and CAV as IM

E.1 Case 1

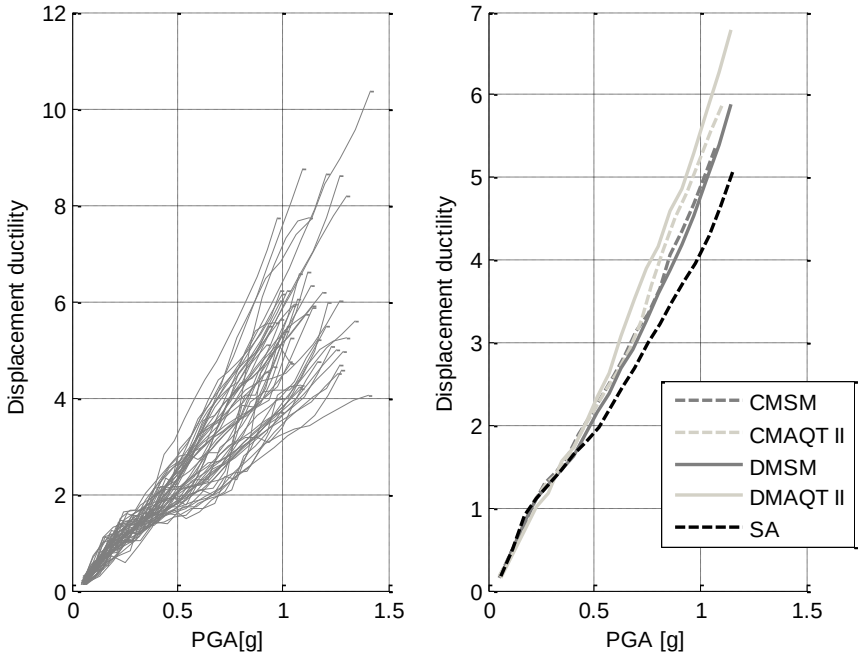

Figure E.1. 1 (a) IDA curves (Ductility vs. PGA) all artificial earthquakes (b) IDA curves (Ductility vs. PGA) by approach for case 1

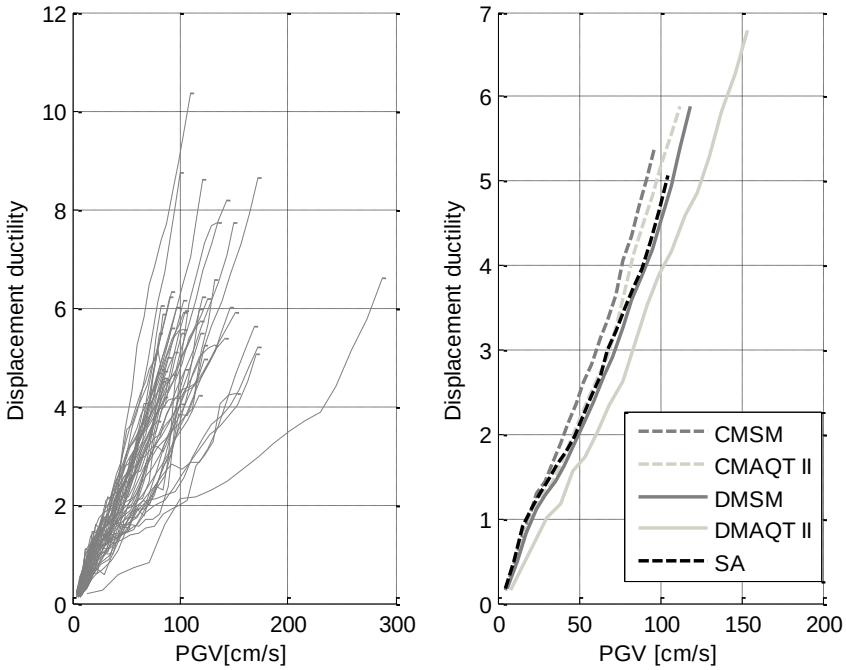

Figure E.1. 2 (a) IDA curves (Ductility vs. PGV) all artificial earthquakes (b) IDA curves (Ductility vs. PGV) by approach for case 1

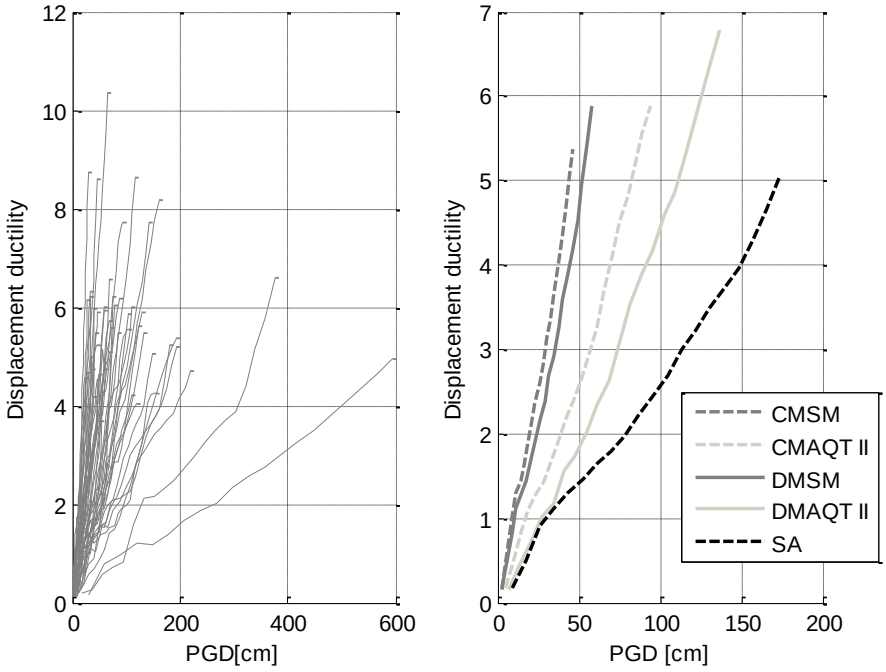

Figure E.1. 3 (a) IDA curves (Ductility vs. PGD) all artificial earthquakes (b) IDA curves (Ductility vs. PGD) by approach for case 1

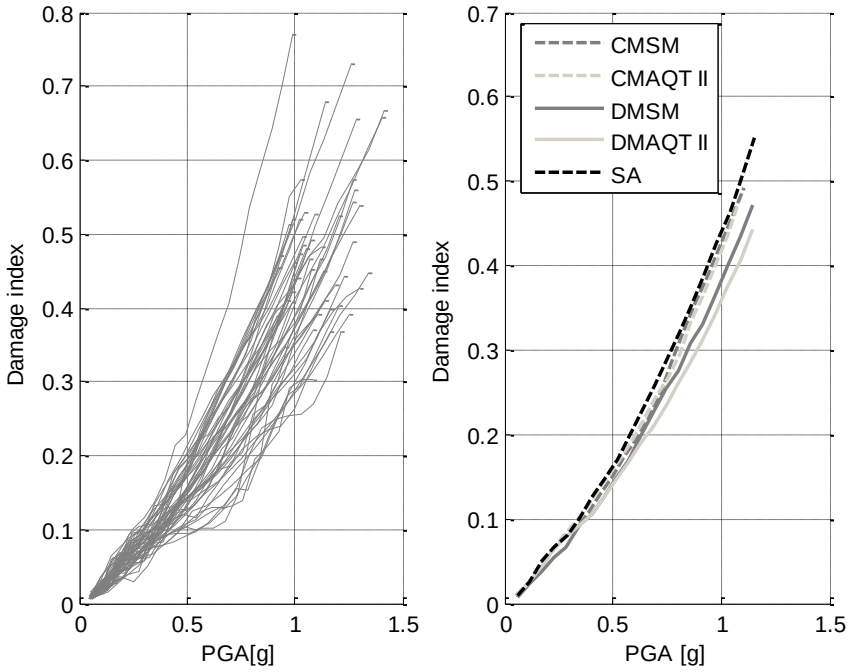

Figure E.1. 4 . (a) IDA curves (DI vs. PGA) all artificial earthquakes (b) IDA curves (DI vs. PGA) by approach for case 1

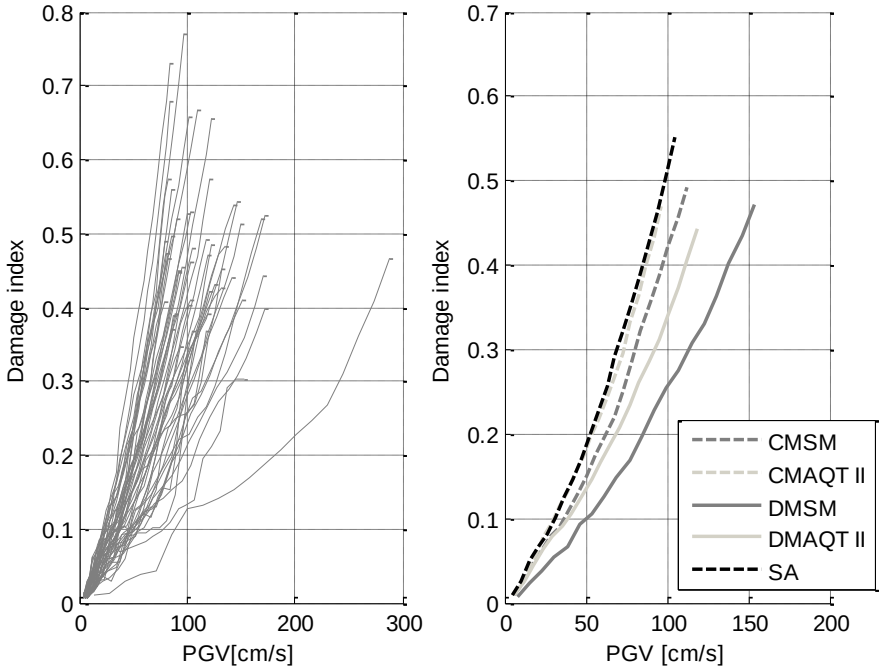

Figure E.1. 5 (a) IDA curves (DI vs. PGV) all artificial earthquakes (b) IDA curves (DI vs. PGV) by approach for case 1

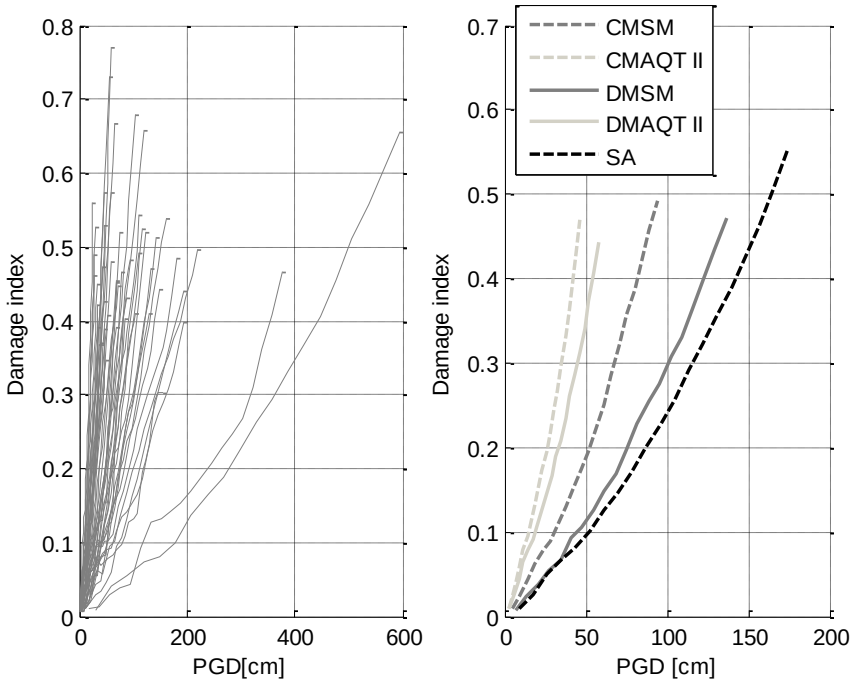

Figure E.1. 6 (a) IDA curves (DI vs. PGD) all artificial earthquakes (b) IDA curves (DI vs. PGD) by approach for case 1

E.2. Case 2

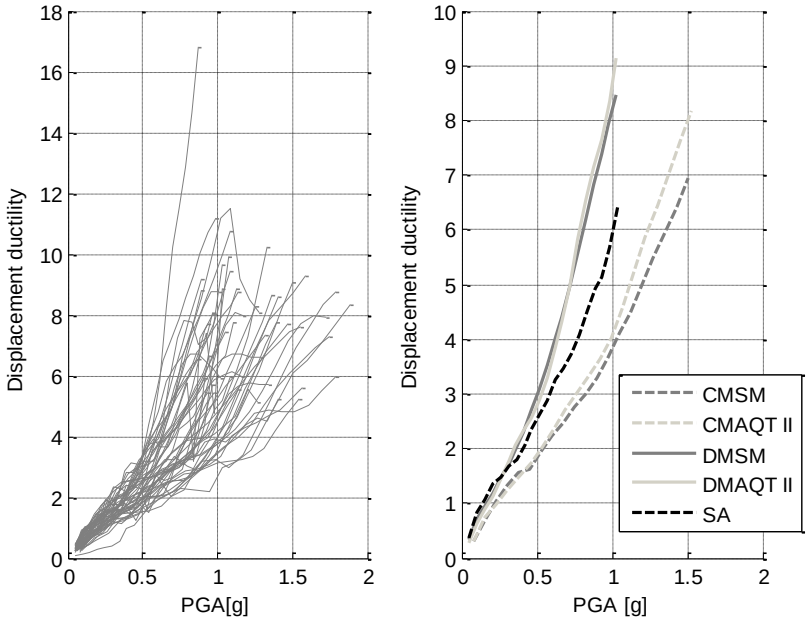

Figure E.2. 1 (a) IDA curves (Ductility vs. PGA) all artificial earthquakes (b) IDA curves (Ductility vs. PGA) by approach for case 2

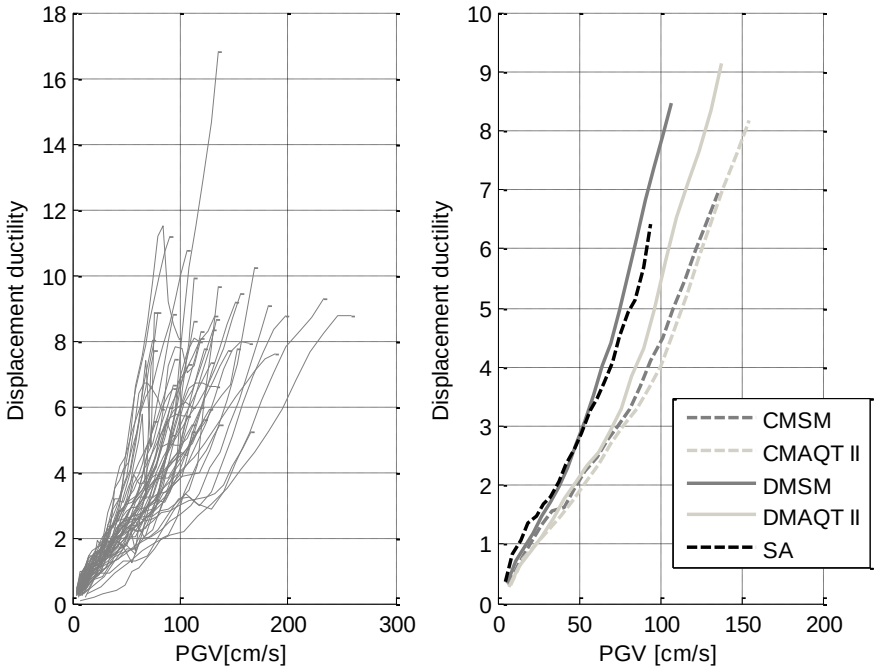

Figure E.2. 2 (a) IDA curves (Ductility vs. PGV) all artificial earthquakes (b) IDA curves (Ductility vs. PGV) by approach for case 2

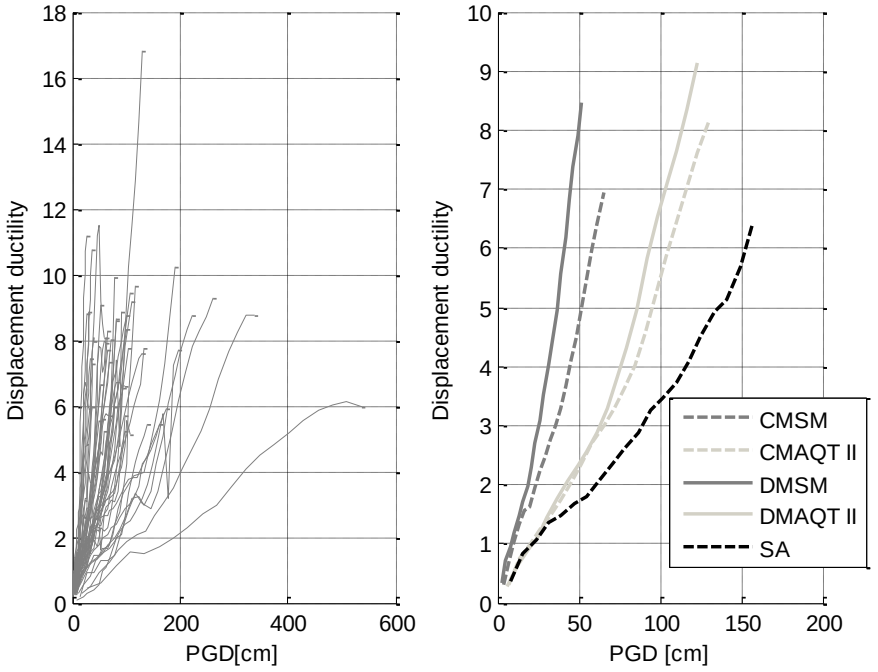

Figure E.2. 3 (a) IDA curves (Ductility vs. PGD) all artificial earthquakes (b) IDA curves (Ductility vs. PGD) by approach for case 2

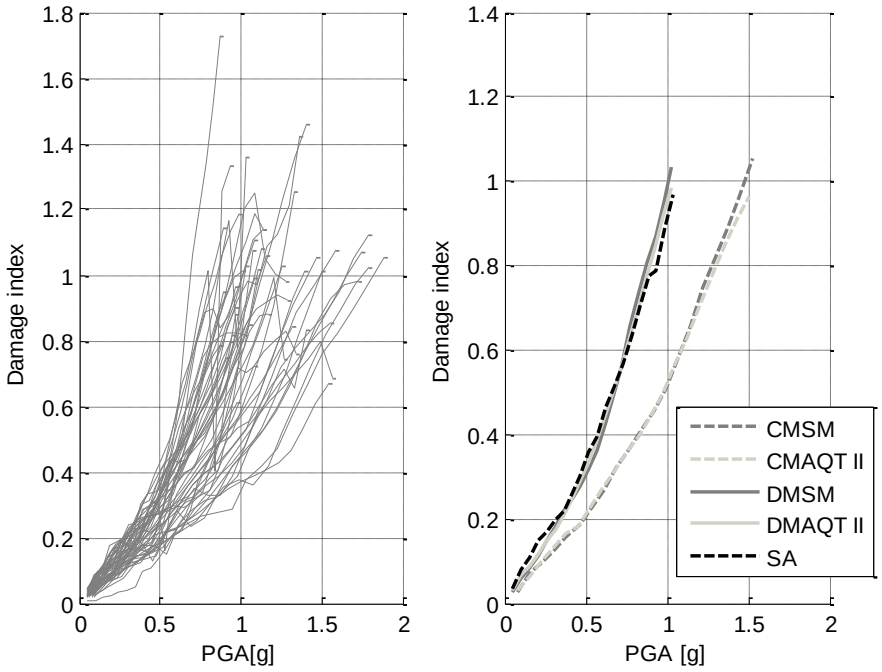

Figure E.2. 4 (a) IDA curves (DI vs. PGA) all artificial earthquakes (b) IDA curves (DI vs. PGA) by approach for case 2

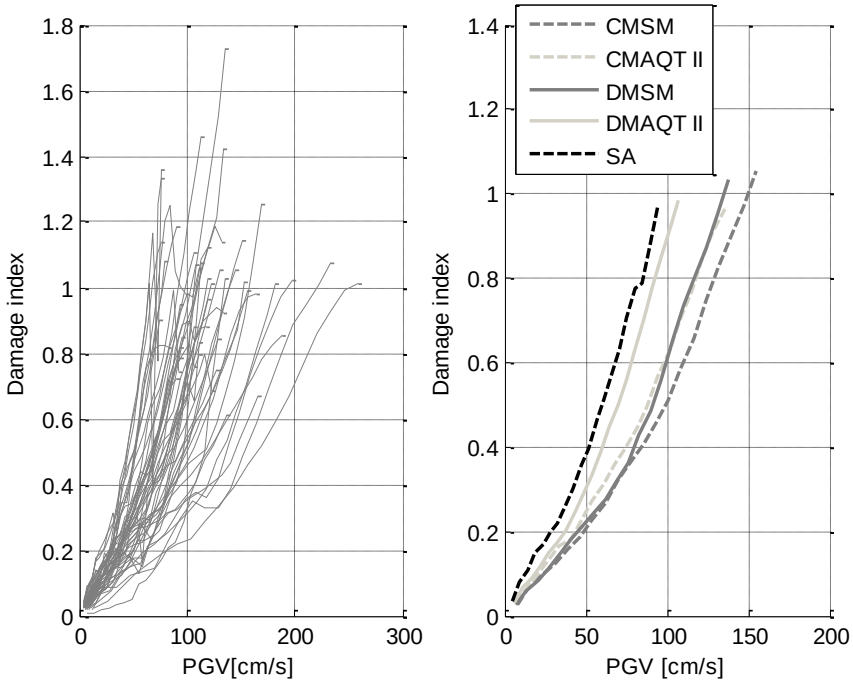

Figure E.2. 5 (a) IDA curves (DI vs. PGV) all artificial earthquakes (b) IDA curves (DI vs. PGV) by approach for case 2

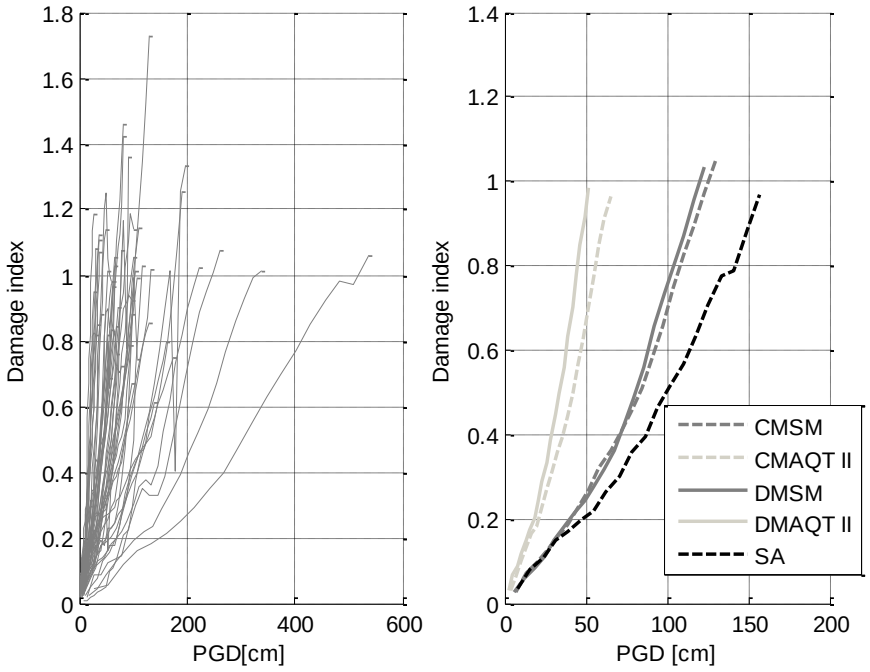

Figure E.2. 6 (a) IDA curves (DI vs. PGD) all artificial earthquakes (b) IDA curves (DI vs. PGD) by approach for case 2

E.3. Case 3

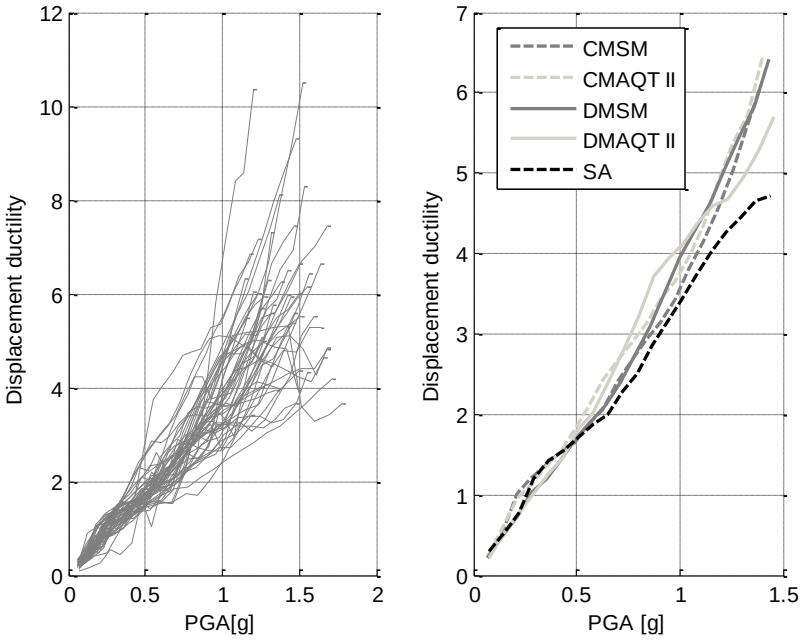

Figure E.3. 1 (a) IDA curves (Ductility vs. PGA) all artificial earthquakes (b) IDA curves (Ductility vs. PGA) by approach for case 3

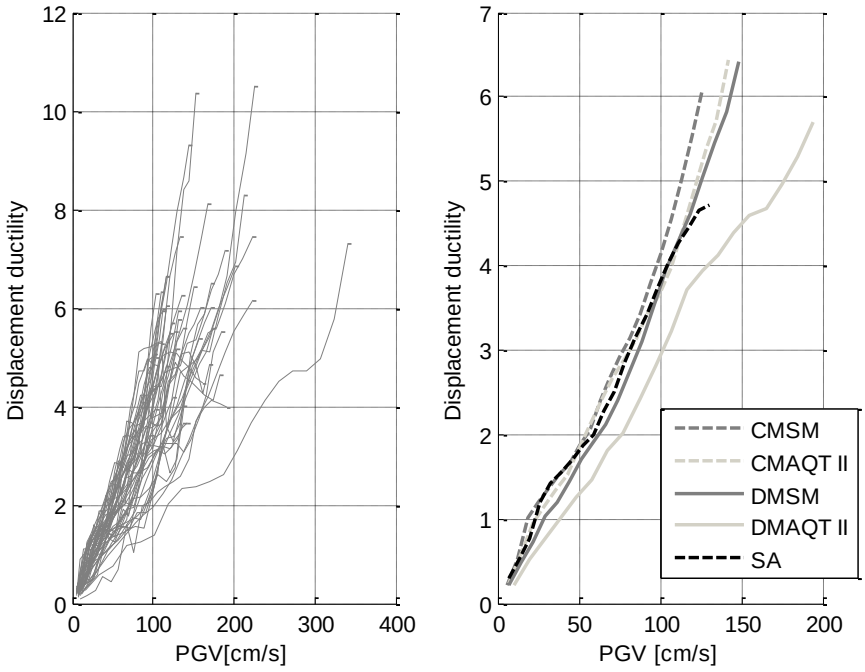

Figure E.3. 2 (a) IDA curves (Ductility vs. PGV) all artificial earthquakes (b) IDA curves (Ductility vs. PGV) by approach for case 3

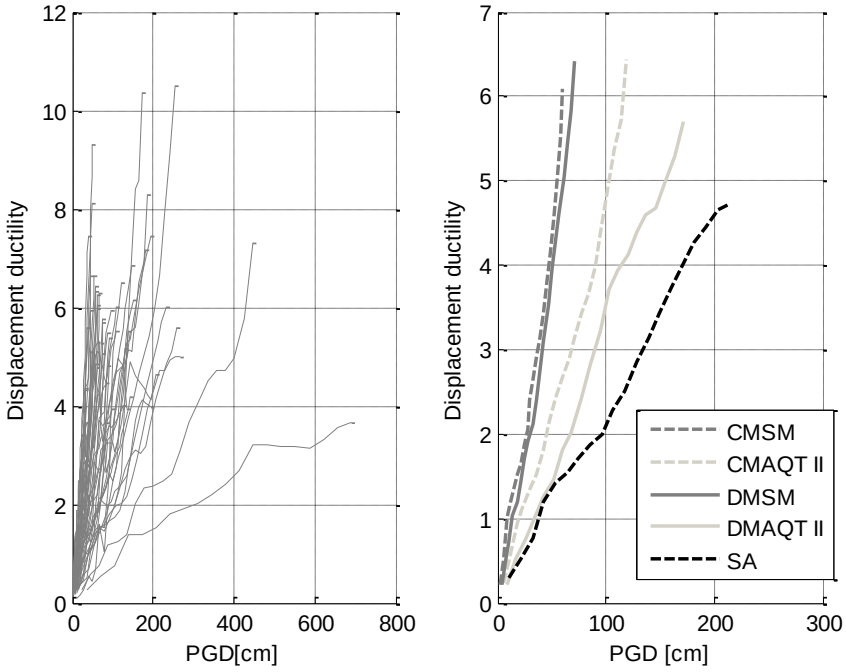

Figure E.3. 3 (a) IDA curves (Ductility vs. PGD) all artificial earthquakes (b) IDA curves (Ductility vs. PGD) by approach for case 3

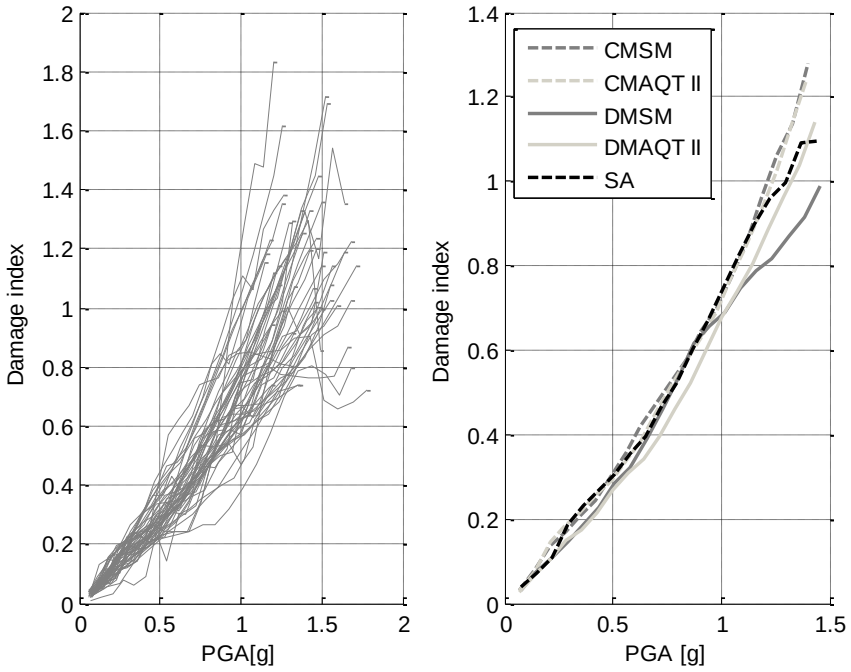

Figure E.3. 4 (a) IDA curves (DI vs. PGA) all artificial earthquakes (b) IDA curves (DI vs. PGA) by approach for case 3

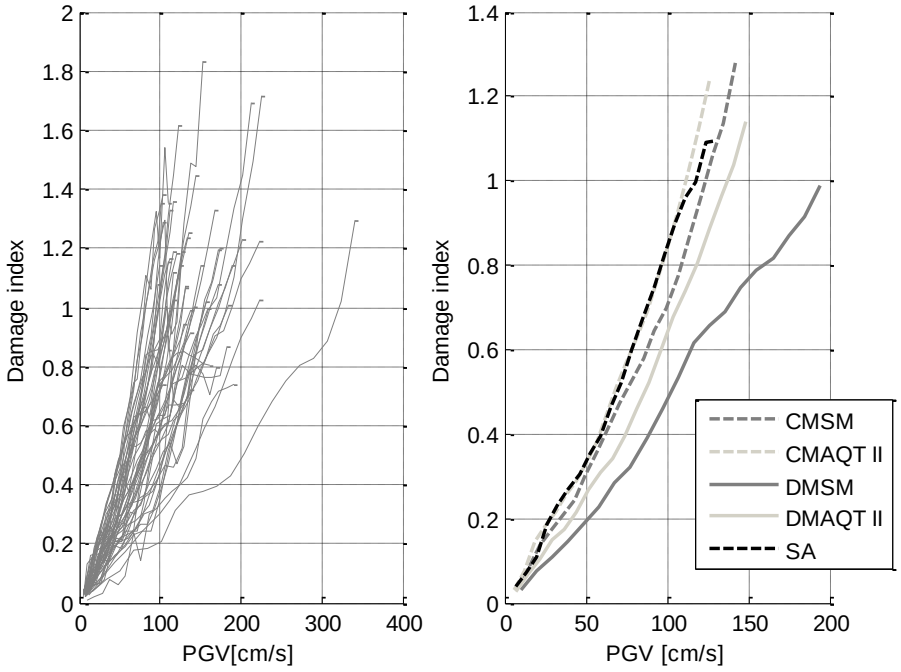

Figure E.3. 5 (a) IDA curves (DI vs. PGV) all artificial earthquakes (b) IDA curves (DI vs. PGV) by approach for case 3

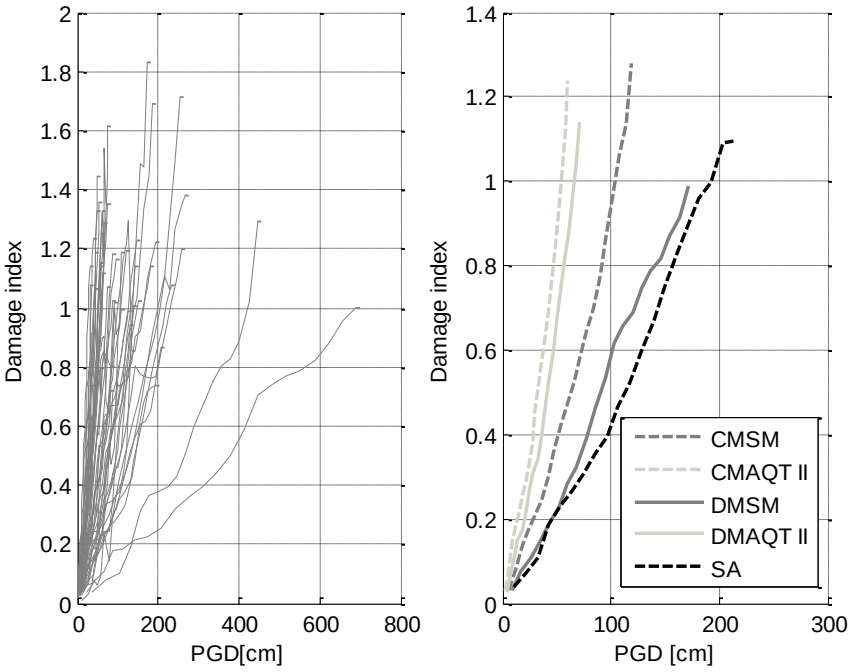

Figure E.3. 6 (a) IDA curves (DI vs. PGD) all artificial earthquakes (b) IDA curves (DI vs. PGD) by approach for case 3

E.4 Case 4

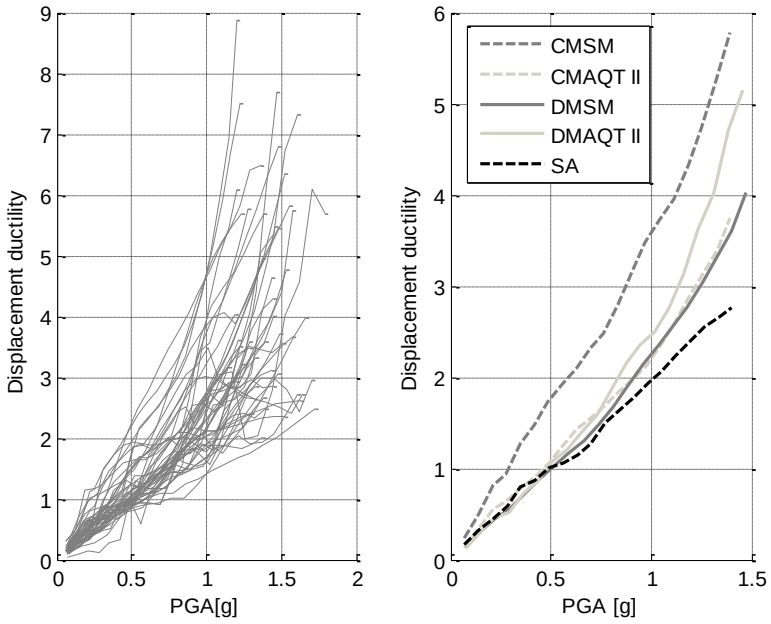

Figure E.4. 1 (a) IDA curves (Ductility vs. PGA) all artificial earthquakes (b) IDA curves (Ductility vs. PGA) by approach for case 4

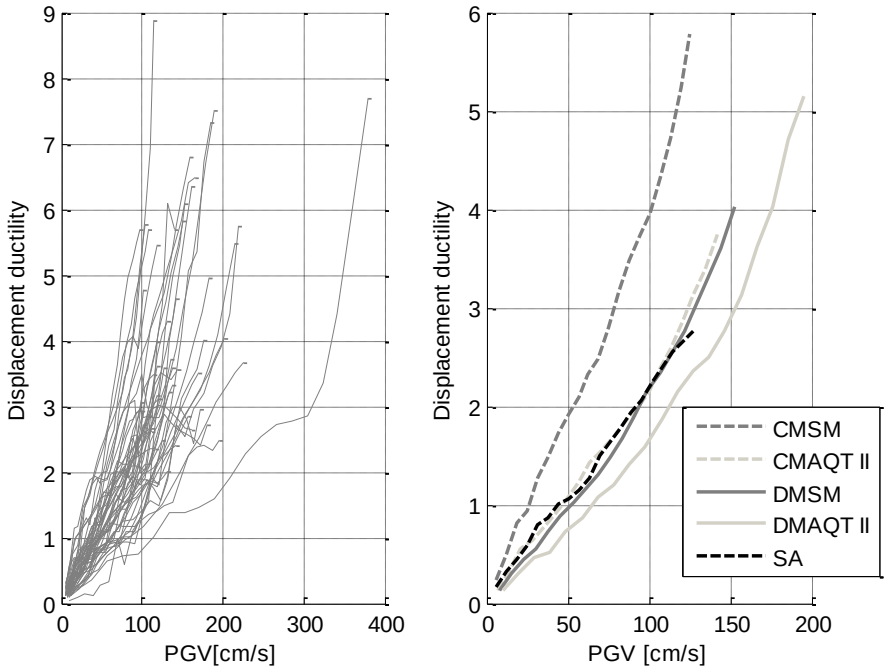

Figure E.4. 2 (a) IDA curves (Ductility vs. PGV) all artificial earthquakes (b) IDA curves (Ductility vs. PGV) by approach for case 4

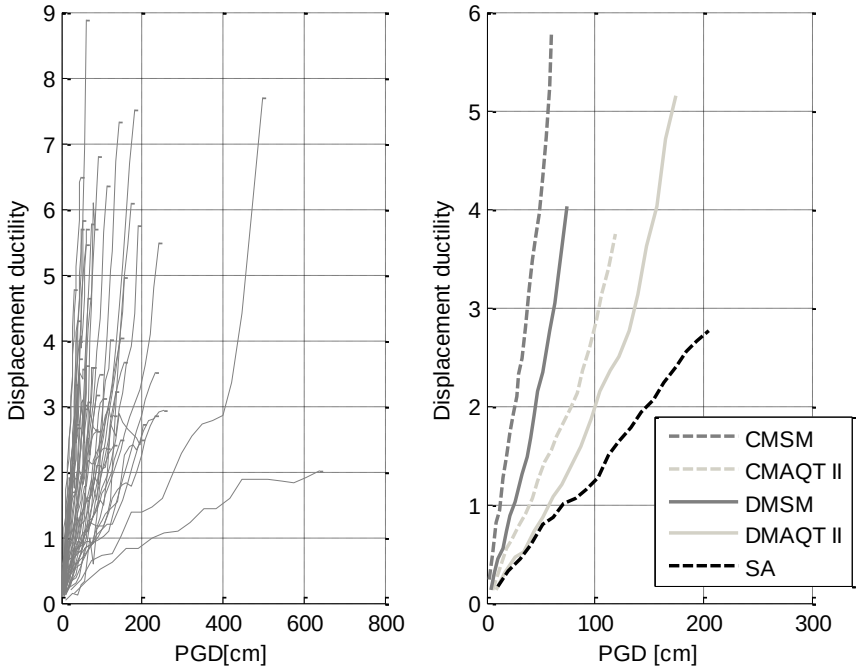

Figure E.4. 3 (a) IDA curves (Ductility vs. PGD) all artificial earthquakes (b) IDA curves (Ductility vs. PGD) by approach for case 4

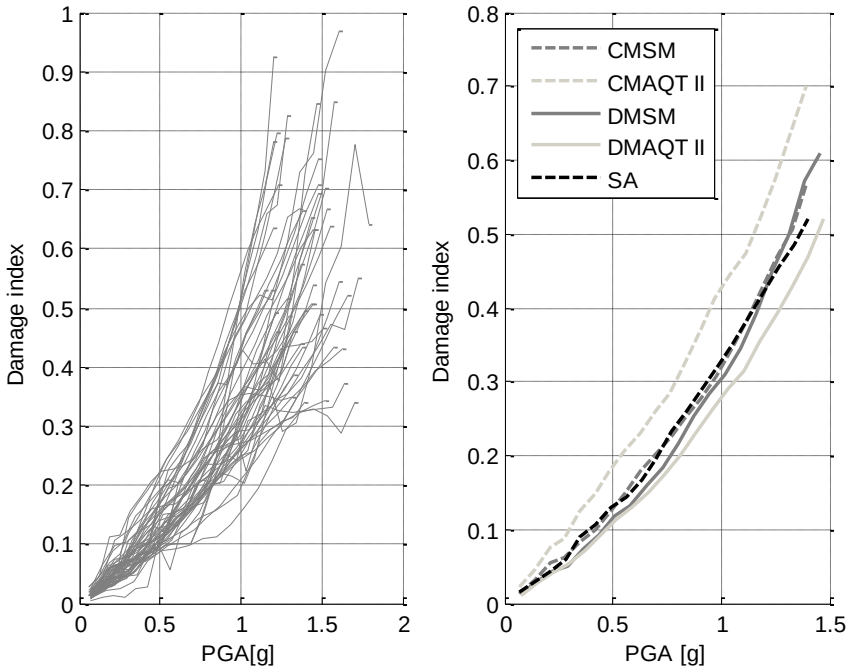

Figure E.4. 4 (a) IDA curves (DI vs. PGA) all artificial earthquakes (b) IDA curves (DI vs. PGA) by approach for case 4

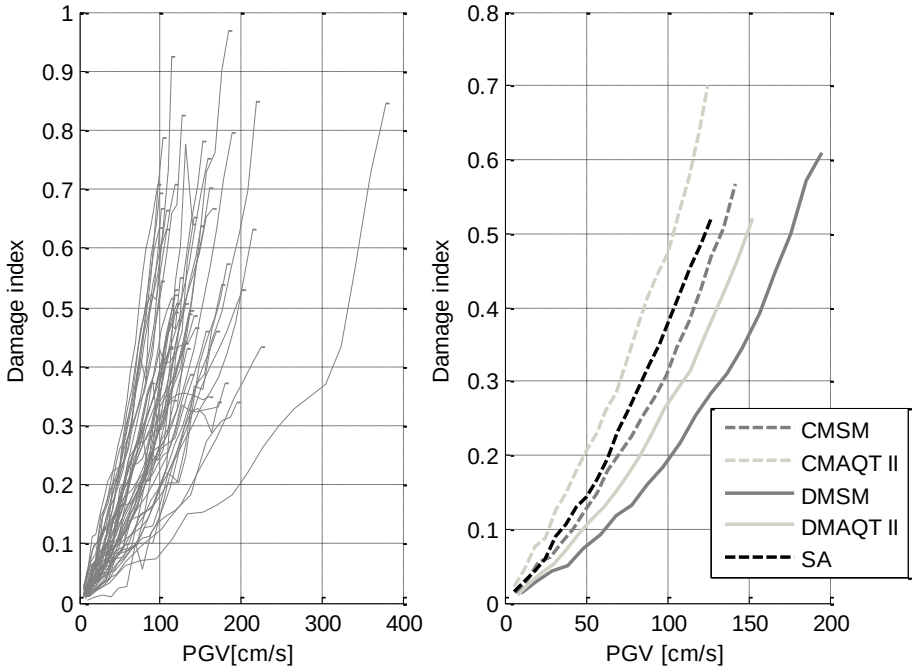

Figure E.4. 5 (a) IDA curves (DI vs. PGV) all artificial earthquakes (b) IDA curves (DI vs. PGV) by approach for case 4

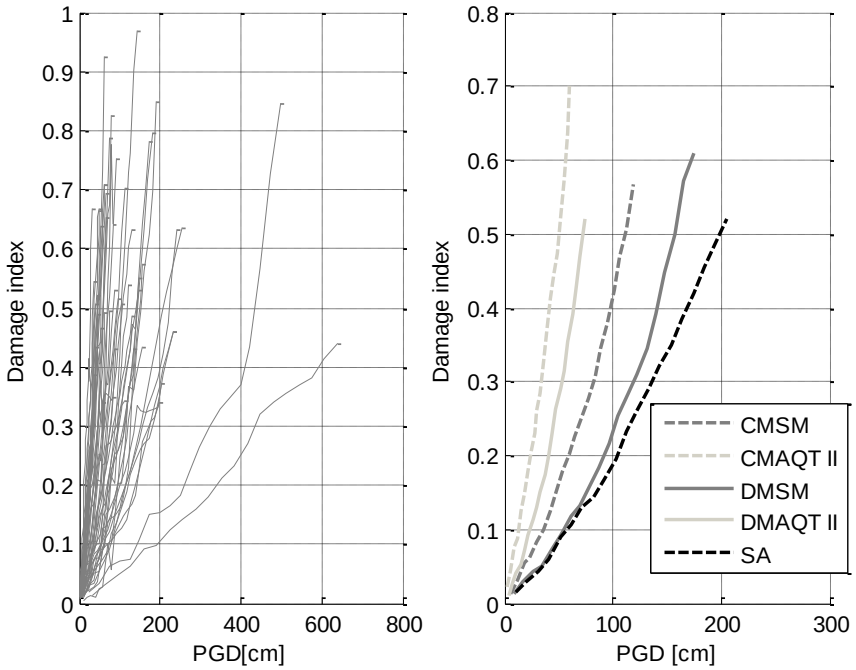

Figure E.4. 6 (a) IDA curves (DI vs. PGD) all artificial earthquakes (b) IDA curves (DI vs. PGD) by approach for case 4